

2010

IDENTIFICATION OF LOCI CONTRIBUTING TO THE SMITH- MAGENIS SYNDROME-LIKE PHENOTYPE AND MOLECULAR EVALUATION OF THE RETINOIC ACID INDUCED 1 GENE

Stephen Williams

Virginia Commonwealth University

Follow this and additional works at: <http://scholarscompass.vcu.edu/etd>

 Part of the [Medical Genetics Commons](#)

© The Author

Downloaded from

<http://scholarscompass.vcu.edu/etd/65>

This Dissertation is brought to you for free and open access by the Graduate School at VCU Scholars Compass. It has been accepted for inclusion in Theses and Dissertations by an authorized administrator of VCU Scholars Compass. For more information, please contact libcompass@vcu.edu.

© Stephen Richardson Williams May 2010
All Rights Reserved

IDENTIFICATION OF LOCI CONTRIBUTING TO THE SMITH-MAGENIS SYNDROME-
LIKE PHENOTYPE AND MOLECULAR EVALUATION OF THE RETINOIC ACID
INDUCED 1 GENE

A dissertation submitted in partial fulfillment of the requirements for the degree of Doctor of
Philosophy at Virginia Commonwealth University.

By

STEPHEN RICHARDSON WILLIAMS
Bachelor of Science (B.S.)
James Madison University, Harrisonburg, Virginia, 2001

Director: Sarah H. Elsea, Ph.D., F.A.C.M.G.
Associate Professor, Departments of Pediatrics and Human and Molecular Genetics

Virginia Commonwealth University
Richmond, Virginia
May, 2010

Acknowledgements

There are many people who contributed to my success at VCU both directly and indirectly and I would like to thank those that had the largest impact on my pursuit of scientific knowledge. First and foremost, I thank my mentor Dr. Sarah H. Elsea. Her knowledge and guidance are unmatched and I feel lucky to have work with and under her. Dr. Elsea provided the motivation to perform well in the classroom and at the bench. She is a forward-thinking scientist and human geneticist who rarely receives the recognition she truly deserves. I think my greatest thanks to her is for driving me to publish solid scientific work and participate in any and all conferences and symposiums. Through these efforts I have been given the opportunity to succeed in the future.

Next, I would like to thank all the members of Elsea lab, both past and present, who aided in my success. I would especially like to thank Dr. Santhosh Girirajan and Dr. Lily H. Truong who are friends and colleagues that encouraged me to think outside the realm of what is probable into that which is possible. I know we will be aiding each other for years to come. I thank Dr. Paula Hauck, Barbara Szomju, Nisha Patel, and David Shin for their guidance when I first entered the Elsea lab. I thank Sara Kohal, Heather Wright, Conschetta Wright, Ria Vyas, Eri Kamura, Brooke Burns, Kristie Schmidt, Sun Kim, and Sureni Mullegama for always supporting me in the lab.

I also thank committee members Dr. Jill Bettinger, Dr. Richard Moran, Dr. Rita Shiang, and Dr. Timothy York. Their guidance and motivation have contributed greatly to the direction and quality of these studies.

I am thankful to my teachers in the Department of Human and Molecular Genetics, Dr. Arti Pandya, Dr. Joyce Lloyd, Dr. Colleen Jackson-Cook, Dr. Mike Grotewiel, Dr. Shawn Holt, Dr. Jim Lister, Dr. Peter O'Connell for their knowledge and willingness to teach.

I also thank my friends Erik Ballagh, Jon Mott, Casey and Jennifer Bohn, Jun Kim, Sami Amr, Nathan Rea and my girlfriend Kelly Shircliff who always supported me in my time at VCU.

Lastly and most importantly, I have to thank my family, Fred R. Williams, Kate S. Williams, Ellen W. McCue, and all the Williams and Sparks for their support. They have always encouraged me to make the best out of every situation and I can only hope to make them proud in the future.

Technical Assistance

Chapter 2 assistance was as follows: Whole genome array comparative genomic hybridization was performed either by Dr. Eli Hatchwell or Empire Genomics. Assistance with collection of clinical information was provided by Dr. Sarah Elsea and Emily Edelman.

Chapter 3 assistance was as follows: Clinical information was gathered in part by Dr. Sarah Elsea, Sureni Mullegama, Dr. William Allen and Dr. Charles Williams. Real time qPCR assistance was provided by Sureni Mullegama. Oligonucleotide array CGH and FISH analysis were performed by Signature Genomics. Jill Rosenfeld assisted with aCGH data analysis.

Chapter 4 assistance was as follows: Collection of clinical information was aided by Dr. Sarah Elsea, Dr. Micheala Aldred, and Dr. Ellen Magenis. MLPA probes were designed by Dr. Micheala Aldred. Arrays were performed by Empire genomics or at the Cleveland Clinic.

Chapter 5 assistance was as follows: Microarray was performed by Nimblegen. Mouse tissues were collected by Brooke Burns or Kristie Schmidt.

Table of Contents

Acknowledgments.....	iii
Technical Assistance.....	v
List of Tables	xi
List of Figures	xii
Abstract	xiv

Chapter	Page
1 Background and literature review	1
Introduction.....	1
Copy Number Variation.....	4
Smith-Magenis syndrome	4
Intellectual disability.....	6
Sleep and circadian rhythm abnormalities	6
Behavioral abnormalities	8
Craniofacial and skeletal abnormalities	8
Other abnormalities.....	10
Variation in SMS deletion	10
Duplication 17p11.2 syndrome (Potoki-Lupski syndrome, PTLS).....	12
Mouse models for Smith-Magenis and Duplication 17p11.2	13
Unexplained intellectual disability	20
2 Identification of loci contributing to the Smith-Magenis-like phenotype	

	Introduction.....	21
	Materials and methods	22
	Subject ascertainment and samples.....	23
	Whole genome array-based comparative genomic hybridization (aCGH)	23
	Fluorescence <i>in situ</i> hybridization	25
	Sequencing of <i>RAI1</i>	25
	Bioinformatic and statistical analyses.....	25
	Results.....	26
	SMS vs. SMS-like phenotypes	26
	Whole genome array comparative genomic hybridization	29
	Pathogenic copy number variants	28
	Non-pathogenic copy number variants	37
	Discussion	41
3	Haploinsufficiency of <i>MBD5</i> associated with a syndrome involving microcephaly, intellectual disabilities, severe speech impairment, and seizures	45
	Introduction	45
	Materials and methods	46
	Patient ascertainment	46
	Cell lines	46
	RNA extraction	47

	Real-time qPCR	47
	<i>RAI1</i> sequencing	48
	Whole-genome array comparative genomic hybridization.....	48
	Oligonucleotide array comparative genomic hybridization.....	48
	Fluorescence <i>in situ</i> hybridization (FISH) analysis	49
	Results.....	49
	Case reports.....	49
	SMS185.....	49
	SMS361.....	55
	Molecular analysis	56
	aCGH	56
	Quantitative real-time PCR.....	58
	Discussion	61
4	Haploinsufficiency of <i>HDAC4</i> results in brachydactyly mental retardation	
	Syndrome	63
	Introduction.....	63
	Materials and methods	64
	Subject ascertainment	64
	Genomic DNA sequence analysis.....	64
	Multiplex ligation-dependent probe amplification and SNP array analysis.....	65
	Results.....	69

	BDMR clinical phenotype	69
	Refinement of the BDMR critical region.....	75
	SMS117 clinical phenotype	80
	Mutation analysis	81
	Discussion	83
	<i>HDAC4</i>	83
	<i>Hdac4</i> ^{-/-} and related mouse models	84
	Clinical implications	85
5	RAI1 transcriptionally regulates <i>CLOCK</i> and is a major contributor to circadian homeostasis	88
	Introduction.....	88
	Circadian Rhythm	91
	Materials and methods	91
	Creation of Plasmids	91
	Transfections	93
	Luciferase assay	93
	Calculation of relative luciferase activity	94
	Statistical analysis	94
	Mouse tissue collection.....	95
	Quantitative PCR	95
	Chromatin immunoprecipitation with microarray (ChIP-Chip)	95
	Candidate gene filtration.....	96

Results.....	97
Chromatin immunoprecipitation with microarray	97
Genes identified for further evaluation	101
<i>CLOCK</i>	101
<i>SNRPN</i>	101
<i>UBE3A</i>	102
<i>BDNF</i>	102
RAI1 transcriptionally activates <i>CLOCK</i> via an intron 1 enhancer element.....	103
Dysregulation of circadian genes in <i>Rail</i> +/- mice	105
Dysregulation of circadian genes in SMS fibroblasts.....	108
Discussion	111
Summary	114
Development	115
Behavior and sleep	116
Future directions	118
References	121
Appendix A	
Appendix B	
Appendix C	
Appendix D	

List of Tables

	Page
Table 1. Clinical features of chromosome 17p11.2 duplication cases.....	14
Table 2. Phenotypes of <i>Rai1</i> engineered mice.....	19
Table 3. Phenotypic features observed in Smith-Magenis syndrome-like cohort	27
Table 4. Pathogenic copy number variants identified in the SMS-like cohort	32
Table 5. Disorders previously associated with the deletions and duplications identified in this study	36
Table 6. Non-pathogenic copy number variations identified in the SMS-like cohort	38
Table 7. Clinical features of cases with 2q23.1 microdeletion syndrome	52
Table 8. <i>HDAC4</i> amplification and sequencing oligonucleotides	66
Table 9. <i>HDAC4</i> cDNA oligonucleotides for amplification and sequencing.....	67
Table 10. MLPA probes for 2q37.3 and <i>HDAC4</i>	68
Table 11. Clinical features of cases with deletions or mutations involving 2q37.3	71
Table 12. List of transcripts which overlap between ChIP-Chip arrays	106
Table 13. Ranked order of top 10 gene regulatory regions identified in ChIP-Chip experiments	100

List of Figures

	Page
Figure 1. Mechanism for non-allelic homologous recombination.....	3
Figure 2. Circadian sleep pattern of SMS subject.....	7
Figure 3. Craniofacial features observed in Smith-Magenis syndrome.....	9
Figure 4. Deletion variation identified in SMS.....	
Figure 5. Mouse synteny to chromosome 17p11.2	14
Figure 6. <i>Rai1</i> +/- mice growth rates compared to WT litter mates	17
Figure 7. CGH array plots for pathogenic CNVs	30
Figure 8. Del2q37 clinical phenotype.....	35
Figure 9. Non-pathogenic copy number variants.....	43
Figure 10. Clinical features of the 2q23.1 deletion syndrome	56
Figure 11. Array analysis of individuals with microdeletions of 2q23.1.....	64
Figure 12. FISH confirmation of 2q23 deletions in patients SMS361 and SMS185.....	66
Figure 13. Quantitative real-time PCR expression analysis of <i>MBD5</i> and <i>EPC2</i> in patient cells	67
Figure 14. Delineation of the BDMR critical region	80
Figure 15. MLPA analysis of <i>HDAC4</i> deletion breakpoints in key 2q37.3 deletions	81
Figure 16. Skeletal anomalies observed in BDMR.....	86
Figure 17. SMS117 <i>HDAC4</i> mutation and impact on HDAC4 protein.....	91
Figure 18. RAI1 localization and genomic and protein structure of RAI1	99
Figure 19. ChIP-Chip arrays	107
Figure 20. RAI1 impact on <i>CLOCK</i> transcription.....	112

Figure 21. <i>Rail</i> and <i>Clock</i> expression in mouse tissues	114
Figure 22. qPCR of circadian genes expressed in mouse hypothalamus.....	115
Figure 23. qPCR of core circadian gene expression in the mouse hypothalamus during day light and night time periods.....	117
Figure 24. Core circadian gene expression in unaffected and SMS fibroblasts	118
Figure 25. Proposed schematic of <i>RAII</i> contribution to proper skeletal development...	125
Figure 26. <i>RAI1</i> regulates <i>CLOCK</i> transcription and is a major element in the circadian cycle	128

Abstract

IDENTIFICATION OF LOCI CONTRIBUTING TO THE SMITH-MAGENIS SYNDROME-LIKE PHENOTYPE AND MOLECULAR EVALUATION OF THE RETINOIC ACID INDUCED 1 GENE

A dissertation submitted in partial fulfillment of the requirements for the degree of Doctor of Philosophy at Virginia Commonwealth University

By

STEPHEN RICHARDSON WILLIAMS

Bachelor of Science (B.S.)

James Madison University, Harrisonburg, Virginia, 2001

Smith-Magenis syndrome (SMS) is a multiple congenital abnormalities intellectual disability syndrome that results from a deletion of chromosome 17p11.2 or mutation of the *retinoic acid induced one* gene (*RAI1*). SMS is characterized by a multitude of phenotypic features including craniofacial defects, short stature, obesity, intellectual disability, self-abusive behavior, sleep disturbance and behavioral abnormalities. Interestingly, although SMS is a clearly defined syndrome with a known molecular change at its foundation, ~40% of all candidate cases sent to the Elsea lab for evaluation do not have a mutation or deletion of *RAI1*. We hypothesize that at least one other locus must be responsible for this Smith-Magenis-like (SMS-like) phenotype.

To address this hypothesis, we first compiled a cohort of 52 subjects who had been referred to the Elsea lab for a clinical diagnosis of SMS. Once these individuals were confirmed to not have an *RAI1* mutation or deletion, their phenotypes were compiled and statically analyzed to distinguish whether SMS and SMS-like cohorts are different in the prevalence of the core phenotypes of SMS such as, but not limited to, sleep disturbance, self-abusive behavior and

developmental delay. SMS-like and SMS cohorts are not different in prevalence for these core features. Next, all SMS-like subjects were sent for whole genome array comparative genomic hybridization (aCGH) to identify duplications or deletions of each individual's genome which contribute to the phenotype observed. We identified 6 pathogenic copy number variants (CNVs) in six individuals which contribute directly to the clinical phenotype, including two del(2)(q37). This study enabled us to draw relationships between SMS and other syndromes that had never been appreciated before and helped to identify pathways in which *RAI1* may function.

Using the data from our SMS-like study we were able to further characterize two known syndromes; Deletion 2q37 syndrome (brachydactyly mental retardation syndrome) and deletion 2q23 syndrome. With regard to deletion 2q37, syndrome we used genomic data from known and new deletion 2q37 subjects to refine the critical region to one gene: the *histone deacetylase 4* gene (*HDAC4*). Using both clinical and molecular clues, we were able to identify one subject from our SMS-like cohort who has an insertion in *HDAC4* which results in a premature stop codon. We conclude from this study that mutation of *HDAC4* results in brachydactyly mental retardation syndrome.

With regard to deletion 2q23 syndrome there were only five known cases in the published literature to which we were able to add two more. Using a similar approach to our del2q37 study we refined the critical region for this syndrome to one gene, the *methyl binding domain 5* gene (*MBD5*). Using a molecular and clinical approach we were able to conclude that haploinsufficiency of *MBD5* results in the core phenotypes seen in del2q23 syndrome including microcephaly, intellectual disabilities, severe speech impairment, and seizures.

Using all the data generated from the three previous studies we set out to characterize the molecular function of *RAI1*. We hypothesize that *RAI1* is a transcription factor that regulates

gene expression of core genes involved in development, neurological function, and circadian rhythm. Using a ChIP-chip based approach we identified 257 transcripts we believe *RAI1* regulates. Following up on these transcripts, using *in vitro* and *in vivo* methods, we have been able to conclude that *RAI1* is a positive regulator of *CLOCK*, the master regulator of the central circadian cycle.

Taken together, these studies have given us insight into the specific molecular changes that contribute to SMS and SMS-like syndromes. We have unveiled pathways and genes which are important to normal human development and behavior and identified novel functions of *RAI1*. These studies will provide the foundation for the future discovery of the pathways affected.

Chapter 1: Background and literature review

Introduction

Smith-Magenis syndrome (SMS, OMIM#182290) is a congenital abnormalities, intellectual disability syndrome that can present with sleep disturbance, self-abusive and aggressive behavior, craniofacial abnormalities, neurological abnormalities, and obesity. First described by Ann Smith and Dr. Ellen Magenis, SMS was initially thought to be a contiguous gene syndrome resulting from a deletion of the 17p11.2 region [3]. However, later molecular evidence revealed one gene contributes to the majority of the phenotypes observed. Data revealed that mutation or deletion of the *retinoic acid induced 1* gene (*RAI1*) resulted in SMS [4]. Thus, SMS is a sporadic, dominant syndrome defined by haploinsufficiency of *RAI1*.

Duplications and deletions of the genome have long been thought to contribute to evolution of all species. While there are rare cases for these copy number changes to confer an advantage to said species, these types of changes are typically detrimental. Deletion and duplication syndromes are a major contributor to the overall number of recognized intellectual disability syndromes which are being identified and characterized at a rapid pace with the advent of new technologies such as whole genome array comparative genomic hybridization (aCGH) [5]. SMS, duplication 17p11.2 syndrome (also known as Potocki-Lupski syndrome), fragile X-syndrome, and Williams syndrome all result from a duplication or deletion of specific regions of the genome.

Typically, deletion syndromes are more common and phenotypically more severe than duplication syndromes, due to haploinsufficiency, one copy not being sufficient, of one or more core genes (a gene imperative to the proper function of the disrupted pathway). When a chromosomal region is duplicated, the resulting phenotype can be more subtle and is thus more

likely to be missed by a clinician, not warranting a molecular evaluation [6]. So, it is more appropriate to state that the incidence of deletion and duplication events in the population is likely very similar, however, the identification of these events is more likely to yield the unveiling of a deletion as the cause of the phenotype observed [7, 8]. This can be seen in SMS versus duplication 17p11.2 syndrome where the intellectual disability, craniofacial, sleep, and metabolic abnormalities are much more severe in SMS and the number of subjects identified with a 17p11.2 duplication is ~75 whereas more than 300 SMS subjects have been confirmed [7]. There is, however, some evidence showing that in the SMS region, on 17p11.2, deletions are twice as likely to occur than duplications [8]. This being said, the molecular events that take place which results in these two outcomes, duplication vs. deletion, are similar and due to non-allelic homologous recombination (NAHR) which is mediated by segmental duplications in the 17p11.2 region [9] (Figure 1).

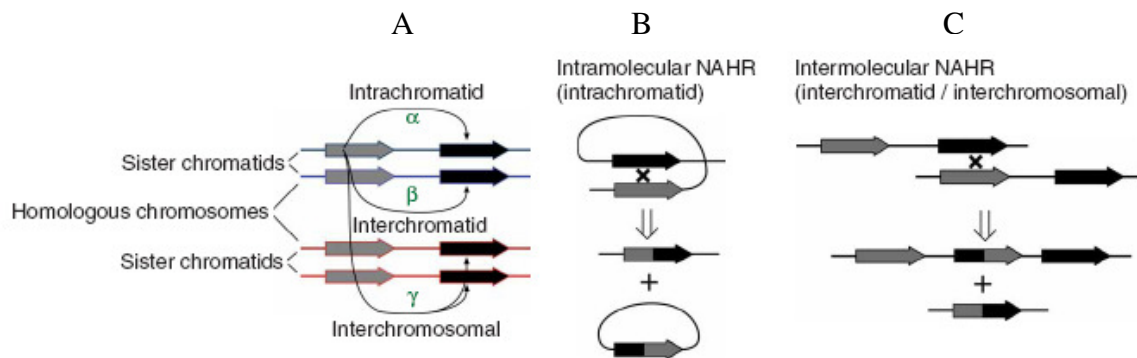


Figure 1. Mechanism for non-allelic homologous recombination. A) Grey and black arrows indicate regions of homology between sister chromatids. NAHR can occur in two forms: B) Intramolecular, wherein sister chromatids misalign leading to deletion of intervening sequences. C) Intermolecular, wherein chromatids from different chromosomes misalign leading to a duplication or deletion allele. Modified from Turner et al. 2008 [8].

Copy Number Variation (CNV)

Copy number variations are defined as segments of DNA ranging from 1 kilobase (kb) to several megabases (Mb), for which copy-number differences have been revealed by comparison of two or more genomes [10]. Investigation into the importance of copy number variations has become an integral part in understanding human evolution and disease. Various molecular events can result from CNV, including gene dosage, gene disruption, gene fusion and position effects, CNVs can cause Mendelian or sporadic traits [11], or be associated with complex diseases [12]. CNVs can also represent singularly benign polymorphic variants that contribute to a combinatorial effect in variation. In fact, it is thought that CNVs contribute more to human variation than do single nucleotide polymorphisms [13]. Additionally, it is thought that CNVs have a much higher *de novo*, locus specific mutation rate than SNPs [11]. Given these facts, it is important to study disorders and syndromes which result from CNV to better understand and recognize regions of the genome that may contribute in large part to disorder or variation.

Smith-Magenis syndrome

Smith-Magenis syndrome is a recognizable syndrome characterized by physical, developmental, neurological, and behavioral features. SMS is typically a *de novo* disorder with an estimated prevalence of 1:15,000–25,000 live births [14] however; there is one report of an SMS subject having a mother who is mosaic for a del(17)(p11.2) [15]. SMS has many clinical phenotypes that overlap with other intellectual disability syndromes, such as Prader-Willi and Williams syndromes, and interestingly only ~46% of those individuals referred the Elsea lab for 17p11.2/*RAI1* molecular evaluation are positive for molecular changes leading to SMS (Elsea, unpublished data).

Physical features consist of distinctive craniofacial and skeletal anomalies including brachycephaly, frontal bossing, hypertelorism, synophrys, up slanting palpebral fissures, midface hypoplasia, a broad square-shaped face flat nasal bridge and a tented upper lip [16]. Dental anomalies include tooth agenesis, especially of premolars, and taurodontism [17]. Cleft lip or palate is also reported at a higher rate than seen in the normal population [18] and hearing loss is present at 60-68%.

The neurological and behavioral phenotypes seen in SMS consists of hypotonia, stereotypies such as self-hugging and hand twirling, self-abusive behavior, hyperactivity, and oral and/or motor dysfunction [18, 19]. An inverted circadian rhythm which results in waking periods during the night and napping periods during the day, and times of activity, complicate the neurological and behavioral phenotypes observed [20].

Skeletal and developmental abnormalities include short stature (<5th percentile), brachycephaly, brachydactyly, scoliosis, fifth-finger clinodactyly, fore arm and elbow limitations, and polydactyly. Additionally obesity is observed and cardiac defects are present at ~30% [18, 20].

Otolaryngological abnormalities such as hearing loss, a hoarse deep voice, and vocal cord nodules and polyps are also common [21, 22, 23]. Additionally, ophthalmologic features are present in 64% of SMS patients and include myopia, iris anomalies such as heterochromic irides or Wolfflin-truckmann spots (iris hamartomas), strabismus, microcornea, and rarely, retinal detachment (which can result from violent behaviors) [18, 24, 25].

Intellectual disability

Intellectual disability (ID) is defined as a person having an IQ <70 and is present in 1–3% of the general population. The cause of ID is unknown in more than half of cases identified [26].

Most SMS individuals have mild to moderate intellectual disability with IQ ranging between 20-78 and most children falling between 40-54 [22]. School-age children with IQs in the low normal range have been identified; however, IQ decreases as the child ages ultimately placing the individual in the mild intellectual disability range by adulthood (Elsea, unpublished data). Delayed speech occurs in ~84% of SMS patients [27]. These individuals have better receptive language skills than expressive language, while their social-emotional functions remain within the normal range [28, 29]. In addition, delayed fine/gross motor skills, problems with sensory integration, and poor adaptive function are seen. Other neurological features include peripheral neuropathy, pes cavus or pes planus, abnormal gait, and decreased sensitivity to pain, which may lead to an increased risk for self-injury.

Sleep and circadian rhythm abnormalities

Sleep disturbance is a hallmark of Smith-Magenis syndrome. It is reported that 75%-100% of all confirmed SMS cases present with sleep disturbance and this is one of the early indicators that an individual may have SMS [19, 22]. Infants typically present with hypersomnolence early in life, and sleep disturbance in older children include difficulty falling asleep, inability to enter or maintain REM sleep, reduced night sleep, shortened and broken sleep cycles with frequent night time and early-morning awakenings and excessive daytime sleepiness [20, 30] (Figure 2).

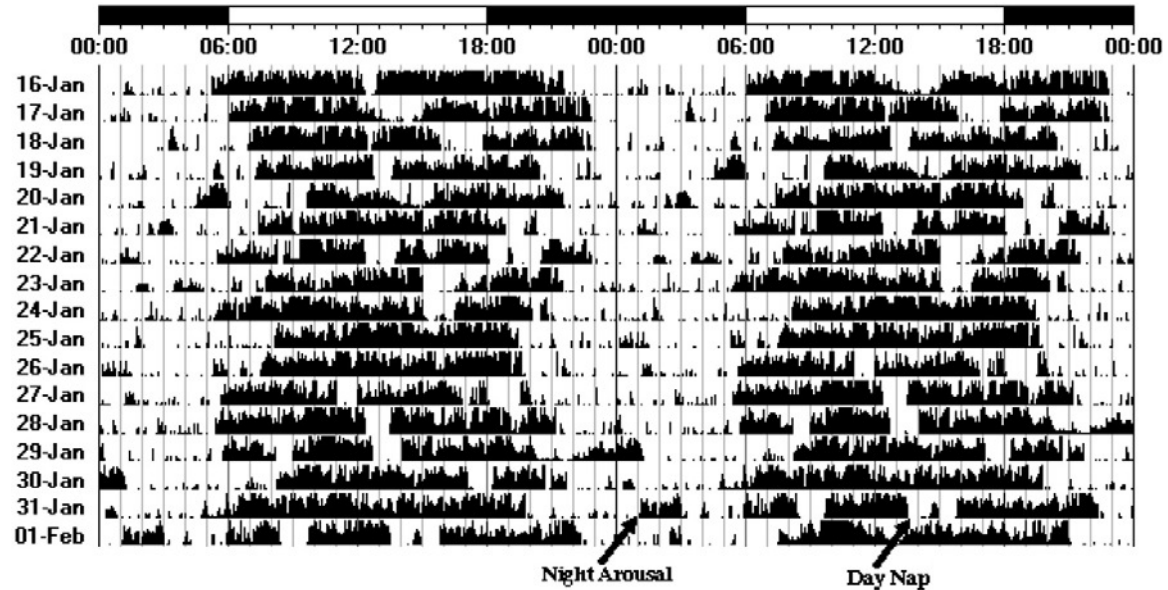


Figure 2. Circadian sleep pattern of SMS subject. 5 year old confirmed SMS subject. Data collected over a 16 day period using a wrist activity meter. Top bar indicates wake periods (white) and sleep periods (black). Vertical black lines indicate periods of activity. Note consistent night time arousals and day time naps. Modified from Gropman et al. 2006 [28].

Thought to be caused by an inverted rhythm of melatonin secretion, these circadian rhythm difficulties can complicate behavioral and learning difficulties (Elsea, unpublished data). However, multiple cases have been reported that have normal melatonin secretion but still have sleep disturbance, indicating a possible molecular role for *RAII* in the sleep cycle and the core molecular pathway of circadian rhythm. [30]

Behavioral abnormalities

The SMS phenotype consists of core behavioral abnormalities. Core phenotypes include attention-seeking, aggression, disobedience, a lack of respect for personal space, distraction, stereotypical and self-injurious behaviors. Interestingly, self-injurious behaviors are seen in ~90% of cases and include head-banging and skin picking, two features unique to SMS, onychotillomania, and polyembolokoilomania are more often seen in older children [31, 32]. Stereotypical behaviors include self-hugging, hand twirling, and body rocking [31, 33]. It is noteworthy that although some SMS subjects are diagnosed with autism early in life (because of delayed speech), this diagnosis typically changes with the acquisition of language skills.

Craniofacial and skeletal abnormalities

Craniofacial and skeletal abnormalities include short stature, broad face, flat nasal bridge, brachycephaly, brachydactyly, scoliosis, crainostenosis, prognathasism, midface hypoplasia, tented upper lip, and cleft lip and/or palate. The range of craniofacial phenotypes is variable early in life but as subjects age there is a “typical” appearance that becomes identifiable (Figure 3)



Figure 3. Craniofacial features observed in Smith-Magenis syndrome. A-C Common deletion. D-F Atypical deletion. G-I *RAI1* mutation. Modified from Girirajan et al. 2006 [34]

Other abnormalities

Along with the typical behavioral, neurological, and craniofacial features there are some phenotypes in SMS that are more variable. Dental abnormalities are observed in ~50% of subjects and include malocclusion, tooth agenesis, taurodontism, gingivitis, and poor overall dental hygiene [17].

Cardiac abnormalities are also seen in a subset of SMS subjects and include ventral septal defect, atrial septal defect, tricuspid stenosis, mitral stenosis, tricuspid and mitral regurgitation, aortic stenosis, pulmonary stenosis, mitral valve prolapse, tetralogy of Fallot, and total anomalous pulmonary venous return [18].

Seizures occur in up to 30% of cases and affect those with a common deletion at the highest rate. However, ~50% of diagnosed SMS cases present with abnormal EEGs [18]. This suggests that up to 20% of individuals with SMS do not reach the threshold for seizure.

Variation in SMS deletion

17p11.2 deletions leading to SMS can be broken down into four main categories; common, large, small and atypical deletions (Figure 4). All deletions encompass the *RAI1* gene but size and position of the deletion can account for phenotypic variance present in the individual. For example, short stature is seen at a higher prevalence in individuals with common deletions than those found to have large deletions [18]. Those with small deletions are more likely to have an abnormal EEG than those with common deletions [18]. Additionally, those with small deletions have a more similar phenotype to individuals with *RAI1* mutations [14].

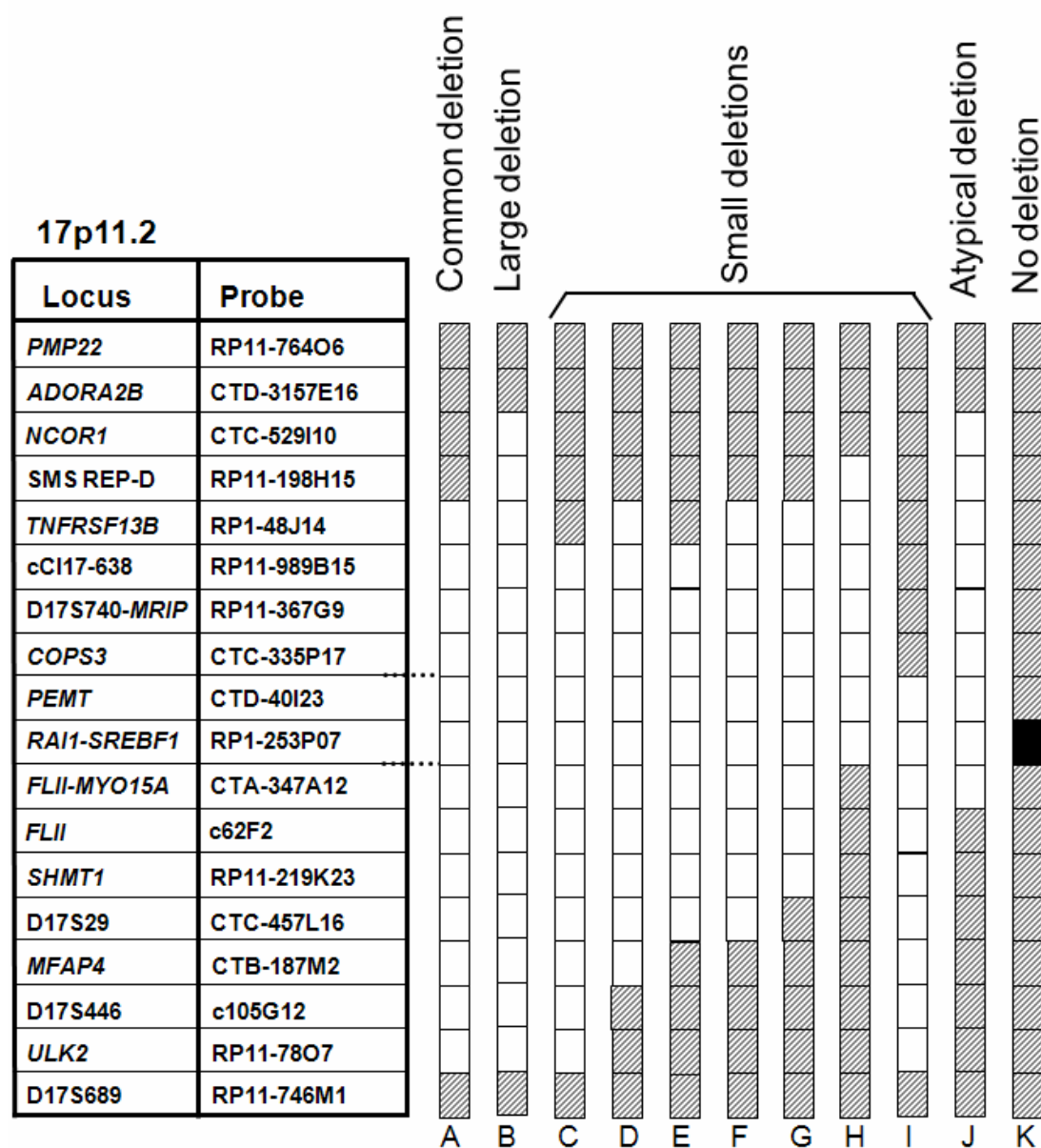


Figure 4. Deletion variation identified in SMS. Loci and FISH probes used to test for presence or absence of these loci are represented in the first two columns. Shaded boxes represent regions not deleted and empty boxes indicate regions that are deleted. Shown are common, large, small and atypical deletions seen in SMS. Note that *RAI1* is found in all deletions. Modified from Girirajan et al. 2006 [34].

Duplication 17p11.2 syndrome (Potoki-Lupski syndrome, PTLS)

Interstitial duplication of 17p11.2 results in duplication 17p11.2 syndrome, also known as Potoki-Lupski syndrome (PTLS). Dup(17)(p11.2) results in mild to severe intellectual disability, infantile hypotonia, failure to thrive, congenital cardiovascular anomalies, sleep-disordered breathing, developmental delay, intellectual disability, hyperactivity, and autism [35, 36]. Craniofacial features include a triangular face, microcephaly, micrognathia, broad nasal bridge, high arched palate, and hypertelorism, while dental anomalies in the form of malocclusion of the teeth have also been reported [37]. Limb abnormalities including flexion deformity of the fingers and club foot have also been described. Other features include cognitive and language impairment, pharyngeal dysphasia, obstructive and central sleep apnea, structural cardiovascular abnormalities, and electroencephalogram (EEG) abnormalities [35, 36]

Less commonly reported features are hearing impairment, structural otolaryngological defects, and ophthalmic abnormalities, such as myopia and iris hamartoma. Other rarely reported features are genitourinary and/or renal anomalies, scoliosis, and hypercholesterolemia [36].

The predicted incidence of dup(17)(p11.2) syndrome are the same as that of SMS (~1:25,000) but is likely under diagnosed because the phenotype can be much more subtle than that of SMS. Only ~75 cases of dup(17)(p11.2) syndrome have been reported [7]. However, a recent report indicates that this region may be subject to germline rates of deletion to duplication of 2.14:1, indicating a molecular preference for deletion over duplication in 17p11.2 [8].

Duplication of this 17p11.2 region can range between a 0.4 Mb to 13.3 Mb with 3.7 Mb being the most common duplication (between distal and proximal repeats flanking RAI1) and 5 Mb being the least common duplication (located between LCR17pA and LCR17pD) having been

recently identified in two individuals [7]. A list of features with regard to the different classifications are seen in Table 1.

Mouse models for Smith-Magenis and duplication 17p11.2 syndromes

Mouse models that mimic human conditions are invaluable tools to help understand the molecular, developmental, and behavioral role of a gene or genes. The sequencing of the mouse genome has allowed for regions of synteny to human genomic sequence to be mapped and utilized for research [38].

Three types of genetically engineered mice are typically used for research and are knockout, gene-trap, and transgenic. Knockout and gene-trap serve the purpose to eliminate a given gene or region from expression and function whereas transgenic mouse models contain genomic material used to over express, or simply express foreign DNA.

Murine chromosome 11qB1.3-B2 is syntenic to human chromosome 17p11.2. An approximate 34 cM region surrounding *RAI1/Rai1* is conserved between mouse and human genomic structure making this region fit for creation of knockout and transgenic mice (Figure 5). Mice lacking *Df(11)17/+* or duplicated for *Dp(11)17/+* a 2 Mb region, containing seven genes, syntenic to human chromosome 17p11.2 were originally created by Waltz et al. 2003 [39] using chromosome engineering technology. These deletion/duplication mice were created to mimic the common deletion seen in SMS and duplication seen in dup(17)(p11.2) syndrome. These mice recapitulate many of the core features observed in SMS and duplication 17p11.2 syndrome.

Table 1. Clinical features of chromosome 17p11.2 duplication cases. Data collected from Girirajan et al. 2007 [40] and Zang et al. 2010 [7].

Clinical features	dup(17)(p10p12) N=4	dup(17)(p11.2p12) N=7	dup(17)(p11.2p11.2) N=8	Uncommon dup(17)(p11.2p12) N=2
Mental retardation	4/4	7/7	8/8	2/2
Pre/postnatal growth retardation	3/4	7/7	3/3	0/2
Motor delay	4/4	7/7	2/3	N
Speech delay	4/4	5/5	2/4	N
History of spontaneous abortions	1/3	N	N	N
Hypotonia	4/4	2/3	2/4	1/1
Feeding difficulties	4/4	3/4	1/3	2/2
Hyperactivity/behavioral abnormalities	1/3	2/5	4/6	2/2
Seizures	2/4	1/6	3/7	0/2
Decreased nerve conduction	¼	5/6	0/8	0/2
Delayed deep tendon reflexes	1/4	6/7	0/8	N
Craniofacial features				
Triangular face	3/3	2/4	1/2	2/2
Microcephaly	4/4	2/3	4/6	N
Micrognathia	3/4	1/4	2/3	N
Hypertelorism	2/4	3/3	1/3	N
Broad nasal bridge	4/4	4/5	2/4	0/2
Low-set/malformed ears	2/4	4/4	3/3	0/1
High arched palate	1/4	3/5	3/4	N
Cleft lip/palate	0/4	0/7	1/4	N
Ophthalmologic disorders	2/4			2/2
Short broad neck	N	1/7	N	0/2
Hearing loss	1/4	1/7	1/3	0/1
Cardiac anomalies	0/4	2/7	0/8	0/2
Renal/urinary tract anomalies	1/4	1/7	2/8	1/1
Short stature	1/4	6/6	5/8	N
Decreased weight	1/4	4/4	3/5	0/2
Bone and limb defects				
Clinodactyly of fifth finger	N	4/7	2/8	N
Flexion contractures	1/4	3/7	0/8	N
Foot anomalies	2/4	6/7	0/8	N
Short sternum	N	1/6	N	N
Dental anomalies	1/4	4/7	5/8	N

Df(11)17/+ mice have features consistent with SMS including craniofacial abnormalities, obesity, seizures and neurobehavioral abnormalities including an abnormal circadian rhythm [39]. Neurological abnormalities were observed including overt clinical seizures and abnormal EEGs which are also seen in SMS [39]. Histological examinations were performed with brains, hearts, spleens, and kidneys, and no obvious defects were identified in any of these tissues [39] which is also consistent with the SMS phenotype.

Dp(11)17/+ (duplication) mice displayed growth retardation, hyperactivity, increased anxiety-related responses in a light-dark test, increased conditioned fear, and decreased startle response with normal sensorimotor gating on a prepulse inhibition assay [39, 41]. No craniofacial anomalies or altered circadian rhythm were observed in the *Dp(11)17/+* mice [39, 41].

Later, using a targeted approach, mice haploinsufficient for *Rai1* were created [42]. These mice were developed to test the phenotypic consequences of *Rai1* inactivation and to provide insight into the phenotypes *Rai1* contributes directly to in SMS. Young *Rai1*^{+/-} mice were under weight as compared to wild-type littermates but by age 23 weeks became significantly larger with progressive weight gain [42] (Figure 6). Eighteen percent of *Rai1*^{+/-} mice had craniofacial abnormalities, including short curved snouts caused by the malformation of the craniofacial skeletal elements [42].

Rai1^{-/-} mice largely were not viable and Mendelian ratios of litters (+/+ 36.2%, +/- 59.3%, -/-4.5%) were skewed indicating significant embryonic lethality. *Rai1*^{-/-} mice that did survive beyond the embryonic stage had growth retardation and craniofacial abnormalities as compared to WT litter mates [42]. Additionally, these showed tone and context dependent impaired fear conditioning, as well as overt seizures [41, 42].

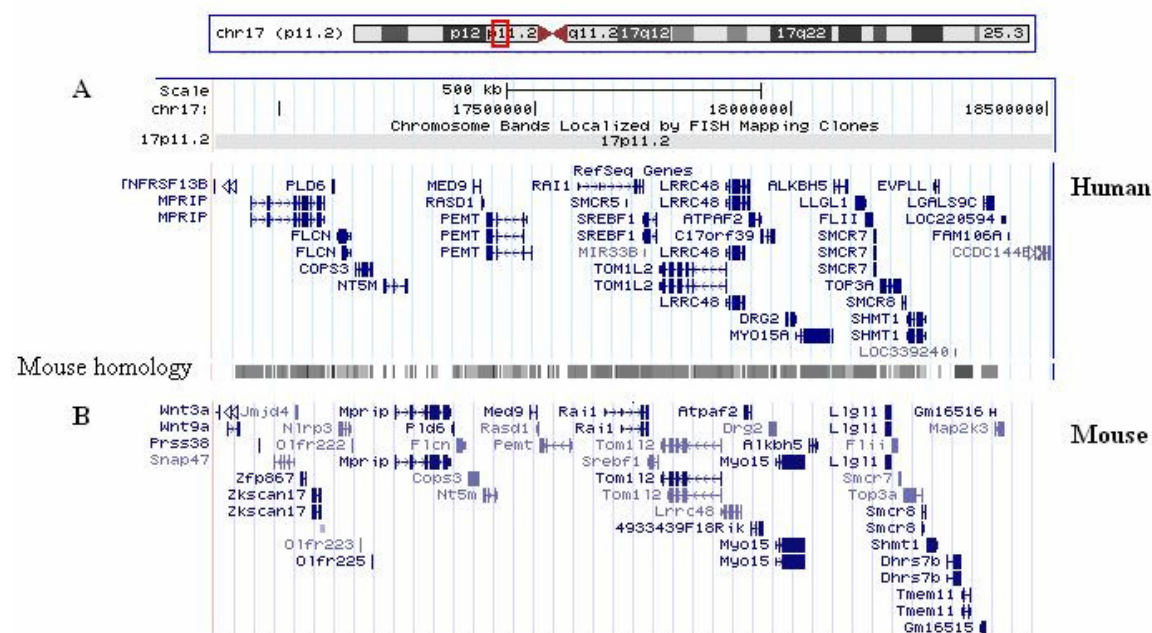


Figure 5. Mouse synteny to chromosome 17p11.2. A) Human 17p11.2. RefSeq Genes (Build: February 2009, GRCh37/hg19). B) Mouse 11qB1.3-B2. RefSeq Genes (Build: July 2007, NCBI37/mm9). Grey bars between sections A and B represent regions of synteny. Modified from UCSC Genome Browser (<http://www.genome.ucsc.edu/>)

Recently, Girirajan et al. [43, 44] generated and performed an in-depth behavioral analysis of bacterial artificial chromosome(BAC) transgenic, *Rail* overexpression mice (*Rail-Tg*) harboring three copies of the *Rail* gene. The authors found that these mice exhibited a variety of defects. Growth retardation was seen with these mice being undersized as compared to WT litter mates which continued as development progressed. However, transgenic mice were able to achieve normal size by 20 weeks [43]. Abnormal maternal behavior was observed wherein *Rail-Tg* mothers could not properly take care of their pups (1/5 survival average, WT or transgenic pups) [44]. When these pups were placed with a WT foster mother (all, 5/5 average) pups survived. Additionally, *Rail* overexpressing mice exhibit a reduction in the levels of 5-HIAA suggesting a defect in the enzyme monoamine oxidase (MAO), which converts serotonin to 5-HIAA. Further, these mice have altered social behavior with impaired nesting behavior, social dominance, aggression, reduced social memory, hyperactivity, anxiety-related behavior, and altered sociability, all 5-HIAA mediated behaviors.

Taken together, the *Df(11)17/+*, *Rail +/-*, *Dp(11)17/+*, and *Rail-Tg* mice have proven to be good models for their respective syndromes. The *Rail +/-* mice have craniofacial, behavioral and developmental abnormalities consistent with those of SMS. Additionally, *Dp(11)17/+* duplication mice have behavioral, neurological and developmental abnormalities consistent with that of dup17p11.2 syndrome. These data reinforce the dosage sensitivity of the *retinoic acid induced 1* gene. A summary of the phenotypes seen in these mice can be seen in Table 2

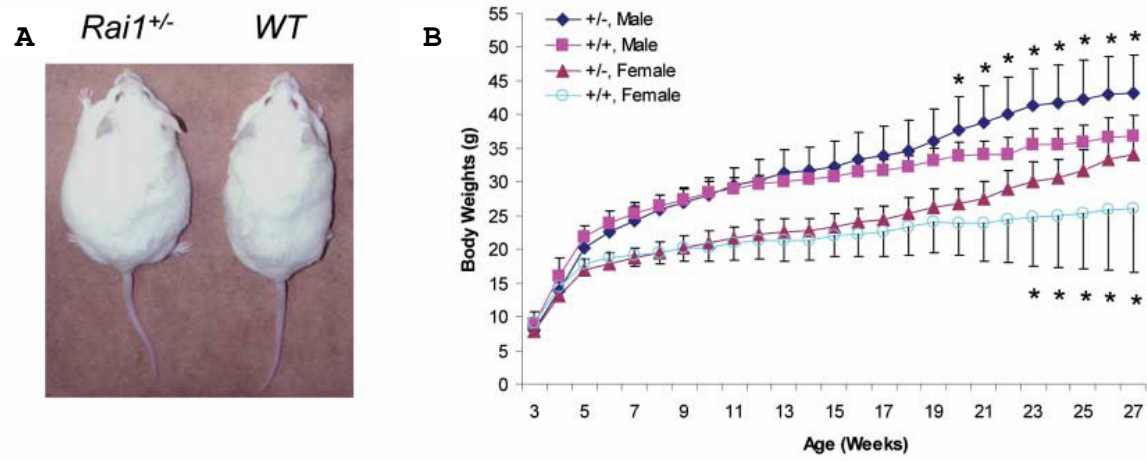


Figure 6. *Rai1*^{+/-} mice growth rates compared to WT litter mates. Note obesity and shortened snout. A) *Rai1*^{+/-} and WT size and craniofacial phenotypes. B) Growth rates of *Rai1*^{+/-} mice. Modified from Bi et al. 2005 [42].

Table 2. Phenotypes of *Rai1* engineered mice. Bi et al. 2005, 2007, Waltz et al. 2003, 2004, 2006, Girirajan et al. 2009.

Feature	Mouse	<i>Df(11)17/+</i> [39, 41]	<i>Rai1</i> +/- [42, 45]	<i>Rai1</i> -/- [45]	<i>Dp(11)1/+</i> [39, 41, 46]	<i>Rai1</i>-Tg [44]
Craniofacial Defect		+	+	+	-	-
Developmental Defect		+	+	+	+	+
Overweight		+	+	-	-	-
Underweight		-	-	+	+	+
Circadian Rhythm Abnormality		+	N/A	N/A	-	N/A
Impaired Conditioned Fear		+	-	+	+	N/A
Hyperactivity		-	-	-	+	+
Seizure		+	+	+	-	-
Abnormal EEG		+	+	+	-	N/A
Abnormal Maternal Behavior		N/A	N/A	N/A	N/A	+
Altered Mendelian Transmission		+	+	-	+	+

“+” indicates presence of feature. “-” indicates absence of feature. “N/A” indicates feature not assessed.

Unexplained intellectual disability

Understanding the molecular basis for intellectual disability continues to be a problematic hurdle to jump in the field of human genetics. ID has a 1-3% prevalence rate in the general population [47, 48] and although there are many well-described ID syndromes associated with known molecular changes such as SMS (del(17)(p11.2)/*RAI1* mutation), Williams syndrome (del(7)(q11.23)), Rett syndrome (*MECP2* mutation), Prader-Willi (paternal del(15)(q11-q13)), the molecular basis for ID in many individuals remains unclear.

The major genomic and molecular contributors to ID are aneuploidy, chromosomal microdeletions or microduplications, translocations, inversions, uniparental disomy (UPD), exonic mutation, splice-site or intronic mutation, and epigenetic or imprinting changes. Chromosomal deletions and duplications account for the vast majority of ID, however in up to 80% of all ID cases the molecular change cannot be identified [49, 50, 51]. The most common clinical diagnoses of individuals with ID are Down syndrome (9.2%), microdeletion 22q11.2 (2.4%), Williams–Beuren syndrome (1.3%), fragile-X syndrome (1.2%), Cohen syndrome (0.7%), and monosomy 1p36.3 (0.6%) [52].

New technologies have evolved to help characterize these ID syndromes, including whole genome array comparative genomic hybridization (aCGH), targeted array, high resolution fluorescence *in situ* hybridization (FISH), and high throughput sequencing (both whole genome and whole exome) have allowed for faster, and more accurate molecular diagnosis the probability of a multiple hit theory exists making the majority of ID fall under the “complex” arena of genetic diagnosis [5].

Chapter 2

Identification of loci contributing to the SMS-like phenotype.

Introduction

Smith-Magenis syndrome (SMS, OMIM#182290) is a complex congenital abnormalities/mental retardation disorder caused by a deletion of chromosome 17p11.2 that includes the *RAI1* gene or a mutation in *RAI1* [4]. Phenotypically, SMS overlaps with other syndromes such as Prader-Willi, Williams, and Down syndromes. While certain features overlap between these syndromes, the phenotype associated with SMS is characterized by a specific combination of traits. In short, SMS can be characterized by developmental delays, craniofacial abnormalities, speech and motor delay, neurological abnormalities, sleep disturbance, and self-injurious behaviors [3]. Due to the dense overlap between mental retardation syndromes, it is imperative that the genetic basis for each clinical phenotype is unraveled to provide the most complete information for families, to target the most appropriate services for the child, and to provide the most accurate recurrence risk assessment.

We have acquired a cohort of individuals with clinical features of Smith-Magenis syndrome in whom a deletion or mutation of *RAI1* cannot be identified. We refer to these cases as “Smith-Magenis syndrome-like” (SMS-like), since they are not phenotypically distinguishable from individuals with a molecularly-confirmed *RAI1* mutation or 17p11.2 deletion. Each case is evaluated on an individual basis, and if the subject meets the phenotypic criteria for a clinical diagnosis of SMS, the coding region of the *RAI1* gene is sequenced. Each subject referred for molecular evaluation had a normal karyotype and 17p11.2 FISH analysis, followed by sequencing of the *RAI1* coding region [53, 54]. Of patients referred to our laboratory for *RAI1* mutation or deletion analysis, 46% (n = 52/112) were confirmed to carry a heterozygous

deletion or mutation of *RAI1*. Although the remaining cases ($n = 60/112$) have significant phenotypic overlap with SMS, they do not have a molecular diagnosis. Thus, we hypothesized that at least one additional locus, possibly functioning in a common pathway with *RAI1*, is contributing to the high frequency of this phenotype. Eight of the remaining cases were not included in this study because of the lack of genetic material for analysis or insufficient clinical data were available for the subject.

Array comparative genomic hybridization (aCGH) has become an invaluable tool in the genomic evaluation of subjects with mental retardation, developmental delay, and congenital anomalies, as well as more complex disorders such as autism and schizophrenia [55, 56]. Using aCGH as our primary tool, we set out to identify genomic regions potentially containing dosage sensitive genes that when deleted or duplicated, lead to an SMS-like phenotype. Analysis of these 52 cases revealed copy number abnormalities of chromosomal regions which contain genes that contribute to neurological integrity, cognition, and development, all of which when disturbed could lead to the phenotypes observed in the SMS and SMS-like groups. Given the phenotypic and genetic information presented herein and the loci identified, these data will improve diagnosis, provide insight into the etiology of mental retardation/congenital abnormalities syndromes, and one day could lead to better treatments and therapy for individuals with these genomic disorders.

Materials and Methods

Subject ascertainment and samples

Subjects were referred to the Elsea laboratory for molecular evaluation of SMS at Michigan State University or Virginia Commonwealth University. Samples were collected in

accordance with Institutional Review Board approved protocols from the appropriate institution. Peripheral blood was collected, and DNA and metaphase chromosomes prepared following standard methods. All samples then evaluated for mutations in the *RAI1* gene. Phenotypic information was collected using medical records, geneticist reports, patient photos, and in some cases a clinical checklist sent to the referring geneticist. All information was collected in accordance with IRB approved protocols.

Whole genome array-based comparative genomic hybridization (aCGH)

aCGH was performed as previously described [40]. The procedures for the construction, hybridization, and data analysis is described below.

Construction of the human BAC CGH array: DNA printing solutions were prepared from sequence connected RPCI-11 BAC by ligation-mediated PCR as described previously [57],[58],[59]. The minimal tiling RPCI BAC array contains ~19,000 BAC clones that were chosen by virtue of their STS content, paired BAC end-sequence and association with heritable disorders and cancer. The backbone of the array consists of ~4600 BAC clones that were directly mapped to specific, single chromosomal positions by fluorescent in situ hybridization (FISH) [57]. Each clone is printed in duplicate on amino-silanated glass slides (Schott Nexterion typeA+) using aMicroGrid II TAS arrayer (Genomic Solutions, Inc.). The BAC DNA products have ~80 µm diameter spots with 150µm center to center spacing creating an array of ~39,000 elements. The printed slides dry overnight and are UV-crosslinked (350mJ) in a Stratalinker 2400 (Stratagene) immediately before hybridization. A complete list of the RPCI-11 BAC clones spotted on the 19K array can be found at: <http://microarrays.roswellpark.org>.

Labeling and hybridization of DNA: Reference and test sample genomic DNAs (1 μ g each) are individually fluorescently labeled using the BioArray CGH Labeling System (Enzo Life Sciences). Initially, DNA is denatured in the presence of a random primer at 99°C for 10 min in a thermocycler, and then quickly cooled to 4°C. The tubes are transferred to ice and labeling occurs with the addition of dNTP-cyanine 3 mix (or dNTP-cyanine 5) and Klenow fragment. Incubation takes place for 4 h at 37°C in a thermocycler. The unincorporated nucleotides were removed using a QIAquick PCR purification column (Qiagen), and the labeled probe is eluted with 2 x 25 μ l washes. Prior to hybridization, the test and reference probes were combined with 100 μ g human Cot-1 DNA (Invitrogen) and precipitated for one hour with sodium acetate and ethanol. The probes are pelleted, resuspended in 110 μ l SlideHyb Buffer #3 (Ambion) containing 5 μ l of 100 μ g/ μ l yeast tRNA (Invitrogen), heated to 95°C for 5 min, then incubated at 37°C for 30 min. Hybridizations to the 19K BAC arrays were performed for 16 h at 55°C using a GeneMachine hybridization station (Genomic Solutions, Inc.) as described [60]. After hybridization, the slides are automatically washed in the GeneTAC station with reducing concentrations of SSC and SDS. aCGH was also performed under similar conditions as a fee for service at Empire Genomics using the same BAC CGH array as previously described [40].

Image and data analyses: The hybridized aCGH slides are scanned using a GenePix 4200AL Scanner (Molecular Devices) to generate high-resolution (5 μ m) images for both Cy3 (test) and Cy5 (control) channels. Image analysis was performed using the ImaGene (version 8.0.0) software from BioDiscovery, Inc. The log₂ test/control ratios were normalized using a sub-grid loess correction. Mapping information was added to the resulting log₂ test/control values. The mapping data for each BAC are found by querying the human genome sequence at

<http://genome.ucsc.edu>, and BACs in regions of segmental duplication or large-scale variation are flagged.

Fluorescence *in situ* hybridization

In order to determine the presence of a 17p11.2 deletion (which would indicate Smith-Magenis syndrome), metaphase chromosomes were prepared for each patient in whom clinical FISH had not been previously reported. *RAI1* FISH was performed as previously described [53]. A minimum of 10 metaphase spreads and 10 interphase nuclei were observed for each case evaluated.

Sequencing of *RAI1*

Overlapping *RAI1* primers covering the entire coding region (exons 3-6, NM_030665) and the intron-exon junctions were designed to PCR-amplify the patient DNA samples. Sequencing of *RAI1* was performed as previously described [34].

Bioinformatic and statistical analyses

Deleted or duplicated BACs were located on the UCSC Genome Browser (<http://www.genome.ucsc.edu/>), Human Mar. 2006 assembly, and genomic position determined for BACs that flanked the deletion or duplication (and were included in the aberration). Prevalence of features in SMS and SMS-like cohorts were analyzed by Fisher's exact test utilizing a web-based program located at <http://www.langsrud.com/fisher.htm>. P-values ≤ 0.05 were considered statistically significant.

Results

SMS vs. SMS-like phenotypes

We have assessed the phenotypes of 52 SMS-like cases and compared the overall features of this cohort to those compiled in a meta-analysis of all the known and reported SMS cases (Table 3) [18]. As evident in the SMS-like cohort, the most common phenotypic features are not different in prevalence between this group and the SMS cohort (Table 3). We propose that even though *RAI1* is the major contributor to SMS, other players in the “SMS pathway”, when duplicated or deleted, result in a similar phenotype. The SMS and SMS-like cohorts are very similar (Table 3). Sleep disturbance, developmental delay, self-injurious behavior, hyperactivity, oral/motor dysfunction, hypotonia, dental anomalies, chronic ear infections, digestive problems, obesity, and neurological abnormalities were not different in prevalence between the two groups and were present in the majority of subjects (Table 3). These commonalities led us to hypothesize that at least one other locus exists and contributes to the global SMS phenotype and/or disruption of a common pathway leads to this phenotype.

Whole genome array comparative genomic hybridization

Once this SMS-like cohort was collected and all testing was negative for classical SMS by molecular techniques (see Methods), DNAs were then evaluated by whole genome array comparative genomic hybridization using a 19,000 RPCI-11 BAC array. We identified 15 copy number variants (CNVs) not previously described in these subjects (Table 4, 5). These variants occur in 21% (11 out of 52) of our population. Within these 15 CNVs, 8 chromosomes are represented, and similar variants are found in multiple cases (Table 4, 5). These CNVs are of

Table 3. Phenotypic features observed in Smith-Magenis syndrome-like cohort.

Common feature	Cohort	
	SMS ¹ (del17p11.2 or <i>RAI1</i> mut)	SMS-like ² (negative for <i>RAI1</i> del or mut)
Developmental delay	100%	100%
Stereotypies	59%	84% *
Self-injury	90%	90%
Sleep disturbance	88%	97%
Self-hugging/tics	63%	55%
Hyperactivity	74%	77%
Seizures	28%	56% *
Hypotonia	71%	72%
Signs of peripheral neuropathy	86%	72%
Oral/motor dysfunction	85%	70%
Craniofacial abnormalities	89%	70% *
Eye abnormalities	87%	59% *
Ear abnormalities	63%	64%
Hearing loss	60%	39%
Ear infections	90%	69% *
Dental anomalies	54%	73%
Cleft lip/palate	15%	2% *
Hoarse voice	86%	50% *
Overweight	33%	53%
Hypercholesterolemia	41%	23%
Heart defect	31%	11% *
Digestive problems	95%	67% *
Short stature	67%	43% *
Brachydactyly	79%	47% *
Scoliosis	32%	34%

¹Values for SMS cohort taken from Edelman et al 2007 (n=105). ²Cases reported in this study (n=52). Statistics calculated with Fisher's Exact Test where *=p-value <0.05. Range of age at evaluation: 2-44 years for SMS-like cases and 4 months -72 years for SMS cases (Edelman et al 2007 [18]).

particular interest because of the potential to further define regions of variation that contribute to the SMS-like phenotype, given common genes that are either deleted or duplicated. Common and possibly polymorphic BACs were excluded by referencing a control group containing 372 individuals from the National Institute of Mental Health (NIMH) Genetics Initiative as control samples [61].

Pathogenic copy number variants

Of the 15 CNVs identified in this cohort, some have been previously described but none have been reported in cases with phenotypic overlap to SMS. Described below are the CNVs believed to be pathogenic and thus, contribute directly to the observed phenotype (Table 4).

- Monosomy 1p36.32-p36.33, identified in SMS203 (Figure. 7, Table 4), is associated with mental retardation, developmental delay, hearing impairment, seizures, growth delay, hypotonia, hyperphagia, brachydactyly, self-abusive behavior, obesity, and a Prader-Willi-associated phenotype [62, 63]. SMS203 is a 44 year old adult female referred for lifelong sleep difficulties and learning and behavioral problems who presented with short stature, obesity, prognathism, dental abnormalities, brachydactyly, scoliosis, eye abnormalities, chronic ear and respiratory infections, and self-injurious behavior. A strong overlap between phenotypes can be seen between both 1p36.33 syndrome and SMS; however, the clinical overlap between these well-described syndromes has not previously been appreciated.
- A single case of del(2)(q23.1) (Figure 7, Table 4) was identified in this cohort. This deletion was previously reported in association with severe psychomotor retardation, speech impairment, epilepsy, microcephaly, ataxia and behavioral disabilities, and described as a pseudo-Angelman

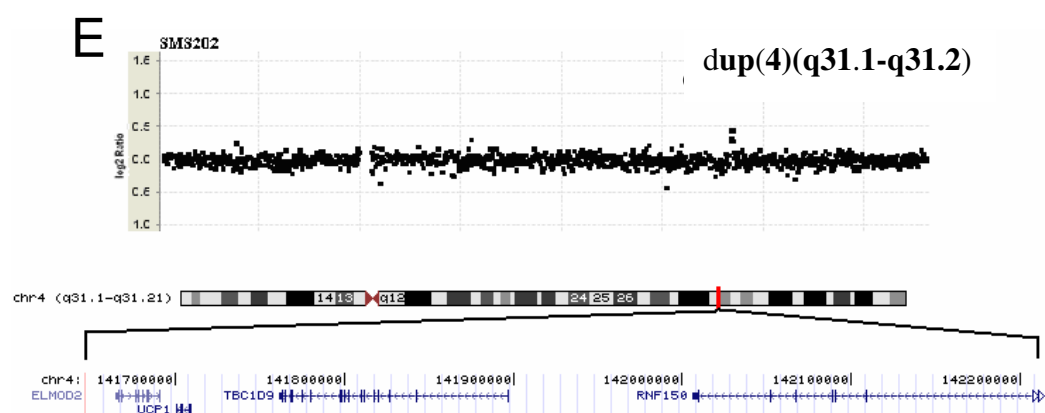
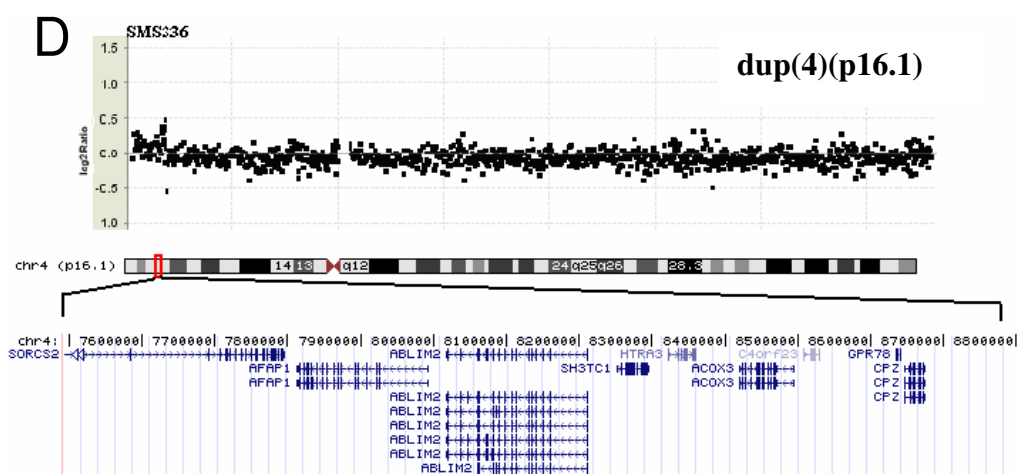
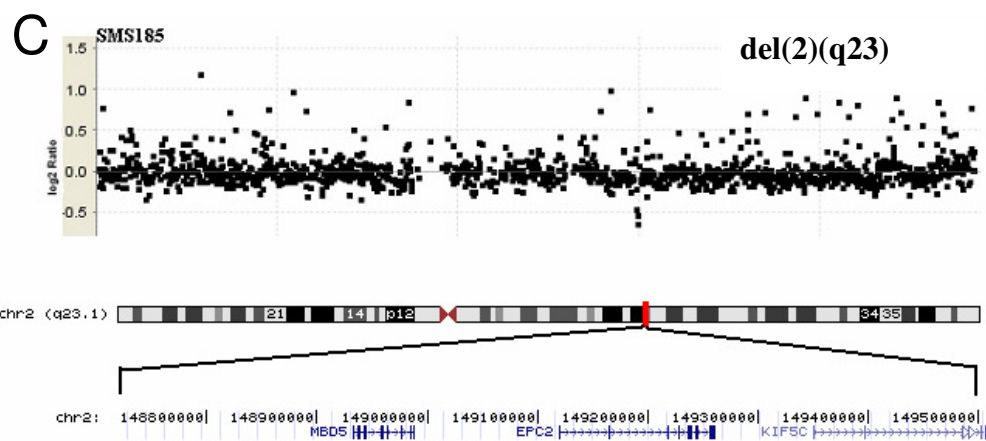


Figure 7. CGH array plots for pathogenic CNVs A) SMS203, del(1)(p36.32-36.33). B) SMS272 and SMS320, del(2)(q37.3) C) SMS185, del(2)(q23.1) D) SMS236, dup(4)(p16.1) and E) SMS202, dup(4)(q31.1-q31.2). Log2 ratio of subject to control shown on y-axis. CNVs were considered significant for duplication or deletion, when flanking BACs held values >0.3 or <-0.3 , respectively, with 3 consecutive BACs involved in a given abnormality. Plots were created using aCGH viewer (<http://falcon.roswellpark.org/aCGHview/>). Genomic data illustrating the extent of each deletion or duplication were modified from UCSC Genome Browser (<http://www.genome.ucsc.edu/>) and RefSeq genes are indicated. Figure not to scale.

Table 4. Pathogenic copy number variants identified in the SMS-like cohort.

Case #	Copy Number Variant (CNV)	Genomic Location (bp)	Size (Mb)
SMS203	del(1)(p36.32p36.33)*	Chr1:2,171,401-3,037,274	0.86
SMS185	del(2)(q23.1)*	Chr2:148,543,058-149,504,469	0.96
SMS272	del(2)(q37.3) ⁺	Chr2:239,764,593-240,938,545	1.17
SMS320	del(2)(q37.3)*	Chr2:237,920,956-240,938,547	3.02
SMS336	dup(4)(p16.1)*	Chr4:7,493,733-8,829,348	1.34
SMS202	dup(4)(q31.1q31.2)*	Chr4:141,648,098-142,218,495	0.57

Deletions contained flanking BACs below $-3.0 \log_2$ ratio. Duplications contained flanking BACs above $3.0 \log_2$ ratio. CNV location taken from UCSC genome browser, Mar. 2006 build, with flanking BACs as reference. CNV confirmation by: *clinical BAC array, ⁺G-Banding.

phenotype [64]. SMS185 is a female who presented at age 3.5 y with mental retardation, short stature, midface hypoplasia, microcephaly, brachydactyly, hoarse voice, heart abnormalities, and hyperactivity but did not exhibit sleep disturbance or self-injurious behavior. Previous methylation testing for Angelman syndrome was negative.

- SMS202 was shown to have a duplication of chromosome 4q31.1-q31.21 (Figure 7, Table 4), which has been associated with mild mental retardation and poor language acquisition [65], features commonly seen in SMS. SMS202 is a 6 year

old female with mental retardation, craniofacial abnormalities, 2-3 toe syndactyly, pes planus, elbow limitations, sleep disturbance, self-injurious behavior, hyperactivity, and stereotypical behaviors.

- SMS336 is a 3 year old male who carries a novel CNV, dup(4)(p16.1) (Figure 7, Table 4), not previously reported in the literature. This region contains 8 known genes and 1 predicted gene, including the VPS10 domain containing receptor 2 gene (*SORCS2*), which is highly expressed in the mouse central nervous system. SMS336 presented with a typical SMS phenotype, including developmental delays, cognitive impairment, short stature, craniofacial, dental, and eye abnormalities, scoliosis, hypotonia, difficulty communicating, hearing loss, chronic ear and respiratory infections, decreased sensitivity to pain, heart abnormalities, obesity, sleep disturbance, hyperactivity, and self-injurious behaviors. This individual also carries a del(14)(q11.2) [66] (Figure 9, Table 6), which is a reported polymorphic CNV.



Figure 8. del2q37 clinical phenotype. A) SMS185 with del(2)(q23.1), age 2 years; B) SMS272 with del(2)(q37.3), age 15 years; and C) SMS320 with del(2)(q37.3), age 3 years.

- A deletion involving 2q37.3 was identified in 2 cases (Figure 7, 8, Table 4):
 - o SMS272 is a 15 year old female with midface hypoplasia, brachycephaly, and brachydactyly (Figure 8b). Her neurobehavioral phenotype consists of stereotypies, and aggressive behavior. She is also obese but does not exhibit sleep disturbance or self-abusive behavior, both of which are typically seen in SMS. A known polymorphic CNV, del(16)(p11.2), was also identified in this case (Figure 7c, 9, Table 6).
 - o SMS320 is a 2 year old female with mental retardation, speech and motor delay, sleep disturbance, stereotypies, attention-seeking, and self-injurious behaviors (Figure 8c). Her craniofacial and skeletal phenotype consists of brachydactyly, brachycephaly, midface hypoplasia, tented upper lip, broad, square face, and synophrys.
- A maternally inherited duplication of 17p12 was identified in SMS348 (Figure 9, Table 6), a 10 year old male who presented with typical features of SMS. Charcot-Marie Tooth disease type 1A (CMT1A) is caused by dup(17)(p12) that includes the *PMP22* gene. The associated demyelination of the peripheral nervous system is well-described and does not involve developmental delays or sleep disturbance [67, 68]. This finding in SMS348 (Figure 9, Table 6), is not causative of the child's developmental phenotype, with the possible exception that in severe cases of CMT1A, peripheral neuropathy may be evident, even in a young child. However, del(17)(p12) was recently shown to confer a 10-fold increased risk for schizophrenia [69] indicating that gene dosage may predispose an individual to a mild increase in risk (Table 5). Dup(17)(p12) was also identified in an aCGH study involving 100 mentally retarded individuals [70].

Table 5. Disorders previously associated with the deletions and duplications identified in this study.

CNV	Associated phenotype
del(1)(p36.33)	Obesity, hyperphagia, dysmorphism, 1p36 deletion syndrome [62],[63]
del(2)(q23.1)	Pseudo-Angelman syndrome [64]
del(2)(q37)	Brachydactyly-mental retardation syndrome/AHO-like [71]
del(8)(p23.1)	Cornelia de Lange alternate locus [72]
dup(15)(q11.2)	Autism [73],[74]
dup(17)(p12)	Schizophrenia [70]/autism [75]/mental retardation [70]/Charcot-Marie-Tooth disease Type 1A [67],[68]

Non-pathogenic copy number variants

Several previously reported non-pathogenic CNVs were detected in this cohort as described in Table 6. Two of these CNVs were detected in more than one case but are within regions of known polymorphisms and thus, not likely to be pathogenic (Figure 9, Table 6). The 8p23.1 region of deletion contains a cluster of defensin genes and *SPAG11B*. While these host defense genes are not excellent candidates for the syndromes described, predicted genes within the deletion region and genes just outside the deleted region, possibly influenced by position effects, cannot be ignored. Additionally, SMS279 also carries a dup(16)(p11.2) which flanks the reported region associated with autism, neurodevelopmental delay, and dysmorphism [76].

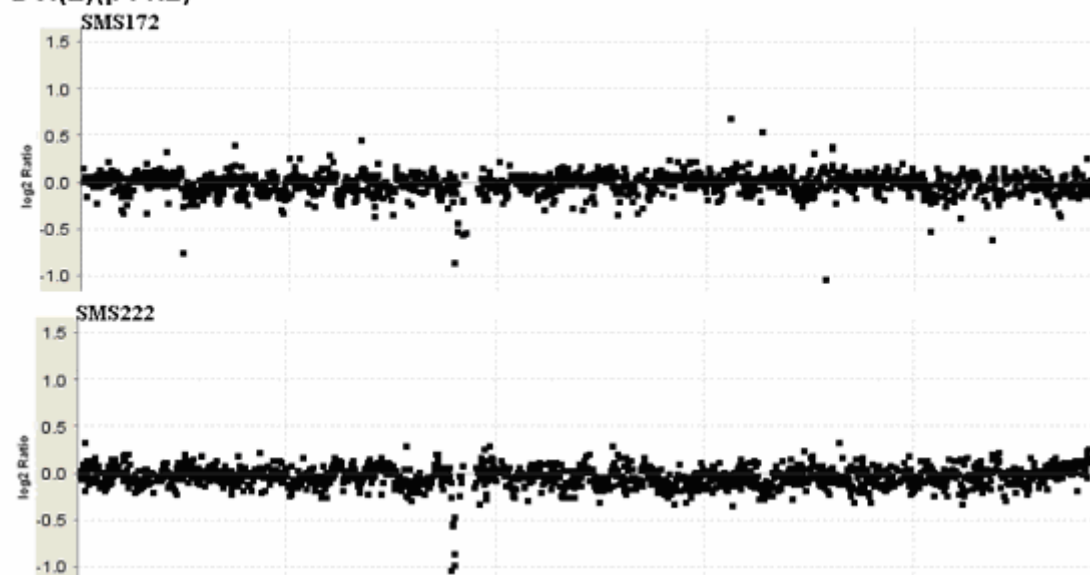
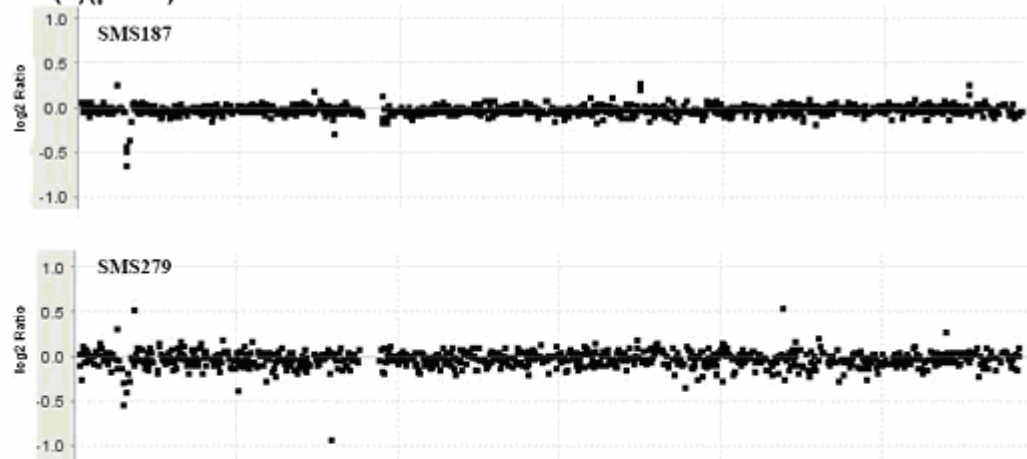
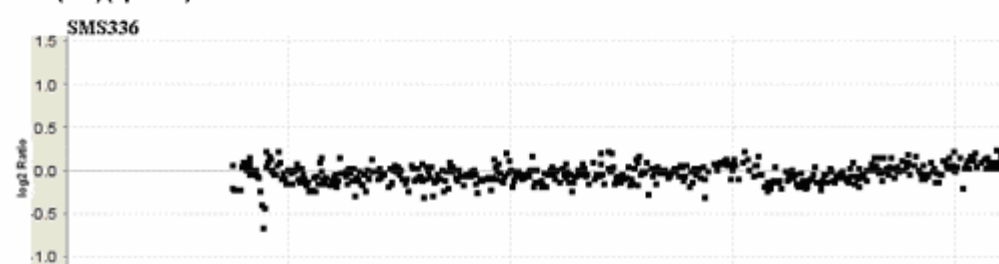
The 2p11.2 region, deleted in 2 cases in this cohort (Figure 9, Table 6), includes several genes that hold potential importance for antibody variation, including *IgA*, *IGVK-A2*, and *IGV3-15*. Position effects could also be altering gene expression in the regions just outside the common deletion, as possible candidates include *FABPI* which is associated with age-dependant obesity in female mice [77] and *FOXI3* which is important in craniofacial development in zebrafish [78].

SMS272, who carries a del(2)(q37), also carries a del(16)(p11.2) distal to the recently reported autism-susceptibility region (Figure 9, Table 6) [79, 80]. A dup(15)(q11.2) was found in SMS202, who also carries a dup(4)(q31.1-q31.2). This deletion region has been associated with autism and may contribute to combinatorial effects along with the dup(4)(q31.1-31.2) that is thought to be pathogenic.

Table 6. Non-pathogenic copy number variations identified in the SMS-like cohort.

Case #	Copy Number Variation	Genomic Location (bp)	Size (Mb)
SMS172	del(2)(p11.2)	Chr2:89,068,208-91,746,640	1.89
SMS222	del(2)(p11.2)	Chr2:89,068,208-90,016,961	0.95
SMS272	del(16)(p11.2)	Chr16:32,456,421-33,593,137	1.14
SMS336	del(14)(q11.2)	Chr14:21,636,643-22,120,718	0.50
SMS202	dup(15)(q11.2)	Chr15:18,617,196-18,882,916	0.27
SMS187	del(8)(p23.1)	Chr8:7,156,827-7,936,168	0.78
SMS279	del(8)(p23.1) dup(16)(p11.2)	Chr8:7,156,827-7,936,168 Chr16:31,855,107-33,295,070	0.78 1.44
SMS348	dup(17)(p12) [#]	Chr17:14,080,569-15,223,450	1.14

Deletions contained flanking BACs below -3.0 log₂ ratio. Duplications contained flanking BACs above 3.0 log₂ ratio. CNV locations taken from UCSC genome browser, Mar. 2006 build, with flanking BACs as reference. [#]Mother also affected with CMT1a.

Del(2)(p11.2)**Del(8)(p23.1)****Del(14)(q11.2)**

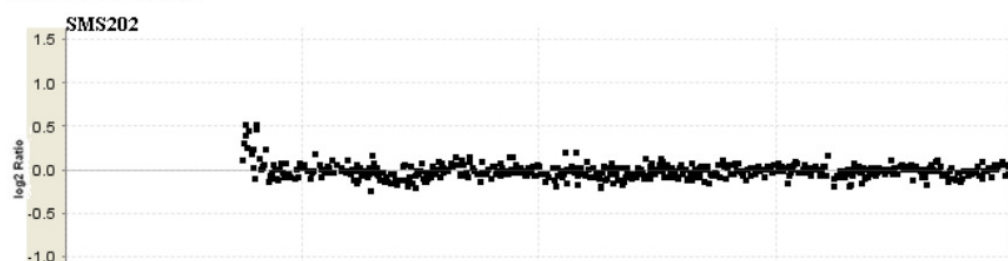
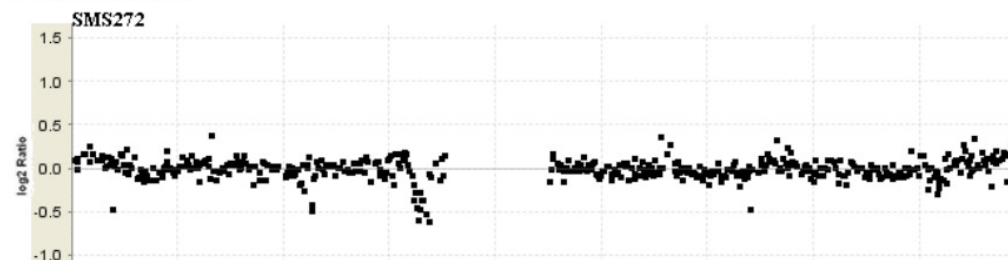
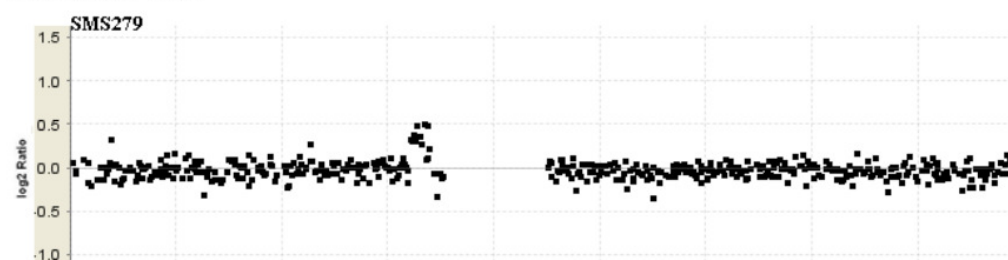
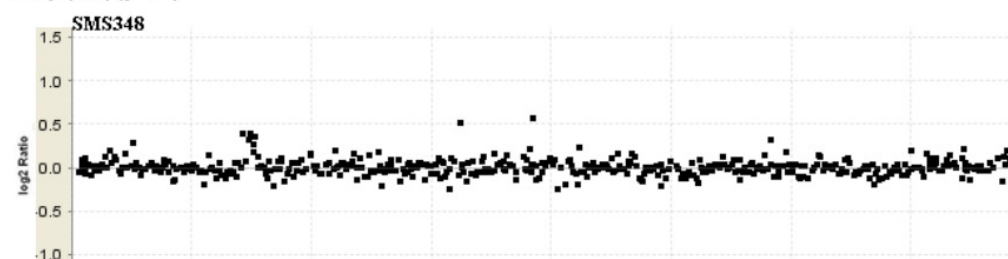
Dup(15)(q11.2)**Del(16)(p11.2)****Dup(16)(p11.2)****Dup(17)(p12)**

Figure 9. Non-Pathogenic copy number variants. Array plots for each subject are shown. Log2 Ratio of subject to control shown on y-axis. Plots were created using aCGH viewer <http://falcon.roswellpark.org/aCGHview/>). Genomic data illustrating the extent of each case deletion or duplication were modified from UCSC Genome Browser (<http://www.genome.ucsc.edu/>). Figure not to scale.

Discussion

In this study, we utilized whole genome aCGH to assess a cohort of 52 clinically well characterized patients referred to our laboratory for molecular evaluation of Smith-Magenis syndrome. We identified duplications or deletions (15 CNVs in 11 subjects) not previously described in these cases, with CNVs in 6 cases that are likely pathogenic and associated with the SMS-like phenotype present in the patient (Tables 4, 6). Some of the same genomic abnormalities can be found in multiple cases, supporting a common etiology for the similar phenotypes. These chromosomal regions include genes that are responsible for fatty acid metabolism, neurological development, cell signaling, circadian rhythm, transport, development, mental health, neuromuscular function, morphology, and cell cycle control. Because of the phenotypic overlap between the SMS and SMS-like cases, a possible indirect role of *RAI1* in the etiology of these phenotypically similar disorders should be explored [81]. Data from this study may give us some insight into the pathways in which *RAI1* functions. *RAI1* is a putative transcription factor that spans ~130 Kb on 17p11.2 and contains 6 exons, 4 of which are coding. Bioinformatic analysis of *RAI1* has identified a bipartite nuclear localization signal and a PHD domain, both of which are consistent with the proposition that *RAI1* functions as a transcription factor. Although the cases were ascertained based on stringent SMS-phenotypic criteria, 52 cases from our cohort neither carried a 17p11.2 lesion nor any pathogenic CNVs. It is possible that these cases carry alterations in the yet-uncharacterized regulatory region of *RAI1* or a point mutation in another critical gene.

We have also identified multiple variants that are associated with reported syndromes (Table 5). This fact speaks to two points: one, there are likely common pathways that lead to the phenotypic overlap between SMS and these known syndromes and two, better delineation of the

phenotypes and training for diagnosis of these syndromes is needed. In addition, there were CNVs that were missed by clinical arrays that did not cover these regions, which supports the fact that diagnostic arrays need better coverage over regions that are associated with known syndromes.

One region of variation, del(2)(q37.3), was found in more than one subject in this cohort (Figure 9, Table 4). Deletion 2q37 syndrome, also known as brachydactyly-mental retardation syndrome or Albright's hereditary osteodystrophy-like syndrome, is well-described and characterized by craniofacial abnormalities, mental retardation, stereotypies, aggressive/self-injurious behavior, distinct brachydactyly, short stature, obesity, eczema, and sparse hair [82, 83]. Although the typical craniofacial and skeletal abnormalities previously reported in association with deletion 2q37 syndrome do not overlap with SMS [16], the neurological, behavioral, and growth abnormalities are similar [18, 24, 34]. Further, SMS272 and SMS320 exhibit the characteristic brachydactyly type E seen in del(2)(q37) syndrome, which is different than the brachydactyly commonly seen in SMS [71, 84]. Both of these subjects also exhibit similar craniofacial abnormalities as those in SMS, as well as many of the other features. These data emphasize not only the phenotypic overlap between these two syndromes but also expand the phenotype of the well-described 2q37 deletion syndrome. These phenotypic and molecular overlaps may lead us to candidate genes and pathways that contribute to these complex features.

Several excellent candidate genes have been identified and warrant further study. Potential candidate genes localized to the overlapping deleted region in 2q37.3 include *HES6*, which has been implicated in mRNA transcription regulation and neurogenesis [85], as well as *SCLY* which is implicated in fatty acid metabolism and *HDAC4* which is involved in chondrogenesis. Given the significant overlapping behavioral and physical phenotype, we

propose that one or more genes present in del(2)(q37) syndrome fall in the same pathway(s) as those leading to SMS.

The 1p36.32-p36.33 region deleted in SMS203 contains more than 10 genes. Deleted in this region is *HES5*, a gene important in neuronal development that when reduced in expression leads to premature depletion of neuronal stem cells [86], which could also lead to some of the neurological phenotypes seen in this patient.

On chromosome 2q23.1, the *MBD5* gene was found to be deleted in a single case using SNP array-based technology to assess subjects with mental retardation [1]. *MBD5* is a methyl-CpG binding domain protein. Interestingly this was the only gene deleted in this patient who presented with mental retardation, seizures, retarded motor development, and limited social interactions, similar to the phenotype of SMS185 in this study.

Duplicated in the chromosome 4p16.1 region (in case SMS336), *SORCS2* is expressed throughout the murine central nervous system, including the olfactory bulb, piriform cortex, amygdala, hippocampus, median geniculate nucleus, interpeduncular nucleus, and some cerebellar Purkinje cells [87]. This gene is thought to be involved with intracellular sorting, and altered dosage may contribute to some of the neurological findings such as hypotonia, decreased sensitivity to pain, sleep disturbance, self-abusive behavior, hyperactivity, and attention deficit disorder.

UPCI is duplicated in SMS202, who carries a dup(4)(q31.1-q31.3). Deletion of this gene has been shown to cause obesity in mice, whereas duplication of *UPCI* is thought to have a protective effect [88]. SMS202 is not overweight; however, because of the *UPCI* pattern of expression in the central nervous system [89], a potential dosage effect should be considered regarding neurological abnormalities.

Candidate gene sequencing in the subjects wherein no CNV was found is a logical next step toward identifying causative genes for the syndromes mapped to the genomic regions discussed above. Further, the documented interaction of RAI1 with candidate genes will aid in the delineation of molecular pathways causative of the phenotypes described. In conclusion, this study is unique in that we have taken a group of patients clinically diagnosed with a very specific phenotype, Smith-Magenis syndrome, and identified potentially alternate causative loci. These findings will help to improve the diagnosis of individuals with phenotypic overlap to SMS, including those with known syndromes that previously were not known to overlap phenotypically, such as del(2)(q37) and del(1)(p36) syndromes. The results presented will help to further improve diagnosis (both molecular and phenotypic) and potentially treatment of microdeletion/microduplication syndromes and will provide insight into the molecular pathways involved in these phenotypically complex disorders.

We propose that, together, Smith-Magenis syndrome and the cases described above, who do not have SMS, encompass a group of disorders that are molecularly related and that patients with developmental delays, self-injurious behaviors, sleep disturbance, stereotypies, and sudden violent outbursts who would otherwise be clinically appropriate for a diagnosis of Smith-Magenis syndrome be considered for whole genome (not targeted) aCGH in order to identify the molecular etiology of the patient's phenotype.

Chapter 3

Haploinsufficiency of *MBD5* associated with a syndrome involving microcephaly, intellectual disabilities, severe speech impairment, and seizures

Introduction

Owing to the phenotypic complexity of many genomic disorders and the fact that most of these disorders result in developmental delays and behavioral problems, overlapping physical and behavioral features between syndromes are commonly observed [90]. Although there are clear phenotypic differences between most syndromes, Smith–Magenis, Down, and Prader–Willi syndromes have many major features in common, including craniofacial features, obesity, and hypotonia, whereas Angelman and Rett syndromes feature seizures and severe developmental delays. Correct identification and diagnosis of specific syndromes are more difficult because of these phenotypic similarities. Ultimately, when comparative genomic hybridization (CGH) data are considered and new syndromic regions of the genome are identified, sorting these cases by phenotype alone may be even more difficult. Microdeletion of chromosome 2q23.1 results in a novel syndrome previously reported in five individuals [64, 70, 91, 92]. In this study, we report two new cases with overlapping 2q23.1 deletions and draw attention to possible candidate genes that could be causative for the characteristic phenotype observed in our cases and in the other five patients reported in literature. A comparison of phenotypes to the other five known cases revealed similar features and confirmed a consistent phenotypic pattern associated with 2q23.1 microdeletion. Although this new microdeletion syndrome has certain phenotypic similarities to various known disorders such as Angelman, Smith–Magenis, and Rett syndromes, it is not a classic phenocopy for any of these conditions. On the basis of our evaluation of the spectrum of

clinical features in our cases and in previously reported ones, we have further delineated the clinical characterization of this new microdeletion syndrome. On the basis of the similar features observed, we established a clinical characterization of the novel microdeletion syndrome. Furthermore, an analysis of all reported cases involving a deletion of 2q23.1 revealed a minimal critical region consisting of a single gene, *MBD5*, as the only deleted gene in one case, and *MBD5* and *EPC2* deleted in all other cases. In this study, we report two new cases of the 2q23.1 deletion syndrome, describe the syndrome phenotype, define the minimal critical region, and analyze the expression of critical region genes toward identification of the causative gene(s) for the disorder.

Materials and Methods

Patient ascertainment

Subjects were referred for molecular evaluation of the Smith–Magenis syndrome (SMS185) and the Prader–Willi syndrome (SMS361). The Institutional Review Boards at Virginia Commonwealth University and Michigan State University approved this study.

Cell lines

Lymphoblastoid cell lines (Epstein–Barr virus-transformed human lymphocytes) from SMS185, her mother (SMS184), her father (SMS183), and from an unaffected control were cultured in RPMI-1640 with 2 mM L-glutamine and 25 mM HEPES (4-(2-hydroxyethyl)-1-piperazineethane-sulfonic acid) (Invitrogen, Carlsbad, CA USA), 10% fetal bovine serum, and 1% penicillin/streptomycin antibiotic-antimycotic solution (Invitrogen) at 37°C in a humidified 5% CO₂ chamber. Cells were grown at the same time period for a span of 3 weeks and

supplemented with fresh media every 2–3 days as needed. Cells were monitored for growth using bright field microscopy and were counted using Trypan blue exclusion with a hemocytometer. After a 3-week growth period, the cells were counted, pelleted, and used immediately for RNA extraction or stored at -80°C for RNA extraction at a later date.

RNA extraction

RNA was extracted from either $5\text{--}10 \times 10^6$ lymphoblast cells using the standard TRIzol protocol (Invitrogen) or from 4 ml whole blood, as described here. The whole blood was mixed with 46 ml Puregene RBC lysis solution, mixed, and let to stand at room temperature for 15 min. White blood cells were pelleted at 600g for 10min at 41°C . The pellet was resuspended in 1 ml RBC lysis solution and incubated at room temperature for 5min. Cells were pelleted at 3000 RPM at 41°C for 2min resuspended in 1 ml cold PBS, and further pelleted at 3000 RPM at 41°C for 2 min. RNA was then isolated using the standard TRIzol protocol (Invitrogen). The concentration and purity of RNA were measured at an absorbance of 260 and 280 nm. RNA was stored at -80°C until ready for use.

Real-time qRT-PCR

First-strand cDNA synthesis using SuperScript II RT (Invitrogen) was prepared with 3 mg of total RNA using Oligo(dT)12-18, and optional RNase OUT treatment, followed by RNA degradation with 2.5 units RNase H (Applied Biosystems Inc., Foster City, CA, USA). For quantitative real-time PCR, predesigned assays on Demand Gene Expression Products (Fermentus, Glen Burnie, MD USA) Taqman MGB probes for MBD5, EPC2, KIF5C, and GAPDH were used (Applied Biosystems Inc.). GAPDH was used as the endogenous control. All

samples of cDNA were run in triplicate in 10 ml reaction volumes. Taqman Universal PCR Master Mix (Applied Biosystems Inc.), the probe, and deionized water were mixed together in a fixed ratio, and 8 ml was added to each well. Diluted cDNA (1:5) was then added to each well. PCR conditions were the Standard 7500 Run mode of the ABI Prism 7900 HT Sequence Detection System (Applied Biosystems Inc.). The cycle threshold (CT) was determined during the geometric phase of the PCR amplification plots, as recommended by the manufacturer. Relative differences in transcript levels were quantified using the DDCT method. Acquired data were analyzed using 7500 Fast System SDS Software (Applied Biosystems Inc.).

RAII sequencing

RAII sequencing was performed as previously described [34] for SMS185. A novel familial polymorphism was found, but no pathogenic mutations were identified in this case. Peripheral blood was collected, from which DNA was prepared immediately or from cell lines established previously. DNA was extracted following standard phenol chloroform methods.

Whole-genome array comparative genomic hybridization (aCGH)

BAC aCGH was performed as previously described [40, 93].

Oligonucleotide array CGH

Oligonucleotide-based microarray analysis was performed for SMS361 using a 105K-feature whole-genome microarray (SignatureChip Oligo Solution made for Signature Genomic Laboratories by Agilent Technologies, Santa Clara, CA, USA) as previously described [94].

Oligonucleotide-based microarray analyses were performed using a 244K feature whole-genome

microarray made for Signature Genomic Laboratories by Agilent Technologies to characterize the extent of the abnormalities in SMS185 and SMS361. Genomic DNA labeling was performed as described for BAC arrays, whereas array hybridization and washing were performed as specified by the manufacturer (Agilent Technologies). Arrays were scanned using an Axon 4000B scanner (Molecular Devices, Sunnyvale, CA, USA) and analyzed using Agilent Feature Extraction software v9.5.1 and Agilent CGH Analytics software v3.5.14. Results were then displayed using custom oligonucleotide array CGH analysis software (Oligoglyphix, Signature Genomic Laboratories, Spokane, WA, USA).

Fluorescence *in situ* hybridization (FISH) analysis

Metaphase FISH was performed using bacterial artificial chromosome (BAC) clone RP11-951G8 from the 2q deleted region as previously described [95]. FISH data are shown in Figure 12.

RESULTS

Case reports

Case 1 (SMS185)

SMS185 is a 13-year-old Caucasian girl first seen for a clinical genetic evaluation when she was 4 years old because of concerns regarding developmental delays, short stature, and microcephaly (Figure 10, Table 7). She was the first child of phenotypically normal and nonconsanguineous parents (mother 25 years and father 19 years). No remarkable detail of pregnancy was mentioned. Birth weight was 3.0 kg and length was 48.26 cm (both between the 25th and 50th percentile) with no perinatal problems. As an infant, she had significant feeding

difficulties due to hypotonia. An atrial septal defect was identified at 1 year of age, with spontaneous closure by 3 years of age. By 16 months of age, microcephaly, global developmental delays, and short stature were evident.

A pediatric developmental evaluation was pursued by 3 years for sleep difficulties and hyperactivity. The initial physical examination at age 4, 5 and 12 years revealed a weight of 16.1 kg (50th percentile), a height of 92.25 cm (just below the third percentile), and a head circumference of 46 cm (~three SD below the mean). She was quite active, with a hoarse voice and no understandable words. Craniofacial examination revealed midface hypoplasia, an upturned nose, apparently widely spaced eyes, and a tented upper lip (Figure 10, Table 7). Skeletal examination revealed short, thick, and tapered fingers, which measured 9.5, 5.5, and 4 cm for total hand, palm, and middle finger lengths, respectively (all below the third percentiles). X-rays of the hands revealed shortened and widened metacarpals and phalanges in a symmetric manner, with no evidence of focally shortened bones.

Follow-up exam at 9, 3, and 12 years revealed a history of the onset of complex-partial seizures at 8 years associated with an abnormal EEG with “mild, diffuse encephalopathy” changes noted, but no areas of focal changes or seizure activity. Her brain MRI scan was normal, and after beginning trileptal, there was no recurrence of seizure activity. A further evaluation at 10, 9, and 12 years noted behavioral difficulties related to significant hyperactivity, minimal expressive speech, a weight of 33.1 kg (30th percentile), a height of 123.2 cm (approximately three SD below the mean), and a head circumference of 50 cm (just below the third percentile). Her physical features were unchanged from the initial examination.

Results of karyotype and FISH analyses to detect a Smith–Magenis syndrome deletion were normal at 4 years of age. Sequencing of the *RAI1* gene did not reveal any pathogenic



Figure 10. Clinical features of the 2q23.1 deletion syndrome. A) Case 1, SMS185 aged 2 years. Note tented upper lip, open mouth, and microcephaly. B) SMS185, 13 years of age, note tented upper lip and prominent incisors. C) Hands of SMS185, 13 years of age; note brachydactyly. D) Case 2, SMS361 aged 8 years. Note tented upper lip with prominent upper incisors and open mouth. E) Hand of SMS361. Note generalized brachydactyly. F) Foot of SMS361, note small foot and short toes with bulbous tips.

Table 7. Clinical features of cases with 2q23.1 microdeletion syndrome. In part created by Sureni Mullegama.

	SMS185 Case 1, This Study	SMS361 Case 2, This Study	Patient 29195 Wagenstaller et al 2007	Patient 1 Jaillard et al 2008	Patient 2 Jaillard et al 2008	Patient 3 Visser et al 2003 Koolen et al 2004	Patient 2 De Vries et al 2005
PHENOTYPE							
SEX	F	F	M	M	M	F	F
AGES OF EVALUATION	4 & 13 years	3 & 9 years	1.5 years	2 & 10 years	3 & 10 years	2, 12 & 14 years	N/A
MENTAL RETARDATION	+	+	+	+	+	+	+
MOTOR DELAY	+	+	+	+	+	+	+
LANGUAGE IMPAIRMENT	Severe	50 words	+	Less than 6 words	Severe	Severe	N/A
BEHAVIORAL PROBLEMS	+ Hyperactivity	+ Social contact seeking behavior Hyperactivity Impulsiveness	+ Limited social interactions	+ Inappropriate laughter	+ Inappropriate laughter Autistic component Self-biting of hands/forearm Decreased sensitivity to pain Stereotypies	N/A	+ Picking of the eyes Hypernea Full hands into mouth
SHORT ATTENTION SPAN	+	+	N/A	+	N/A	N/A	N/A

SLEEPING DIFFICULTIES	+	-	N/A	-	+	N/A	N/A
POST-NATAL GROWTH RETARDATION	+	-	N/A	+	+	+	+
SHORT STATURE	+	+	N/A	-	-	+	+
SEIZURES	+	+	+	+	+	+	+
ATAXIA	-	+	N/A	+	+	N/A	N/A
FEEDING DIFFICULTIES	+	+	N/A	+	+	N/A	N/A
INFANTILE HYPOTONIA	+	+	N/A	+	+	N/A	N/A
CONSTIPATION	+	+	N/A	+	+	N/A	N/A
	+	+		+	+	+	+
<u>CRANIOFACIAL MANIFESTATIONS</u>							
▪ MICROCEPHALY	+	15%	N/A	+	+	+	+
▪ BRACHYCEPHALY	-	-	N/A	-	+	-	-
▪ MIDFACE HYPOPLASIA	+	+	N/A	-	+	-	-
▪ HYPERTELORISM	+/- Apparently widely-spaced eyes	-	N/A	+	-	N/A	N/A
▪ FLAT NOSE	-	-	+	+	-	Small nose	N/A

▪ WIDE MOUTH	+	+	+	+	+	N/A	+
▪ TENTED UPPER LIP	+	+	N/A	+	+	N/A	N/A
▪ OPEN MOUTH	+	+	+	+	+	N/A	N/A
▪ SMALL CHIN	-	+	N/A	+	+	-	-
▪ DENTAL ANOMALIES	+	+	N/A	-	+	+	N/A
▪ MACROGLOSSIA	-	-	N/A	-	+	-	-
<u>EYE FINDINGS</u>		Optic nerve hypoplasia Mild myopia 30% right intermittent esotropia		Hypermetropia Astigmatism			
<u>HAND/FOOT ABNORMALTIES</u>	+	+	+	+	+	+	+
▪ 5TH FINGER CLINODACTYLY	-	+	N/A	-	+	+	+
• BRACHYDACTYLY	- Small hands and feet	- Small hands and feet	N/A	-	+	N/A	N/A
<u>OTHER</u>		Lumbar lordosis Toes bulbous at tips Bitemporal narrowing Relative obesity	Hypoactive Sandal gap	Micropenis Scoliosis Valgus feet Recurrent ear infections	Calm baby Hypogenitalism Pseudoarthrosis of the clavicle	Sandal gap Large ears	

mutations (data not shown). DNA methylation for the Angelman syndrome was normal at 9 years.

Case 2 (SMS361)

SMS361 is a 10-year-old Hispanic girl who was first seen at 26 months of age for developmental delay (Table 7). She was born to an 18-year-old gravida 1 mother. She was thought to have Down syndrome at birth, but chromosome testing was negative by report. Her family history was unremarkable.

She had a generalized tonic-clonic seizure at 8 months of age, but her EEG and CT scans were normal. She was treated with valproic acid and has had only 1–2 seizures/year. At 4 years of age, a repeat EEG showed spike and wave epileptiform discharges from the frontal lobes. This pattern has been observed on and off during successive EEGs, with the latest EEG at 7 years of age demonstrating a left-sided spike and wave pattern from the left frontal lobe. Several brain MRIs were normal. She walked after 2 years of age. Her speech was delayed, but she did learn new words. At the age of 2 years and 11 months, she knew about a total of 50 words in English and Spanish. She did not start putting two words together until after 9 years of age. Her speech was unclear, although she continues to add words to her vocabulary. She can follow simple commands, but her attention span is limited.

A physical examination at 9 years of age showed truncal obesity, with a height of 122 cm (5th percentile), weight of 41.0 kg (90th percentile), and an occipitofrontal circumference of 50.5 cm (15th percentile). She was hyperactive, impulsive, and had a short attention span, moving from object to object in the examination room

(Table 7). She had social contact-seeking behavior, maintained good eye contact, and had a happy demeanor. She had an unusual facial appearance with a tented upper lip and bitemporal narrowing. She had light-colored irides. Her hands were small (total hand length of 13 cm, less than third percentile) and showed clinodactyly of the fifth digits (although her hand X-ray showed no shortened fourth metacarpal). Her total foot length was 17.5 cm (less than third percentile) and the toes were bulbous at the tips (Figure 10). Ophthalmologic examination revealed mild optic nerve hypoplasia, mild myopia, and a 30% right intermittent esotropia. Her caregiver reports a healthy appetite but no food seeking was described.

Molecular analyses

aCGH

Array comparative genomic hybridization: SMS185 was evaluated by whole-genome array comparative hybridization (aCGH BAC array) [96], revealing a ~700kb deletion of 2q23.1 and confirmed by a clinical BAC array (data not shown). To further refine the break points of this deletion, a high-resolution oligo array (Agilent 244K) was performed, defining the deletion region to be ~930 kb at chr2:148,447,496–149,377,297 (NCBI36/hg18 coordinates, Figure 11), encompassing four known genes, *ORC4L*, *MBD5*, *EPC2*, and *KIF5C*. SMS361 was evaluated by both 105K and 244K oligo arrays (Figure 11), as described in the methods section.

Array data revealed a 3.51-Mb deletion of chromosome 2q22.3–q23.3 (chr2:146,798,229–150,310,317, NCBI36/hg18 coordinates) encompassing nine known or predicted genes, *PABPCP2*, *ACVR2A*, *ORC4L*, *MBD5*, *EPC2*, *KIF5C*, *LYPD6B*, *LYPD6*, and *MMADHC*.

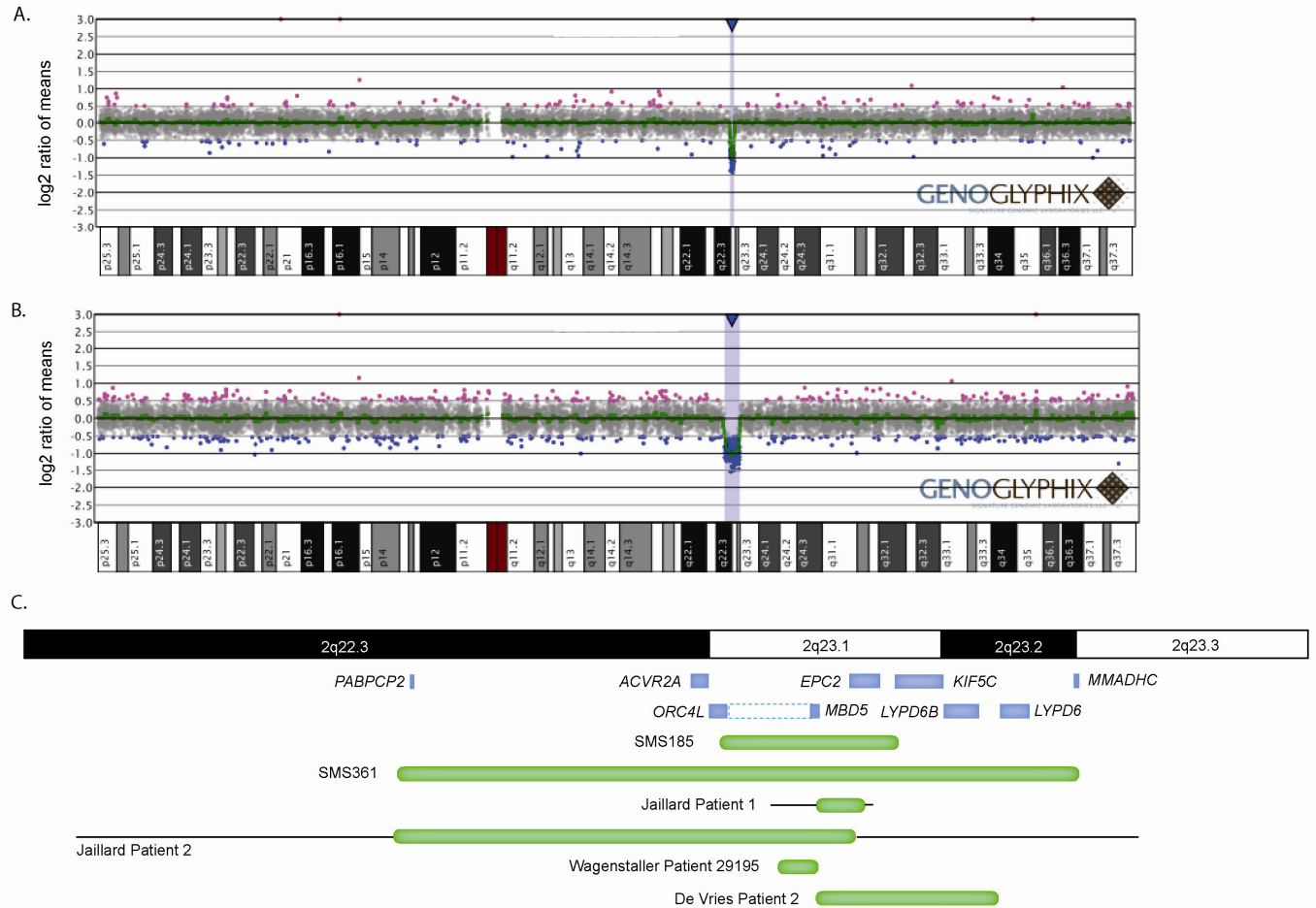


Figure 11. Array analysis of individuals with microdeletions of 2q23.1. A, B) Oligonucleotide microarray profiles for (a) a single-copy loss of 930 kb at chr(2)(q23.1); (chr2: 148,447,496–149,377,297) in SMS185 and (b) a single-copy loss of 3.51 Mb at chr(2)(q22.3-q23.3) (chr2: 146,798,229–150,310,317) in SMS361. For microarray plots, probes are ordered on the x axis according to physical mapping positions, with distal 2p to the left and distal 2q to the right. C) Summary of the deletion sizes in individuals with microdeletions encompassing 2q23.1. Green bars indicate the minimum deletion sizes in individuals in this study and those in the literature, and black lines extend to show maximum deletion sizes. Genes in the region are indicated by blue boxes. Coding exons for *MBD5* are included in the solid blue box, whereas 5' noncoding exons described by Wagenstaller et al [1] are within the dashed blue box. Modified from Williams et al. 2009 [2]. Arrays performed by Signature Genomics.

Metaphase FISH with RP11–951G8 confirmed a deletion in five out of five cells examined for both SMS185 and SMS361 (Figure 12). Array data indicate a common, overlapping region between these two cases that includes *ORC4L*, *MBD5*, *EPC2*, and *KIF5C* (Figure 11).

Quantitative real-time PCR

Loss of genes or gene function due to chromosomal deletion does not necessarily correlate to a reduction in gene expression; however, haploinsufficiency of one or more genes is typically the pathological defect in microdeletion syndromes. To determine the genes that have a reduced expression in the overlapping 2q23.1 region, both subjects were assessed for *MBD5*, *EPC2*, and *KIF5C* mRNA levels in white blood cells. Correlating directly to the confirmed deletions, both SMS185 and SMS361 have an ~50% reduced expression of *MBD5* and *EPC2* mRNA compared with normal controls (Figure 13).

Normal levels of expression were observed for *KIF5C*; however, *KIF5C* has a very low expression in peripheral blood, and thus, levels may not be reflective of the expression in the brain (data not shown). *KIF5C* expression may be affected in both the larger and smaller deletion cases, as the smaller deletion includes the 5' region of the *KIF5C* gene, which may alter gene expression. The reduction in expression of *MBD5* and *EPC2* supports the potential role of each of these genes in the pathophysiology of this disorder.

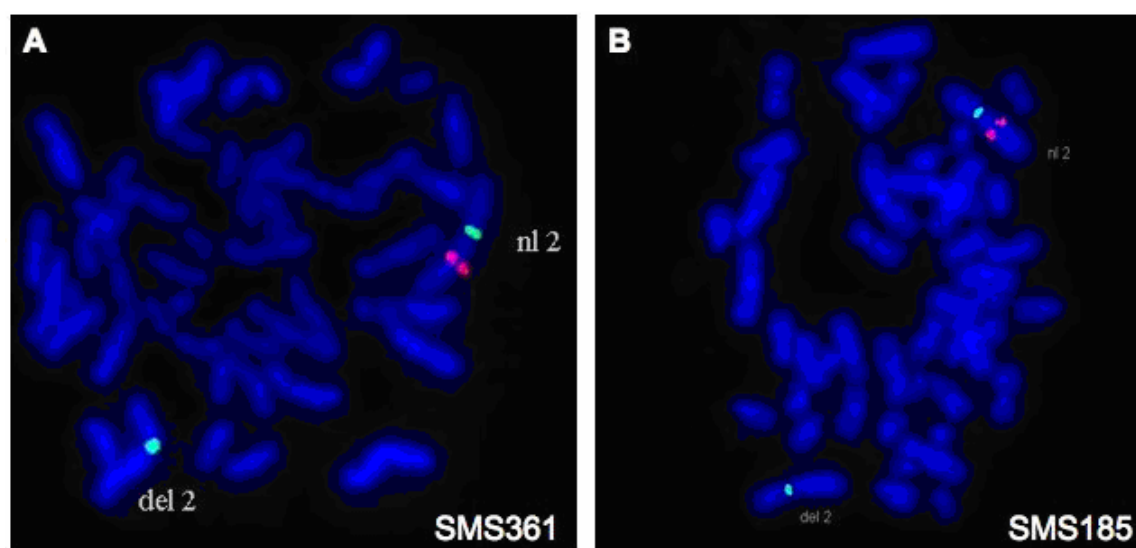


Figure 12. FISH confirmation of 2q23 deletions in patients SMS361 (A) and SMS185 (B). for both images, BAC clone RP11-951G8 from 2q23.1 is labeled in red and a chromosome 2 centromere probe is labeled in green as a control. The red signal is missing, while the green signal is retained on one chromosome 2 homologue, indicating a deletion. Performed by Signature Genomics.

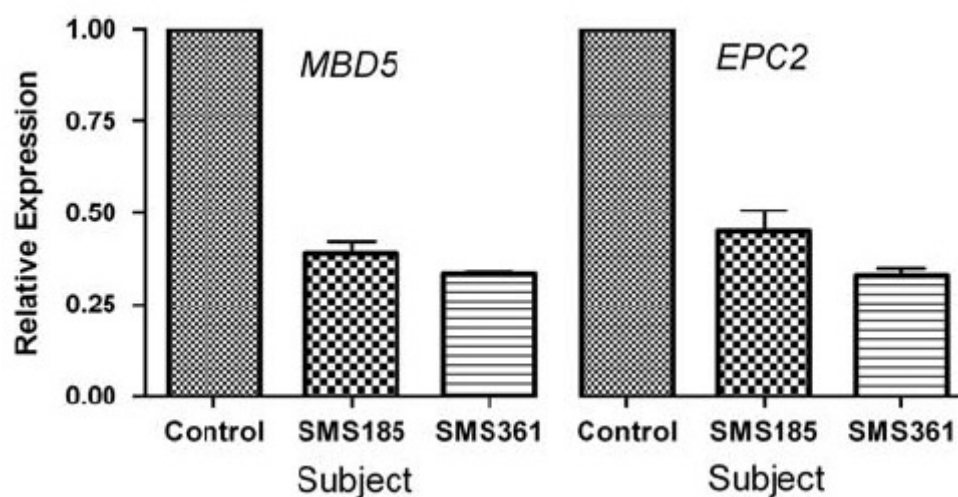


Figure 13. Quantitative real-time PCR expression analysis of *MBD5* and *EPC2* in patient cells. *MBD5* and *EPC2* relative gene expressions in SMS185 (EBV-derived lymphoblastoid cell line) and SMS361 (fresh white blood cells) are shown. Gene expression is shown relative to *GAPDH* expression and control cells, with relative expression values based on the $\Delta\Delta C_t$ value with normal control set to 1. Control cells were cultured or isolated at the same time and with the same methods as test cells. All experiments were performed in triplicate and average values for all combined experiments are shown (n=2–5). Data generated, in part, by Sureni Mullegama.

DISCUSSION

In this study, we present two subjects, SMS185 and SMS361, with a del(2)(q23.1). These individuals have a distinct clinical phenotype that includes severe cognitive impairment, seizures, relative obesity, small hands and feet, and mild craniofacial dysmorphism, including one child with microcephaly.

A recent report described two patients with overlapping deletions of this region on chromosome 2 exhibiting a ‘pseudo-Angelman’ phenotype [64]. Both the subjects in this study tested negative for an abnormal *SNRPN* DNA methylation patterning of the 15q11.2 region, which rules out a diagnosis of Angelman syndrome. However, they do have features consistent with the ‘pseudo-Angelman’ phenotype described by Jaillard et al (2008) [64]. In addition to the report by Jaillard et al (2008) [64], three other cases of 2q23.1 deletion have been previously described [70, 91, 92] (Figure 11). The common phenotypes observed in these subjects are severe mental retardation, motor delay, severe language impairment (sometimes accompanied by hoarse voice), behavioral abnormalities (including hyperactivity and inappropriate laughter), postnatal growth retardation, relative obesity, and seizures (Table 7). In addition, a distinctive craniofacial phenotype is also apparent that includes small head size, wide and open mouth, a tented upper lip, and prominent incisors (Figure 10). Skeletal abnormalities include generalized brachydactyly (Figure 10, Table 7).

The more variable phenotypes between the cases reported here and those in previous studies include craniofacial abnormalities such as brachycephaly and relative hypertelorism (likely associated with microcephaly), as well as eye findings and genital abnormalities. Overall, these individuals with varying overlapping deletions of 2q23.1 present with a very similar global phenotype, which leads us to believe that a common gene(s) might be involved.

Additionally, after completion of this study a study by van Bon et al. 2010 [97] confirmed the findings reported in the present study. All subjects fell within the global phenotype described and it was concluded that haploinsufficiency of *MBD5* was responsible for the clinical manifestations observed. It was also mentioned that *EPC2* and *KIF5C* are likely modifiers of overall variability [97].

It is worthwhile to mention that reported duplications of the 2q23 region are rare and tend to be much larger in size than the deletions described in this and previous reports [98, 99, 100]. The reported duplication 2q23 cases presented with craniofacial abnormalities, low set ears, and heart, kidney, genital, skeletal, and neurological abnormalities, with death resulting in early infancy [101]. The phenotype observed in dup(2)(q23) further supports a gene dosage as a mechanism and the importance of the genes in this region. When considering all of the reported deletions involving 2q23.1 (Figure 11), a critical region emerges that includes a single gene, *MBD5*. *MBD5* (methyl-CpG binding domain protein 5) is expressed neuronally and likely functions in the regulation of gene expression [102, 103]. *MBD5* contains a methyl-binding domain, sharing sequence homology to MECP2, which when mutated or deleted, results in Rett syndrome. We have shown in this study that *MBD5* is haploinsufficient in patient white blood cells and lymphoblastoid cells (Figure 13), providing further evidence of its role in this syndrome and the need for proper gene dosage for normal development and behavior. We do not, however, rule out the possibility that *KIF5C* and/or *EPC2* may contribute to variability or severity of the syndrome. These data, taken together with the previous report of a small deletion within *MBD5* [1, 64] and the recent study by van Bon et al. [97], indicate that haploinsufficiency of *MBD5* is the likely common pathological defect for most features of this syndrome.

Chapter 4

Haploinsufficiency of *HDAC4* results in brachydactyly mental retardation syndrome

Introduction

Chromosome deletions involving the 2q37 region result in brachydactyly mental retardation syndrome (BDMR, OMIM 600430), also known as Albright hereditary osteodystrophy-like syndrome (AHO-like). BDMR is a complex disorder that presents with a spectrum of clinical features, including developmental delay, autism spectrum disorder, craniofacial and skeletal abnormalities, cardiac defects, behavioral problems, and neurological anomalies. Approximately 100 individuals have been reported with a deletion involving the chromosome 2q37 region [83]. To date, the critical region for this syndrome has not been clearly defined, and a variety of phenotypes have been mapped to the 2q37.1→2qter region [83]. Variable expressivity and reduced penetrance for most major features complicate genotype:phenotype correlations in this syndrome and further impair diagnosis.

In a study of 52 individuals referred for a phenotype consistent with Smith-Magenis syndrome (SMS) but for whom no 17p11.2 deletion or *RAI1* mutation could be found, we identified by whole genome array comparative genomic hybridization (aCGH) several copy number variants responsible for the SMS-like phenotypes observed in these individuals [96]. Interestingly, we identified 2 cases that carried overlapping deletions of the 2q37 region [96]. After a literature review, we discovered that the phenotypic overlap between these two distinct syndromes was striking. Utilizing this unique aCGH data set and additional cases, we refined the critical region for BDMR, reducing the likely candidates to a single gene, *HDAC4*. Given

the apparent phenotypic overlap between SMS and BDMR, we then investigated more closely the specific phenotypes in our cohorts with Smith-Magenis syndrome-like and/or AHO-like features and identified one subject who lacked a 2q37 deletion but had striking phenotypic overlap with known 2q37 deletion cases. Sequencing of the coding region of *HDAC4* in this case revealed a *de novo* single base insertion that truncates the protein. *HDAC4* (histone deacetylase 4) is known to be critical for proper skeletogenesis and chondrogenesis [104], as well as neuronal survival [105]. Taking into consideration the overlapping deletion data and *de novo* mutation presented here, we assert that haploinsufficiency of *HDAC4* results in the brachydactyly mental retardation syndrome.

Materials and methods

Subject ascertainment

Subjects were referred to the Elsea laboratory for molecular evaluation of SMS at Michigan State University, or Virginia Commonwealth University, or to the Aldred Laboratory at the Cleveland Clinic for AHO-like phenotype. Samples and medical records were collected in accordance with Institutional Review Board approved protocols from the appropriate institution. Peripheral blood was collected, and DNA and metaphase chromosomes were prepared following standard methods. Phenotypic information was collected from medical records, geneticist reports, and patient photos.

Genomic DNA sequence analysis

Total DNA was isolated from cultured peripheral white blood cells using the QIAamp DNA Minikit (QIAGEN, GmbH, Hilden, Germany). PCR was performed using intronic primers from the *HDAC4* gene generated using Primer3 (v. 0.4.0) (<http://frodo.wi.mit.edu/primer3/>),

which flank both the 5' and 3' regions of each *HDAC4* exon (Table X). PCR products were treated with ExoSAP-IT (USB, Cleveland, OH) to digest PCR primers. Sequencing and analysis of electropherograms were done as previously described [54]. PCR products were sequenced and analyzed on both the forward and reverse DNA strands. Sequencing primers are provided in the Tables 8, 9.

Multiplex ligation-dependent probe amplification and SNP array analysis

MLPA was performed as previously described [106] using five custom-designed probe sets that were approximately equally spaced across the genomic extent of *HDAC4* (Table 10). Breakpoints outside of the *HDAC4* gene were defined using Illumina CNV370 single nucleotide polymorphism arrays and Beadstudio software to identify copy number changes.

Table 8. *HDAC4* amplification and sequencing oligonucleotides.

Exon	Primer	Primer Sequence	T _m (C)	Amplicon
1	1F	GGCTCGGCGCTTGAACGTCT	64	220
1	1R	TGGGCAAAGAAAGCCCCGCT	64	
2	2F	TGCGCGCAGTTTCTGAAGCC	64	214
2	2R	CCCCTCGCCCTCTCTGCACT	64	
3	3F	CCAGGGACAGCAAAGGGCGG	66	376
3	3R	CGGAGGCAGGGCTGGAGTCA	66	
4	4F	AGCCCGGAATGGCCCTGACT	63	654
4	4R	TACTCCCCGTGTGCTGCCCC	63	
5	5F	TAGCCGTCCCCAGCCCTTCC	64	412
5	5R	CTGCCGCACGAGTGATCCCC	64	
6	6F	GGGGCAGTGCCTGGGTAAA	64	285
6	6R	CTGCAGGTGATTCTTCTCTAAGTGG	64	
7	7F	TGAGCTCCCTGCGCTCTCCC	64	400
7	7R	GGGGGTTGACAGCGTGAGGC	64	
8	8F	GGGCATTCGGGCCACAGGTC	64	320
8	8R	AGGCCACTTTCCTCACCCCA	64	
9	9F	ATGTTTGGCCGTGACAGACT	60	219
9	9R	AAGGACCCATCACCACCAC	60	
10	10F	AGCATCCTGGCTGTGCTTT	58	242
10	10R	CCAGGCCCATTTGTGCTC	58	
11	11F	TTCCCCTCTGCTGTTTCTTC	58	398
11	11R	GTTCCCTCTTTCTGCCTCCT	58	
12	12F	GACCCAGCTCTCTGTGCTTC	60	377
12	12R	ACCACAGAAGATGCCACCTG	60	
13	13F	CAACACGGCCGTTTCTTC	60	243
13	13R	ACCCTCAGGCTGCACAAA	60	
14	14F	ATGACACGCTGATGCTGAAG	58	237
14	14R	TAAGCCCAAAGAACCACCTG	58	
15	15F	CTGTCTGTGGAGCTGAAGCA	60	222
15	15R	ACCCAATATGGGAGGAAAGG	60	
16	16F	CCTCGTTGTCCACAAATG	58	220
16	16R	ACCACTGGGACTCGAGAAGA	58	
17	17F	TCACTGTGGGGTGTTGTTTC	58	232
17	17R	CAGCCTGATGAGAGGGAGAC	58	
18	18F	AGGGTGCAGCAAGAACTGT	58	245
18	18R	CCTAAGGGAGGGAAGGAAGA	58	
19	19F	CTCCAGCGTCAGTTCTCTCC	60	223
19	19R	CCTAAGCTTCCCACATCCAA	60	
20	20F	TGCCTCAGCCCTGAAGTAGT	60	179
20	20R	GGCCCTTATATACCCACCT	60	
21	21F	CGTGTGTTTCTCTCCTTCTGG	60	215
21	21R	GACACGCTCATCTCCAACAA	60	
22	22F	ACCCAGTAACGCCTTCTCCT	60	234
22	22R	TAAAAAGGGGACCTGACACG	60	
23	23F	TCTTACGATGCCATGAGACG	60	242
23	23R	GGGTCTCTGGGGTCTTCTTA	60	
24	24F	GTCTCGGAACACCCGTCTAA	60	240
24	24R	GTATAGGGGGACAGGGATGG	60	
25	25F	ACTTTCCTCACCCACACCAC	60	246
25	25R	GGTTCTGACCCTGAATAGTGTG	60	

26	26F	CACAGCCTTTAACCCACGTT	60	183
26	26R	TGGCTGAGCTTCAAGACAGA	60	

Table 9. *HDAC4* cDNA oligonucleotides for amplification and sequencing.

Coding exon (cDNA)	Primer	Sequence	Tm	Amplicon (bp)
1-8	cDNA 1F	GAGTTTGGAGCTCGTTGGAG	56	1135
1-8	cDNA 1R	AAGGATGGCGATGTGTAGAGG	56	
1-8	Sequencing Primer 1F	GCAGCTCAAGAACAAGGAG	NA	NA
1-8	Sequencing Primer 1R	CTCTTTGCCCTTCTCCTTG TTC	NA	NA

Table 10. MLPA probes for 2q37.3 and *HDAC4*. Designed by Dr. Michaela Aldred

Name	Sequence	Ensembl Build 41
rs870790A	GGGTTCCCTAAGGGTTGGATTCTTAGGACCTGAAAGTCTGAACCAGCATTCCAA	239980739
rs870790B	GTGGGAGTATTGTTCAAGCGGTGATGGAATTGTCTAGATTGGATCTTGCTGGCAC	239980805
HDAC4-2A	GGGTTCCCTAAGGGTTGGAGAGGCTCGGCGCTTGAACGTCTG	239939431
HDAC4-2B	TGACCCAGCCCTCACCGTCCCGGTACTCTAGATTGGATCTTGCTGGCAC	239939479
HDAC4-3A	GGGTTCCCTAAGGGTTGGATGGCCGAGACCAGCCAGTGGAGCTG	239823237
HDAC4-3B	CTGAATCCTGCCCCGCGTGAACCACATTCTAGATTGGATCTTGCTGGCAC	239823287
HDAC4-i9A	GGGTTCCCTAAGGGTTGGAGCACTTGCCCTTCACTCTTCACCTTCCA	239726184
HDAC4-i9B	ATTTGGGGTGAGGGAAAGTGGCCTGTGTCTAGATTGGATCTTGCTGGCAC	239726238
HDAC4-i26A	GGGTTCCCTAAGGGTTGGACTCCTTCCAGTGCCAAAGCCCCTTAGAGAC	239639900
HDAC4-i26B	GCATGAGGAGCATTAGATCCTGAACAGATGGATCTAGATTGGATCTTGCTGGCAC	239639961

Results

Utilizing recent studies of SMS-like [96] and known deletion 2q37 subjects [107], we were able to make genotype:phenotype correlations allowing refinement of the critical region for BDMR to ~chr2: 239,639,900-240,938,547 within the 2q37.3 band, including the *HDAC4* gene.

BDMR clinical phenotype

The deletion 2q37 syndrome phenotype consists of a variety of findings that overlap with other syndromes such as Smith-Magenis, Prader-Willi, Angelman, and fragile-X syndromes (Table 11). Common features include mild facial dysmorphism, congenital heart defects, distinct brachydactyly type E, intellectual disabilities, developmental delay, seizures, autism spectrum disorder, and obesity [83, 107]. Genotype:phenotype correlations have been attempted in the past but have failed to identify a single gene that may contribute to the core findings observed in BDMR.

Deletion cases we previously reported showed the classical BDMR phenotype (Table 11). SMS272 is obese Native American with cognitive and developmental delays and was originally referred for features of Smith-Magenis syndrome (SMS). Skeletal features include brachydactyly type E (shortened 3rd, 4th, and 5th, metacarpals with shortened and proximately paced 4th left toe), midface hypoplasia, and brachycephaly (Figure 16, Table 11). She also exhibits stereotypies and aggressive behavior but lacks two of the key features, sleep disturbance and self-abusive behavior, which are common in SMS. She carries a small, 1.17 Mb, 2q37.3 deletion which was later confirmed on karyotype (Figure 14).

SMS320 was referred for developmental, speech, and motor delays, sleep disturbance, stereotypies, attention-seeking, and self-injurious behaviors. Her craniofacial and skeletal

phenotype consists of brachydactyly, brachycephaly, midface hypoplasia, tented upper lip, and a broad, square face (Table 11). While originally referred for SMS, she carries a larger deletion of 2q37.3 that spans 3.02 Mb (Figure 14).

Subject 122 presented with developmental delay, mild facial dysmorphism, BDE and receptive language and social communication disorder. A detailed clinical description was published previously [107]. Case 122 carries a 3.21 Mb 2q37 deletion (Figure 14).

Subject 10780, who carries a 3.2 Mb deletion within 2q37 (Figure 14), presented with, developmental delay, short stature, facial dysmorphism, brachydactyly type E, and grand mal seizures (Table 11). A detailed clinical description has been published previously [71]

Table 11. Clinical features of cases with deletions or mutations involving 2q37.3.

PHENOTYPE	SMS117 <i>HDAC4</i> mutation	SMS272 del(2)(q37.3) including <i>HDAC4</i> [96]	SMS320 del(2)(q37) including <i>HDAC4</i> [96]	122 del(2)(q37) including <i>HDAC4</i> [107]	10780 del(2)(q37) including <i>HDAC4</i> [71]	2282 del(2)(q37.3) not including <i>HDAC4</i>
Sex	F	F	F	F	F	F
Age at evaluation	16 and 25 years	15 and 17 years	3 years	6 years	12 years	7 years
Developmental delay	+	+	+	+	+	+
Motor delay	+	-	+	+	+	+
Language impairment	+	+	+	+	+	+
Behavioral problems	Self-injurious behavior Pulling out of fingernails	Aggressive behavior Hand wringing Eye squint	Self-injurious behavior Head banging Skin picking Hand biting Hyperactivity	receptive language and social communication disorders	N/A	Autistic behavior Repetitive behaviors
Stereotypies		Self-hug, tics	Self-hug	N/A	N/A	N/A
Sleeping difficulties	+	-	+	N/A	N/A	N/A
Decreased sensitivity to pain	+	+	+	N/A	N/A	N/A
Hearing loss	+		-	-	-	-
Short stature	+/-	-	-	+	+	-
Seizures	essential tremor	-	-	-	+	+
Feeding difficulties	+	-	-	-	N/A	-
Obesity/overweight	+	+	+	-	-	+
Craniofacial manifestations						

Broad face	+	+	+	+	+	+
Upslanting eyes	+	+	+	-	-	
Brachycephaly	+	+	+			
Midface hypoplasia	+	+	+		+	+
Broad, upturned nose	+	+	+		+	-
Skeletal abnormalities						
Brachydactyly	+, type E	+, type E	-	+	+	-
Proximally placed 4th toe, shortened 4th metatarsal	+	+	-	+	+	-
OTHER	Subvalvar aortic stenosis; mitral stenosis; pacemaker Hypothyroidism Hirsutism Spina bifida occulta Very friendly	Sinus arrhythmia Myopia Very friendly		2-3 toe syndactyly	Craniosynostosis	Hypothyroidism Precocious puberty

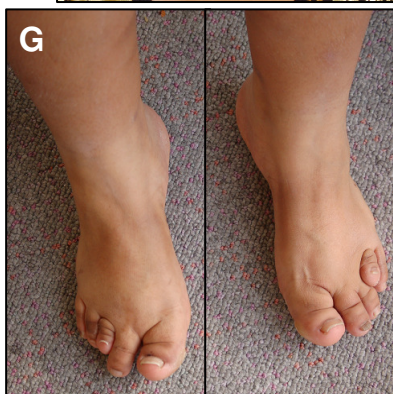
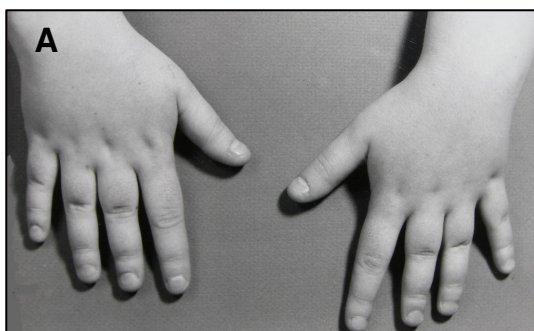


Figure 14. Skeletal anomalies observed in BDMR. A) Hands of case SMS117. B) Feet of SMS117, showing shortened 4th metatarsal and wide spacing between toes. C) Radiograph of left hand of SMS117 showing shortened 3rd, 4th, and 5th metacarpals. D) Radiograph of SMS117 feet showing proximally placed and shortened 4th metatarsal and bilaterally widely spaced 1st, 2nd, and 3rd toes. E). Photo of SMS272 at 17 years of age. F) Hands of SMS272. Note shortened 3rd and 4th fingers. G) Feet of SMS272 with shortened 3rd toes and proximally placed and shortened 4th toes. H) Radiograph documenting shortened 3rd and 4th metacarpals in the hands of SMS272.

Refinement of the BDMR critical region

Refining the critical region for deletion 2q37 syndrome has proven difficult because of poor genotype:phenotype correlation and a paucity of interstitial deletions that would help define minimal overlapping candidate regions. However, because of deletions identified within a small overlapping region within the 2q37.3 band [96, 107], we were able to narrow the critical region to ~200 kb region including *HDAC4* (Figure 14), with SMS272 critical to this analysis due to the very small deletion identified by aCGH. Further supporting the refinement of this region to ~200 kb is subject 2282 who does not have the BDE phenotype. However this patient does have developmental delay, facial dysmorphism and autistic behaviors (Table 11), indicating that other aspects of 2q37 deletion syndrome are complex and like many deletion/mutation syndromes multiple genes may contribute to the full spectrum of the phenotype.

Two del(2)(q37.3) subjects were analyzed by MLPA to assess the specific location of the break points observed (Figure 15, Table 10). As shown in Figure 15 , the proximal breakpoints of the deletions are within the *HDAC4* gene. The breakpoint identified in case 122 is in the second intron of *HDAC4*, while the breakpoint for case 10780 is in intron 9 (Figure 15). Both deletions should result in haploinsufficiency for *HDAC4* as the promoter and initial coding exons are deleted in both cases (*HDAC4* is transcribed on the minus strand of DNA). These two subjects have a strikingly similar phenotype to that of SMS117 and to other BDMR cases, including intellectual disabilities, developmental delay, brachydactyly type E, and facial dysmorphism. Case 10780 also has short stature with obesity, further strengthening the case for mutations in *HDAC4* to contribute to the core phenotypes of BDMR.

Further supporting the notion that deletion of *HDAC4* is responsible for the brachydactyly type E phenotype, subject 2282 has a 2.68 Mb terminal deletion with a breakpoint

that is distal of *HDAC4* (Figure 14). This individual presented with developmental delay, obesity, autistic behaviors and a history of seizures but had no evidence of metacarpal or metatarsal shortening. Facial dysmorphism included a broad face with bi-temporal narrowing and small nose with flat nasal bridge. There was no evidence of heart or other major organ defect. An additional case, subject 2232, was diagnosed with a terminal 2q37 deletion approximately 7 Mb in size (Figure 14). Unfortunately no clinical details were available and thus this case is not included in Table 11.

These molecular and clinical data supported mutation analysis of *HDAC4* as the logical next step toward identification of a single gene that, when mutated, results in BDMR. Further supporting sequence analysis of cases with the BDMR phenotype but without 2q37 deletion is the *Hdac4*^{-/-} mouse [104], which has a significant skeletal phenotype [104]. Although important in electron transport, *NDUFA10* was eliminated as a probable cause for BDMR.

Figure 15. Delineation of the BDMR critical region. A) Ideogram of chromosome 2 band q37.3. B) Schematic representation of 2q37.3 region and RefSeq Genes included (www.genome.ucsc.edu, accessed Feb. 25, 2010). C) Horizontal bars indicate the regions of deletion in each of these key 2q37 deletion syndrome cases. The brachydactyly mental retardation syndrome critical region is indicated by the vertical bars. The SMS117 *HDAC4* point mutation is indicated by the small red vertical line.

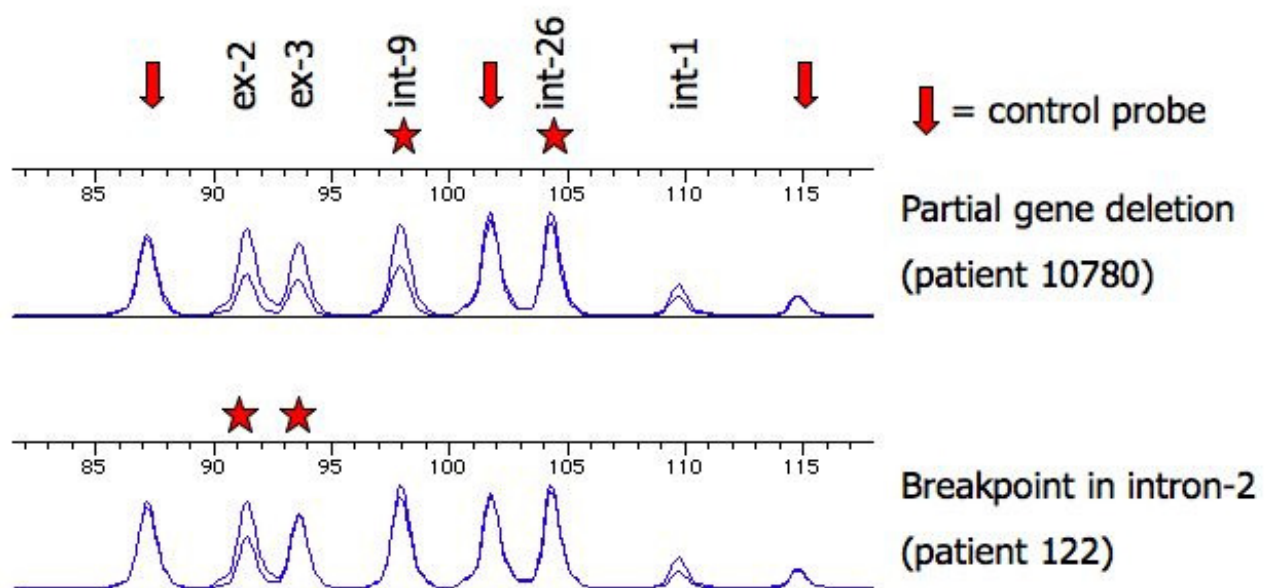


Figure 16. MLPA analysis of *HDAC4* deletion breakpoints in key 2q37.3 deletions.

Top: Analysis of patient 10780 showed an *HDAC4* deletion extending at least through intron 9 but the breakpoint occurring prior to intron 26. *Bottom:* Patient 122 revealed a deletion including intron 1 and exon 2, with the breakpoint occurring between the probes for exon 2 and exon 3. Stars indicate regions between which the breakpoint occurs for each case. Control probes are indicated by the arrows and show 2 alleles of equal intensity for each.

SMS117 Clinical phenotype

SMS117, who is deletion 2q37 negative, is a female French-Canadian born at 43 weeks to nonconsanguineous parents (Figures 16, 17 Table 11). Birth was complicated by two induction attempts. Weight at birth was 2.85 kg (10-25%), and length was 51 cm (25-50%). The 1st year was marked with feeding difficulties. Subvalvular aortic stenosis was identified at 4 months. Psychomotor development was delayed, with walking at 18 months, and speaking in sentences at 6 years of age. The clinical phenotype worsened with age. She received a mitral valve replacement and permanent pacemaker at 5 years. At 13.5 years, she was referred to genetics where she presented with dysmorphic features, including midface hypoplasia, broad face and nose, brachycephaly, frontal bossing, a down turned lower lip, and upslanted eyes. At 25 years, physical exam revealed obesity (96 kg, >95%; 157cm, 10-25%). Neurologically, decreased deep tendon reflexes, and cerebral atrophy were also observed, as well as sensorineural hearing loss (>40 dB) for which she wears two hearing aids. Cerebral atrophy was identified by head CT, and spina bifida occulta was also observed. Decreased sensitivity to pain, onychotillomania, hyperactivity, and a decreased attention span were also observed, in addition to a hospitalization for hypersomnolence and precipitous loss of consciousness. Sleep abnormalities began at 3 years of age with several arousals throughout the night, which lasted until the age of 8; however at 24 years, she can sleep for up to 18 hours if not awakened. A complete absence of REM sleep as per 44 hours of EEG video telemetry was noted. Skeletal features include brachydactyly type E with proximally placed 3rd, 4th, and 5th fingers (shortened 3rd, 4th, and 5th metacarpals on X-ray) and bilateral proximally placed 4th toes and bilateral widely spaced 1st, 2nd, and 3rd toes (Figure 16). Total hand length was 14 cm (<3%) and total foot length was 22.5 cm (10-25%). There is a striking similarity between the morphology of the

hands and feet of SMS117 (*HDAC4* mutation) and SMS272 (2q37 deletion) (Figure 16), lending further support to the importance of *HDAC4* in this syndrome. Family history was unremarkable; however, the patient's father died at age 50 years of a pulmonary embolism, and no other abnormalities were reported.

Mutation analysis

All coding exons for *HDAC4*, in SMS117, were sequenced and assessed for mutation (PCR primers found in Table 8). When analyzing the nucleotide sequence for exon 19, an insertion of a single cytosine was observed (c.2399_2400insC; Figure 17). Because this insertion lies within a run of five cytosines, the exact location of the insertion cannot be determined, but this does not impact the resulting location of the premature stop codon (Gly801TrpfsX1) (Figure 17).

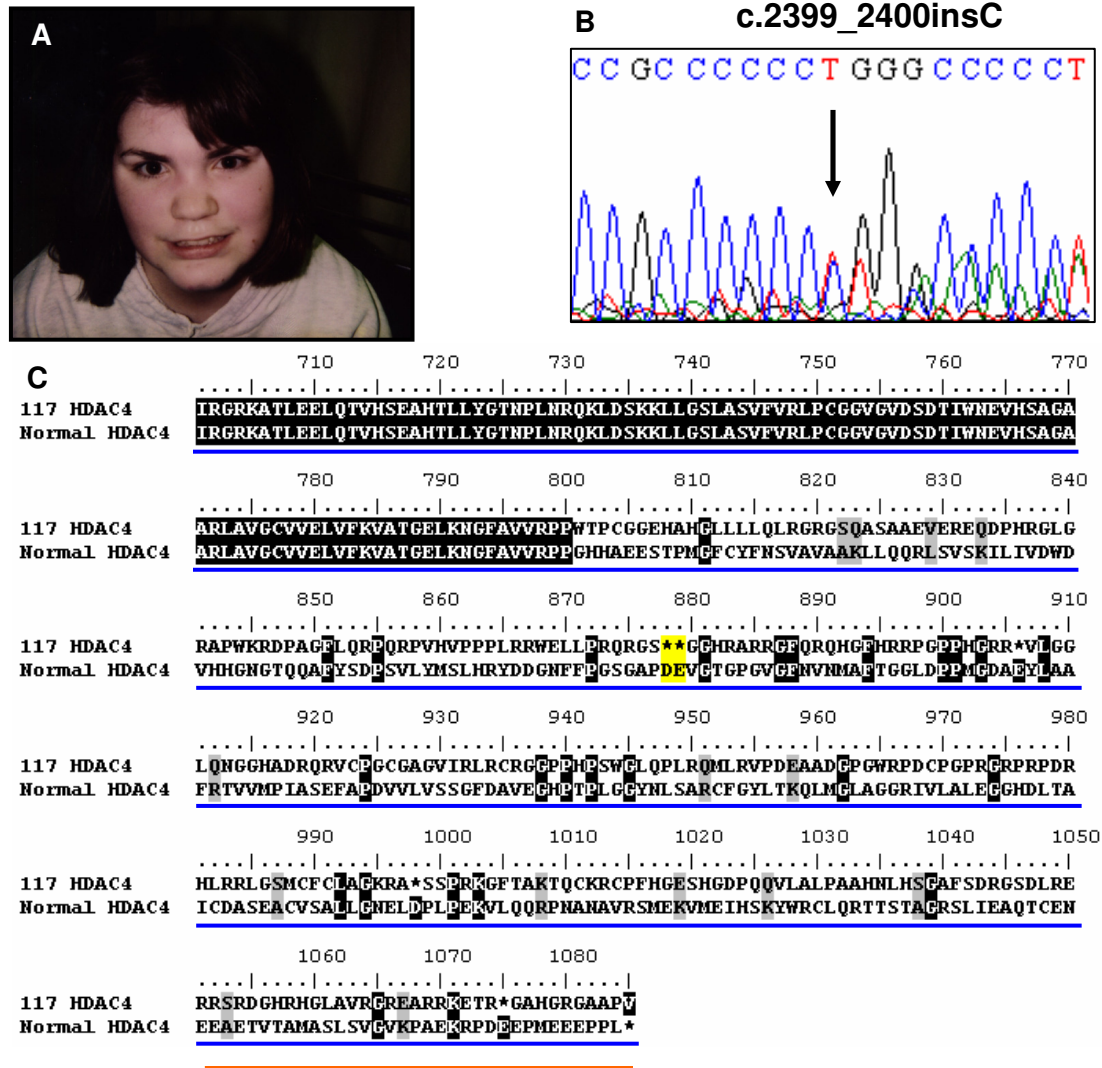


Figure 17. SMS117 HDAC4 mutation and impact on HDAC4 protein. A) SMS117 at 13 years. B) Electropherogram trace showing nucleotide insertion of a single cytosine at c.2399 in the *HDAC4* gene. C) Partial amino acid alignment of the normal HDAC4 protein with the altered protein likely produced in SMS117 due to frame shift mutation. Premature stop codon highlighted in yellow. The histone deacetylase domain resides at amino acids 655-1084 (Blue line), and the nuclear export signal is at amino acids 1051-1084 (Orange line). The mutation disrupts the HDAC domain and removes the nuclear export signal

Discussion

We describe five individuals with del(2)(q37.3) four of which include or interrupt the *HDAC4* gene, as well as one individual with a *HDAC4* insertion which results in a frame shift and truncated protein. Additional cases from the literature supporting this conclusion include patient 2 from Shrimpton et al (2004) with BDE, short stature and cognitive delay and a recent report of a patient with BDE, developmental delay, autism and seizures Felder et al, 2009. Although *HDAC4* was not specifically examined in these two cases, the breakpoints mapped in close proximity to *HDAC4* suggesting this gene was likely disrupted. Taken together, we conclude that haploinsufficiency of *HDAC4* results in brachydactyly mental retardation syndrome.

HDAC4

HDAC4 is a class II HDAC which acts as a co-repressor for DNA-binding transcription factors. Acting in concert with HDAC9 and HDAC3, HDAC4 acts to inhibit a variety of transcription factors including, MEF2C and RUNX2, and serves to deacetylate histones, both of which are essential for proper skeletal development. This deacetylation condenses chromatin making it inaccessible to factors that drive transcription. Additionally, class II HDACs are antagonists of cardiac hypertrophy needed for proper cardiac development [108]. Because of this molecular evidence it is logical to conclude that deletion or mutation of HDAC4 would lead to the core phenotypes seen in BDMR.

HDAC4 mutation

The impact of this insertion, found in SMS117, on the HDAC4 protein is significant. The

premature stop codon interrupts the histone deacetylase domain potentially limiting or preventing all histone deacetylase activity from this *HDAC4* allele. This deacetylase activity is essential for protein function, as HDAC4 has the ability to deacetylate all four core histones [109]. Fischle et al. [110] showed that if amino acids 1002–1058 or 803–846 of HDAC4 (the most conserved domain of HDAC4 across species) are deleted, interaction with HDAC3 and all histone deacetylase activity are eliminated. As shown in Figure 17, the insertion of a cytosine at codon 801 causes a frame-shift that significantly reduces amino acid identity (5%) or similarity (5%) between the SMS117 mutant and wild type alleles. Taken together, these data provide evidence that the mutant HDAC4 protein is completely void of histone deacetylase activity and can no longer bind with HDAC3. Further, when mutated from histidine to alanine, a charged polar to nonpolar change at p.802 and p.803, Fischle et al. showed that binding to N-CoR was eliminated [110]. N-CoR is essential for HDAC3 recruitment and HDAC activity of the complex. The SMS117 mutation of *HDAC4* shows a p.H802T, and p.H803P change at these essential amino acids leading to charged polar to uncharged polar and charged polar to nonpolar changes, respectively, potentially having a great impact on the activity of this mutant protein (Figure 17).

Hdac4^{-/-} and related mouse models

The *Hdac4*^{-/-} mouse has a variety of significant phenotypes and was shown to have early onset chondrocyte hypertrophy and premature bone ossification [104]. These mice present with severe bone malformations and are much smaller than wild-type littermates due to premature ossification of the developing bone. A reflection of the importance of *HDAC4* in bone malformation in humans can be seen when studying the hands and feet of SMS117 and SMS272

(Figure 16). In addition, in the same manuscript by Vega et al. 2004, it was shown that HDAC4 also directly controls Runt-related transcription factor 2 (*Runx2*) activity. The *Hdac4*^{-/-} mouse model directly mimics the phenotype seen with constitutive *Runx2* expression in chondrocytes [111, 112].

MEF2C activity which is necessary for proper chondrocyte hypertrophy and bone development is also regulated by HDAC4 [113, 114]. Mice deleted for the *Mef2c* gene have impaired hypertrophy, cartilage angiogenesis, ossification, and longitudinal bone growth, a converse phenotype to that of the *Hdac4*^{-/-} mouse [115], consistent with HDAC4 acting as a negative co-repressor of *MEF2C*.

Clinical implications

In the analysis of twenty 2q37 deletion cases, Aldred et al. concluded that the region most likely associated with congenital heart defects in the BDMR syndrome included the *HDAC4* gene. In this report, we support this finding with the fact that SMS117 has a significant cardiac defect. The role of HDAC4 in cardiac development is further supported by data that implicate MEF2C, which is regulated by HDAC4, in cardiac development [116]. Additional studies and cases are required to confirm this hypothesis.

Based upon our findings reported here, we conclude that haploinsufficiency of the *HDAC4* gene results in BDMR. Data support a significant role for HDAC4 in normal skeletal development, specifically in metacarpal and metatarsal growth and craniofacial development, and in neuronal function, with a prominent role in behavior. Autism or autism spectrum disorder (ASD) has been reported in many cases with 2q37.3 deletions, and with behavioral and developmental findings consistent with the cases we report here [107, 117, 118, 119]. However,

two of our older cases are reported to be "very friendly" but with poor communication skills, while the younger subjects have significant speech delay and poor communication with behavioral problems often prohibiting positive interactions. These findings suggest that reduced expression or function of HDAC4 is a contributor to the ASD phenotype observed in many cases with 2q37 deletion but that interpersonal skills may improve with age and with reduction of negative behaviors. Given that the genetic basis of autism is highly complex, it is not surprising that autistic behavior was also reported in case 2282 with a terminal 2q deletion that does not include *HDAC4* and in a published case with a much smaller subtelomeric deletion suggesting that multiple genes at 2q37 may be involved in this phenotype [120]. A more proximal locus, *CENTG2* at 2q37 (now renamed *AGAPI*), has also been suggested by two-point linkage analysis in autism families, although this was not supported by multipoint analysis [121].

Additionally, a recent publication by Klopocki et al. 2010 [122], has linked mutations in the parathyroid hormone related protein (*PTHLH*) to result in brachydactyly type E. Interestingly, *Pthlh* was identified as an inhibitor of Runx2 (regulated by Hdac4) in mice [123], and *Pthlh*^{-/-} mice results in lethal short-limbed chondrodysplasia and speaks to the probability of common pathway involved in the development of metacarpals and metatarsals in the hands and feet in humans.

Given the significant phenotypic overlap with Smith-Magenis syndrome, BDMR and SMS should be considered together in the differential diagnosis. While type E brachydactyly is unique to BDMR, it is only penetrant in 50-60% of cases, so its absence does not remove the possibility of a positive diagnosis for BDMR. Also, other phenotypes within the syndrome also show variable expressivity, especially heart defects and behavioral problems. Given this variability, a genetic "two hit" model is the most likely applicable to neuropsychiatric disorder

[124] and given the range of phenotypes and variable expressivity seen dependent on deletion size this makes sense with regard to BDMR. The diagnostic challenges and the elucidation of core phenotypes from syndrome to syndrome make it important to note all molecular findings and detail specific phenotypic findings in all cases.

As such, we recommend molecular evaluation in cases with phenotypic findings consistent with BDMR and/or SMS for deletions involving chromosomes 2q37.3 and 17p11.2, respectively (karyotype, FISH, and/or aCGH). For those cases without 2q37.3 deletion and with type E brachydactyly, sequencing of *HDAC4* is appropriate. For those subjects without a deletion of 17p11.2 and without type E brachydactyly, *RAI1* sequence analysis should be undertaken, and if negative, followed by *HDAC4* sequencing. We anticipate additional mutations in the *HDAC4* gene will be identified lending further support to this gene playing an essential role in proper cognitive, bone, and cardiac development in humans.

Chapter 5

RAI1 transcriptionally regulates *CLOCK* and is a major contributor to circadian homeostasis

Introduction

The retinoic acid induced one gene is the gene that when mutated or deleted results in Smith-Magenis syndrome. However, little is known about the molecular function of RAI1. Given the phenotypic consequences of *RAI1* mutation or deletion, *RAI1* must be involved in pathways associated with development, behavior, neurological function, and circadian rhythm.

Mutations in transcription factors have long been associated with human disease, including ATRX syndrome, myeloid leukemia and autoimmune dysfunction [125]. Because transcription factors can regulate many genes, deciphering their global function can be difficult. With concern to *RAI1*, there is an additional layer of complexity because, other than bioinformatic analysis, very little is known about the true molecular function of RAI1.

Rai1, originally called *Gt1*, was identified in mouse P19 embryonal carcinoma cells which can be differentiated into neurons and glial cells when treated with retinoic acid [126], and three human isoforms are predicted by bioinformatic analysis. RAI1 contains a plant homeodomain (PHD), and a bipartite nuclear localization signal, which are commonly seen in transcription factors (Figure 18). PHD domains typically bind zinc and are involved in chromatin remodeling, whereas nuclear localization signals have the ability to recruit chaperone proteins, therefore facilitating transport into the nucleus [127]. Transcription factors will then either bind directly to nuclear DNA or other proteins which will form the initiation complex, to start of transcription via RNA polymerase II. However, transcription factors can also repress

transcription acting to a negatively regulate transcription by blocking the enhancer binding regions.

Past studies have shown that Rai1 is expressed in all tested tissues and highly expressed in neural tissue [126]. We have previously shown that an RAI1 protein tagged with GFP (RAI1-GFP) localizes to the nucleus (Figure 18) (Burnes et al. in review). Complicating the story, the three predicted isoforms of RAI1 may serve different functions dependent on spatial and temporal expression.

Identification of genes targeted by transcription factors can be difficult. Before the advent of newer technologies, initial screens for gene targets of transcription factors could be a very labor intensive task [128]. Traditionally, the project would start with a chromatin immunoprecipitation using agarose beads bound to an antibody specific for the protein of interest. The protein would be pulled down with chromatin bound to the protein of interest, in complex with the antibody coated beads, and these chromatin fragments would be cloned into plasmids. Sequencing of these plasmids would follow. Hundreds of these individual clones would have to be sequenced making this process very time consuming [128]. Recently, chromatin immunoprecipitation coupled with microarray has become an important tool in deciphering the targets of transcription factors. Global ChIP-chip is a high throughput and effective tool for screening the regulatory regions of all known genes and has reduced the time needed to identify targets of transcription factors [129]. Through this set of studies we set out to identify genes regulated by RAI1.

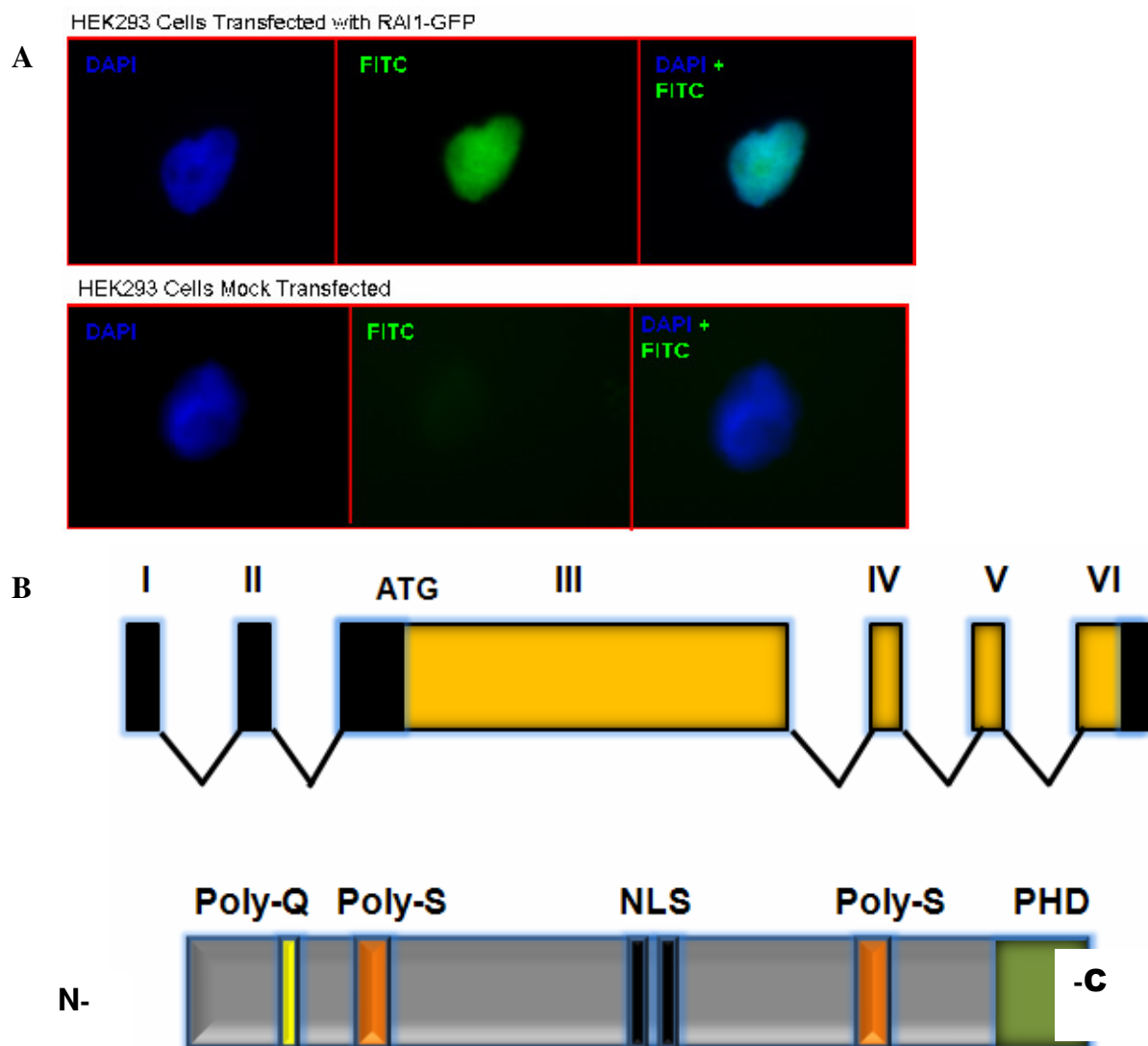


Figure 18. RAI1 localization and genomic and protein structure of *RAI1*. A) HEK293 cells transfected with RAI1a-GFP. B) The top panel shows genomic structure of *RAI1* (isoform A) with 6 exons (4 coding: yellow and 2 noncoding: black). The bottom panel shows the protein structure of RAI1 including the polyglutamine (Poly-Q) and polyserine (Poly-S) tracts, the bipartite nuclear localization signals (NLS), and a C-terminal PHD (plant homeodomain). Created, in part, by Santhosh Girirajan.

Circadian Rhythm

Circadian rhythm

Mammalian circadian rhythm is an essential regulator of not only the sleep-wake cycle but also body temperature, feeding cycles, hormone secretion, drug and xenobiotic metabolism, glucose homeostasis, and cell-cycle progression [130]. The master regulator of the circadian clock resides in the suprachiasmatic nucleus located in the mammalian hypothalamus. The primary synchronizer of this clock is the 24 hour light dark cycle. Over this 24 hour light dark cycle, a feed back loop of gene transcription and subsequent degradation of gene products occur signaling the mentioned processes to react accordingly. Because of the complexity of this circadian loop, disturbances in the timing of gene expression can have a major impact on not only one's sleep pattern, but also ones disease susceptibility and behavioral stability. Genes involved in fatty acid metabolism, energy metabolism, and cholesterol biosynthesis seem to be expressed in a circadian manner [130] so one can anticipate that sleep disturbance could be tied to obesity and increased risk for disease. Interestingly, mice with a homozygous mutation in the gene *Clock* (one of the first and most important circadian genes identified) are obese and hyperphagic [131]. Further, altered circadian rhythm has been linked to bipolar disorder [132], and variants in *CLOCK* have been linked to sleep disorders in humans [133]. It has been shown through caregiver surveys that partial alleviation of the sleep disturbance in patients with SMS can result in behavioral improvement [134]

Materials and methods

Creation of Plasmids

$RAII^{Flag}$: *RAII* coding sequence was cloned into pEntr/D-TOPO using standard manufacturer protocols (Invitrogen, Carlsbad, CA). A 5' TOPO poly linker was added to cDNA

PCR forward primer (CACC) to ensure proper directional cloning. Following PCR 2 uL of PCR product was mixed with 1uL salt solution, 2 uL ddH₂O, and 1 uL pEntr/D-TOPO. The reaction was transformed into One Shot® Competent *E. coli* (Invitrogen, Carlsbad, CA) according to manufacturer's instructions. Cells were spread on LB plates containing 50 µg/ml kanamycin. After 18 hours colonies were picked and mixed with LB broth containing 50 ug/ml kanamycin and shaken for 18 hours at 37⁰C. Plasmid DNA was isolated using Fermentus GeneJET™ plasmid mini kit (Burlington, Ontario, Canada) according to standard manufacturer's instructions. Inserts were confirmed using *RAII* cDNA primers and sequenced using standard Sanger techniques. Next, *RAII*^{pEntr/D-TOPO} was recombined with pDest26^{Flag} [135] using the standard gateway protocol provided by Invitrogen(Carlsbad, CA) to create pDest26*RAII*^{Flag}.

CLOCK^{Luc}: The *CLOCK* 1st intron element was PCR amplified using standard techniques (forward primer: 5'-GGACCTTTGCAAGAGCCCAAG-3', reverse primer: 5'-GCAGAGCACAGAGGGCTTTTAGGCCGATGT-3') and cloned into StrataClone™ PCR Cloning vector using the standard protocol provide by the manufacture(Agilent Technologies, Santa Clara, CA) creating CLOCK^{Strata} plasmid. The insert was confirmed by standard Sanger sequencing, and removed by restriction digest with *KpnI* and *SacI* enzymes (New England Biolabs, Ipswich, MA). The resulting product was run on a 2% agarose gel for 30 min and purified using Qiagen (Germantown, MD) Qiaquick gene extraction kit according to standard manufacturer's protocols. *KpnI* and *SacI* enzymes were then used to "prepare" the pGL3pro vector (Promega Corp, Madison, WI) and the cut out insert from CLOCK^{Strata} was directionally ligated into the pGL3pro vector to create CLOCK^{Luc} using standard T4 ligation protocols provided by the manufacturer (Promega Corp, Madison, WI).

Transfections

Human embryonic kidney (HEK293T) cells were maintained in 6-well dishes containing Dulbecco's modified Eagle's medium with 10% (v/v) FBS, 2 mM L-glutamine, and 100 µg/ml of penicillin/streptomycin (Invitrogen, Carlsbad, CA) at 37°C in a 5% CO₂ incubator. The cells were counted using trypan blue exclusion to ensure >90% viability. Transfections with pUC19, psvβ-Gal, BDNF^{Luc} and RAI1^{Flag} were performed by lipofection using LipofectamineTM 2000 (Invitrogen, Carlsbad, CA) according to the manufacturer's instructions. Briefly, ~4 x 10⁵ cells were plated in 2.0 ml of growth medium without antibiotics 24 hours prior to transfection. A total of 4 µg of total plasmid DNA, using pUC19 plasmid as “filler” DNA, was diluted in 250 µl OptiMEM® Reduced Serum Medium (Invitrogen, Carlsbad, CA). Similarly, 10 µl of LipofectamineTM 2000 was diluted in 250 µl of OptiMEM® Reduced Serum Medium, mixed well, and incubated for 5 minutes. After incubation, diluted plasmid DNA was mixed with diluted LipofectamineTM 2000 to a total volume of 500 µl and incubated for 20 minutes. Plasmid:Lipofectamine complexes (500 µl) were added to each well and mixed by rocking. The cells were then incubated at 37°C in a 5% CO₂ incubator, for 24 hours before Trizol RNA extraction using standard protocols provided by Invitrogen (Carlsbad, CA).

Luciferase assay

Twenty-four hours after DNA transfections cells were washed with 2 mL DPBS (Invitrogen, Carlsbad, CA), and Tropix Glacto-LightTM (Applied Biosystems, Bedford, MA) standard protocol was used. Briefly, 250 µL of lysis solution was added to each well of the six well plate and scraped until all cells were detached. Lysates were collected and centrifuged at

12,000 RPM for 2 min to pellet cell debris. Next, of the resulting supernatant 50 uL was transferred to a 4 wells of a 96 well white luminometer plate. Two wells were treated with 70 uL diluted Galacton® substrate (1:100, Galacton:Reaction buffer diluent) and incubated for 30 min. To the 2 wells that contained the diluted Galacton® substrate, 100 uL of Accelerator(-II) was added. To the 2 wells that did not contain the diluted Galacton® substrate, 100 uL of Steady-Glo® Luciferase substrate (Promega Corp, Madison, WI) was added. Each well was read using the Wallac 1420 VICTOR2™ luminometer (PerkinElmer, Waltham, MA) on a maximum linear scale.

Calculation of relative luciferase activity

Relative luciferase activity, from each individual transfection, was calculated by dividing the average number of light units read from the wells containing the Steady-Glo® Luciferase substrate (Promega Corp, Madison, WI) by the average number of light units from the wells containing the Galacton® substrate and Accelerator(-II). The equation ($\Delta\text{Luc}/\Delta\beta\text{-Gal}=\text{Relative luciferase activity}$) was used. Wells containing pUC19, *psvβ-Gal*, and *CLOCK^{Luc}* was used as baseline luciferase activity. Each experiment was performed independently no less than three times.

Statistical analysis

P-values were generated by averaging relative luciferase activity from each independent study and performing a two-tailed student's t-test. Standard deviations were generated using Excel.

Mouse tissue collection

Rail^{+/-} mice were obtained from the Jackson labs [42]. These mice were bred with wild-type C57Bl/6J females to obtain *Rail*^{+/-} and wild type pups. Genotyping was performed using PCR primers, reported in Bi et al 2005, specific for the *Rail*-targeted allele and the wild type allele [42]. Mice euthanized in the day time hours were taken at ~8 hours Zeitgeber time and mice euthanized in the night time hours were taken at ~16 hours Zeitgeber time. WT C57Bl/6J and *Rail*^{+/-} mice were euthanized by CO₂ anesthesia and tissues were collected in accordance with standard protocols and frozen at -80°C.

Quantitative PCR

qPCR was performed as previously described [81].

Chromatin immunoprecipitation with microarray (ChIP-Chip)

HEK293t cells were transfected with *RAI1*^{Flag} plasmid as stated above by scaling the reaction up for a T75 culture dish. ChIP-Chip was processed with mouse IgG Dynabeads (Invitrogen, Carlsbad, CA) and monoclonal anti-Flag IgG antibody produced in mouse (Sigma Aldrich, St. Lewis, MO) according to manufacture's protocols using Nimblegen "ChIP sample preparation protocol v2" (Roche Nimblegen, Madison, WI). Briefly, after 24 hours, transfected cells were formaldehyde treated to cross-link protein complexes with nuclear chromatin and frozen at -80°C overnight. Nuclei were next isolated by cytoplasmic lysis and centrifugation. Isolated nuclei were then sonicated on ice with a Branson Sonifier, used at 25% power, to shear DNA:protein complexes to between ~200 and 800bp. Lysates were then centrifuged at 4,000

RPM at 4°C to pellet debris. Protein:chromatin products were then mixed with IgG Dynabeads, that had been washed and mixed with anti-Flag IgG antibody at 4°C for 24 hours, for 16 hours overnight. Using a DynaMag™-Spin magnet (Invitrogen, Carlsbad, CA) protein:chromatin products were isolated and nuclear extracts discarded. Chromatin:protein complexes were then washed 6 times according to manufacturers protocols and the crosslink was reversed by using heat treatment at 65°C for 16 hours. Following reverse crosslink chromatin products were whole genome amplified, as per recommendation by Nimblegen, by using WGA2-10RXN kit (Sigma-Aldrich, St. Lewis, MO).

Arrays were processed by Nimblegen using the Nimblegen HG18 RefSeq promoter array according to standard manufacturer's protocols. Control chromatin was processed as per manufacturers instructions using nuclear DNA isolated from HEK293t cells that were non-transfected and non-cross linked but were sonicated as stated above. Data were pre processed by Nimblegen according to standard manufacturer's protocols. *RAI1^{Flag}* binding sites were generated by using genomic data points, Peak_Start and Peak_End, from Nimblegen pre-processed data files.

Candidate gene filtration

Ideally, regions of potential RAI1 binding would replicate between both ChIP-Chip experiments but this was not a defined criteria. RAI1 probable "hits" were defined by false discovery rate (FDR<.20), preprocessed by Nimblegen, reproducibility between arrays, known biological function, and Signal Map peak score (Roche Nimblegen, Madison, WI). FDR "is generated from the scaled log₂-ratio data. NimbleScan detects peaks by searching for 4 or more probes whose signals are above the specified cutoff values, ranging from 90% to 15%, using a

500bp sliding window. The cutoff values are a percentage of a hypothetical maximum, which is the mean + 6[standard deviation]. The ratio data is then randomized 20 times to evaluate the probability of “false positives.” Each peak is then assigned a FDR score based on the randomization (Roche Nimblegen, Madison, WI).” Peak scores were identified by loading preprocessed .GFF files. Peak scores are between 1-4 and only scores between 1-2 were considered. Peak scores are based off of an algorithm created by Nimblegen.

Results

Chromatin immunoprecipitation with microarray

Genes identified by ChIP-Chip:

Two independent ChIP-Chips were performed by transfecting RAI1^{Flag} plasmid into HEK293 cells. HEK293 cells were used because of their ease of transfection and biological relevance as RAI1 is highly expressed in the human kidney [136].

By performing the two ChIP-chip experiments in HEK293 cells we were able to identify 257 transcripts which overlap between the arrays (Figure 19, Table 12). As suspected, we identified genes important in circadian rhythm, cognition, chromatin modification, development, and neurological stability were identified (Figure 19, Table 12). To refine our candidate gene list which would be further explored we used SignalMap software (provided by Roche Nimblegen), and known biological function to pick the best transcripts of interest. Peak scores range from 1-4. Peaks created in SignalMap which held a value of 1 or 2 were identified as best hits. A value of 1 or 2 correlates with a low false discovery rate and high log2 ratio of test/control indicating a high scoring peak. A ranked order of top genes can be seen in Table 13.

Table 12. List of gene regulatory regions which overlap between RAI1 ChIP-Chip arrays.

ABCB1	CHODL	HIST1H2AC	LOC642891	OR52A1	POU1F1	TNFSF5IP1
AGL	CHRNA5	HIST1H2BL	LOC646215	OR52N5	PRKACB	TRPC3
AKAP7	CLEC5A	HIST1H2BM	LOC81558	OR56B1	RAP1B	TRPM8
AKR1C1	CNTF	HIST1H3H	LPHN2	OR5B2	RGS21	TUSC1
AKR1C3	COG6	HIST1H4B	LRRN3	OR5BU1	RHOB	TXNDC13
ALS2CR16	COMMD3	HIST1H4J	LRRTM4	OR5H14	RP1-32F7.2	UBE3A
AMELY	CRBN	HLA-DPA1	LST-3TM12	OR5H6	RP11-35N6.1	UFM1
AMY2B	CREM	HLA-DPB1	LUM	OR5K3	RP11-54H7.1	UGT2A1
ANXA1	CRYGS	HS322B1A	MAS1L	OR5K4	RP13-11B7.1	UNQ9356
APIN	CYLC2	HSFY1	MEF2A	OR5M3	RREB1	UTS2D
APRT	CYorf15A	HSFY2	MEP1A	OR5R1	RSRC1	UTY
ARHGEF7	CYorf15B	HSN2	MGAT4C	OR5T2	SERPINI2	VWA2
ASAH2	DEFB112	HTR2B	MGC33530	OR5V1	SGCG	WDSOF1
ASB4	DGKB	IFNA10	MGC34713	OR5W2	SGCZ	XRN1
ATF6	DIAPH3	IL12RB2	MGC35043	OR6M1	SHOX2	YIPF7
ATP5E	DNAJC5B	IL15	MGC35212	OR8H1	SI	ZNF306
AZI2	DSPP	IL17D	MKRN3	OR8H2	SLC12A1	ZNF614
BAZ2B	DTNA	IMPG2	MMP13	OR8I2	SLC16A7	
BCHE	ELOVL2	INVS	MTRF1L	OR8K3	SLC25A32	
BMP5	EYA1	JMJD1A	MUC7	OR9G1	SLC26A7	
C10orf61	FAM55D	KCNK10	MYL1	OR9G9	SLCO1B3	
C10orf68	FBXL7	KCNMB4	N/A	OTUD6B	SLITRK6	
C14orf10	FBXO4	KCTD4	NAP1L3	PALLD	SMC6L1	
C14orf150	FGB	KIAA0391	OGN	PCDH11X	SNPH	
C20orf103	FGF7	KIAA1712	OMD	PCDH15	SNRPN	
C21orf34	FGL2	KLF14	OR10T2	PCDHA1	SPAG6	
C3orf58	FH	KLHL4	OR11H4	PCDHA11	SPANXA1	
C4BPB	FLJ22662	KLHL9	OR13C3	PCDHA3	SPANXA2	
C4orf7	FLJ32745	KLRC4	OR13F1	PCDHB16	SPANXE	
C9orf102	FLJ43706	KLRK1	OR1Q1	PCDHB8	SPATA18	
C9orf150	FLJ44048	KRT12	OR2B11	PCDHGA12	TAF2	
CAB39L	FLJ46120	KRT24	OR2J3	PCDHGA9	TAIP-2	
CCDC46	FO XK2	KRTAP1-1	OR2L2	PDE1A	TAS2R7	
CD69	FYTTD1	KRTAP1-3	OR2L3	PHIP	TAS2R8	
CDH12	GABRG1	KRTAP4-12	OR2M5	PHYHIPL	TDRD4	
CDY2B	GALNT13	KRTAP6-3	OR2T10	PIGF	TEX15	
CENTD1	GLRA3	LCE3B	OR2T4	PLCB4	TFEC	
CEP76	GPR52	LEF1	OR4A47	PLRG1	TMEM77	
CEPT1	HHLA2	LOC129285	OR4C16	PMCH	TMPRSS11B	
CHL1		LOC401137	OR51A7	PNLIP	TNFSF18	

Full gene names are provided in Appendix E.

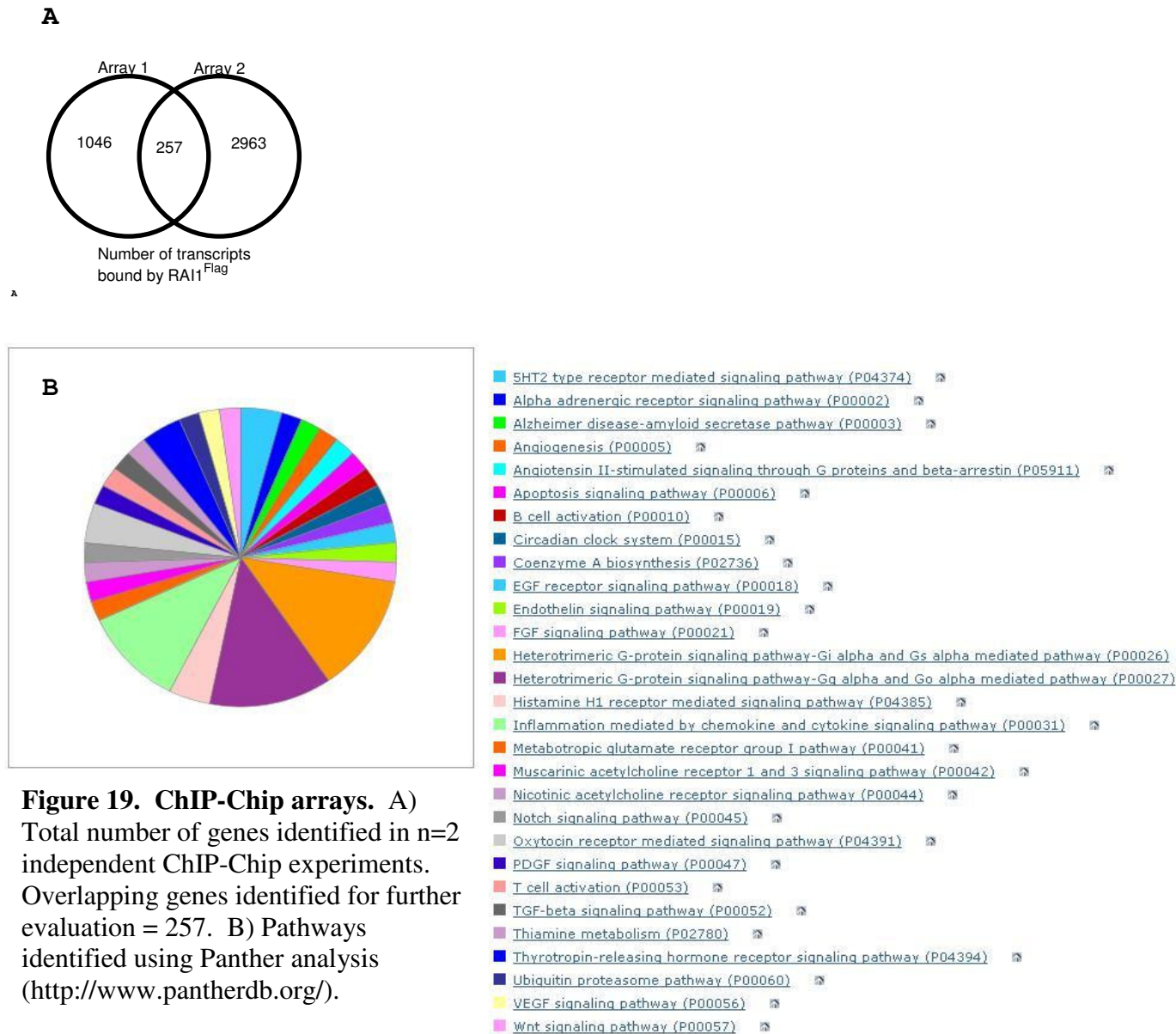


Figure 19. ChIP-Chip arrays. A) Total number of genes identified in n=2 independent ChIP-Chip experiments. Overlapping genes identified for further evaluation = 257. B) Pathways identified using Panther analysis (<http://www.pantherdb.org/>).

Table 13. Ranked order of top 10 gene regulatory regions identified in ChIP-Chip experiments. Disease relevance collected from Panther (www.pantherdb.org) and PubMed (<http://www.ncbi.nlm.nih.gov/sites/entrez?db=pubmed>)

Gene Symbol	Gene Name	Disease Relevance	FDR
<i>SNRPN</i>	Small nuclear ribonucleoprotein polypeptide	Prader-Willi and Angelman syndromes	0.05
<i>UBE3A</i>	Ubiquitin protein ligase E3A	Angelman syndrome	0.10
<i>BDNF</i>	Brain-derived neurotrophic factor	Obesity, neurotransmission, metabolism	0.18
<i>CLOCK</i>	Circadian locomotor output cycles kaput	Sleep, circadian rhythm mood disorder, schizophrenia, insomnia, obesity	0.19
<i>MEF2A</i>	Myocyte enhancer factor 2A	Muscle development, neuronal differentiation, cell growth control, apoptosis	0.15
<i>BMP5</i>	Bone morphogenetic protein 5	Skeletal development, dendritic growth	0.01
<i>TRPC3</i>	Transient receptor potential cation channel, subfamily C, member 3	Alzheimer syndrome, BDNF function	0.14
<i>BCHE</i>	Butyrylcholinesterase	Neurotransmission, drug metabolism, skeletal muscle development, butyrylcholinesterase deficiency	0.15
<i>CREM</i>	cAMP responsive element modulator	Apoptosis, transcription, cell cycle regulation	0.09

Genes identified for further evaluation

CLOCK: The mammalian circadian *locomotor output cycles kaput* (*CLOCK*) was identified and cloned by King et al. [137] in 1997. *CLOCK* is thought to be the master regulator of the central clock of circadian rhythm. The protein product of the *CLOCK* gene is a basic-helix-loop-helix transcription factor and heterodimerizes with BMAL1 to activate transcription of a variety of downstream genes essential for proper modulation of circadian rhythm. The period genes (*PER1*, *PER2*, *PER3*), the cryptochrome genes (*CRY1*, *CRY2*), the nuclear receptor subfamily 1 group D member 2 (*NR1D2/Rev-Erb β*), and RAR-related orphan receptor A genes (*RORA*, *RORB*, *RORC*). All of these genes have an E-box (consensus sequence: CANNTG) to which the CLOCK/BMAL1 complex binds.

SNRPN: The *small nuclear ribonucleoprotein polypeptide N* (*SNRPN*) resides in the Prader-Willi/Angelman syndromes region on chromosome 15q11.2. The protein encoded by this gene is one polypeptide of a small nuclear ribonucleoprotein complex and belongs to the snRNP SMB/SMN family. The protein may play a role in pre-mRNA processing. Although individual snRNPs are believed to recognize specific nucleic acid sequences through RNA-RNA base pairing, the specific role of *SNRPN* is unknown. The genomic location of *SNRPN* is on the opposite strand of the *SNURF* gene (*SNRPN* upstream reading frame) being transcribed on the sense strand. The 5' UTR of *SNRPN* has been identified as an imprinting center. The most common cause for Prader-Willi syndrome (PWS) is paternal microdeletion of *SNRPN* (del(15)(q11-q13)pat) resulting in ~70% of cases, while the second most common cause is maternal uniparental disomy (UPD) of chromosome 15 (15 (upd(15)mat)) [138]. Interestingly, there is strong overlap between the physical and behavioral phenotypes seen in PWS and SMS. This gene is being pursued by Anam Bashir (Elsea Lab)

UBE3A: *Ubiquitin protein ligase E3A (UBE3A)* is located on chromosome 15q11.2 and functions to target proteins for degradation. Ubiquitination is an important step in all cells as dysfunctional gene products must be removed from the cellular machinery by cellular structures such as proteasomes. *UBE3A* is ubiquitously expressed from both the paternal and maternal alleles except for the brain where only the maternal copy of the gene is expressed and the paternal copy is imprinted. Maternal deletion, mutation, or imprinting error of *UBE3A* results in Angelman syndrome (AS). The most common lesions leading to AS are a common large deletion of 15q11-q13 (~70%), paternal uniparental disomy (~1%), and an imprinting defect (~4%) [138]. Additionally, *UBE3A* mutation account for approximately 8% of cases [139]. Paternal UPD led investigators to the conclusion that AS involves a maternally expressed gene. Based on the finding of point mutations in patients with AS, *UBE3A* has been identified as the gene affected in AS. Interestingly, imprinted *UBE3A* expression is restricted to the brain only.

BDNF: *Brain-derived neurotrophic factor (BDNF)* is located on chromosome 11. It is primarily active in the hippocampus, cortex, basal forebrain, cerebellum and olfactory bulb. It is also found in the retina, central nervous system (CNS), motor neurons, kidneys, and the prostate. BDNF functions in neuronal survival, growth and differentiation of new neurons and synapses, as well as control of food intake. *BDNF* has recently been reported to regulate food intake and glucose homeostasis in genetically obese animal models [140]. The *Bdnf*^{+/-} mouse exhibits hyperphagic behavior and dramatic obesity [141]. Haploinsufficiency for *Bdnf* in mice was found to cause increased food intake, early-onset obesity, hyperactivity, and cognitive impairment [141]. Previous studies have also shown that up regulation of *Bdnf* rescued synaptic

plasticity, long-term memory deficits and behaviors of the mutant Huntington's disease mice [142]. *In vitro* overexpression of *Bdnf* increased axonal length and axonal branching in Rett syndrome, while preventing the decrease in dendritic length commonly seen with the disease [143]. This gene is being pursued by Sun Kim (Elsea lab)

RAI1 transcriptionally activates *CLOCK* via an intron 1 enhancer element

The downstream targets of *CLOCK* are well characterized. However, the transcriptional regulator of *CLOCK* has not been defined. Using peak data acquired from our dual ChIP-Chip assays we were able to identify a ~350 bp region where RAI1^{Flag} possibly binds. This element resides in intron 1 (Chr4:56072089- 56072440). Primers designed to flank this region were used to amplify this piece of genomic DNA, which was first cloned into the StrataClone TA cloning vector and then was subcloned into the pGL3-Promoter vector (*CLOCK*^{Luc}) which contains an SV40 promoter that provides baseline luciferase activity.

When RAI1^{Flag} is transfected with *CLOCK*^{Luc} there is a greater than 2-fold increase in luciferase activity (Figure 19). Taken together, the ChIP-Chip and luciferase data suggest that RAI1 binds, directly or in a complex, to the 1st intron of *CLOCK*, enhancing its transcriptional activity *in vitro*. Given these findings, it was logical to move forward with *in vivo* studies utilizing the *Rai1*^{+/-} mice.

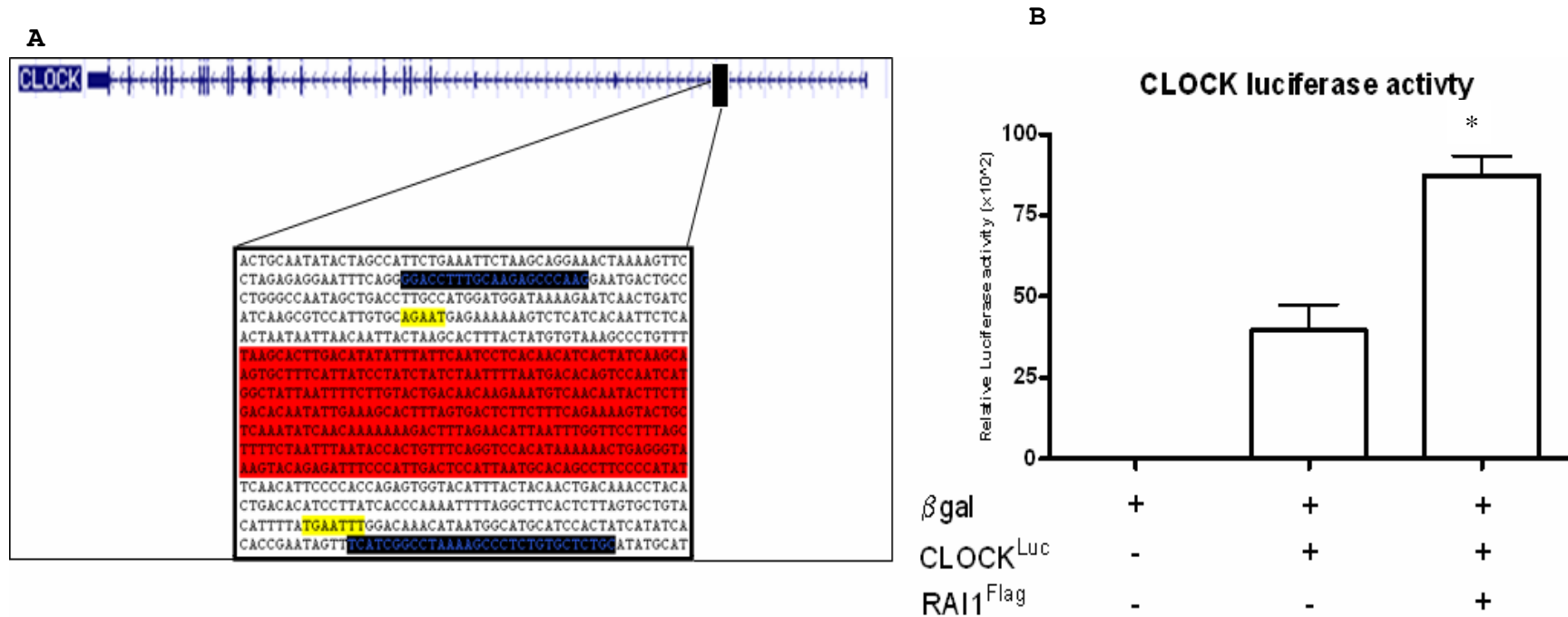


Figure 20. RAI1 impact on *CLOCK* transcription. A) Intron 1 *CLOCK* enhancer region used for luciferase assays. Shown in red: ~350bp region identified in Nimblegen array as most likely binding region of RAI1^{Flag}. Shown in yellow: Proposed RAI1 consensus binding sites as reported by Eri Kamura (Elsea Lab). Shown in black: PCR primers used to clone region (CLOCK^{Luc}) used for luciferase assays (724 bp). B) Luciferase activity of co-transfection of RAI1^{Flag} with CLOCK^{Luc} plasmids. N=3 studies with readings taken in duplicate. *, P=0.009.

Dysregulation of circadian genes in *Rai1*^{+/-} mice

Rai1^{+/-} mice are obese, hyperphagic, have decreased sensitivity to pain, low muscle strength, and an altered circadian rhythm [42, 45, 144]. Expression analysis of *Rai1*^{+/-} kidney and whole brain shows a marked decrease in both *Rai1* and *Clock* (mouse orthologue to *CLOCK*) (Figure 20). Additionally, expression of *Rai1* and *Clock* in the mouse hypothalamus showed reduced expression (Figure 21). Further, we analyzed the expression of downstream targets of *Clock* including *Per2*, *Npas2*, and *Nr1d2* in the mouse hypothalamus, all of which had reduced expression as compared to WT C57Bl/6J littermates during the day time hours. These data show that there is circadian dysregulation of gene expression in the *Rai1*^{+/-} mouse hypothalamus.

Next it was important to measure circadian gene expression in the mouse hypothalamus during the day time and night time hours to ensure that rhythmicity was not restored with regard to external cues such as feeding. Our results show that during the dark phase the expression of core circadian genes is dysregulated including *Per2* which when knocked out in mice results in a severe circadian phenotype [145] and *Nr1d2* which was identified as one of the top genes with reduced expression in a study of human cells knocked down for RAI1 [81] (Figure 22). Interestingly, *Clock* expression is upregulated in night time, suggesting a malfunction of the autoregulatory feedback loop.

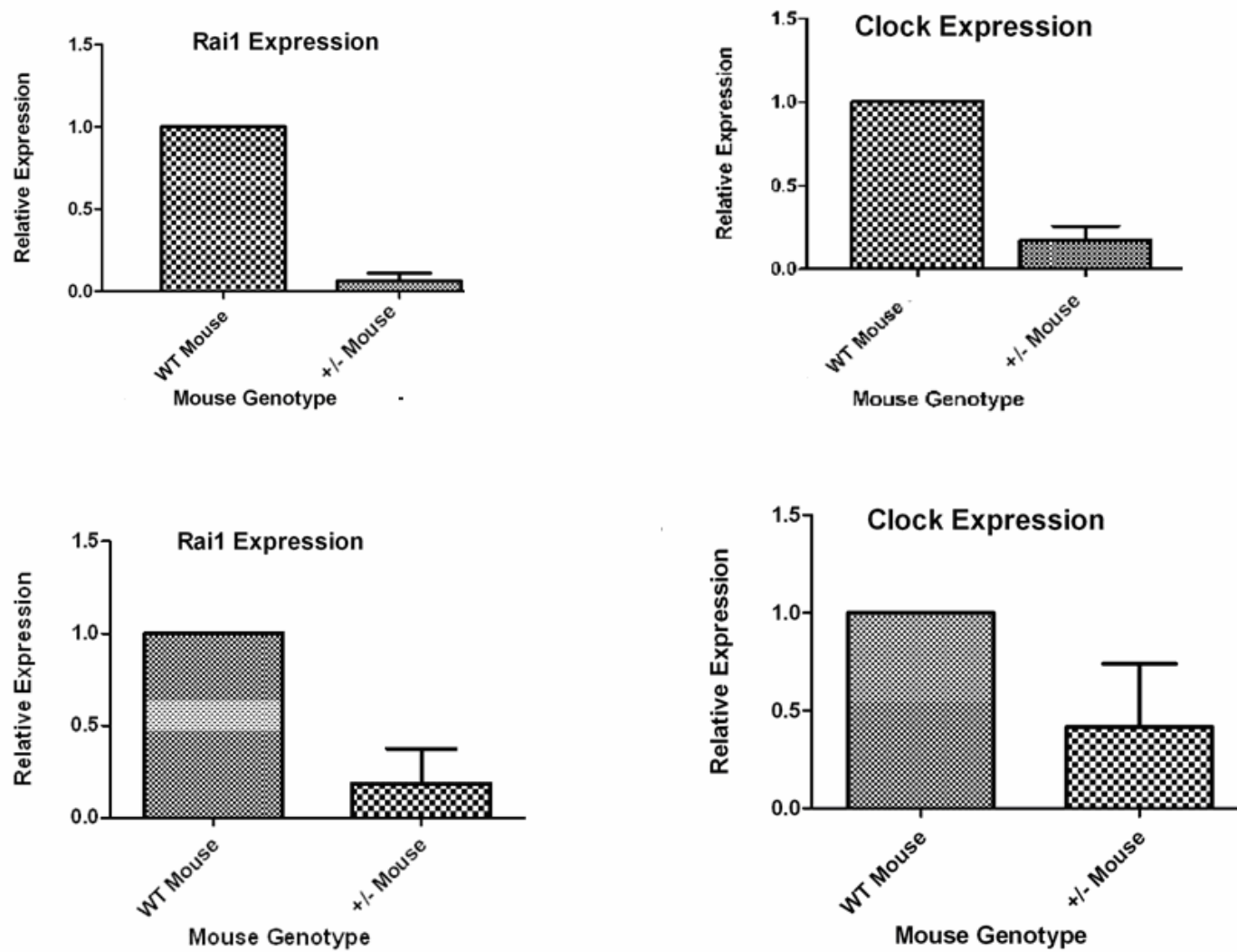


Figure 21. *Rai1* and *Clock* expression in mouse tissues. A-B) Mouse Brain. C-D) Mouse Kidney. N=3 mice per tissue. All mice sacrificed during the day time hours.

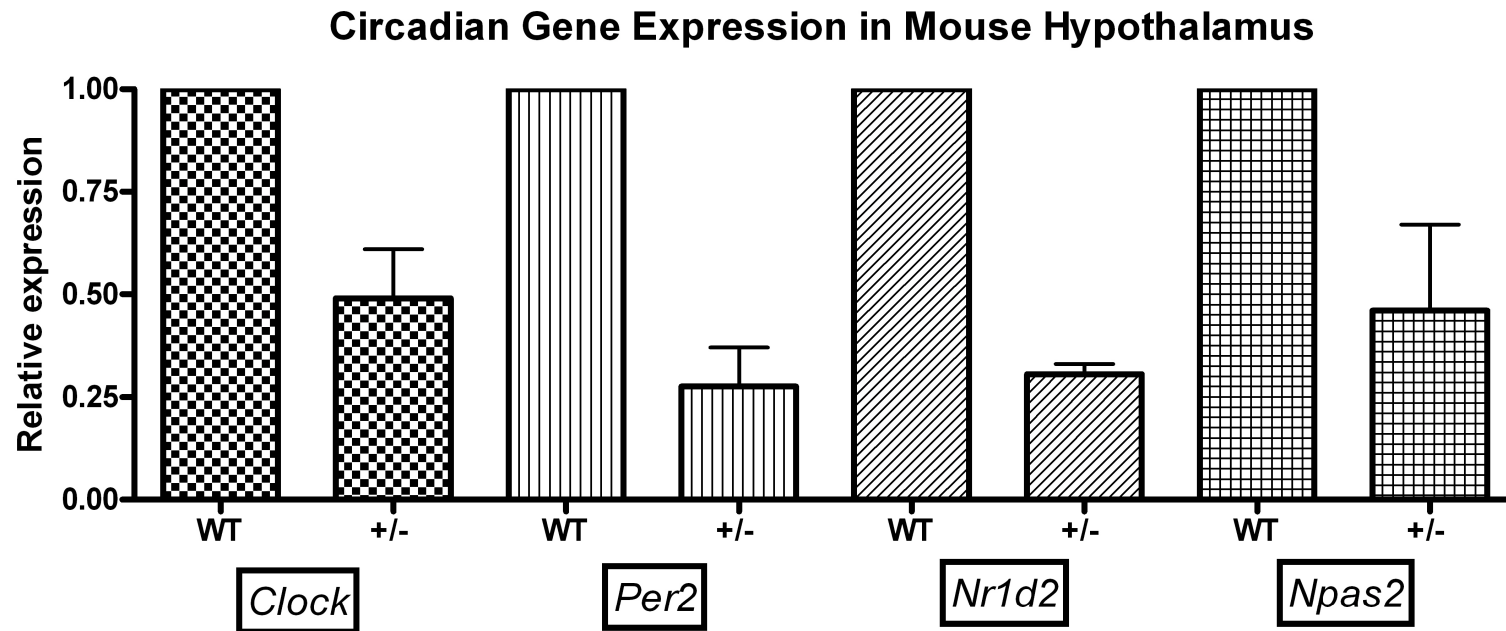


Figure 22. qPCR of circadian genes expressed in mouse hypothalamus. N=3 mice per tissue. All mice sacrificed during light phase.

Dysregulation of circadian genes in SMS fibroblasts

Human fibroblasts follow a 24 hr rhythmicity *in vitro* just as they would *in vivo*. To assess the circadian cycling of *RAI1*, *CLOCK*, and *NR1D2* we took RNA samples from unaffected (GM637), deletion (SMS182), and mutation (SMS175) cell lines. Transcription of all of these genes is dysregulated when compared to unaffected fibroblasts. It is worth while to note that the hypothesis to date, with regard to the inverted circadian rhythm seen in SMS, is that an inverted secretion of melatonin causes sleep disturbance. The data presented here suggest that this inverted circadian rhythm is likely due to a dysregulation of circadian gene expression, and the inverted melatonin secretion seen in the majority of cases is likely a byproduct of said dysregulation. Further supporting our hypothesis is the fact that C57BL6 mice do not secrete melatonin [146].

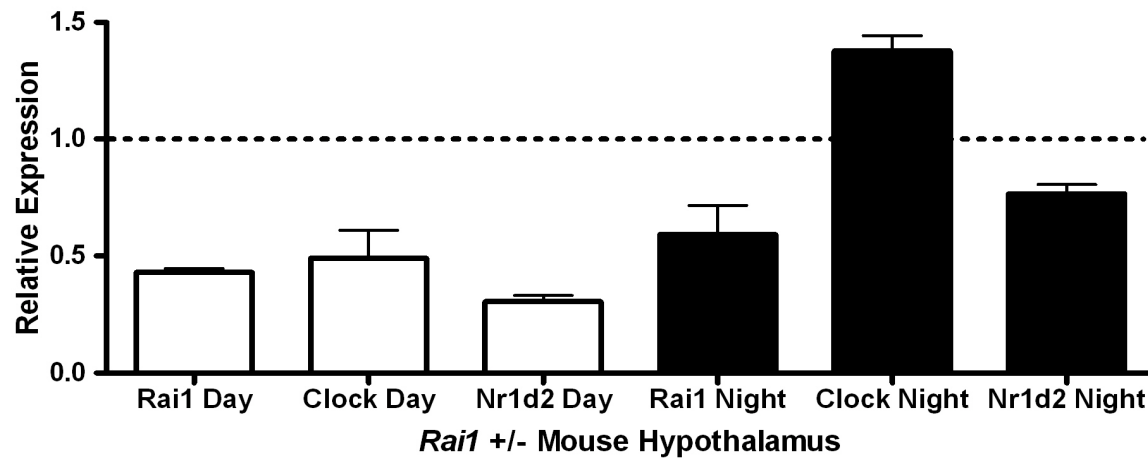


Figure 23. qPCR of core circadian gene expression in the mouse hypothalamus during day light (white boxes) and night time (black boxes) periods. Circadian rhythm remains disrupted during both light and dark phase hours relative to WT baseline at the same phase (1, dotted line). N=3 mice per tissue.

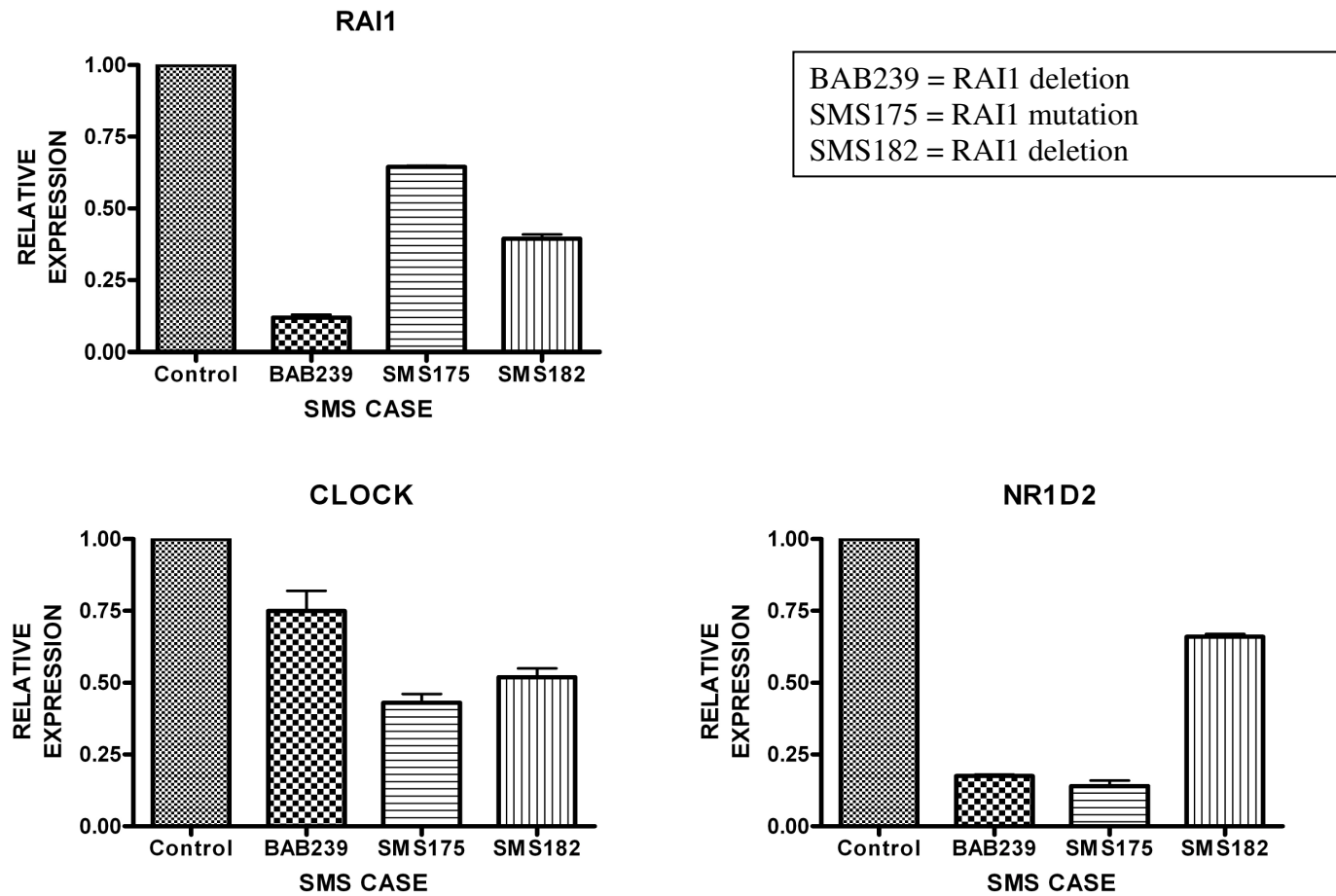


Figure24. Core circadian gene expression in unaffected and SMS fibroblasts. N=3 qPCR experiments per cell line performed in triplicate.

Discussion

The circadian rhythm defect seen in Smith-Magenis syndrome is thought to contribute to a more severe behavioral phenotype [14]. It is thought that if sleep rhythmicity is resolved, treatment of behavior becomes easier. This is why it is imperative to understand the molecular defects that result from *RAI1* mutation or deletion.

RAI1 is a proposed transcription factor containing a PHD domain and nuclear localization signal. However, it was previously unknown in what biochemical pathways *RAI1* functions and what genes it may regulate. Identification of the molecular changes and subsequent affected pathways that result from *RAI1* haploinsufficiency holds the potential for chemical, habitual, or nutritional based interventions.

The *Clock/Clock* mutant mice were created by King et al. in 1996 [147]. By using a forward genetics approach, mutagenesis followed breeding and positional cloning, the authors identified a mutant mouse with an A to T splice site mutation which results in deletion of 51 amino acids of the protein. This mutation disrupts exons 16, 17, and 18 of the 24-exon gene product. This *Clock* mutant mouse was bred to generate the *Clock/Clock* mutant mouse which has an erratic and unpredictable circadian sleep cycle, with loss of periodicity, as compared to WT littermates indicating its importance in circadian homeostasis [137]. As a complementary approach to positional cloning, Antoch et al. 1997 [148] used *in vivo* complementation with BAC clones expressed in transgenic mice to identify the circadian *Clock* gene. A *Clock* transgene completely rescued both the long-period and the loss-of-rhythm phenotypes in *Clock* mutant mice. These over expressing *Clock* mice revealed a shortened period length leading to the fact that *Clock* is a dosage sensitive gene. Surprisingly, when DeBruyne et al. created the *Clock*^{-/-}

complete knockout there was no loss of rhythmicity, indicating that multiple genes may play a critical role as “master regulators” or have compensatory effects [149].

As it is important to not only study the influence *RAI1* has on *CLOCK* it is also necessary to analyze further downstream effects. The *period circadian protein homolog 2* (*PER2*) is a very important circadian transcript involved with the correct rhythmicity of circadian cycling. The *Per2* homozygous mutation mouse (*Per2^{m/m}*) was created by Zheng et al. in 1999 [150]. This mouse contains a deletion in the PAS domain of the mouse *Per2* gene. The PAS domain is highly conserved in circadian clock genes from a variety of species [150]. The *Per2^{m/m}* mouse exhibits a variety of circadian phenotypes including a shorter circadian period in normal 12 hour light/12 hour dark conditions, followed by loss of circadian rhythmicity in constant darkness as measured by wheel running measurements [150]. Additionally, *Per1* mRNA levels were reduced in *Per2^{m/m}* mice, indicating that *Per2* is upstream of *Per1* [150].

Further, Girirajan et al. 2009 [81] identified *NR1D2* in a *RAI1* knockdown study in HEK293t cells. This study included siRNA knock-down of *RAI1* followed by microarray analysis. *NR1D2* was one of the top genes down regulated in this study and adds to the validity of our findings.

Polymorphisms in the key players of circadian rhythm (*CLOCK*, *BMAL1*, *PER3*) have been implicated in a variety of mood disorders in humans [151, 152]. Additionally, single nucleotide polymorphisms (SNPs) in *CLOCK* have been associated with defects including, bipolar disorder [153], insomnia with bipolar disorder [154, 155], major depressive disorder [156] and obesity. Additionally *BMAL1* [157, 158], *PER3* [157] and *TIMLESS* [158] have all been associated with bipolar disorder. The behavioral phenotype seen in Smith-Magenis syndrome has also been described as manic in some cases lending to the idea that disruption of

the circadian rhythm may not only complicate the behavioral phenotype but contribute directly to it.

Given the important role that *CLOCK* plays in circadian rhythm and its association with human disease, many studies have been performed to identify the function of *CLOCK*, but its transcriptional regulator(s) has remained vague. Here we present data that suggest that *RAI1* is an important enhancer of *CLOCK* transcription. Using both *in vivo* and *in vitro* tools we were able to show that *RAI1* regulates *CLOCK* via an enhancer region located in intron 1 which contains two proposed *RAI1* consensus binding sites identified by Eri Kamura (Elsea lab) [159].

These data suggest that *RAI1* plays an important role in maintaining circadian rhythmicity and because circadian rhythms impact development, sleep, and behavior these findings should help to further delineate the pathways involved in syndromes wherein these functions are disrupted. Additionally, as better treatments are developed to target these pathways, we may one day be able to correct many of the sleep and behavioral phenotypes seen in Smith-Magenis syndrome.

Chapter 6

Summary

These studies have identified new loci associated with a Smith-Magenis-like phenotype. We have shown that SMS and SMS-like cohorts are not different with regard to the core phenotypes seen most commonly in SMS. We have also shown that alternate loci, that when deleted or duplicated, can result in a phenotype similar to SMS. Additionally, we have been able to make phenotypic connections between SMS and SMS-like syndromes which has already improved diagnosis of these disorders (Chapter 2).

The broad aCGH study allowed us to explore in detail the deletion 2q23 syndrome. Using overlapping deletions from our case, as well as new and reported cases, we were able to better define the phenotype of this syndrome, as well as narrow the critical region to one gene, *MBD5*. We believe that haploinsufficiency of *MBD5* contributes to the major phenotypes in deletion 2q23 syndrome, including microcephaly, intellectual disabilities, severe speech impairment, and seizures (Chapter 3). We believe that mutation screening of *MBD5* in individuals with a similar phenotype is an appropriate next step in confirming the weight of contribution that *MBD5* holds in this rare syndrome.

Additionally, using a similar approach as in Chapter 3 we were able to refine the critical region for Brachydactyly Mental Retardation syndrome (deletion 2q37 syndrome) and identified an insertion mutation of *HDAC4* in one case, SMS117. Mutation of *HDAC4* likely contributes to the major phenotypes seen in BDMR and identification of more mutation cases is likely in the future (Chapter 4).

Lastly, we were able to characterize, in part, the molecular function of *RAI1*, the gene that when mutated or deleted results in Smith-Magenis syndrome. There is a strong circadian

phenotype associated with SMS wherein subjects have consistent night awakenings with frequent day time napping. We believe that *RAI1* plays a significant role in the central circadian pathway. Using both *in vivo* and *in vitro* methods, we have shown that *RAI1* regulates *CLOCK* gene expression, which is a novel breakthrough, as the transcriptional regulators of *CLOCK* have not been defined (Chapter 5).

Taken together these studies have further defined and refined the molecular root for each syndrome. However, the question remains: “What specific pathways and genes are logical to explore in the future with regard to these syndromes and the impact of *RAI1* on human development and behavior?”

Development

In an exploratory bioinformatic study by Danielle Bartholomew (Elsea lab) *MEF* binding sites in the 5' untranslated region of *RAI1* were identified. As stated above *MEF2C* activity is necessary for proper chondrocyte hypertrophy and bone development. *MEF2C* is also inhibited by *HDAC4*. Additionally, the *bone morphogenic protein 5* gene (*BMP5*), a member of the transforming growth factor-beta superfamily of regulatory molecules, was identified in our ChIP-Chip studies lending to the idea that *RAI1* regulates it on the transcriptional level. *BMP5* is necessary for proper skeletogenesis, and *BMP5* mutant mice have a variety of skeletal and soft tissue abnormalities [160]. It is also worthwhile to note that *BMP5* has been shown to elicit dendritic growth *in vitro* [161], which may contribute to some of the neurological phenotypes seen in SMS. In these studies we have shown that mutation of *HDAC4* results in many of the features seen in SMS as well as distinct brachydactyly not seen in SMS, which is logical considering *HDAC4* may be upstream of *RAI1* (Figure 24). My belief is that *MEF2C* is a

positive regulator of *RAI1* transcription which is modulated by HDAC4. I also believe that *RAI1* may be a positive regulator of *BMP5* ultimately leading to proper skeletal development (Figure 24). However, it must be mentioned that HDAC4 is also a regulator of *RUNX2* which is known to be necessary for proper skeletogenesis suggesting multiple pathways involved. Additionally, as shown in Tables 12 and 13 *RAI1* may regulate *MEF2A* suggesting a possible autoregulatory feedback loop with regard to *RAI1* function in skeletogenesis.

Behavior and sleep

The behavioral phenotypes seen in SMS and SMS-like syndromes are significant. They include, but are not limited to, verbal outbursts, temper tantrums, self-abusive behavior, and stereotypies. These phenotypes all have a strong neurological element and are complicated by sleep disturbance. It has been shown that solving the sleep problems seen in SMS may relieve many of the behavioral phenotypes [14]. It is my proposition that *RAI1* plays a major role in circadian rhythm and that when *RAI1* is mutated or deleted the resulting behavioral phenotypes are a direct result of this haploinsufficiency.

We have shown here that *RAI1* is a positive regulator of *CLOCK*, the master regulator of central circadian gene expression. We used both animal models and cell based studies to show the disruption of the circadian cycle in SMS subjects. *CLOCK* has been shown to be associated with a variety of disorders including schizophrenia, bipolar disorder, mania and depression all of which have elements seen in the SMS phenotype. A schematic of the influence *RAI1* has on the circadian cycle can be seen in Figure 25.

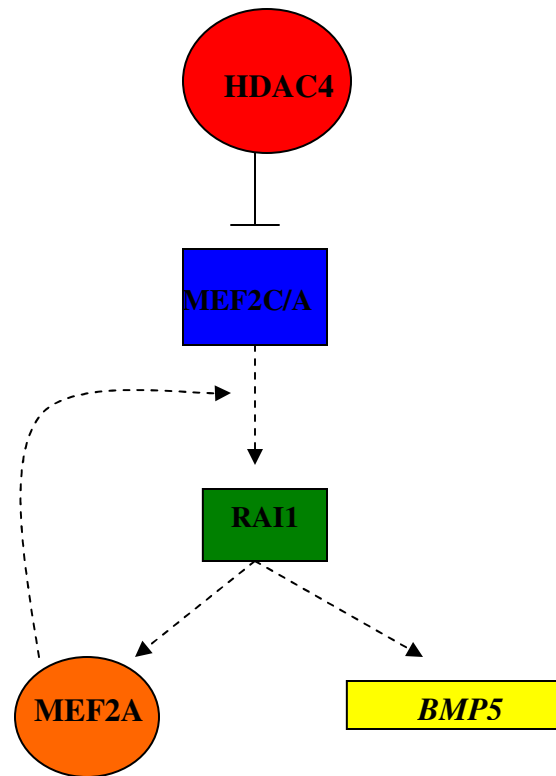


Figure 25. Proposed schematic of *RAI1* contribution to proper skeletal development. HDAC4 negatively regulates MEF2C on the protein level which then leads to reduced *RAI1* transcription leading to skeletal, neurological and behavioral phenotypes . Reduced *RAI1* transcription then leads to reduced *BMP5* and *MEF2A* transcription which may then lead to neurological and skeletal phenotypes as well as malfunction of the proposed feedback loop.

Theoretically, if *CLOCK* expression is reduced, downstream gene expression would also be reduced. This could have a variety of impacts; molecularly, this reduction of *CLOCK* and downstream genes would also result in dysregulation of the regulatory feedback loops. Clinically, this could result in an altered sleep cycle, mood disorder and even learning disability and developmental problems.

Future directions

With regard to the SMS-like study and resulting studies (Chapters 2-4), I would like to see more subjects ascertained and screened for *HDAC4* and *MBD5* mutations. I would also like to see molecular characterization of these mutations. For example, cDNA from subjects with mutations could be collected and cloned into a variety of vectors. A Flag vector already in use in the Elsea lab could be used to perform IP studies to identify presence or absence of specific binding partners. Also, stable transfection of these mutant alleles could help to identify whether they are functionally active and able to perform their transcriptional roles on downstream genes. The molecular follow up will allow further insight into the pathways involved in these syndromes and how mutation specifically affects pathways. I would also like to see a detailed panel of molecular tests, including aCGH, MLPA and gene sequencing, and phenotypic check lists developed such that the proper diagnosis for these individuals may be more easily acquired in the future, helping families, clinicians, and the subjects themselves.

With regard to the molecular function of *RAI1*, I would like to see a variety of studies performed. First and foremost I think that follow up with the remaining genes of interest from the ChIP-Chip study is imperative, specifically the top 10 genes identified in Table 13. Additionally, I would like to see a study performed that identifies binding partners of *RAI1*.

This can be easily performed utilizing the *RAI1*^{Flag} plasmid already available with IP and mass spec analysis. Alternatively, the *RAI1* coding sequence could easily be cloned into a vector containing a HIS-tag and column chromatography could be utilized which may reduce some of the background associated with IP. If *RAI1* binds to a well characterized protein, this will allow us further insight into the molecular functions of *RAI1* and possibly lead us to proteins that regulate *RAI1* on the transcriptional level. Cloning of the *RAI1* promoter would also help with this endeavor (being pursued by Dr. Deborah Zies). I would also like to see the *Rai1*^{+/-} mice crossed with the *Clock*^{-/-} mice which do not have a circadian phenotype. If the resulting mice do have a strong circadian phenotype we may be able to identify alternative circadian pathways that *RAI1* influences outside of *CLOCK* transcription. These studies will not only help SMS and SMS-like subjects but could have impact on the general public and those with psychiatric disorders.

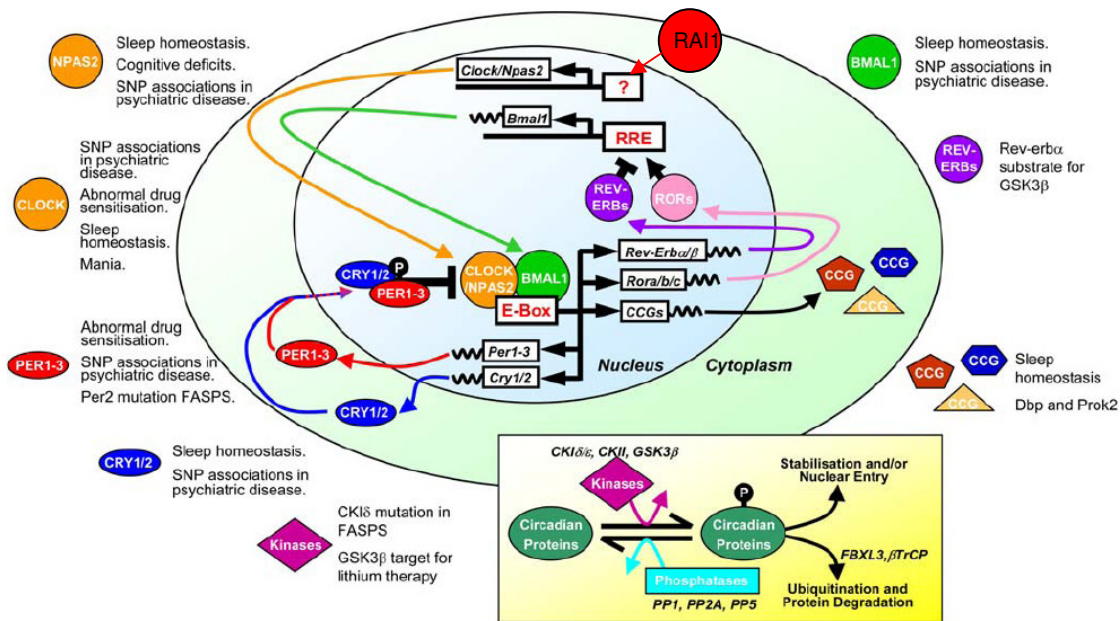


Figure 26. RAI1 regulates clock transcription and is a major element in the circadian cycle. Modified from Nolan et al. 2008.

References

- 1 Wagenstaller J, Spranger S, Lorenz-Depiereux B, Kazmierczak B, Nathrath M, Wahl D, Heye B, Glaser D, Liebscher V, Meitinger T, Strom TM. Copy-number variations measured by single-nucleotide-polymorphism oligonucleotide arrays in patients with mental retardation. *Am J Hum Genet* 2007;**81**(4):768-79.
- 2 Williams SR, Mullegama SV, Rosenfeld JA, Dagli AI, Hatchwell E, Allen WP, Williams CA, Elsea SH. Haploinsufficiency of MBD5 associated with a syndrome involving microcephaly, intellectual disabilities, severe speech impairment, and seizures. *Eur J Hum Genet*; **18**(4):436-41.
- 3 Smith AC, McGavran L, Robinson J, Waldstein G, Macfarlane J, Zonona J, Reiss J, Lahr M, Allen L, Magenis E. Interstitial deletion of (17)(p11.2p11.2) in nine patients. *Am J Med Genet* 1986;**24**(3):393-414.
- 4 Slager RE, Newton TL, Vlangos CN, Finucane B, Elsea SH. Mutations in RAI1 associated with Smith-Magenis syndrome. *Nat Genet* 2003;**33**(4):466-8.
- 5 Shinawi M, Cheung SW. The array CGH and its clinical applications. *Drug Discov Today* 2008.
- 6 Yatsenko SA, Treadwell-Deering D, Krull K, Lewis RA, Glaze D, Stankiewicz P, Lupski JR, Potocki L. Trisomy 17p10-p12 due to mosaic supernumerary marker chromosome: delineation of molecular breakpoints and clinical phenotype, and comparison to other proximal 17p segmental duplications. *Am J Med Genet A* 2005;**138**(2):175-80.
- 7 Zhang F, Potocki L, Sampson JB, Liu P, Sanchez-Valle A, Robbins-Furman P, Navarro AD, Wheeler PG, Spence JE, Brasington CK, Withers MA, Lupski JR. Identification of

- uncommon recurrent Potocki-Lupski syndrome-associated duplications and the distribution of rearrangement types and mechanisms in PTLS. *Am J Hum Genet*; **86**(3):462-70.
- 8 Turner DJ, Miretti M, Rajan D, Fiegler H, Carter NP, Blayney ML, Beck S, Hurles ME. Germline rates of de novo meiotic deletions and duplications causing several genomic disorders. *Nat Genet* 2008;**40**(1):90-5.
 - 9 Lee JA, Carvalho CM, Lupski JR. A DNA replication mechanism for generating nonrecurrent rearrangements associated with genomic disorders. *Cell* 2007;**131**(7):1235-47.
 - 10 Feuk L, Carson AR, Scherer SW. Structural variation in the human genome. *Nat Rev Genet* 2006;**7**(2):85-97.
 - 11 Lupski JR. Genomic rearrangements and sporadic disease. *Nat Genet* 2007;**39**(7 Suppl):S43-7.
 - 12 Bi W, Yan J, Stankiewicz P, Park SS, Walz K, Boerkoel CF, Potocki L, Shaffer LG, Devriendt K, Nowaczyk MJ, Inoue K, Lupski JR. Genes in a refined Smith-Magenis syndrome critical deletion interval on chromosome 17p11.2 and the syntenic region of the mouse. *Genome Res* 2002;**12**(5):713-28.
 - 13 Redon R, Ishikawa S, Fitch KR, Feuk L, Perry GH, Andrews TD, Fiegler H, Shapero MH, Carson AR, Chen W, Cho EK, Dallaire S, Freeman JL, Gonzalez JR, Gratacos M, Huang J, Kalaitzopoulos D, Komura D, MacDonald JR, Marshall CR, Mei R, Montgomery L, Nishimura K, Okamura K, Shen F, Somerville MJ, Tchinda J, Valsesia A, Woodwark C, Yang F, Zhang J, Zerjal T, Zhang J, Armengol L, Conrad DF, Estivill

- X, Tyler-Smith C, Carter NP, Aburatani H, Lee C, Jones KW, Scherer SW, Hurles ME. Global variation in copy number in the human genome. *Nature* 2006;**444**(7118):444-54.
- 14 Elsea SH, Girirajan S. Smith-Magenis syndrome. *Eur J Hum Genet* 2008;**16**(4):412-21.
 - 15 Zori RT, Lupski JR, Heju Z, Greenberg F, Killian JM, Gray BA, Driscoll DJ, Patel PI, Zackowski JL. Clinical, cytogenetic, and molecular evidence for an infant with Smith-Magenis syndrome born from a mother having a mosaic 17p11.2p12 deletion. *Am J Med Genet* 1993;**47**(4):504-11.
 - 16 Allanson JE, Greenberg F, Smith AC. The face of Smith-Magenis syndrome: a subjective and objective study. *J Med Genet* 1999;**36**(5):394-7.
 - 17 Tomona N, Smith AC, Guadagnini JP, Hart TC. Craniofacial and dental phenotype of Smith-Magenis syndrome. *Am J Med Genet A* 2006;**140**(23):2556-61.
 - 18 Edelman E, Girirajan S, Finucane B, Patel P, Lupski J, Smith A, Elsea S. Gender, genotype, and phenotype differences in Smith-Magenis syndrome: a meta-analysis of 105 cases. *Clin Genet* 2007;**71**(6):540-50.
 - 19 Smith AC, Dykens E, Greenberg F. Sleep disturbance in Smith-Magenis syndrome (del 17 p11.2). *Am J Med Genet* 1998;**81**(2):186-91.
 - 20 Gropman AL, Elsea S, Duncan WC, Jr., Smith AC. New developments in Smith-Magenis syndrome (del 17p11.2). *Curr Opin Neurol* 2007;**20**(2):125-34.
 - 21 Di Cicco M, Padoan R, Felisati G, Dilani D, Moretti E, Guerneri S, Selicorni A. Otorhinolaryngologic manifestation of Smith-Magenis syndrome. *Int J Pediatr Otorhinolaryngol* 2001;**59**(2):147-50.
 - 22 Greenberg F, Lewis RA, Potocki L, Glaze D, Parke J, Killian J, Murphy MA, Williamson D, Brown F, Dutton R, McCluggage C, Friedman E, Sulek M, Lupski JR. Multi-

- disciplinary clinical study of Smith-Magenis syndrome (deletion 17p11.2). *Am J Med Genet* 1996;**62**(3):247-54.
- 23 Liburd N, Ghosh M, Riazuddin S, Naz S, Khan S, Ahmed Z, Riazuddin S, Liang Y, Menon PS, Smith T, Smith AC, Chen KS, Lupski JR, Wilcox ER, Potocki L, Friedman TB. Novel mutations of MYO15A associated with profound deafness in consanguineous families and moderately severe hearing loss in a patient with Smith-Magenis syndrome. *Hum Genet* 2001;**109**(5):535-41.
 - 24 Chen RM, Lupski JR, Greenberg F, Lewis RA. Ophthalmic manifestations of Smith-Magenis syndrome. *Ophthalmology* 1996;**103**(7):1084-91.
 - 25 Finucane BM, Jaeger ER, Kurtz MB, Weinstein M, Scott CI, Jr. Eye abnormalities in the Smith-Magenis contiguous gene deletion syndrome. *Am J Med Genet* 1993;**45**(4):443-6.
 - 26 Moeschler JB, Shevell M. Clinical genetic evaluation of the child with mental retardation or developmental delays. *Pediatrics* 2006;**117**(6):2304-16.
 - 27 Madduri N, Peters SU, Voigt RG, Llorente AM, Lupski JR, Potocki L. Cognitive and adaptive behavior profiles in Smith-Magenis syndrome. *J Dev Behav Pediatr* 2006;**27**(3):188-92.
 - 28 Gropman AL, Duncan WC, Smith AC. Neurologic and developmental features of the Smith-Magenis syndrome (del 17p11.2). *Pediatr Neurol* 2006;**34**(5):337-50.
 - 29 Smith AC, Dykens E, Greenberg F. Behavioral phenotype of Smith-Magenis syndrome (del 17p11.2). *Am J Med Genet* 1998;**81**(2):179-85.
 - 30 Boudreau EA, Johnson KP, Jackman AR, Blancato J, Huizing M, Bendavid C, Jones M, Chandrasekharappa SC, Lewy AJ, Smith AC, Magenis RE. Review of disrupted sleep

- patterns in Smith-Magenis syndrome and normal melatonin secretion in a patient with an atypical interstitial 17p11.2 deletion. *Am J Med Genet A* 2009;**149A**(7):1382-91.
- 31 Dykens EM, Finucane BM, Gayley C. Brief report: cognitive and behavioral profiles in persons with Smith-Magenis syndrome. *J Autism Dev Disord* 1997;**27**(2):203-11.
 - 32 Greenberg F, Guzzetta V, Montes de Oca-Luna R, Magenis RE, Smith AC, Richter SF, Kondo I, Dobyns WB, Patel PI, Lupski JR. Molecular analysis of the Smith-Magenis syndrome: a possible contiguous-gene syndrome associated with del(17)(p11.2). *Am J Hum Genet* 1991;**49**(6):1207-18.
 - 33 Dykens EM, Smith AC. Distinctiveness and correlates of maladaptive behaviour in children and adolescents with Smith-Magenis syndrome. *J Intellect Disabil Res* 1998;**42** (Pt 6):481-9.
 - 34 Girirajan S, Vlangos CN, Szomju BB, Edelman E, Trevors CD, Dupuis L, Nezarati M, Bunyan DJ, Elsea SH. Genotype-phenotype correlation in Smith-Magenis syndrome: evidence that multiple genes in 17p11.2 contribute to the clinical spectrum. *Genet Med* 2006;**8**(7):417-27.
 - 35 Treadwell-Deering DE, Powell MP, Potocki L. Cognitive and behavioral characterization of the Potocki-Lupski syndrome (duplication 17p11.2). *J Dev Behav Pediatr*;**31**(2):137-43.
 - 36 Potocki L, Bi W, Treadwell-Deering D, Carvalho CM, Eifert A, Friedman EM, Glaze D, Krull K, Lee JA, Lewis RA, Mendoza-Londono R, Robbins-Furman P, Shaw C, Shi X, Weissenberger G, Withers M, Yatsenko SA, Zackai EH, Stankiewicz P, Lupski JR. Characterization of Potocki-Lupski syndrome (dup(17)(p11.2p11.2)) and delineation of a

- dosage-sensitive critical interval that can convey an autism phenotype. *Am J Hum Genet* 2007;**80**(4):633-49.
- 37 Potocki L, Chen KS, Park SS, Osterholm DE, Withers MA, Kimonis V, Summers AM, Meschino WS, Anyane-Yeboa K, Kashork CD, Shaffer LG, Lupski JR. Molecular mechanism for duplication 17p11.2- the homologous recombination reciprocal of the Smith-Magenis microdeletion. *Nat Genet* 2000;**24**(1):84-7.
- 38 Waterston RH, Lindblad-Toh K, Birney E, Rogers J, Abril JF, Agarwal P, Agarwala R, Ainscough R, Alexandersson M, An P, Antonarakis SE, Attwood J, Baertsch R, Bailey J, Barlow K, Beck S, Berry E, Birren B, Bloom T, Bork P, Botcherby M, Bray N, Brent MR, Brown DG, Brown SD, Bult C, Burton J, Butler J, Campbell RD, Carninci P, Cawley S, Chiaromonte F, Chinwalla AT, Church DM, Clamp M, Clee C, Collins FS, Cook LL, Copley RR, Coulson A, Couronne O, Cuff J, Curwen V, Cutts T, Daly M, David R, Davies J, Delehaunty KD, Deri J, Dermitzakis ET, Dewey C, Dickens NJ, Diekhans M, Dodge S, Dubchak I, Dunn DM, Eddy SR, Elnitski L, Emes RD, Eswara P, Eyraas E, Felsenfeld A, Fewell GA, Flicek P, Foley K, Frankel WN, Fulton LA, Fulton RS, Furey TS, Gage D, Gibbs RA, Glusman G, Gnerre S, Goldman N, Goodstadt L, Grafham D, Graves TA, Green ED, Gregory S, Guigo R, Guyer M, Hardison RC, Haussler D, Hayashizaki Y, Hillier LW, Hinrichs A, Hlavina W, Holzer T, Hsu F, Hua A, Hubbard T, Hunt A, Jackson I, Jaffe DB, Johnson LS, Jones M, Jones TA, Joy A, Kamal M, Karlsson EK, Karolchik D, Kasprzyk A, Kawai J, Keibler E, Kells C, Kent WJ, Kirby A, Kolbe DL, Korf I, Kucherlapati RS, Kulbokas EJ, Kulp D, Landers T, Leger JP, Leonard S, Letunic I, Levine R, Li J, Li M, Lloyd C, Lucas S, Ma B, Maglott DR, Mardis ER, Matthews L, Mauceli E, Mayer JH, McCarthy M, McCombie WR, McLaren S,

- McLay K, McPherson JD, Meldrim J, Meredith B, Mesirov JP, Miller W, Miner TL, Mongin E, Montgomery KT, Morgan M, Mott R, Mullikin JC, Muzny DM, Nash WE, Nelson JO, Nhan MN, Nicol R, Ning Z, Nusbaum C, O'Connor MJ, Okazaki Y, Oliver K, Overton-Larty E, Pachter L, Parra G, Pepin KH, Peterson J, Pevzner P, Plumb R, Pohl CS, Poliakov A, Ponce TC, Ponting CP, Potter S, Quail M, Reymond A, Roe BA, Roskin KM, Rubin EM, Rust AG, Santos R, Sapojnikov V, Schultz B, Schultz J, Schwartz MS, Schwartz S, Scott C, Seaman S, Searle S, Sharpe T, Sheridan A, Shownkeen R, Sims S, Singer JB, Slater G, Smit A, Smith DR, Spencer B, Stabenau A, Stange-Thomann N, Sugnet C, Suyama M, Tesler G, Thompson J, Torrents D, Trevaskis E, Tromp J, Ucla C, Ureta-Vidal A, Vinson JP, Von Niederhausern AC, Wade CM, Wall M, Weber RJ, Weiss RB, Wendl MC, West AP, Wetterstrand K, Wheeler R, Whelan S, Wierzbowski J, Willey D, Williams S, Wilson RK, Winter E, Worley KC, Wyman D, Yang S, Yang SP, Zdobnov EM, Zody MC, Lander ES. Initial sequencing and comparative analysis of the mouse genome. *Nature* 2002;**420**(6915):520-62.
- 39 Walz K, Caratini-Rivera S, Bi W, Fonseca P, Mansouri DL, Lynch J, Vogel H, Noebels JL, Bradley A, Lupski JR. Modeling del(17)(p11.2p11.2) and dup(17)(p11.2p11.2) contiguous gene syndromes by chromosome engineering in mice: phenotypic consequences of gene dosage imbalance. *Mol Cell Biol* 2003;**23**(10):3646-55.
- 40 Girirajan S, Williams SR, Garben JY, Nowak NJ, Hatchwell E, Elsea S. 17p11.2p12 triplication and del(17)q11.2q12 in a severely affected child with dup(17)p11.2p12 syndrome *Clin Genet* 2007;**71**:1-12, In Press.

- 41 Walz K, Spencer C, Kaasik K, Lee CC, Lupski JR, Paylor R. Behavioral characterization of mouse models for Smith-Magenis syndrome and dup(17)(p11.2p11.2). *Hum Mol Genet* 2004;**13**(4):367-78.
- 42 Bi W, Ohyama T, Nakamura H, Yan J, Visvanathan J, Justice MJ, Lupski JR. Inactivation of Rai1 in mice recapitulates phenotypes observed in chromosome engineered mouse models for Smith-Magenis syndrome. *Hum Mol Genet* 2005;**14**(8):983-95.
- 43 Girirajan S, Patel N, Slager RE, Tokarz ME, Bucan M, Wiley JL, Elsea SH. How much is too much? Phenotypic consequences of Rai1 overexpression in mice. *Eur J Hum Genet* 2008;**16**(8):941-54.
- 44 Girirajan S, Elsea SH. Abnormal maternal behavior, altered sociability, and impaired serotonin metabolism in Rai1-transgenic mice. *Mamm Genome* 2009;**20**(4):247-55.
- 45 Bi W, Yan J, Shi X, Yuva-Paylor LA, Antalffy BA, Goldman A, Yoo JW, Noebels JL, Armstrong DL, Paylor RE, Lupski JR. Rai1 deficiency in mice causes learning impairments and motor dysfunctions whereas Rai1 heterozygous mice display minimal behavioral phenotypes. *Hum Mol Genet* 2007.
- 46 Walz K, Paylor R, Yan J, Bi W, Lupski JR. Rai1 duplication causes physical and behavioral phenotypes in a mouse model of dup(17)(p11.2p11.2). *J Clin Invest* 2006;**116**(11):3035-41.
- 47 McLaren J, Bryson SE. Review of recent epidemiological studies of mental retardation: prevalence, associated disorders, and etiology. *Am J Ment Retard* 1987;**92**(3):243-54.
- 48 Roeleveld N, Zielhuis GA, Gabreels F. The prevalence of mental retardation: a critical review of recent literature. *Dev Med Child Neurol* 1997;**39**(2):125-32.

- 49 Flint J, Knight S. The use of telomere probes to investigate submicroscopic rearrangements associated with mental retardation. *Curr Opin Genet Dev* 2003;**13**(3):310-6.
- 50 Hunter AG. Outcome of the routine assessment of patients with mental retardation in a genetics clinic. *Am J Med Genet* 2000;**90**(1):60-8.
- 51 Knight SJ, Lese CM, Precht KS, Kuc J, Ning Y, Lucas S, Regan R, Brenan M, Nicod A, Lawrie NM, Cardy DL, Nguyen H, Hudson TJ, Riethman HC, Ledbetter DH, Flint J. An optimized set of human telomere clones for studying telomere integrity and architecture. *Am J Hum Genet* 2000;**67**(2):320-32.
- 52 Rauch A, Hoyer J, Guth S, Zweier C, Kraus C, Becker C, Zenker M, Huffmeier U, Thiel C, Ruschendorf F, Nurnberg P, Reis A, Trautmann U. Diagnostic yield of various genetic approaches in patients with unexplained developmental delay or mental retardation. *Am J Med Genet A* 2006;**140**(19):2063-74.
- 53 Vlangos CN, Wilson M, Blancato J, Smith AC, Elsea SH. Diagnostic FISH probes for del(17)(p11.2p11.2) associated with Smith-Magenis syndrome should contain the RAI1 gene. *Am J Med Genet A* 2005;**132**(3):278-82.
- 54 Girirajan S, Elsas LJ, 2nd, Devriendt K, Elsea SH. RAI1 variations in Smith-Magenis syndrome patients without 17p11.2 deletions. *J Med Genet* 2005;**42**(11):820-8.
- 55 Shevell MI, Bejjani BA, Srour M, Rorem EA, Hall N, Shaffer LG. Array comparative genomic hybridization in global developmental delay. *Am J Med Genet B Neuropsychiatr Genet* 2008;**147B**(7):1101-8.
- 56 Slavotinek AM. Novel microdeletion syndromes detected by chromosome microarrays. *Hum Genet* 2008;**124**(1):1-17.

- 57 Nowak NJ, Miecznikowski J, Moore SR, Gaile D, Bobadilla D, Smith DD, Kernstine K, Forman SJ, Mhawech-Fauceglia P, Reid M, Stoler D, Loree T, Rigual N, Sullivan M, Weiss LM, Hicks D, Slovak ML. Challenges in array comparative genomic hybridization for the analysis of cancer samples. *Genet Med* 2007;**9**(9):585-95.
- 58 Nowak NJ, Snijders AM, Conroy JM, Albertson DG. The BAC resource: tools for array CGH and FISH. *Curr Protoc Hum Genet* 2005;**Chapter 4**:Unit 4 13.
- 59 Snijders AM, Nowak N, Segreaves R, Blackwood S, Brown N, Conroy J, Hamilton G, Hindle AK, Huey B, Kimura K, Law S, Myambo K, Palmer J, Ylstra B, Yue JP, Gray JW, Jain AN, Pinkel D, Albertson DG. Assembly of microarrays for genome-wide measurement of DNA copy number. *Nat Genet* 2001;**29**(3):263-4.
- 60 Miliaras D, Conroy J, Pervana S, Meditskou S, McQuaid D, Nowak N. Karyotypic changes detected by comparative genomic hybridization in a stillborn infant with chorioangioma and liver hemangioma. *Birth Defects Res A Clin Mol Teratol* 2007;**79**(3):236-41.
- 61 Christian SL, Brune CW, Sudi J, Kumar RA, Liu S, Karamohamed S, Badner JA, Matsui S, Conroy J, McQuaid D, Gergel J, Hatchwell E, Gilliam TC, Gershon ES, Nowak NJ, Dobyns WB, Cook EH, Jr. Novel submicroscopic chromosomal abnormalities detected in autism spectrum disorder. *Biol Psychiatry* 2008;**63**(12):1111-7.
- 62 Eugster EA, Berry SA, Hirsch B. Mosaicism for deletion 1p36.33 in a patient with obesity and hyperphagia. *Am J Med Genet* 1997;**70**(4):409-12.
- 63 Reish O, Berry SA, Hirsch B. Partial monosomy of chromosome 1p36.3: characterization of the critical region and delineation of a syndrome. *Am J Med Genet* 1995;**59**(4):467-75.

- 64 Jaillard S, Dubourg C, Gerard-Blanluet M, Delahaye A, Pasquier L, Dupont C, Henry C, Tabet AC, Lucas J, Aboura A, David V, Benzacken B, Odent S, Pipiras E. 2q23.1 microdeletion identified by array-CGH: an emerging phenotype with Angelman-like features? *J Med Genet* 2008.
- 65 Elghezal H, Sendi HS, Monastiri K, Lapierre JM, Romdhane SI, Mougou S, Saad A. Large duplication 4q25-q34 with mild clinical effect. *Ann Genet* 2004;**47**(4):419-22.
- 66 Zahir F, Firth HV, Baross A, Delaney AD, Eydoux P, Gibson WT, Langlois S, Martin H, Willatt L, Marra MA, Friedman JM. Novel deletions of 14q11.2 associated with developmental delay, cognitive impairment and similar minor anomalies in three children. *J Med Genet* 2007;**44**(9):556-61.
- 67 Lupski JR, de Oca-Luna RM, Slaugenhaupt S, Pentao L, Guzzetta V, Trask BJ, Saucedo-Cardenas O, Barker DF, Killian JM, Garcia CA, Chakravarti A, Patel PI. DNA duplication associated with Charcot-Marie-Tooth disease type 1A. *Cell* 1991;**66**(2):219-32.
- 68 Patel PI, Franco B, Garcia C, Slaugenhaupt SA, Nakamura Y, Ledbetter DH, Chakravarti A, Lupski JR. Genetic mapping of autosomal dominant Charcot-Marie-Tooth disease in a large French-Acadian kindred: identification of new linked markers on chromosome 17. *Am J Hum Genet* 1990;**46**(4):801-9.
- 69 Kirov G, Grozeva D, Norton N, Ivanov D, Mantripragada KK, Holmans P, Craddock N, Owen MJ, O'Donovan MC. Support for the involvement of large cnvs in the pathogenesis of schizophrenia. *Hum Mol Genet* 2009.
- 70 de Vries BB, Pfundt R, Leisink M, Koolen DA, Vissers LE, Janssen IM, Reijmersdal S, Nillesen WM, Huys EH, Leeuw N, Smeets D, Sistermans EA, Feuth T, van Ravenswaaij-

- Arts CM, van Kessel AG, Schoenmakers EF, Brunner HG, Veltman JA. Diagnostic genome profiling in mental retardation. *Am J Hum Genet* 2005;**77**(4):606-16.
- 71 Wilson LC, Leverton K, Oude Luttikhuis ME, Oley CA, Flint J, Wolstenholme J, Duckett DP, Barrow MA, Leonard JV, Read AP, et al. Brachydactyly and mental retardation: an Albright hereditary osteodystrophy-like syndrome localized to 2q37. *Am J Hum Genet* 1995;**56**(2):400-7.
- 72 Baynam G, Goldblatt J, Walpole I. Deletion of 8p23.1 with features of Cornelia de Lange syndrome and congenital diaphragmatic hernia and a review of deletions of 8p23.1 to 8pter? A further locus for Cornelia de Lange syndrome. *Am J Med Genet A* 2008;**146A**(12):1565-70.
- 73 Sebat J, Lakshmi B, Malhotra D, Troge J, Lese-Martin C, Walsh T, Yamrom B, Yoon S, Krasnitz A, Kendall J, Leotta A, Pai D, Zhang R, Lee YH, Hicks J, Spence SJ, Lee AT, Puura K, Lehtimäki T, Ledbetter D, Gregersen PK, Bregman J, Sutcliffe JS, Jobanputra V, Chung W, Warburton D, King MC, Skuse D, Geschwind DH, Gilliam TC, Ye K, Wigler M. Strong association of de novo copy number mutations with autism. *Science* 2007;**316**(5823):445-9.
- 74 Marshall CR, Noor A, Vincent JB, Lionel AC, Feuk L, Skaug J, Shago M, Moessner R, Pinto D, Ren Y, Thiruvahindrapuram B, Fiebig A, Schreiber S, Friedman J, Ketelaars CE, Vos YJ, Ficicioglu C, Kirkpatrick S, Nicolson R, Sloman L, Summers A, Gibbons CA, Teebi A, Chitayat D, Weksberg R, Thompson A, Vardy C, Crosbie V, Luscombe S, Baatjes R, Zwaigenbaum L, Roberts W, Fernandez B, Szatmari P, Scherer SW. Structural variation of chromosomes in autism spectrum disorder. *Am J Hum Genet* 2008;**82**(2):477-88.

- 75 Szatmari P, Paterson AD, Zwaigenbaum L, Roberts W, Brian J, Liu XQ, Vincent JB, Skaug JL, Thompson AP, Senman L, Feuk L, Qian C, Bryson SE, Jones MB, Marshall CR, Scherer SW, Vieland VJ, Bartlett C, Mangin LV, Goedken R, Segre A, Pericak-Vance MA, Cuccaro ML, Gilbert JR, Wright HH, Abramson RK, Betancur C, Bourgeron T, Gillberg C, Leboyer M, Buxbaum JD, Davis KL, Hollander E, Silverman JM, Hallmayer J, Lotspeich L, Sutcliffe JS, Haines JL, Folstein SE, Piven J, Wassink TH, Sheffield V, Geschwind DH, Bucan M, Brown WT, Cantor RM, Constantino JN, Gilliam TC, Herbert M, Lajonchere C, Ledbetter DH, Lese-Martin C, Miller J, Nelson S, Samango-Sprouse CA, Spence S, State M, Tanzi RE, Coon H, Dawson G, Devlin B, Estes A, Flodman P, Klei L, McMahon WM, Minshew N, Munson J, Korvatska E, Rodier PM, Schellenberg GD, Smith M, Spence MA, Stodgell C, Tepper PG, Wijsman EM, Yu CE, Roge B, Mantoulan C, Wittemeyer K, Poustka A, Felder B, Klauck SM, Schuster C, Poustka F, Bolte S, Feineis-Matthews S, Herbrecht E, Schmotzer G, Tsiantis J, Papanikolaou K, Maestrini E, Bacchelli E, Blasi F, Carone S, Toma C, Van Engeland H, de Jonge M, Kemner C, Koop F, Langemeijer M, Hijmans C, Staal WG, Baird G, Bolton PF, Rutter ML, Weisblatt E, Green J, Aldred C, Wilkinson JA, Pickles A, Le Couteur A, Berney T, McConachie H, Bailey AJ, Francis K, Honeyman G, Hutchinson A, Parr JR, Wallace S, Monaco AP, Barnby G, Kobayashi K, Lamb JA, Sousa I, Sykes N, Cook EH, Guter SJ, Leventhal BL, Salt J, Lord C, Corsello C, Hus V, Weeks DE, Volkmar F, Tauber M, Fombonne E, Shih A, Meyer KJ. Mapping autism risk loci using genetic linkage and chromosomal rearrangements. *Nat Genet* 2007;**39**(3):319-28.

- 76 Behjati F, Shafaghathi Y, Firouzabadi SG, Kahrizi K, Bagherizadeh I, Najmabadi H, Bint S, Ogilvie C. M-banding characterization of a 16p11.2p13.1 tandem duplication in a child with autism, neurodevelopmental delay and dysmorphism. *Eur J Med Genet* 2008.
- 77 Martens MA, Wilson SJ, Reutens DC. Research Review: Williams syndrome: a critical review of the cognitive, behavioral, and neuroanatomical phenotype. *J Child Psychol Psychiatry* 2008;**49**(6):576-608.
- 78 Ohyama T, Groves AK. Expression of mouse Foxi class genes in early craniofacial development. *Dev Dyn* 2004;**231**(3):640-6.
- 79 Kumar RA, KaraMohamed S, Sudi J, Conrad DF, Brune C, Badner JA, Gilliam TC, Nowak NJ, Cook EH, Jr., Dobyns WB, Christian SL. Recurrent 16p11.2 microdeletions in autism. *Hum Mol Genet* 2008;**17**(4):628-38.
- 80 Weiss LA, Shen Y, Korn JM, Arking DE, Miller DT, Fossdal R, Saemundsen E, Stefansson H, Ferreira MA, Green T, Platt OS, Ruderfer DM, Walsh CA, Altshuler D, Chakravarti A, Tanzi RE, Stefansson K, Santangelo SL, Gusella JF, Sklar P, Wu BL, Daly MJ. Association between microdeletion and microduplication at 16p11.2 and autism. *N Engl J Med* 2008;**358**(7):667-75.
- 81 Girirajan S, Truong H, Blanchard C, Elsea S. A functional network module for Smith-Magenis syndrome. *Clin Genet* 2009.
- 82 Bijlsma EK, Aalfs CM, Sluitjer S, Oude Luttikhuis ME, Trembath RC, Hoovers JM, Hennekam RC. Familial cryptic translocation between chromosomes 2qter and 8qter: further delineation of the Albright hereditary osteodystrophy-like phenotype. *J Med Genet* 1999;**36**(8):604-9.

- 83 Falk RE, Casas KA. Chromosome 2q37 deletion: clinical and molecular aspects. *Am J Med Genet C Semin Med Genet* 2007;**145C**(4):357-71.
- 84 Schlesinger AE, Potocki L, Poznanski AK, Lupski JR. The hand in Smith-Magenis syndrome (deletion 17p11.2): evaluation by metacarpophalangeal pattern profile analysis. *Pediatr Radiol* 2003;**33**(3):173-6.
- 85 Jhas S, Ciura S, Belanger-Jasmin S, Dong Z, Llamosas E, Theriault FM, Joachim K, Tang Y, Liu L, Liu J, Stifani S. Hes6 inhibits astrocyte differentiation and promotes neurogenesis through different mechanisms. *J Neurosci* 2006;**26**(43):11061-71.
- 86 Kageyama R, Ohtsuka T, Kobayashi T. Roles of Hes genes in neural development. *Dev Growth Differ* 2008;**50 Suppl 1**:S97-103.
- 87 Hermey G, Plath N, Hubner CA, Kuhl D, Schaller HC, Hermans-Borgmeyer I. The three sorCS genes are differentially expressed and regulated by synaptic activity. *J Neurochem* 2004;**88**(6):1470-6.
- 88 Feldmann HM, Golozoubova V, Cannon B, Nedergaard J. UCP1 ablation induces obesity and abolishes diet-induced thermogenesis in mice exempt from thermal stress by living at thermoneutrality. *Cell Metab* 2009;**9**(2):203-9.
- 89 Kim-Han JS, Dugan LL. Mitochondrial uncoupling proteins in the central nervous system. *Antioxid Redox Signal* 2005;**7**(9-10):1173-81.
- 90 Jedeke KB. The overlapping spectrum of rett and angelman syndromes: a clinical review. *Semin Pediatr Neurol* 2007;**14**(3):108-17.
- 91 Koolen DA, Vissers LE, Nillesen W, Smeets D, van Ravenswaaij CM, Sistermans EA, Veltman JA, de Vries BB. A novel microdeletion, del(2)(q22.3q23.3) in a mentally

- retarded patient, detected by array-based comparative genomic hybridization. *Clin Genet* 2004;**65**(5):429-32.
- 92 Visser LE, de Vries BB, Osoegawa K, Janssen IM, Feuth T, Choy CO, Straatman H, van der Vliet W, Huys EH, van Rijk A, Smeets D, van Ravenswaaij-Arts CM, Knoers NV, van der Burgt I, de Jong PJ, Brunner HG, van Kessel AG, Schoenmakers EF, Veltman JA. Array-based comparative genomic hybridization for the genomewide detection of submicroscopic chromosomal abnormalities. *Am J Hum Genet* 2003;**73**(6):1261-70.
- 93 Ballif BC, Theisen A, Coppinger J, Gowans GC, Hersh JH, Madan-Khetarpal S, Schmidt KR, Tervo R, Escobar LF, Friedrich CA, McDonald M, Campbell L, Ming JE, Zackai EH, Bejjani BA, Shaffer LG. Expanding the clinical phenotype of the 3q29 microdeletion syndrome and characterization of the reciprocal microduplication. *Mol Cytogenet* 2008;**1**:8.
- 94 Ballif BC, Theisen A, McDonald-McGinn DM, Zackai EH, Hersh JH, Bejjani BA, Shaffer LG. Identification of a previously unrecognized microdeletion syndrome of 16q11.2q12.2. *Clin Genet* 2008;**74**(5):469-75.
- 95 Shaffer LG, McCaskill C, Han JY, Choo KH, Cuttillo DM, Donnenfeld AE, Weiss L, Van Dyke DL. Molecular characterization of de novo secondary trisomy 13. *Am J Hum Genet* 1994;**55**(5):968-74.
- 96 Williams SR, Girirajan S, Tegay D, Nowak N, Hatchwell E, Elsea SH. Array comparative genomic hybridization of 52 subjects with a Smith-Magenis-like phenotype: identification of dosage-sensitive loci also associated with schizophrenia, autism, and developmental delay. *J Med Genet* 2009(In Press).

- 97 van Bon BW, Koolen DA, Brueton L, McMullan D, Lichtenbelt KD, Ades LC, Peters G, Gibson K, Moloney S, Novara F, Pramparo T, Dalla Bernardina B, Zoccante L, Balottin U, Piazza F, Pecile V, Gasparini P, Guerzi V, Kets M, Pfundt R, de Brouwer AP, Veltman JA, de Leeuw N, Wilson M, Antony J, Reitano S, Luciano D, Fichera M, Romano C, Brunner HG, Zuffardi O, de Vries BB. The 2q23.1 microdeletion syndrome: clinical and behavioural phenotype. *Eur J Hum Genet*; **18**(2):163-70.
- 98 Marchese S DG, Garver K, Stadler M. De novo 46,XX,dup(2)(q21-q31) ascertained by prenatal cytogenetic analysis. *Am J Hum Genet* 1984;**36**:103.
- 99 Matos A, Nogueira A, Criado B, Pereira S, Castedo S, Montenegro N. Prenatal diagnosis of partial trisomy 2q. Case report. *Prenat Diagn* 1997;**17**(9):874-6.
- 100 Schumacher RE, Rocchini AP, Wilson GN. Partial trisomy 2q. *Clin Genet* 1983;**23**(3):191-4.
- 101 Farrell SA, Sajoo A, Maybury D, Speevak MD. Pure partial trisomy of 2q22-q23 secondary to a paternally inherited direct insertion: a rare duplication. *Clin Genet* 2003;**64**(3):255-7.
- 102 Nagase T, Kikuno R, Hattori A, Kondo Y, Okumura K, Ohara O. Prediction of the coding sequences of unidentified human genes. XIX. The complete sequences of 100 new cDNA clones from brain which code for large proteins in vitro. *DNA Res* 2000;**7**(6):347-55.
- 103 Roloff TC, Ropers HH, Nuber UA. Comparative study of methyl-CpG-binding domain proteins. *BMC Genomics* 2003;**4**(1):1.

- 104 Vega RB, Matsuda K, Oh J, Barbosa AC, Yang X, Meadows E, McAnally J, Pomajzl C, Shelton JM, Richardson JA, Karsenty G, Olson EN. Histone deacetylase 4 controls chondrocyte hypertrophy during skeletogenesis. *Cell* 2004;**119**(4):555-66.
- 105 Chen B, Cepko CL. HDAC4 regulates neuronal survival in normal and diseased retinas. *Science* 2009;**323**(5911):256-9.
- 106 Aldred MA, Vijayakrishnan J, James V, Soubrier F, Gomez-Sanchez MA, Martensson G, Galie N, Manes A, Corris P, Simonneau G, Humbert M, Morrell NW, Trembath RC. BMPR2 gene rearrangements account for a significant proportion of mutations in familial and idiopathic pulmonary arterial hypertension. *Hum Mutat* 2006;**27**(2):212-3.
- 107 Aldred MA, Sanford RO, Thomas NS, Barrow MA, Wilson LC, Brueton LA, Bonaglia MC, Hennekam RC, Eng C, Dennis NR, Trembath RC. Molecular analysis of 20 patients with 2q37.3 monosomy: definition of minimum deletion intervals for key phenotypes. *J Med Genet* 2004;**41**(6):433-9.
- 108 Zhang CL, McKinsey TA, Chang S, Antos CL, Hill JA, Olson EN. Class II histone deacetylases act as signal-responsive repressors of cardiac hypertrophy. *Cell* 2002;**110**(4):479-88.
- 109 Grozinger CM, Hassig CA, Schreiber SL. Three proteins define a class of human histone deacetylases related to yeast Hda1p. *Proc Natl Acad Sci U S A* 1999;**96**(9):4868-73.
- 110 Fischle W, Dequiedt F, Hendzel MJ, Guenther MG, Lazar MA, Voelter W, Verdin E. Enzymatic activity associated with class II HDACs is dependent on a multiprotein complex containing HDAC3 and SMRT/N-CoR. *Mol Cell* 2002;**9**(1):45-57.

- 111 Takeda S, Bonnamy JP, Owen MJ, Ducy P, Karsenty G. Continuous expression of Cbfa1 in nonhypertrophic chondrocytes uncovers its ability to induce hypertrophic chondrocyte differentiation and partially rescues Cbfa1-deficient mice. *Genes Dev* 2001;**15**(4):467-81.
- 112 Ueta C, Iwamoto M, Kanatani N, Yoshida C, Liu Y, Enomoto-Iwamoto M, Ohmori T, Enomoto H, Nakata K, Takada K, Kurisu K, Komori T. Skeletal malformations caused by overexpression of Cbfa1 or its dominant negative form in chondrocytes. *J Cell Biol* 2001;**153**(1):87-100.
- 113 Black BL, Olson EN. Transcriptional control of muscle development by myocyte enhancer factor-2 (MEF2) proteins. *Annu Rev Cell Dev Biol* 1998;**14**:167-96.
- 114 McKinsey TA, Zhang CL, Olson EN. MEF2: a calcium-dependent regulator of cell division, differentiation and death. *Trends Biochem Sci* 2002;**27**(1):40-7.
- 115 Arnold MA, Kim Y, Czubryt MP, Phan D, McAnally J, Qi X, Shelton JM, Richardson JA, Bassel-Duby R, Olson EN. MEF2C transcription factor controls chondrocyte hypertrophy and bone development. *Dev Cell* 2007;**12**(3):377-89.
- 116 Munoz JP, Collao A, Chiong M, Maldonado C, Adasme T, Carrasco L, Ocaranza P, Bravo R, Gonzalez L, Diaz-Araya G, Hidalgo C, Lavandero S. The transcription factor MEF2C mediates cardiomyocyte hypertrophy induced by IGF-1 signaling. *Biochem Biophys Res Commun* 2009;**388**(1):155-60.
- 117 Smith M, Escamilla JR, Filipek P, Bocian ME, Modahl C, Flodman P, Spence MA. Molecular genetic delineation of 2q37.3 deletion in autism and osteodystrophy: report of a case and of new markers for deletion screening by PCR. *Cytogenet Cell Genet* 2001;**94**(1-2):15-22.

- 118 Reddy KS. Cytogenetic abnormalities and fragile-X syndrome in Autism Spectrum Disorder. *BMC Med Genet* 2005;**6**:3.
- 119 Felder B, Radlwimmer B, Benner A, Mincheva A, Todt G, Beyer KS, Schuster C, Bolte S, Schmotzer G, Klauck SM, Poustka F, Lichter P, Poustka A. FARP2, HDLBP and PASK are downregulated in a patient with autism and 2q37.3 deletion syndrome. *Am J Med Genet A* 2009;**149A**(5):952-9.
- 120 Wolff DJ, Clifton K, Karr C, Charles J. Pilot assessment of the subtelomeric regions of children with autism: detection of a 2q deletion. *Genet Med* 2002;**4**(1):10-4.
- 121 Wassink TH, Piven J, Vieland VJ, Jenkins L, Frantz R, Bartlett CW, Goedken R, Childress D, Spence MA, Smith M, Sheffield VC. Evaluation of the chromosome 2q37.3 gene CENTG2 as an autism susceptibility gene. *Am J Med Genet B Neuropsychiatr Genet* 2005;**136B**(1):36-44.
- 122 Klopocki E, Hennig BP, Dathe K, Koll R, de Ravel T, Baten E, Blom E, Gillerot Y, Weigel JF, Kruger G, Hiort O, Seemann P, Mundlos S. Deletion and Point Mutations of PTHLH Cause Brachydactyly Type E. *Am J Hum Genet*; **86**(3):434-9.
- 123 Guo J, Chung UI, Yang D, Karsenty G, Bringham FR, Kronenberg HM. PTH/PTHrP receptor delays chondrocyte hypertrophy via both Runx2-dependent and -independent pathways. *Dev Biol* 2006;**292**(1):116-28.
- 124 Girirajan S, Rosenfeld JA, Cooper GM, Antonacci F, Siswara P, Itsara A, Vives L, Walsh T, McCarthy SE, Baker C, Mefford HC, Kidd JM, Browning SR, Browning BL, Dickel DE, Levy DL, Ballif BC, Platky K, Farber DM, Gowans GC, Wetherbee JJ, Asamoah A, Weaver DD, Mark PR, Dickerson J, Garg BP, Ellingwood SA, Smith R, Banks VC, Smith W, McDonald MT, Hoo JJ, French BN, Hudson C, Johnson JP, Ozmore JR,

- Moeschler JB, Surti U, Escobar LF, El-Khechen D, Gorski JL, Kussmann J, Salbert B, Lacassie Y, Biser A, McDonald-McGinn DM, Zackai EH, Deardorff MA, Shaikh TH, Haan E, Friend KL, Fichera M, Romano C, Gecz J, DeLisi LE, Sebat J, King MC, Shaffer LG, Eichler EE. A recurrent 16p12.1 microdeletion supports a two-hit model for severe developmental delay. *Nat Genet*; **42**(3):203-9.
- 125 Capili AD, Schultz DC, Rauscher IF, Borden KL. Solution structure of the PHD domain from the KAP-1 corepressor: structural determinants for PHD, RING and LIM zinc-binding domains. *Embo J* 2001; **20**(1-2):165-77.
- 126 Imai Y, Suzuki Y, Matsui T, Tohyama M, Wanaka A, Takagi T. Cloning of a retinoic acid-induced gene, GT1, in the embryonal carcinoma cell line P19: neuron-specific expression in the mouse brain. *Brain Res Mol Brain Res* 1995; **31**(1-2):1-9.
- 127 Bienz M. The PHD finger, a nuclear protein-interaction domain. *Trends Biochem Sci* 2006; **31**(1):35-40.
- 128 Nie L, Vazquez AE, Yamoah EN. Identification of Transcription Factor-DNA Interactions Using Chromatin Immunoprecipitation Assays. *Methods Mol Biol* 2009; **493**:311-22.
- 129 Kirmizis A, Farnham PJ. Genomic approaches that aid in the identification of transcription factor target genes. *Exp Biol Med (Maywood)* 2004; **229**(8):705-21.
- 130 Takahashi JS, Hong HK, Ko CH, McDearmon EL. The genetics of mammalian circadian order and disorder: implications for physiology and disease. *Nat Rev Genet* 2008; **9**(10):764-75.

- 131 Turek FW, Joshu C, Kohsaka A, Lin E, Ivanova G, McDearmon E, Laposky A, Losee-Olson S, Easton A, Jensen DR, Eckel RH, Takahashi JS, Bass J. Obesity and metabolic syndrome in circadian Clock mutant mice. *Science* 2005;**308**(5724):1043-5.
- 132 Salvatore P, Ghidini S, Zita G, De Panfilis C, Lambertino S, Maggini C, Baldessarini RJ. Circadian activity rhythm abnormalities in ill and recovered bipolar I disorder patients. *Bipolar Disord* 2008;**10**(2):256-65.
- 133 Mendlewicz J. Disruption of the circadian timing systems: molecular mechanisms in mood disorders. *CNS Drugs* 2009;**23 Suppl 2**:15-26.
- 134 De Leersnyder H. Inverted rhythm of melatonin secretion in Smith-Magenis syndrome: from symptoms to treatment. *Trends Endocrinol Metab* 2006;**17**(7):291-8.
- 135 Amr S, Heisey C, Zhang M, Xia XJ, Shows KH, Ajlouni K, Pandya A, Satin LS, El-Shanti H, Shiang R. A homozygous mutation in a novel zinc-finger protein, ERIS, is responsible for Wolfram syndrome 2. *Am J Hum Genet* 2007;**81**(4):673-83.
- 136 Seranski P, Heiss NS, Dhorne-Pollet S, Radelfof U, Korn B, Hennig S, Backes E, Schmidt S, Wiemann S, Schwarz CE, Lehrach H, Poustka A. Transcription mapping in a medulloblastoma breakpoint interval and Smith-Magenis syndrome candidate region: identification of 53 transcriptional units and new candidate genes. *Genomics* 1999;**56**(1):1-11.
- 137 King DP, Zhao Y, Sangoram AM, Wilsbacher LD, Tanaka M, Antoch MP, Steeves TD, Vitaterna MH, Kornhauser JM, Lowrey PL, Turek FW, Takahashi JS. Positional cloning of the mouse circadian clock gene. *Cell* 1997;**89**(4):641-53.
- 138 Horsthemke B, Buiting K. Imprinting defects on human chromosome 15. *Cytogenet Genome Res* 2006;**113**(1-4):292-9.

- 139 Hitchins MP, Rickard S, Dhalla F, Fairbrother UL, de Vries BB, Winter R, Pembrey ME, Malcolm S. Investigation of UBE3A and MECP2 in Angelman syndrome (AS) and patients with features of AS. *Am J Med Genet A* 2004;**125A**(2):167-72.
- 140 Lebrun B, Bariohay B, Moyse E, Jean A. Brain-derived neurotrophic factor (BDNF) and food intake regulation: a minireview. *Auton Neurosci* 2006;**126-127**:30-8.
- 141 Gray J, Yeo GS, Cox JJ, Morton J, Adlam AL, Keogh JM, Yanovski JA, El Gharbawy A, Han JC, Tung YC, Hodges JR, Raymond FL, O'Rahilly S, Farooqi IS. Hyperphagia, severe obesity, impaired cognitive function, and hyperactivity associated with functional loss of one copy of the brain-derived neurotrophic factor (BDNF) gene. *Diabetes* 2006;**55**(12):3366-71.
- 142 Simmons DA, Rex CS, Palmer L, Pandeyarajan V, Fedulov V, Gall CM, Lynch G. Up-regulating BDNF with an ampakine rescues synaptic plasticity and memory in Huntington's disease knockin mice. *Proc Natl Acad Sci U S A* 2009;**106**(12):4906-11.
- 143 Larimore JL, Chapleau CA, Kudo S, Theibert A, Percy AK, Pozzo-Miller L. Bdnf overexpression in hippocampal neurons prevents dendritic atrophy caused by Rett-associated MECP2 mutations. *Neurobiol Dis* 2009;**34**(2):199-211.
- 144 Girirajan S, Elsea SH. Distorted Mendelian transmission as a function of genetic background in Rai1-haploinsufficient mice. *Eur J Med Genet* 2009;**52**(4):224-8.
- 145 Zheng B, Albrecht U, Kaasik K, Sage M, Lu W, Vaishnav S, Li Q, Sun ZS, Eichele G, Bradley A, Lee CC. Nonredundant roles of the mPer1 and mPer2 genes in the mammalian circadian clock. *Cell* 2001;**105**(5):683-94.
- 146 Goto M, Oshima I, Tomita T, Ebihara S. Melatonin content of the pineal gland in different mouse strains. *J Pineal Res* 1989;**7**(2):195-204.

- 147 King DP, Takahashi JS. Forward genetic approaches to circadian clocks in mice. *Cold Spring Harb Symp Quant Biol* 1996;**61**:295-302.
- 148 Antoch MP, Song EJ, Chang AM, Vitaterna MH, Zhao Y, Wilsbacher LD, Sangoram AM, King DP, Pinto LH, Takahashi JS. Functional identification of the mouse circadian Clock gene by transgenic BAC rescue. *Cell* 1997;**89**(4):655-67.
- 149 Debruyne JP, Noton E, Lambert CM, Maywood ES, Weaver DR, Reppert SM. A clock shock: mouse CLOCK is not required for circadian oscillator function. *Neuron* 2006;**50**(3):465-77.
- 150 Zheng B, Larkin DW, Albrecht U, Sun ZS, Sage M, Eichele G, Lee CC, Bradley A. The mPer2 gene encodes a functional component of the mammalian circadian clock. *Nature* 1999;**400**(6740):169-73.
- 151 Hampp G, Ripperger JA, Houben T, Schmutz I, Blex C, Perreau-Lenz S, Brunk I, Spanagel R, Ahnert-Hilger G, Meijer JH, Albrecht U. Regulation of monoamine oxidase A by circadian-clock components implies clock influence on mood. *Curr Biol* 2008;**18**(9):678-83.
- 152 Albrecht U. Circadian clocks in mood-related behaviors. *Ann Med*.
- 153 Benedetti F, Serretti A, Colombo C, Barbini B, Lorenzi C, Campori E, Smeraldi E. Influence of CLOCK gene polymorphism on circadian mood fluctuation and illness recurrence in bipolar depression. *Am J Med Genet B Neuropsychiatr Genet* 2003;**123B**(1):23-6.
- 154 Serretti A, Cusin C, Benedetti F, Mandelli L, Pirovano A, Zanardi R, Colombo C, Smeraldi E. Insomnia improvement during antidepressant treatment and CLOCK gene polymorphism. *Am J Med Genet B Neuropsychiatr Genet* 2005;**137B**(1):36-9.

- 155 Serretti A, Benedetti F, Mandelli L, Lorenzi C, Pirovano A, Colombo C, Smeraldi E. Genetic dissection of psychopathological symptoms: insomnia in mood disorders and CLOCK gene polymorphism. *Am J Med Genet B Neuropsychiatr Genet* 2003;**121B**(1):35-8.
- 156 Pirovano A, Lorenzi C, Serretti A, Ploia C, Landoni S, Catalano M, Smeraldi E. Two new rare variants in the circadian "clock" gene may influence sleep pattern. *Genet Med* 2005;**7**(6):455-7.
- 157 Nievergelt CM, Kripke DF, Barrett TB, Burg E, Remick RA, Sadovnick AD, McElroy SL, Keck PE, Jr., Schork NJ, Kelsoe JR. Suggestive evidence for association of the circadian genes PERIOD3 and ARNTL with bipolar disorder. *Am J Med Genet B Neuropsychiatr Genet* 2006;**141B**(3):234-41.
- 158 Mansour HA, Wood J, Logue T, Chowdari KV, Dayal M, Kupfer DJ, Monk TH, Devlin B, Nimgaonkar VL. Association study of eight circadian genes with bipolar I disorder, schizoaffective disorder and schizophrenia. *Genes Brain Behav* 2006;**5**(2):150-7.
- 159 Kamura E. Exploring the Methylation Status of RAI1 and the RAI1 Consensus Binding Sequence. 2009.
- 160 Kingsley DM, Bland AE, Grubber JM, Marker PC, Russell LB, Copeland NG, Jenkins NA. The mouse short ear skeletal morphogenesis locus is associated with defects in a bone morphogenetic member of the TGF beta superfamily. *Cell* 1992;**71**(3):399-410.
- 161 Beck HN, Drahushuk K, Jacoby DB, Higgins D, Lein PJ. Bone morphogenetic protein-5 (BMP-5) promotes dendritic growth in cultured sympathetic neurons. *BMC Neurosci* 2001;**2**:12.

Appendix A

Overexpression of *RAII* in HEK293t cells

As stated in Chapter 1, duplication of 17p11.2 results in dup17p11.2 syndrome (aka Potocki-Lupski syndrome). This syndrome is rarer than SMS, but because duplication of this genomic region, including *RAII*, gives rise to a recognizable syndrome, it points to the fact that *RAII* is a dosage-sensitive gene. Additionally, Girirajan et al. 2008, 2009 [43],[44] showed that *Rail-Tg* mice have altered maternal behavior, altered sociability, and impaired serotonin metabolism [44]. Further, these mice have growth retardation, increased locomotor activity, and abnormal anxiety-related responses. *Rail-Tg* mice also have an altered gait with short strides and long sways, impaired ability on a cage top hang test, decreased forelimb grip strength, and a dominant social behavior. Additional analyses of homozygous transgenic mice revealed a dosage-dependent exacerbation of the phenotype, including extreme growth retardation, severe neurological deficits, and increased hyperactivity [43].

These results laid the groundwork to examine the molecular changes that occur because of *RAII* overexpression. We used transient over expression followed by gene expression microarray to explore the consequence of *RAII* overexpression.

Materials and methods

Transfections

Transfections of HEK293t cells with *RAII*^{Flag} were performed as described Chapter 5.

RNA isolation

RNA was isolated using the standard Trizol protocol provided by Invitrogen (Invitrogen, Carlsbad, CA)

Microarray

Microarray was performed as previously described [81] using the Affymetrix Human Genome, HG-U133A 2.0 Array chipset. Control RNA was isolated from non transfected HEK293t cells.

Results

Table A1. Top upregulated genes identified in HEK293t cells overexpressing *RAII*.
RAII/Control Signal

Log Ratio	Gene Symbol	Gene Name	Pathway	Biological Process
5.5	<i>TRPC1</i>	transient receptor potential cation channel, subfamily C, member 1	---	transport
5.5	<i>HNRNPU</i>	heterogeneous nuclear ribonucleoprotein U	mRNA_processing_Reactome	RNA processing
5.3	<i>MAT2A</i>	methionine adenosyltransferase II, alpha	---	S-adenosylmethionine biosynthetic process protein amino acid phosphorylation /// SRP-dependent cotranslational protein targeting to membrane /// signal transduction
5	<i>SRP72</i>	signal recognition particle 72kDa	---	
5	<i>SARIA</i>	SAR1 gene homolog A	---	transport cytoskeletal anchoring /// regulation of cell shape
5	<i>EZR</i>	ezrin	---	L-serine biosynthetic process
5	<i>PSAT1</i>	phosphoserine aminotransferase 1	---	selenocysteine incorporation /// cell redox homeostasis
4.9	<i>SELT</i>	selenoprotein T	---	
4.8	<i>ASL</i>	argininosuccinate lyase	---	urea cycle response to tumor cell
4.8	<i>TP53</i>	tumor protein p53	Apoptosis	
4.8	<i>PRIM2</i>	primase, DNA, polypeptide 2 (58kDa)	DNA_replication_Reactome	DNA replication protein modification process ///regulation of protein metabolic process
4.7	<i>UBE2M</i>	ubiquitin-conjugating enzyme E2M	---	

4.7	<i>TMED2</i>	transmembrane emp24 domain trafficking protein 2	---	transport negative regulation of transcription from RNA polymerase II promoter ///
4.7	<i>ENO1</i>	enolase 1, (alpha) mitochondrial ribosomal protein S12	Glycolysis_and_Gluconeogenesis	glycolysis
4.6	<i>MRPS12</i>	---	---	translation
4.6	<i>RNFT1</i>	ring finger protein, transmembrane 1	---	---
4.5	<i>DUSP3</i>	dual specificity phosphatase 3	---	protein amino acid dephosphorylation
4.5	<i>MAN1A1</i>	mannosidase, alpha, class 1A, member 1 homeodomain	---	protein amino acid glycosylation
4.5	<i>HIPK3</i>	interacting protein kinase 3 ADAM	---	transcription
4.5	<i>ADAM10</i>	metallopeptidase domain 10	Hypertrophy_model	in utero embryonic development signal transduction /// small GTPase mediated signal transduction
4.5	<i>ARFRP1</i>	ADP-ribosylation factor related protein 1	---	nucleobase, nucleoside, nucleotide and nucleic acid metabolic process protein folding ///
4.4	<i>SLC29A1</i>	solute carrier family 29 member 1	---	response to stress /// response to unfolded protein muscle contraction /// muscle
4.4	<i>HSPA8</i>	heat shock 70kDa protein 8	Circadian_Exercise	development glycolysis ///
4.3	<i>UTRN</i>	utrophin phosphoglycerate kinase 1	---	phosphorylation
4.3	<i>PGK1</i>	ganglioside-induced differentiation- associated protein 1	Glycolysis_and_Gluconeogenesis	---
4.3	<i>GDAP1</i>	---	---	---

Table A2. Top downregulated genes identified in HEK293t cells overexpressing *RAI1*

Log Ratio	Gene Symbol	Gene Title	Pathway	Biological process term
-5.5	<i>ANKRD36B</i>	ankyrin repeat domain 36B	---	cellular di-, tri-valent inorganic anion homeostasis
-4.5	<i>CDC42BPA</i>	CDC42 binding protein kinase alpha spen homolog, transcriptional regulator	---	protein amino acid phosphorylation
-4.2	<i>SPEN</i>	---	---	transcription

-4.2	<i>SFRS11</i>	splicing factor, arginine/serine-rich 11	---	mRNA processing
-4.2	<i>SEMA6A</i>	sema domain, transmembrane domain, and cytoplasmic domain, 6A	---	apoptosis ///nervous system development /// axon guidance /// organ morphogenesis
-4.1	<i>NKTR</i>	natural killer-tumor recognition sequence	---	protein folding skeletal development /// carbohydrate metabolic process /// nervous system development
-4.1	<i>SMA4</i>	Glucuronidase, beta pseudogene 1	---	
-4	<i>SRRM2</i>	serine/arginine repetitive matrix 2	---	mRNA processing
-3.9	<i>RBM41</i>	RNA binding motif protein 41	---	---
-3.7	<i>MSH5</i>	mutS homolog 5 (E. coli) /// chromosome 6 open reading frame 26	Ovarian_Infertility_Genes	mismatch repair
-3.7	<i>GOLGA8A</i>	golgi autoantigen, golgin subfamily a, 8A	---	---
-3.7	<i>CEP350</i>	centrosomal protein 350kDa	---	protein targeting
-3.7	<i>ATHL1</i>	ATH1, acid trehalase-like 1	---	carbohydrate metabolic process
-3.7	<i>EBF2</i>	early B-cell factor 2	---	transcription
-3.7	<i>MCM3APAS</i>	minichromosome maintenance complex component 3 associated protein	---	---
-3.7	<i>WNK1</i>	antisense WNK lysine deficient protein kinase 1	---	protein amino acid phosphorylation
-3.6	<i>ATRX</i>	alpha thalassemia/mental retardation syndrome X-linked	---	DNA repair /// DNA repair /// DNA methylation

Discussion

In this study we have overexpressed *RAI1* in HEK293t cells to evaluate the molecular consequences of this action. Given that *RAI1* is a dosage sensitive gene these were important experiments to perform and examine pathways affected. We have identified gene which play critical roles in circadian rhythm, epigenetic regulation, DNA repair, RNA processing, transcription and a variety of other critical pathways. These studies will help to identify the

molecular role *RAII* plays in the cell and help to understand the consequence of abnormal *RAII* dosage.

Appendix B

Short Report

17p11.2p12 triplication and del(17)q11.2q12 in a severely affected child with dup(17)p11.2p12 syndrome

Girirajan S, Williams SR, Garbern JY, Nowak N, Hatchwell E, Elsea SH. 17p11.2p12 triplication and del(17)q11.2q12 in a severely affected child with dup(17)p11.2p12 syndrome.

Clin Genet 2007; 72: 47–58. © Blackwell Munksgaard, 2007

Multiple congenital anomalies/mental retardation syndromes due to genomic rearrangements involving chromosome 17p11.2 include deletion resulting in Smith–Magenis syndrome and a reciprocal duplication of the same region resulting in the 17p11.2 duplication syndrome. We present the clinical and molecular analysis of an 8-year-old male with a dup(17p11.2p12) who was evaluated for unusual severity of the phenotype. Fluorescent *in situ* hybridization (FISH) analysis not only confirmed the 17p duplication but also identified an ~25% mosaicism for tetrasomy 17p11.2p12. Whole-genome array comparative genomic hybridization (aCGH) was performed to identify other genomic rearrangements possibly contributing to the severe phenotype and the unusual features in the patient. The 17p duplication was determined by FISH and aCGH to encompass ~7.5 Mb, from *COX10* to *KCNJ12*. An ~830 Kb deletion of 17q11.2q12, including exon 1 of an amiloride-sensitive cation channel neuronal gene, *ACCN1*, was also identified by aCGH; breakpoints of the deletion were confirmed by FISH. Sequencing the non-deleted allele of *ACCN1* did not show any mutations. Western analysis of human tissue-specific proteins revealed that *ACCN1* is expressed not only in the brain as previously reported but also in all tissues examined, including heart, liver, kidneys, and spleen. The large-sized 17p11.2p12 duplication, partial triplication of the same region, and the 17q11.2q12 deletion create a complex chromosome 17 rearrangement that has not been previously identified. This is the first case of triplication reported for this chromosome. Our study emphasizes the utility of whole-genome analysis for known cases with deletion/duplication syndromes with unusual or severe phenotypes.

**S Girirajan^a, SR Williams^a,
 JY Garbern^b, N Nowak^{c,d},
 E Hatchwell^e and SH Elsea^{a,f}**

^aDepartment of Human Genetics, Virginia Commonwealth University, Richmond, VA, USA, ^bCenter for Molecular Medicine and Genetics, Wayne State University School of Medicine, Detroit, MI, USA, ^cDepartment of Biochemistry and Center of Excellence in Bioinformatics and Life Sciences, State University of New York at Buffalo, NY, USA, ^dDepartment of Cancer Prevention, Roswell Park Cancer Institute, Buffalo, NY, USA, ^eDepartment of Pathology, State University of New York at Stony Brook, NY, USA, and ^fDepartment of Pediatrics, Virginia Commonwealth University, Richmond, VA, USA

Key words: *ACCN1* – aCGH – cardiac anomalies – 17p11.2p12 triplication – 17q11.2q12 deletion – 17p11.2p12 duplication – FISH – mental retardation – tetrasomy 17p11.2p12

Corresponding author: Dr Sarah H. Elsea, PhD, FACMG, Departments of Pediatrics and Human Genetics, 1101 E Marshall St, 12-018 Sanger Hall, PO BOX 980441, Medical College of Virginia, Virginia Commonwealth University, Richmond, VA 23298, USA.
 Tel.: +804 628 0987;
 fax: +804 628 1609;
 e-mail: selsea@vcu.edu

Received 26 January 2007, revised and accepted for publication 19 April 2007

Rearrangements due to homologous and non-homologous mechanisms within region-specific low copy repeats or segmental duplications cause deletions/duplications in disease-associated genomic regions (1). The genomic fragility of the short arm of chromosome 17 is due to extensive segmental duplications, especially in the Charcot–Marie–Tooth disease type 1A/Smith–Magenis syndrome (CMT1A/SMS) regions (1). Clinically

recognized genomic disorders of proximal 17p include Charcot–Marie–Tooth disease type 1A caused by a duplication of the peripheral myelin protein 22 (*PMP22*) gene (2), hereditary neuropathy with liability to pressure palsies caused by a deletion of *PMP22* (3), and Smith–Magenis syndrome, associated with an interstitial deletion of 17p11.2 containing the retinoic acid induced 1 gene (*RAI1*) (4–10). Duplication of the SMS region

and larger regions of the short arm of chromosome 17 has also been reported but less frequently (11–28).

Although less clearly defined, the clinical features of patients with duplication 17p consist of mild to severe mental retardation, developmental delay, failure to thrive, behavioral features, craniofacial anomalies, and short stature (16, 29). Craniofacial features include a triangular face, microcephaly, micrognathia, broad nasal bridge, high arched palate, and hypertelorism, while dental anomalies in the form of malocclusion of the teeth have also been reported (24). Limb abnormalities including flexion deformity of the fingers and club foot have also been described (12, 13, 15, 16, 18, 20, 21).

In this paper, we report the molecular and clinical evaluation of a child with severe phenotype carrying complex rearrangements of chromosome 17. A combination of fluorescent *in situ* hybridization (FISH) and array comparative genomic hybridization (CGH) was used to identify and confirm a 17p11.2p12 duplication, 17p11.2p12 mosaic triplication, and also 17q11.2q12 deletion in this patient. Both *de novo* rearrangements are seen on the same chromosome 17 homologue. While our study emphasizes the utility of interphase FISH for the identification of triplications; aCGH results indicate that identification of a single genomic rearrangement does not preclude the possibility of another genomic abnormality.

Materials and methods

Patient samples

Research samples were collected at Michigan State University and Wayne State University in accordance with Institutional Review Board approved protocols of Virginia Commonwealth University. Peripheral blood samples were collected, and metaphase chromosomes and DNA were prepared using standard cytogenetic methods.

Fluorescent *in situ* hybridization

In order to delineate the chromosome 17p duplication, probes were chosen from our previously published SMS contig map of bacterial artificial chromosome (BAC) and P1-derived artificial chromosome clones (30), and also from University of Southern California, Santa Cruz (UCSC) genome browser (May 2004 version). Probes to confirm the chromosome 17q deletion were obtained from the initial aCGH clones and verified using UCSC genome browser (March 2006 version). The FISH probes from centromeric to telomeric with their representative loci used to map the 17p11.2p12 rearrangement include: RP11-746M1

(D17S689), CTC-457L16 (D17S29), RP1-253P07 (*RAI1*), RP1-48J14 (*TNFRSF13B*), and RP11-764O6 (*PMP22*). The FISH probes used to map the 17q11.2q12 deletion (Table 1) include: RP11-329H16 (*CCL2*, *CCL7*, *CCL8*, and *CCL11*), RP11-47G8, RP11-79K15, and RP11-797M22 (all *ACCN1* probes). FISH was performed as previously described (5). For every probe analyzed by FISH, ~100 interphase nuclei and metaphase spreads were observed. Parental samples were also evaluated to rule out any familial rearrangement and mosaicism.

Table 1. aCGH probes (from telomere to centromere) used to map the chromosome 17 duplication and deletion^a

Probes	Loci
Chromosome 17p11.2p12	
RP11-661L20	<i>ELAC2</i>
RP11-210C3	<i>HS3ST3A</i>
RP11-668O24	<i>COX10</i>
RP11-78J16	<i>HS3ST3B1</i>
RP11-64B12	<i>FLJ45831</i>
RP11-465O5	<i>PMP22/TEKT3</i>
RP11-90G21	<i>FAM18B2</i>
RP11-459E6	<i>ADORA2B</i>
RP11-455I21	<i>NCOR1</i>
RP11-410D6	<i>PIGL</i>
RP11-404D6	<i>UBB</i>
RP11-803H14	<i>ZNF624</i>
RP11-793G13	<i>TNFRSF13B</i>
RP11-472C16	<i>COPS3/NT5M</i>
RP11-384M20	<i>TOM1L2/ATPAF2</i>
RP11-936C14	<i>DRG2/LLGL1</i>
RP11-80K17	<i>TRIM70/FBXW10</i>
RP11-977H13	<i>PRPSAP2</i>
RP11-160E2	<i>GRAP</i>
RP11-135L13	<i>EPN2/MAPK7</i>
RP11-1007K2	<i>AKAP10</i>
RP11-1065P14	<i>SPECC1</i>
RP11-746M1	<i>USP22</i>
RP11-64J19	<i>TMEM11/MAP2K3</i>
RP11-45G12	<i>KCNJ12</i>
RP11-730C17	<i>WSB1</i>
RP11-803B22	<i>KSR1</i>
Chromosome 17q11.2q12	
RP11-299F7	Exons 8–10 (<i>ACCN1</i>)
RP11-98K21	Exons 2–6 (<i>ACCN1</i>)
RP11-797M22	Intron 1 (<i>ACCN1</i>)
RP11-90A23	Intron 1 (<i>ACCN1</i>)
RP11-79K15	Intron 1 (<i>ACCN1</i>)
RP11-47G8	Intron 1 (<i>ACCN1</i>)
RP11-1137H3	Exon 1 (<i>ACCN1</i>)
RP11-329H16	<i>CCL2</i> , <i>CCL7</i> , <i>CCL8</i> , <i>CCL11</i>
RP11-521P1	<i>CCL1</i> , <i>CCL13</i>
RP11-42E9	<i>TMEM132E</i>

^aA list of aCGH probes used to map the proximal 17p duplication and the 17q deletion along with their representative loci are shown. The shaded regions represent the extent of the 17p duplication and the deletion. Flanking unshaded regions represent genes/loci with normal copy number.

Genotyping

Four sequence tagged site markers localized to 17p11.2 (cen-D17S783, D17S805, D17S1794, and D17S900-tel) were used to determine the origin of the duplication. Polymerase chain reaction (PCR) for the markers was performed using fluorescently labeled reverse primers on the DNA samples from the patient and the parents. Genotyping was performed using an ABI Prism® 3100 Genetic Analyzer and analysis performed using GENESCAN analysis software (Applied Biosystems, Foster City, CA).

Whole-genome array-comparative genomic hybridization

The design of the tiling path BAC array was based around a pre-existing set of 6800 clones which had been assembled at the Roswell Park Cancer Institute (RPCI) to generate a first generation array used previously for cancer genomics (<http://microarrays.roswellpark.org>). This set of 6800 clones was used as a 'scaffold' around which an additional set of 13,000 clones were assembled to fill in the gaps, according to the following criteria: no gaps greater than 10 kb in the final design, overlap was only required if the gap was greater than 10 kb, and only RPCI-11 clones were used to fill in the gaps. A minimum number of BACs were used to fulfill the criteria and Perl scripts were written in order to access data from a full set of BAC end-pairs (www.genome.ucsc.edu).

Reference DNA, 500 ng from each parent, and 1 µg of the patient's (test) DNA was fluorescently labeled using the BioPrime aCGH Labeling System (GE Healthcare, Piscataway, NJ). Hybridization to the 19K CGH arrays was performed using a GeneMachine hybridization station (Genomic Solutions, Ann Arbor, MI) as described previously (31). Following post-hybridization washes, the slides were spun dry and scanned immediately at 5 µm resolution using a GenePix 4000B laser scanner

(Axon Inc., Sunnyvale, CA). Image analysis was performed using the BlueFuse package from Cambridge BlueGnome (Cambridge, UK). aCGH clones used for mapping both the duplication (17p11.2p12) and deletion (17q11.2q12) are listed in Table 1.

ACCN1 sequence analysis

DNA from whole blood was isolated by the phenol-chloroform method. PCR to amplify coding exons of *ACCN1* was performed with 100 ng genomic DNA, 20 pmol each of forward and reverse primers, 10 mM Tris-HCl, 50 mM KCl, 1.5 mM MgCl₂, 200 µM dNTPs, and 1 U *Taq* DNA polymerase in a total reaction volume of 25 µl. Standard PCR conditions were followed with annealing temperatures for all the primers ranging between 55°C and 64°C. PCR products (5 µl) were either purified by digesting with 2 U of shrimp alkaline phosphatase and 10 U of exonuclease I (USB Corp, Cleveland, OH) at 37°C, 15 min followed by 80°C, 15 min to remove excess primers or were gel purified using a Qiagen gel extraction kit (Qiagen Inc, Valencia, CA). Sequencing and analysis of electropherograms were performed as described previously (9). Primers used for amplifying the *ACCN1* gene are shown in Table 2.

Western analysis

Human tissue-specific protein medleys (20 or 40 µg with 0.5 mM DTT; Clontech, Mountain View, CA) were boiled, run on a NuPAGE™ 4–12% Bis-Tris gel using a XCell SureLock™ Mini-cell (Invitrogen, Carlsbad, CA), and transferred to 0.45 µm polyvinylidene fluoride membrane (Millipore Corporation, Bedford, MA), using XCell II™ Blot Module (Invitrogen). The blot was then blocked in phosphate-buffered saline with Tween 20 (PBST) (137 mM NaCl, 2.7 mM KCl, 8 mM

Table 2. Polymerase chain reaction primers used to amplify and sequence *ACCN1*

	Forward primer	Reverse primer
Exon 1	aaacactcacccctgtcagc	ccccactcacccctccatatt
Exon 1 (variant)	ttccactgctgcggact	tggttaacactgcaagaggcctgg
Exon 2	ttgtctcttgatgccaaa	cccatcctctgtccctctct
Exon 3	ttgccatgtaaggcaacct	tgcccaattttagggaacaa
Exon 4	gagccaggagttaaaaacca	cccaaacactggatgcttct
Exon 5	agctctgggggtgactgt	tcctctccatctccctctcc
Exon 6	gcaaaagtgggccatttca	gcaggggctgtgtcttactc
Exon 7	gagtcaggcttcttgcttg	gctgggggtcttcttattct
Exon 8	cctccaataagccatcagc	aaaacctccatccctctg
Exon 9	gggcttgctgctacggtatgt	ctggctctggcatgactct
Exon 10	aaggattccattcagccctga	caaggatgcgtcgtgttg

Na_2HPO_4 , 2 mM KH_2PO_4 and 0.05% Tween-20) containing 10% non-fat dry milk overnight at 4°C. The blot was then incubated with rabbit anti-*ACCN1* antibody (1:2000 dilution, Upstate/Chemicon, Temecula, CA) or anti-Lamin A antibody (1:20,000, Invitrogen) at 37°C for 1 h, washed 6×, 5 min each, with PBST containing 2% non-fat dry milk; incubated with horseradish peroxidase conjugated goat-anti-rabbit secondary antibody (1:20,000, Vector labs, Burlingame, CA) for 1 h at 37°C, washed 6×, 5 min each with PBST; and detected with Western Lightning™ Chemiluminescence Reagent Plus (PerkinElmer, Boston, MA).

Results

Clinical findings

SMS224 is an 8-year-old male with cognitive delay, facial dysmorphisms, severe behavioral abnormalities, weak extremities, sensorimotor neuropathy, and congenital heart disease (Fig. 1a). Initial evaluation by a high-resolution G-banding technique revealed a partial duplication of chromosome 17p.

The pre-natal period was complicated by maternal exposure to parvovirus B19 followed by delivery at 36 weeks. The post-natal period was complicated by neonatal unconjugated hyperbilirubinemia

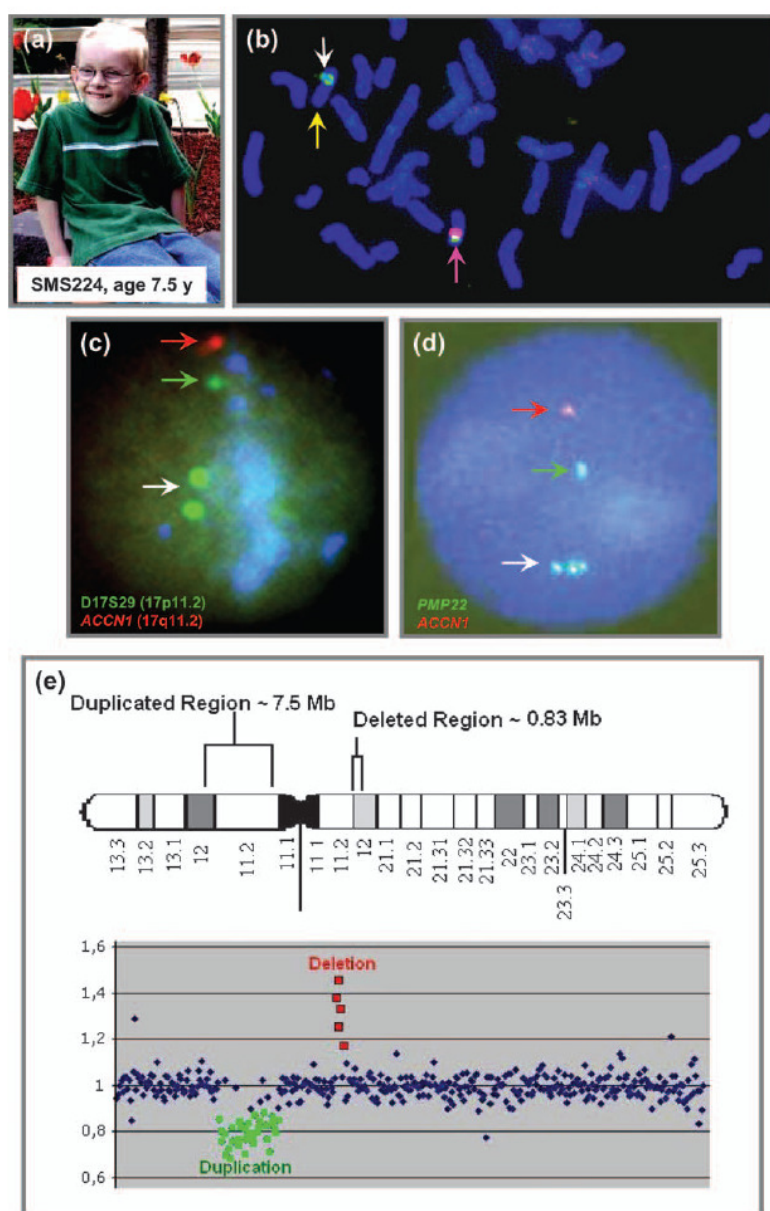


Fig. 1. Molecular analysis of SMS224: (a) Photo of SMS224 at the age of 7.5 years. (b) FISH analysis on a metaphase spread showing *ACCN1* (RP11-90A23) deletion (yellow arrow) and 17p11.2 (CTC-457L16/D17S29) duplication (white arrow) on the same homologue of chromosome 17. The normal chromosome 17 homologue is indicated (pink arrow). (c) FISH on an interphase nucleus shows a duplication (white arrow) and a normal copy (green arrow) for a 17p11.2 probe (CTC-457L16/D17S29). A single copy of *ACCN1* (RP11-90A23) is also indicated (red arrow). (d) FISH on an interphase nucleus shows a triplication for the *PMP22* (RP11-764O6) probe on one chromosome 17 (white arrow) and a single copy of *PMP22* on the normal chromosome 17; *ACCN1* probe (RP11-90A23) shows a single copy (red arrow). (e) Array CGH data for SMS224 showing gain of DNA indicated by a peak that spans 17(p11.2)(p12) and loss of DNA on 17(q11.2)(q12) represented by an ideogram of chromosome 17 (top).

and paresis of the right leg because of a thoracolumbar syrinx detected by magnetic resonance imaging (MRI). Syrinx decompression by shunt insertion was performed at about 1 year of age, after which his physical capacity and activity improved. Significant feeding difficulties and hypotonia were observed during early infancy with poor weight gain, and he was subsequently diagnosed with oropharyngeal dysphagia for which he was under nasogastric intubation until 6 months of age. A history of constipation prompted a rectal biopsy for Hirschsprung disease, which was normal. Because the subject developed recurrent, unexplained fevers and seemed to be anhidrotic, he was evaluated by a clinical geneticist who did not find evidence for anhidrotic ectodermal dysplasia. Developmentally, he has exhibited delays in physical and verbal milestones, as well as delays in social, emotional, and cognitive functioning. His first steps were at 18 month of age but have become independent for ambulation although he has a mild steppage gait. He currently has very little speech and has been communicating his needs by pointing or leading people to what he wants. He has normal dentition and normal tooth eruption.

Initially, a number of studies were performed including tests for urine and plasma amino acids, organic acids, peroxisomal panel, acylcarnitine panel, and immunological testing, all of which were normal. Subsequent analysis for fragile X and FISH studies for velocardiofacial syndrome were negative. Further clinical evaluations revealed a series of medical problems. An echocardiogram showed a number of congenital abnormalities including a bicuspid aortic valve, dilated aortic root and ascending aortic aneurysm, patent foramen ovale, and a ventriculoseptal defect for which he underwent a valve-sparing root and ascending aortic replacement surgeries. He also had mild mitral regurgitation and left ventricular hypertrophy with a shortening fraction of 36%. He also had several episodes per week of unexplained sinus tachycardia, with heart rates up to 190 beats/min, associated with syncope and cyanosis and that were investigated by cardiac catheterization. In addition to confirming the echocardiographic findings, he was found to have a narrow right coronary artery ostium. Episodic syncope was thought to be caused by poor flow into the right coronary artery, resulting in transient reduction in cardiac output, or by a Bezold–Jarisch reflex precipitated by obstruction to flow at the aortic valve. Syncopal spells resolved after replacement of the aortic root, aortic valve, and ascending aorta, and regrafting of the right coronary artery.

Frequent episodes of altered consciousness, compatible with non-convulsive seizures, were also

seen in this child. Electroencephalogram studies documented multifocal epileptiform discharges on several occasions and almost continuous spike and slow wave activity during sleep. Occasionally, postictal periods were characterized by transient improvement in his ability to form coherent sentences. MRI of the brain showed patchy white matter abnormalities. 3-D time-of-flight magnetic resonance angiogram (MRA) of the circle of Willis showed no evidence of an arteriovenous malformation or aneurysm, although a slight asymmetry in the flow of the carotid arteries, the right being slightly smaller than the left, was documented. Magnetic resonance spectroscopy was also within normal limits.

Parents of SMS224 note that he had difficulty recognizing faces and following objects at 3–4 years of age. Ophthalmologic examination revealed severe hyperopia and some amblyopia for which refractive correction was given. External eye exams revealed no ptosis or proptosis, and no preferential fixation or nystagmus was noted. His eye movements were conjugate with intact corneal reflexes. The patient was sensitive to bright light and preferred dim light. Examination of the anterior segments showed no abnormalities; pupils were reactive to light with no relative afferent pupillary defect. Dilated fundus examination revealed a pink, healthy optic disc with no pallor or swelling. The history of photophobia was suspected for a cone dystrophy, although, his central vision was normal. A possible retinal dystrophy because of the deletion of *ACCNI*, implicated in light-induced damage to the retina, was considered; retinal fundus and electroretinogram studies showed no abnormalities.

Sleep studies revealed severe sleep disordered breathing with hypercapnia. He was reportedly very difficult to wake up as a baby but now has reversed and was reported as an extremely light sleeper. He also has obstructive and central apnea. SMS224 also had enlarged tonsils and adenoids for which he underwent surgery. Hearing exams revealed a moderately severe hearing loss. In addition, the patient was evaluated for malignant hyperthermia because of unexplained fevers and inappropriate sweating that is accompanied by muscle twitching, leukocytosis, and hyperglycemia after general anesthesia that usually resolved within 24 h. A malrotation of the left kidney was also identified by ultrasound.

Upon physical examination at the age of 7 years, he was unable to follow verbal cues and does not follow simple commands. He reached for objects and would accurately grasp them in a coarse fashion and in a purposeful manner. At the age of 7.5 years, his height was 120 cm (~50th percentile),

weight 22 kg (<5th percentile). His facial features showed a prominent forehead, downslanting palpebral fissures, mild mandibular hypoplasia, and a normal palate and uvula. He had dental caries and a notch in his left lower incisor superiorly. He had long fingers, hyperextensibility at the elbows and proximal interphalangeal joints, and flat arches of the feet. Cardiovascular examination was significant with a 3/6 harsh ejection systolic murmur with no diastolic murmur heard. His lungs were clear to auscultation bilaterally. Neurologically, he had some truncal hypotonia with increased tone symmetrically in both legs. Extremity examination showed metatarsus adductus bilaterally. He had delayed deep tendon reflexes, a withdrawal plantar response. He was non-verbal, ambulatory without assistance, and he had coarse motor control of his upper and lower extremities with a coarse gait and a slight foot slap when walking.

Peripheral nerve biopsy showed reduced packing density with expansion of the intervening endoneurial connective tissue consistent with moderately severe nerve fiber loss. On ultrastructural examination, many of the myelinated fibers showed retraction between axoplasm and myelin sheath; occasionally, rare fibers showed several concentrically arranged profiles of Schwann cell cytoplasm external to the myelinating Schwann cell, suggestive of early onion bulb formation. Gastrocnemius muscle biopsy showed moderately scattered atrophic fibers, relatively small diameter type 2 fibers, and mild fiber type grouping that is most prominent in the type 2 fiber population. Endomysial capillaries appeared dilated and prominent with thickening of the basal lamina. Electron microscopy showed well-formed myofibrils with no definite increase in myofiber glycogen, lipid, or mitochondrial content noted. Electromyography and nerve conduction studies (~15 m/sec) showed signs of demyelinating polyneuropathy, compatible with CMT1A.

There is no relevant family history of consanguinity, peripheral neuromuscular disease, or mental retardation. There is a history of miscarriages on the maternal side wherein the mother has had four miscarriages, and the grandmother has had seven. There is also a family history of cardiovascular manifestation with his sister having a dilated aorta and his maternal half-sister having a dilated aorta and long QT syndrome. In addition, there is a history on his paternal grandfather's side of individuals having undergone aortic replacement or rupture, including a cousin having an aortic rupture in his twenties. A possibility of Marfan syndrome in this family was assessed and subsequently ruled-out after a thorough clinical evaluation. A summary of clinical features in

SMS224 compared with published data on patients with different sized chromosome 17 duplications is given in Table 3.

Molecular findings

Initial cytogenetic analysis of peripheral blood from SMS224 by karyotyping and standard GTG banding techniques showed a partial duplication of chromosome 17: 46,XY,dup(17)(p11.2p12). FISH studies confirmed the duplication and also identified a mosaic triplication or partial tetrasomy in ~25% of the interphase nuclei. The duplication maps ~7.5 Mb region within 17(p11.2p12) including the CMT1A and the SMS regions and encompassing more than 100 genes including (from telomere to centromere) *COX10*, *PMP22*, *ADORA2B*, *UBB*, *TNFRSF13B*, *RAI1*, *DRG2*, *PRPSAP2*, *EPN2*, *SPECC1*, *USP22* and *KCNJ12* (Table 1, Fig. 1b–d). Genotyping of patient and parental DNAs to determine the parent of origin for the 17p11.2 duplication revealed the presence of one paternal allele and both maternal alleles indicating a maternal inter-chromosomal recombination event. Further, aCGH was performed to identify any other genomic rearrangements that might contribute to the unusual features in this patient. Array CGH not only confirmed the breakpoints of the 17(p11.2p12) duplication but also identified a deletion containing exon 1 of the amiloride-sensitive cation channel neuronal 1 (*ACCNI*) gene and a cluster of genes coding for cytokine receptors (*CCL2*, *CCL7*, *CCL8*, and *CCL11*) on chromosome 17(q11.2q12) (Table 1, Fig. 1f). FISH was performed to confirm the extent of the deletion using locus specific probes; RP11-797M22, RP11-90A23, RP11-79K15, RP11-47G8, and RP11-329H16 (see Methods). The deletion was confirmed in all the cells examined by FISH. Parental chromosome analyses for both rearrangements on chromosome 17 using FISH and aCGH were negative.

Genotype–phenotype correlation

Comparison of clinical features of published cases with different sized chromosome 17 duplications to SMS224 shows that our patient has many features consistent with a large-sized duplication such as severe cognitive impairment, severe mental retardation, facial dysmorphism, cardiovascular, and renal defects (Table 3). To identify clinical features solely due to the 17p rearrangement, ~40 clinical characteristics of reported cases with duplication 17p including dup17p11.2p11.2, dup17p11.2p12, dup17p11.2p10, and trisomy 17p were analyzed. While the 31 cases reported in the literature do show variability (summarized in Table 3), a common

Table 3. Clinical features of trisomy 17p, dup17p10p12, dup17p11.2p12, dup17p11.2p11.2, and SMS224^a

Clinical features ^b	Trisomy 17p <i>n</i> = 12	Dup(17) (p10p12) <i>n</i> = 4	Dup(17) (p11.2p12) <i>n</i> = 7	Dup(17) (p11.2p11.2) <i>n</i> = 8	SMS224
Mental retardation	10/10	4/4	7/7	8/8	+
Pre- /post-natal growth retardation	12/12	3/4	7/7	3/3	+
Motor delay	12/12	4/4	7/7	2/3	+
Speech delay	2/2	4/4	5/5	2/4	+
Maternal history of spontaneous abortions	3/8	1/3	<i>n</i>	<i>n</i>	+
Hypotonia	6/10	4/4	2/3	2/4	+
Feeding difficulties	7/7	4/4	3/4	1/3	+
Hyperactivity/behavioral abnormalities	<i>n</i>	1/3	2/5	4/6	+
Seizures	2/12	2/4	1/6	3/7	+
Decreased nerve conduction	1/1	1/4	5/6	0/8	+
Delayed deep tendon reflexes	1/1	1/4	6/7	0/8	+
Craniofacial features					
Triangular face	<i>n</i>	3/3	2/4	1/2	+
Microcephaly	12/12	4/4	2/3	4/6	—
Micrognathia	11/12	3/4	1/4	2/3	—
Hypertelorism	8/12	2/4	3/3	1/3	—
Broad nasal bridge	11/12	4/4	4/5	2/4	—
Low-set/malformed ears	12/12	2/4	4/4	3/3	+
High arched palate	7/12	1/4	3/5	3/4	+
Cleft lip/palate	4/12	0/4	0/7	1/4	—
Ophthalmologic disorders					
Downslanting palpebral fissures	9/12	2/4	6/6	4/4	+
Ptosis	6/12	2/4	1/7	<i>n</i>	—
Myopia or hyperopia	<i>n</i>	2/4	2/7	1/3	+
Strabismus	<i>n</i>	0/4	1/7	1/2	—
Others eye anomalies	7/10	0/4	0/8	0/8	+
Short broad neck	7/12	<i>n</i>	1/7	<i>n</i>	—
Hearing loss	3/3	1/4	1/7	1/3	+
Cardiac anomalies					
Valvular defects	5/12	0/4	2/7	0/8	+
Dilated aorta/aneurysms/coarctation	1/12	0/4	0/7	0/8	+
Renal/urinary tract anomalies	3/12	1/4	1/7	2/8	+
Short stature	11/12	1/4	6/6	5/8	—
Decreased weight	11/12	1/4	4/4	3/5	+
Bone and limb defects					
Clinodactyly of fifth finger	7/12	<i>n</i>	4/7	2/8	—
Flexion contractures	10/12	1/4	3/7	0/8	—
Foot anomalies	5/12	2/4	6/7	0/8	—
Short sternum	7/12	<i>n</i>	1/6	<i>n</i>	<i>n</i>
Dental anomalies	<i>n</i>	1/4	4/7	5/8	—
Widely placed nipples	5/10	<i>n</i>	1/1	<i>n</i>	<i>n</i>
Single palmar crease	4/9	<i>n</i>	<i>n</i>	<i>n</i>	<i>n</i>
Malignant hyperthermia	<i>n</i>	<i>n</i>	<i>n</i>	<i>n</i>	+
Syringomyelia	<i>n</i>	<i>n</i>	<i>n</i>	<i>n</i>	+

^aThe numbers are based on published case reports of trisomy 17p [Bartsch-Sandhoff et al. (12); Feldman et al. (13); Jinno et al. 1982; Kulharya et al. 1998; Latta et al. 1974; Martsof et al. (29); Mascarello et al. (15); Mikhail et al. 2006; Palutke et al. (11); Schrandner-Stumpel et al. (17); Shabtai et al. 1979; Yamamoto et al. 1979], dup(17)(p10p12) [Docherty et al. (14); Shaw et al. (27); Stankiewicz et al. 2001; Yatsenko et al. (28)] dup(17)(p11.2p12), [Kozma et al. (18); Lupski et al. 1992; Magenis et al. (16); Pellegrino et al. (20); Potocki et al. 1999; Roa et al. (22); Upadhyaya et al. (19)], and dup(17)(p11.2p11.2) [Balarin et al. (23), Brown et al. (21), Potocki et al. (24), Schneider et al. (25)].

^bNote that the denominators in each of the features are not equal to '*n*' numbers because of: incomplete or missing data and/or age not appropriate for assessment of that particular feature.

phenotype for dup17p syndrome did emerge. SMS224 has the clinical features common to these patients, such as characteristic craniofacial features, pre- and post-natal growth retardation, feeding difficulties, hyperactivity, cognitive impairment, speech delay, and hypotonia (Table 3). Further, the presence of delayed tendon reflexes,

decreased nerve conduction, and peripheral neuromuscular disease is consistent with the involvement of *PMP22* (duplication of which causes CMT1A). However, limb abnormalities including flexion deformity of fingers, clinodactyly of fifth finger, and club foot that are commonly seen in patients with 17p duplications were not seen in our

patient. Published cases of CMT1A homozygous for the 17p11.2 duplication have variable severity of clinical features suggesting that the severity and variability of the disease are not determined solely by the copy number of *PMP22* (32). Thus, the more severe manifestations and the unusual, previously unreported features in SMS224 (Table 3) can be because of the following: increased dosage of genes within the triplicated segment, involvement of genes such as *AKAP10*, *SPECC1*, *USP22*, *TMEM*, *MAP2K3*, and *KCNJ12* that are outside the SMS and CMT1A regions but within the chromosome 17p rearrangement breakpoints, or because of haploinsufficiency of genes on chromosome 17q11.2q12 (*ACCNI* and/or cytokine gene cluster).

Certain clinical manifestations seen in SMS224 such as severe cardiac manifestations, multiform epileptic seizures, thoracolumbar syrinx, and malignant hyperthermia are unusual and are not reported in patients with duplication 17p (Table 3). These features could be associated with the 17q11.2q12 deletion encompassing *ACCNI* and the cluster of cytokines or may be because of another, undetected, genetic abnormality.

Contribution of *ACCNI* towards severe phenotype in SMS224

ACCNI (also known as *BNAC1*, *BNC1*, *ASIC2*, or *MDEG*) maps to the long arm of chromosome 17 and is composed of 10 exons encoding a member of the degenerin/epithelial sodium channel (DEG/ENaC) superfamily (Fig. 2a) (33). Alternative splicing has been observed at this locus and two

variants, encoding distinct isoforms differing in the first 184 amino acids, have also been identified (Fig. 2a). *ACCNI* is expressed during early embryogenesis and throughout post-natal life in the central and peripheral nervous systems of humans, specifically the brain (34). The members of this family are amiloride-sensitive sodium channels that contain intracellular N- and C-termini, 2 hydrophobic transmembrane regions (TM1 and TM2), and a large extracellular loop, which has many cysteine residues with conserved spacing (Fig. 2b) (35). *ACCNI* is glycosylated at the two N-linked asparagine residues 365 and 392 during post-translational processing (Fig. 2b) (36, 37). The pre-transmembrane domain (pre-TM2) and the second transmembrane segment (TM2) form the amiloride-binding site and determine the selectivity of the channel (Fig. 2b) (38). Also, the conserved domain at the N-terminal end and the cysteine rich domain near the transmembrane domain 2 (TM2) are important for the basic function of the channel (39).

This class of acid-sensing channels also contributes to learning and memory as well as acidosis-induced injury, where they may act as mediators of stimuli that respond to the acidosis that accompanies stroke, epilepsy, and trauma under pathological conditions (40, 41). Comparison of clinical features in patients with NF1 with large 17q11.2 deletions encompassing *ACCNI* shows that variable mental retardation is the only common feature possibly contributed by *ACCNI* (42). To support this, Venturin et al. (43) performed a deletion gene

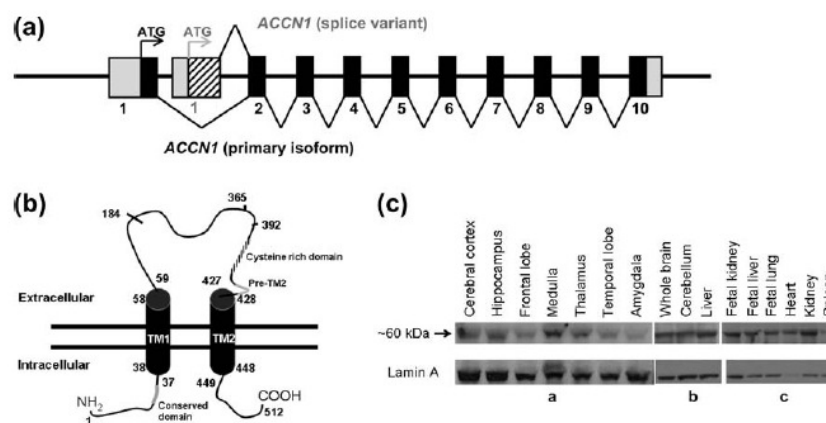


Fig. 2. Genomic structure, protein structure, and expression of *ACCNI*: (a) The genomic architecture of *ACCNI* with 10 exons (filled boxes) and 5' and 3' UTRs (open boxes) is shown. Alternatively, spliced first exon (striped box) is also shown. (b) Schematic representation of *ACCNI* showing intracellular N-terminus region, transmembrane domains (TM1 and TM2, black cylinders), a large extracellular loop, a pre-transmembrane domain (pre-TM2, gray segment), and a C-terminal intracellular tail (37). The amino acid residues forming the different components of *ACCNI* are depicted. N-linked asparagine residues 365 and 392 are glycosylated during post-translational modification. (36) Other regions of importance are the conserved domain at the N-terminal end (gray segment) and the cysteine-rich domain (striped segment) near the TM2. (c) Western blot analysis of human tissue-specific protein medleys shows an ~60 kDa band corresponding to *ACCNI* (see Methods). Blots contain 40 μ g (a & b) or 20 μ g (c) of each protein lysate (see Methods).

content analysis in patients with NF1 micro-deletion and identified six genes including *ACCNI*, where haploinsufficiency may contribute to the mental retardation in these patients. Further, the *ACCNI* family of neuronal degenerins has been implicated in neurodegeneration in *Caenorhabditis elegans* and epilepsy in humans (34, 44). Adult *Accn1* knockout mice exhibit light-induced retinal degeneration as a result of uncontrolled rod photo transduction (34, 45).

To further understand the expression pattern of ACCN1 in human tissues, western analysis was performed using human tissue-specific protein medleys (Fig. 2c). Results indicate that the major isoform of ACCN1 (~60 kDa) is expressed in all of the major organs namely, fetal and adult brain (cerebral cortex, cerebellum, medulla, hippocampus, thalamus, amygdala, and frontal and temporal lobes), liver, heart, kidney, and spleen. *ACCNI* expression is not confined to the brain as previously reported (Fig. 2c) (34). Alignment of the ACCN1 protein sequences of human, chimp, mouse, and rat showed that human and mouse

sequences are 99.2% identical and 99.4% similar; humans and rats have 99% identity and 99.2% similarity whereas humans and chimps share 100% identity (Fig. 3).

To further assess any possible role for *ACCNI* in the phenotype in SMS224, the entire *ACCNI* gene was sequenced including the coding exons and the splice variants (Table 2). Sequence analysis of the non-deleted allele of *ACCNI* and its splice variant showed no mutations.

Discussion

In this report, we describe a male patient with a multiple congenital abnormalities/mental retardation syndrome associated with unusual systemic manifestations and a severe phenotype. His initial cytogenetic findings showed a chromosome 17p11.2p12 duplication involving both the SMS and CMT1A regions. It is clear that other patients with duplications of the proximal 17p region have mild clinical abnormalities, but the severity seen in our patient prompted further genome-wide studies.

Human	1	SERVSYYFSYQHVTKVDEVVAQSLVPPAVTLCNLNGFRFSRLTTNDLYHAGELLALLDVN
Chimp	1	SERVSYYFSYQHVTKVDEVVAQSLVPPAVTLCNLNGFRFSRLTTNDLYHAGELLALLDVN
Mouse	1	SERVSYYFSYQHVTKVDEVVAQSLVPPAVTLCNLNGFRFSRLTTNDLYHAGELLALLDVN
Rat	1	SERVSYYFSYQHVTKVDEVVAQSLVPPAVTLCNLNGFRFSRLTTNDLYHAGELLALLDVN
Human	61	LQIPDPHLADPSVLEALRQKANFKHYKPKQFSMLEFLHRVGHDLKDMMLYCKFKGQECGH
Chimp	61	LQIPDPHLADPSVLEALRQKANFKHYKPKQFSMLEFLHRVGHDLKDMMLYCKFKGQECGH
Mouse	61	LQIPDPHLADPTVLEALRQKANFKHYKPKQFSMLEFLHRVGHDLKDMMLYCKFKGQECGH
Rat	61	LQIPDPHLADPTVLEALRQKANFKHYKPKQFSMLEFLHRVGHDLKDMMLYCKFKGQECGH
Human	121	QDFTTVFTKYGKCYMFNSGEDGKPLLTTVKGGTGNGLEIMLDIQQDEYLPWIGETEETTF
Chimp	121	QDFTTVFTKYGKCYMFNSGEDGKPLLTTVKGGTGNGLEIMLDIQQDEYLPWIGETEETTF
Mouse	121	QDFTTVFTKYGKCYMFNSGEDGKPLLTTVKGGTGNGLEIMLDIQQDEYLPWIGETEETTF
Rat	121	QDFTTVFTKYGKCYMFNSGEDGKPLLTTVKGGTGNGLEIMLDIQQDEYLPWIGETEETTF
Human	181	EAGVKVQIHSQSEPPPIQELGFGVAPGQTFVATQEQRLTYLPPPWGECRSSEMGLDFFP
Chimp	181	EAGVKVQIHSQSEPPPIQELGFGVAPGQTFVATQEQRLTYLPPPWGECRSSEMGLDFFP
Mouse	181	EAGVKVQIHSQSEPPPIQELGFGVAPGQTFVATQEQRLTYLPPPWGECRSSEMGLDFFP
Rat	181	EAGVKVQIHSQSEPPPIQELGFGVAPGQTFVATQEQRLTYLPPPWGECRSSEMGLDFFP
Human	241	VYSITACRIDCETRYIVENCNCRMVHMPGDAPFCTPEQHKCEAEPALGLLAEKDSNYCLC
Chimp	241	VYSITACRIDCETRYIVENCNCRMVHMPGDAPFCTPEQHKCEAEPALGLLAEKDSNYCLC
Mouse	241	VYSITACRIDCETRYIVENCNCRMVHMPGDAPFCTPEQHKCEAEPALGLLAEKDSNYCLC
Rat	241	VYSITACRIDCETRYIVENCNCRMVHMPGDAPFCTPEQHKCEAEPALGLLAEKDSNYCLC
Human	301	RTPCNLTRYNKELSMVKIPSKTSAKYLEKKFNKSEKYISENILLVDIFFEALNYETIEQK
Chimp	301	RTPCNLTRYNKELSMVKIPSKTSAKYLEKKFNKSEKYISENILLVDIFFEALNYETIEQK
Mouse	301	RTPCNLTRYNKELSMVKIPSKTSAKYLEKKFNKSEKYISENILLVDIFFEALNYETIEQK
Rat	301	RTPCNLTRYNKELSMVKIPSKTSAKYLEKKFNKSEKYISENILLVDIFFEALNYETIEQK
Human	361	KAYEVAALLGDIGGQMGLFIGASILTILELFDYIYELIKEKLLDLLGKEEPEGSHDENVS
Chimp	361	KAYEVAALLGDIGGQMGLFIGASILTILELFDYIYELIKEKLLDLLGKEEPEGSHDENVS
Mouse	361	KAYEVAALLGDIGGQMGLFIGASILTILELFDYIYELIKEKLLDLLGKEEPEGSHDENMS
Rat	361	KAYEVAALLGDIGGQMGLFIGASILTILELFDYIYELIKEKLLDLLGKEEPEGSHDENMS
Human	421	TCDTMPNHSETISHTVNVPLQTILGLTLEBIAC
Chimp	421	TCDTMPNHSETISHTVNVPLQTILGLTLEBIAC
Mouse	421	TCDTMPNHSETISHTVNVPLQTILGLTLEBIAC
Rat	421	TCDTMPNHSETISHTVNVPLQTILGLTLEBIAC

Fig. 3. ACCN1 is highly conserved through species. Boxshade alignment of human ACCN1 (Q16515, NM_001094), chimp (NP_001085, uncurated sequences from UCSC genome browser), rat (Q62962, NM_001034014), and mouse Accn1 (Q925H0, NM_1034013) sequences are shown.

FISH experiments identified a mosaic tetrasomy of the same chromosomal region as the duplication. Array CGH analysis mapped the extent of this chromosome 17p rearrangement, spanning from *COX10* to *KCNJ12* and also found a 17q11.2q12 deletion encompassing the first exon of *ACCN1* and a cluster of cytokine genes. A detailed clinical evaluation of this patient identified a complex and severe phenotype, including several previously unreported systemic manifestations. Genotype–phenotype analysis suggests that the severity of the phenotype in this patient is either because of the tetrasomy of ~100 genes on proximal 17p, some of which can be dosage sensitive, or because of the unusually large-sized duplication encompassing genes outside the SMS/CMT1A regions. The unusual features, hitherto not reported in patients with partial or complete duplication 17p, are possibly because of hemizygous deletion of the genes *ACCN1* and the cytokine cluster on 17(q11.2q12). SMS224 is legally blind and disruption of *ACCN1* may play a role in this aspect of the phenotype. Although an electroretinogram showed no indications of retinal degeneration in this patient, age-related progression of retinal degeneration cannot be ruled out. The cluster of cytokine genes, *CCL2*, *CCL7*, *CCL8*, and *CCL11*, is a family of secreted proteins involved in immunoregulatory and inflammatory processes. Further investigations need to be carried out to decipher the role of this group of genes in contributing to the phenotype in our patient.

A detailed analysis of the family history from SMS224 documented the presence of certain manifestations that might have a hereditary basis suggesting a role for genes/loci other than that

involved in the chromosome 17 rearrangement. There is a maternal history of miscarriages, suggesting the possibility of an inherited abnormality in the family even though parental karyotypes were normal. In addition, SMS224 was diagnosed with a dilated aortic root early in life and had aortic valve replacement surgeries. The sister of this patient was diagnosed with a dilated aortic root, and the half-sister from the mother's side also was diagnosed with a dilated aorta, long QT syndrome, scoliosis, extra teeth, and extreme flexibility. Also, the paternal side of the family has a history of aortic pathologies. While Marfan syndrome was ruled out in this family, the possibility of another locus elsewhere in the genome contributing to this connective tissue-associated phenotype requires further studies. Congenital bicuspid valve leading to aortic dilation has been reported earlier in sporadic and familial cases (46, 47). Thus, identification of more patients with similar hereditary defects might shed light in to the mode of inheritance and, possibly, help in the identification of susceptible loci.

We also report here for the first time a patient with tetrasomy 17p11.2p12. Triplications or partial tetrasomies for other chromosomal regions have been reported (Table 4) (48–62). Constitutional triplications of genomic regions have been associated with various disorders that include mental retardation syndromes, Pelizaeus–Merzbacher syndrome, Parkinsonism and recently, hereditary pancreatitis (63–66). The majority of chromosomal triplications reported so far are interstitial, with the exception of those cases reported by Devriendt et al. and Batanian et al. (48, 50) that have a triplication of the terminal chromosomal fragment.

Table 4. Summary of reported cases of intrachromosomal triplications

Clinical features	Triplicated segment	Reference
Multiple congenital anomalies associated with mental retardation, skeletal and craniofacial features, developmental delay	2q37	Rauch et al. (55)
	2q11.1q21	Wang et al. (61)
	3q25.3q29	Ounap et al. (54)
	5p14p15.33	Harrison et al. (52)
	7p21.3p22	Rivera et al. 1998
	8p22p23	Shieh et al. (58)
	9p13p22	Verheij et al. (60)
	9p22pter	Batanian et al. (48)
	10q26	Devriendt et al. (50)
	12p11.22p12.3	Eckel et al. (51)
	13q14	Brecevic et al. (49)
	13q22q23	Reddy and Logan 2001
	15q11q13	Roberts et al. (57)
	15q24q26	James et al. (53)
	22q11.2	Yobb et al. (62)
Hereditary pancreatitis	7q34 (<i>PRSS1</i>)	Marechal et al. (63)
Parkinsonism	Parkin gene (6q25.2q27)	Lucking et al. (64)
	A synuclein (4q21)	Singleton et al. (65)
Pelizaeus–Merzbacher disease	PLP (Xq22)	Wolf et al. (66)

The mechanism of duplication coupled with mosaic triplication in our patient could be because of an aberrant recombination during meiosis I followed by an intrachromosomal mitotic event resulting in mosaicism, similar to that described for other mosaic triplication cases (56). It is observed, in general, that tetrasomy of an autosomal segment causes a similar but more severe phenotype than trisomy of the same segment as demonstrated in tetrasomy 9p, 18p, and 15(q12-q13) (49). Thus, we can attribute the severity of the phenotype in our patient to increased copy number of dosage sensitive genes in 17p11.2p12 and unusual features to 17q11.2q12 deletion.

In conclusion, our study emphasizes the need for whole genome analysis in multiple congenital abnormalities/mental retardation disorders with unusual and severe phenotypes. Without the use of aCGH, this patient may never have been diagnosed with a 17q11.2q12 deletion possibly affecting his prognosis and treatment. Further, some duplications identified by cytogenetic analysis may, in fact, be triplications and therefore warrant further investigations by interphase FISH.

Acknowledgements

We thank our patient and his family for their interest and pursuit of research efforts. Drs Harold Dietz, Catherine Keegan, John Gerlach, and Michael Netzloff and Rebecca McFalda for helpful discussions, patient referral, and evaluation. This work was funded by a grant from the US National Institutes of Health (R01 HD38534) to S. H. E. and resources from Virginia Commonwealth University (to S. H. E.), and also the Roswell Park Cancer Center Support Grant CA16056 (to N. N.).

References

- Lee JA, Lupski JR. Genomic rearrangements and gene copy-number alterations as a cause of nervous system disorders. *Neuron* 2006; 52: 103–121.
- Lupski JR, de Oca-Luna RM, Slaugenhaupt S et al. DNA duplication associated with Charcot–Marie–Tooth disease type 1A. *Cell* 1991; 66: 219–232.
- Chance PF, Alderson MK, Leppig KA et al. DNA deletion associated with hereditary neuropathy with liability to pressure palsies. *Cell* 1993; 72: 143–151.
- Smith AC, McGavran L, Robinson J et al. Interstitial deletion of (17)(p11.2p11.2) in nine patients. *Am J Med Genet* 1986; 24: 393–414.
- Vlangos CN, Yim DK, Elsea SH. Refinement of the Smith–Magenis syndrome critical region to approximately 950kb and assessment of 17p11.2 deletions. Are all deletions created equally? *Mol Genet Metab* 2003; 79: 134–141.
- Vlangos CN, Wilson M, Blancato J et al. Diagnostic FISH probes for del(17)(p11.2p11.2) associated with Smith–Magenis syndrome should contain the RAI1 gene. *Am J Med Genet A* 2005; 132: 278–282.
- Slager RE, Newton TL, Vlangos CN et al. Mutations in RAI1 associated with Smith–Magenis syndrome. *Nat Genet* 2003; 33: 466–468.
- Bi W, Saifi GM, Shaw CJ et al. Mutations of RAI1, a PHD-containing protein, in nondeletion patients with Smith–Magenis syndrome. *Hum Genet* 2004; 115: 515–524.
- Girirajan S, Elsas LJ 2nd, Devriendt K et al. RAI1 variations in Smith–Magenis syndrome patients without 17p11.2 deletions. *J Med Genet* 2005; 42: 820–828.
- Girirajan S, Vlangos CN, Szomju BB et al. Genotype–phenotype correlation in Smith–Magenis syndrome: evidence that multiple genes in 17p11.2 contribute to the clinical spectrum. *Genet Med* 2006; 8: 417–427.
- Palutke W, Chen H, Woolley P Jr et al. An extra small metacentric chromosome identified as a deleted chromosome no. 17. *Clin Genet* 1976; 9: 454–458.
- Bartsch-Sandhoff M, Hieronimi G. Partial duplication of 17p. A new chromosomal syndrome. *Hum Genet* 1979; 49: 123–127.
- Feldman GM, Baumer JG, Sparkes RS. Brief clinical report: the dup(17p) syndrome. *Am J Med Genet* 1982; 11: 299–304.
- Docherty Z, Hulten MA, Honeyman MM. De novo tandem duplication 17p11 leads to cen. *J Med Genet* 1983; 20: 138–142.
- Mascarello JT, Jones MC, Hoyme HE et al. Duplication (17p) in a child with an isodicentric (17p) chromosome. *Am J Med Genet* 1983; 14: 67–72.
- Magenis RE, Brown MG, Allen L et al. De novo partial duplication of 17p [dup(17)(p12–p11.2)]: clinical report. *Am J Med Genet* 1986; 24: 415–420.
- Schrander-Stumpel C, Schrander J, Fryns JP et al. Trisomy 17p due to a t(8;17)(p23;p11.2)pat translocation. Case report and review of the literature. *Clin Genet* 1990; 37: 148–152.
- Kozma C, Meck JM, Loomis KJ et al. De novo duplication of 17p [dup(17)(p12 – p11.2)]: report of an additional case with confirmation of the cytogenetic, phenotypic, and developmental aspects. *Am J Med Genet* 1991; 41: 446–450.
- Upadhyaya M, Roberts SH, Farnham J et al. Charcot–Marie–Tooth disease 1A (CMT1A) associated with a maternal duplication of chromosome 17p11.2–>12. *Hum Genet* 1993; 91: 392–394.
- Pellegrino JE, Pellegrino L, Spinner NB et al. Developmental profile in a patient with monosomy 10q and dup(17p) associated with a peripheral neuropathy. *Am J Med Genet* 1996; 61: 377–381.
- Brown A, Phelan MC, Patil S et al. Two patients with duplication of 17p11.2: the reciprocal of the Smith–Magenis syndrome deletion? *Am J Med Genet* 1996; 63: 373–377.
- Roa BB, Greenberg F, Gunaratne P et al. Duplication of the PMP22 gene in 17p partial trisomy patients with Charcot–Marie–Tooth type-1 neuropathy. *Hum Genet* 1996; 97: 642–649.
- Balarin MA, da Silva Lopes VL, Varella-Garcia M. A dup(17)(p11.2p11.2) detected by fluorescence in situ hybridization in a boy with Alport syndrome. *Am J Med Genet* 1999; 82: 183–186.
- Potocki L, Chen KS, Park SS et al. Molecular mechanism for duplication 17p11.2 – the homologous recombination reciprocal of the Smith–Magenis microdeletion. *Nat Genet* 2000; 24: 84–87.
- Schneider MC, Hughes CR, Forrester S et al. Mild phenotype due to tandem duplication of 17p11.2. *Am J Med Genet* 2000; 94: 296–299.
- Stankiewicz P, Shaw CJ, Dapper JD et al. Genome architecture catalyzes nonrecurrent chromosomal rearrangements. *Am J Hum Genet* 2003; 72: 1101–1116.
- Shaw CJ, Stankiewicz P, Christodoulou J et al. A girl with duplication 17p10-p12 associated with a dicentric chromosome. *Am J Med Genet A* 2004; 124: 173–178.
- Yatsenko SA, Treadwell-Deering D, Krull K et al. Trisomy 17p10-p12 due to mosaic supernumerary marker chromosome: delineation of molecular breakpoints and clinical

- phenotype, and comparison to other proximal 17p segmental duplications. *Am J Med Genet A* 2005; 138: 175–180.
29. Martsolf JT, Larson L, Jalal SM et al. Complete trisomy 17p a relatively new syndrome. *Ann Genet* 1988; 31: 172–174.
 30. Lucas RE, Vlangos CN, Das P et al. Genomic organisation of the approximately 1.5 Mb Smith–Magenis syndrome critical interval: transcription map, genomic contig, and candidate gene analysis. *Eur J Hum Genet* 2001; 9: 892–902.
 31. Cowell JK, Nowak NJ. High-resolution analysis of genetic events in cancer cells using bacterial artificial chromosome arrays and comparative genome hybridization. *Adv Cancer Res* 2003; 90: 91–125.
 32. LeGuern E, Gouider R, Mabin D et al. Patients homozygous for the 17p11.2 duplication in Charcot-Marie-Tooth type 1A disease. *Ann Neurol* 1997; 41: 104–108.
 33. Waldmann R, Voilley N, Mattei MG et al. The human degenerin MDEG, an amiloride-sensitive neuronal cation channel, is localized on chromosome 17q11.2–17q12 close to the microsatellite D17S798. *Genomics* 1996; 37: 269–270.
 34. Waldmann R, Champigny G, Voilley N et al. The mammalian degenerin MDEG, an amiloride-sensitive cation channel activated by mutations causing neurodegeneration in *Caenorhabditis elegans*. *J Biol Chem* 1996; 271: 10433–10436.
 35. Darboux I, Lingueglia E, Champigny G et al. dGNaCl, a gonad-specific amiloride-sensitive Na⁺ channel. *J Biol Chem* 1998; 273: 9424–9429.
 36. Saugstad JA, Roberts JA, Dong J et al. Analysis of the membrane topology of the acid-sensing ion channel 2a. *J Biol Chem* 2004; 279: 55514–55519.
 37. Snyder PM, McDonald FJ, Stokes JB et al. Membrane topology of the amiloride-sensitive epithelial sodium channel. *J Biol Chem* 1994; 269: 24379–24383.
 38. Kellenberger S, Gautschi I, Schild L. A single point mutation in the pore region of the epithelial Na⁺ channel changes ion selectivity by modifying molecular sieving. *Proc Natl Acad Sci U S A* 1999; 96: 4170–4175.
 39. Bianchi L, Driscoll M. Protons at the gate: DEG/ENaC ion channels help us feel and remember. *Neuron* 2002; 34: 337–340.
 40. Wemmie JA, Chen J, Askwith CC et al. The acid-activated ion channel ASIC contributes to synaptic plasticity, learning, and memory. *Neuron* 2002; 34: 463–477.
 41. Xiong ZG, Zhu XM, Chu XP et al. Neuroprotection in ischemia: blocking calcium-permeable acid-sensing ion channels. *Cell* 2004; 118: 687–698.
 42. Riva P, Corrado L, Natacci F et al. NF1 microdeletion syndrome: refined FISH characterization of sporadic and familial deletions with locus-specific probes. *Am J Hum Genet* 2000; 66: 100–109.
 43. Venturin M, Guarnieri P, Natacci F et al. Mental retardation and cardiovascular malformations in NF1 microdeleted patients point to candidate genes in 17q11.2. *J Med Genet* 2004; 41: 35–41.
 44. Biagini G, Babinski K, Avoli M et al. Regional and subunit-specific downregulation of acid-sensing ion channels in the pilocarpine model of epilepsy. *Neurobiol Dis* 2001; 8: 45–58.
 45. Ettaiche M, Guy N, Hofman P et al. Acid-sensing ion channel 2 is important for retinal function and protects against light-induced retinal degeneration. *J Neurosci* 2004; 24: 1005–1012.
 46. Clementi M, Notari L, Borghi A et al. Familial congenital bicuspid aortic valve: a disorder of uncertain inheritance. *Am J Med Genet* 1996; 62: 336–338.
 47. McKusick VA. Association of congenital bicuspid aortic valve and Erdheim's cystic medial necrosis. *Lancet* 1972; 1: 1026–1027.
 48. Batanian JR, Chen X, Grange DK. Mosaic isodicentric chromosome 9 triplication (9p22-pter) and no deletion in an abnormal infant presenting with clinical features of trisomy 9: a new type of isodicentric chromosome formation. *Am J Hum Genet* 1994; 55: A98.
 49. Brecevic L, Basaran S, Dutly F et al. Tandem triplication of chromosome 13q14 with inverted interstitial segment in a 4 year old girl. *J Med Genet* 2000; 37: 964–967.
 50. Devriendt K, Matthijs G, Holvoet M et al. Triplication of distal chromosome 10q. *J Med Genet* 1999; 36: 242–245.
 51. Eckel H, Wimmer R, Volleth M et al. Intrachromosomal triplication 12p11.22–p12.3 and gonadal mosaicism of partial tetrasomy 12p. *Am J Med Genet A* 2006; 140: 1219–1222.
 52. Harrison KJ, Teshima IE, Silver MM et al. Partial tetrasomy with triplication of chromosome (5) (p14–p15.33) in a patient with severe multiple congenital anomalies. *Am J Med Genet* 1998; 79: 103–107.
 53. James PA, Aftimos S, Oei P. Partial tetrasomy 15 due to a unique inverted triplication of chromosome 15q24–q26. *Am J Med Genet A* 2004; 130: 208–210.
 54. Ounap K, Ilus T, Bartsch O. A girl with inverted triplication of chromosome 3q25.3–> q29 and multiple congenital anomalies consistent with 3q duplication syndrome. *Am J Med Genet A* 2005; 134: 434–438.
 55. Rauch A, Pfeiffer RA, Trautmann U. Deletion or triplication of the alpha 3 (VI) collagen gene in three patients with 2q37 chromosome aberrations and symptoms of collagen-related disorders. *Clin Genet* 1996; 49: 279–285.
 56. Reddy KS, Logan JJ. Intrachromosomal triplications: molecular cytogenetic and clinical studies. *Clin Genet* 2000; 58: 134–141.
 57. Roberts SE, Dennis NR, Browne CE et al. Characterisation of interstitial duplications and triplications of chromosome 15q11–q13. *Hum Genet* 2002; 110: 227–234.
 58. Shieh JT, Hudgins L, Cherry AM et al. Triplication of 8p22–8p23 in a patient with features similar to Kabuki syndrome. *Am J Med Genet A* 2006; 140: 170–173.
 59. Thomas PK, Marques W Jr, Davis MB et al. The phenotypic manifestations of chromosome 17p11.2 duplication. *Brain* 1997; 120 (Pt 3): 465–478.
 60. Verheij JB, Bouman K, van Lingen RA et al. Tetrasomy 9p due to an intrachromosomal triplication of 9p13–p22. *Am J Med Genet* 1999; 86: 168–173.
 61. Wang J, Reddy KS, Wang E et al. Intrachromosomal triplication of 2q11.2–q21 in a severely malformed infant: case report and review of triplications and their possible mechanism. *Am J Med Genet* 1999; 82: 312–317.
 62. Yobb TM, Somerville MJ, Willatt L et al. Microduplication and triplication of 22q11.2: a highly variable syndrome. *Am J Hum Genet* 2005; 76: 865–876.
 63. Le Marechal C, Masson E, Chen JM et al. Hereditary pancreatitis caused by triplication of the trypsinogen locus. *Nat Genet* 2006; 38: 1372–1374.
 64. Lucking CB, Bonifati V, Periquet M et al. Pseudodominant inheritance and exon 2 triplication in a family with parkin gene mutations. *Neurology* 2001; 57: 924–927.
 65. Singleton AB, Farrer M, Johnson J et al. Alpha-synuclein locus triplication causes Parkinson's disease. *Science* 2003; 302: 841.
 66. Wolf NI, Sistermans EA, Cundall M et al. Three or more copies of the proteolipid protein gene PLP1 cause severe Pelizaeus–Merzbacher disease. *Brain* 2005; 128: 743–751.

Copyright of *Clinical Genetics* is the property of Blackwell Publishing Limited and its content may not be copied or emailed to multiple sites or posted to a listserv without the copyright holder's express written permission. However, users may print, download, or email articles for individual use.

Appendix C

Diagnosing Smith–Magenis Syndrome and Duplication 17p11.2 Syndrome by *RAI1* Gene Copy Number Variation Using Quantitative Real-Time PCR

Hoa T. Truong,¹ Sara Solaymani-Kohal,² Kevin R. Baker,³ Santhosh Girirajan,⁴ Stephen R. Williams,⁴ Christopher N. Vlangos,⁴ Ann C.M. Smith,^{5,6} David J. Bunyan,³ Paul E. Roffey,¹ Christopher L. Blanchard,¹ and Sarah H. Elsea⁴

Smith–Magenis syndrome (SMS) and duplication 17p11.2 (dup17p11.2) syndrome are multiple congenital anomalies/mental retardation disorders resulting from either a deletion or duplication of the 17p11.2 region, respectively. The retinoic acid induced 1 (*RAI1*) gene is the causative gene for SMS and is included in the 17p11.2 region of dup17p11.2 syndrome. Currently SMS and dup17p11.2 syndrome are diagnosed using a combination of clinically recognized phenotypes and molecular cytogenetic analyses such as fluorescent *in situ* hybridization (FISH). However, these methods have proven to be highly expensive, time consuming, and dependent upon the low resolving capabilities of the assay. To address the need for improved diagnostic methods for SMS and dup17p11.2 syndrome, we designed a quantitative real-time PCR (Q-PCR) assay that measures *RAI1* copy number using the comparative C_t method, $\Delta\Delta C_t$. We tested our assay with samples blinded to their previous SMS or dup17p11.2 syndrome status. In all cases, we were able to determine *RAI1* copy number status and render a correct diagnosis accordingly. We validated these results by both FISH and multiplex ligation-dependent probe amplification (MLPA). We conclude that Q-PCR is an accurate, reproducible, low-cost, and reliable assay that can be employed for routine use in SMS and dup17p11.2 diagnosis.

Introduction

SMITH–MAGENIS SYNDROME (SMS, OMIM #182290) is a multiple congenital anomalies/mental retardation disorder that includes distinctive facial features, cognitive and behavioral characteristics, self-injurious behaviors, and sleep disturbance (Smith *et al.*, 1986; Greenberg *et al.*, 1991; Greenberg *et al.*, 1996; Allanson *et al.*, 1999; Girirajan *et al.*, 2005). Nonallelic homologous recombination (NAHR) between SMS repeats (SMS-REPs) or other low copy repeats (LCRs) within the 17p11.2 region gives rise to SMS or the recombination reciprocal, duplication 17p11.2 (dup17p11.2) syndrome (Chen *et al.*, 1997; Potocki *et al.*, 2000; Bi *et al.*, 2003). Individuals with dup17p11.2 syndrome also present with congenital anomalies, neurological and behavioral characteristics, as well as other clinical features that are distinct from that of SMS (Magenis *et al.*, 1986; Potocki *et al.*, 2007; Girirajan

et al., 2007b). The phenotypic spectrum of both SMS and dup17p11.2 syndrome is outlined in Table 1.

The majority of SMS patients carry an interstitial deletion of 17p11.2. Of these, 70% have a common deletion that spans ~3.5 Mb, while the remainder harbor larger or smaller deletions. The phenotypic manifestations observed in SMS are believed to be due to either the haploinsufficiency of the retinoic acid induced 1 gene (*RAI1*), which lies within this interstitial deletion region, or mutation of the *RAI1* gene (Slager *et al.*, 2003; Vlangos *et al.*, 2003; Bi *et al.*, 2004; Girirajan *et al.*, 2005). Although *RAI1* has not been implicated as the causative gene in dup17p11.2 syndrome, it is contained within the recently refined 1.3 Mb critical region for this syndrome (Potocki *et al.*, 2007).

The prevalence of SMS is approximated at 1:25,000, and the prevalence of dup17p11.2 syndrome should be equivalent to that of its recombination reciprocal (Greenberg *et al.*,

¹Faculty of Science, Charles Sturt University, Wagga Wagga, NSW, Australia.

²University of the West of England, Bristol, United Kingdom.

³Wessex Regional Genetics Laboratory, Salisbury District Hospital, Salisbury, United Kingdom.

⁴Departments of Pediatrics and Human Genetics, Virginia Commonwealth University, Richmond, Virginia.

⁵Office of the Clinical Director, NHGRI, National Institutes of Health, Bethesda, Maryland.

⁶Georgetown University Medical Center, Washington, District of Columbia.

TABLE 1. CLINICAL MANIFESTATIONS OF SMITH-MAGENIS SYNDROME AND DUP17P11.2 SYNDROME

SMS				
Craniofacial/skeletal	Otolaryngologic	Neurological/behavioral	Ocular	Other
Brachycephaly Midface hypoplasia Prognathism Tented upper lip Broad, square face Synophrys Brachydactyly Short stature Scoliosis	Chronic ear infections Hearing loss Hoarse, deep voice	Variable mental retardation Speech delay Motor delay Hypotonia Seizures Sleep disturbance Self hugging Attention seeking Self-injurious behaviors - Onychotillomania - Polyembolokoilomania - Head banging	Myopia Strabismus	Cardiovascular anomalies Renal/urinary track abnormality Dental anomalies Hypercholesterolemia
Dup17p11.2				
Craniofacial/skeletal	Neurological/behavioral		Ocular	Other
Microcephaly Triangular face Pre- and postnatal growth delay	Variable mental retardation Speech delay Motor delay Hypotonia Failure to thrive in infancy Sleep apnea Hyperactivity		Hypermetropia	EEG abnormalities Low cholesterol Cardiovascular anomalies Oral-pharyngeal dysphagia Dental anomalies

1991; Potocki *et al.*, 2007). In the past decade, SMS diagnosis has relied upon a combination of clinical recognition of characteristic features, cytogenetic analysis, and molecular screening (Gropman *et al.*, 2006). The majority of cases of SMS have been diagnosed using G-banded chromosome analysis and/or fluorescent *in situ* hybridization (FISH). In patients where the SMS phenotype is present but there is no cytogenetically detectable deletion, the *RAI1* gene has been sequenced for mutations (Slager *et al.*, 2003; Bi *et al.*, 2004; Girirajan *et al.*, 2005). Routine G-banded chromosome analyses and/or FISH have typically been used to diagnose dup17p11.2 patients (Potocki *et al.*, 2007).

The incidence rate, however, is likely to be an underestimation due to the subtle phenotypes presented in both syndromes, the diversity in size of the deletions/duplications involved in perpetuating the syndrome, and also the reliability of the currently available diagnostic procedures (Struthers *et al.*, 2002; Potocki *et al.*, 2007). Many of the clinical and neurobehavioral features that are characteristic markers used in SMS diagnosis are subtle during infancy and early childhood but become increasingly pronounced with age, leading to a delayed diagnosis in many cases (Gropman *et al.*, 2006). Likewise, many of the features associated with dup17p11.2 syndrome escape recognition until later infancy or childhood (Potocki *et al.*, 2007).

Currently available cytogenetic methodologies that are routinely used in SMS and dup17p11.2 syndrome diagnoses have limitations. These include the low resolving power of G-banded karyotyping to visualize subtle deletions or duplications, the inability of FISH to detect deletions that may be smaller than the probes utilized, and the need for interphase rather than routine metaphase FISH to fully delineate duplicated regions. Further, from a practical diagnostic per-

spective, the cost, the time, and the labor intensity of these cytogenetic methodologies are considered to be quite high.

Together, all of these factors point to the need for an efficient, quick, and reliable diagnostic tool to aid in the identification of individuals with SMS or dup17p11.2 syndrome. This would allow a more timely diagnosis and will ensure that intervention measures for clinical manifestations are put into place as soon as possible. We have established a quantitative real-time PCR (Q-PCR) assay that is capable of measuring copy number variation in the 17p11.2 region, but more specifically, it measures the number of copies of the *RAI1* gene. We have validated this method by conducting a blinded study with samples that have a known deletion or duplication of *RAI1* and verified our results using FISH and multiplex ligation-dependent probe amplification (MLPA). Our approach is highly specific, fast, and reliable, making it an attractive method for routine use in SMS and dup17p11.2 diagnosis.

Materials and Methods

Subjects

To validate the Q-PCR assay for use in SMS and dup17p11.2 syndrome diagnosis, 17 SMS, 1 dup17p11.2, and 4 normal samples were blinded to the previously confirmed diagnoses of SMS or dup17p11.2 syndrome. Normal *RAI1* deletion and *RAI1* duplication control samples were also included in each run. Once the study was complete, all samples were decoded to reveal their copy number status, allowing for verification of the results obtained with FISH and MLPA. Additionally, the *RAI1* Q-PCR assay was tested on 42 samples of unrelated healthy individuals who were not previously tested for a deletion or duplication of the *RAI1* gene. Samples used in this study were collected in accor-

dance to approved IRB protocols by either Virginia Commonwealth University (VCU3784) or the SMS Natural History Study (01-HG-0109) at the National Institutes of Health.

Genomic DNA

Patient and control genomic DNA was extracted by the phenol chloroform method from whole blood or from lymphoblastoid cell lines or saliva, using the QIAamp DNA Minikit (QIAGEN, GmbH, Hilden, Germany) or the Oragene DNA Purification Kit (DNA Genotek, Ottawa, Canada), respectively, and approximately 50 ng used per reaction. The concentration and purity of the genomic DNA preparations were measured at an absorbance of 260 and 280 nm. DNA was stored at -20°C until ready for use.

Fluorescence in situ hybridization

FISH was used to confirm previous clinical and cytogenetic diagnoses in all 18 patient samples used in the blinded study. The following BAC and PAC clones mapping to chromosome 17p11.2 were used for preparation of FISH probes: CTC-529I10, CTC-157E16, RP11-314M5, RP11-253P07 (representing the *RAI1* locus), and RP11-746M1. FISH was performed as previously described (Vlangos *et al.*, 2003).

Multiplex ligation-dependent probe amplification

The *RAI1* copy number status of the blinded samples was also tested using the P064B MLPA Mental Retardation 1 SALSA Kit (MRC-Holland, Amsterdam, The Netherlands), covering chromosome 17p11.2. Because probes specific for *RAI1* were not contained within this kit, additional probes were created. The design, location, sequence, and size of *RAI1* probes used in conjunction with the commercially available kit are outlined in Table II of Girirajan *et al.* (2007a). MLPA was performed as previously described (Girirajan *et al.*, 2007a).

MLPA data analysis

MLPA PCR products were separated on an ABI PRISM[®] 3100 Genetic Analyser and interpreted using Genotyper (v3.7) software (Applied Biosystems, Foster City, CA). *RAI1* copy number was determined by exporting peak heights into an Excel spreadsheet, which had been designed to assess the ratio of each test peak relative to all other peaks for the given individual. Further, ratios of test peaks to control peaks and ratios of control peaks to control peaks for each sample were compared to those of two normal individuals, which were included in each run (Bunyan *et al.*, 2004). The dosage quotient for a normal individual with two copies of *RAI1* is expected to be 1.0, 0.5 for a deletion (SMS), and 1.5 for a duplication (dup17p11.2 syndrome).

Quantitative real-time PCR

PCR was performed using an AB 7500 FAST Sequence Detection System (Applied Biosystems). Each reaction was performed in a total volume of 10 μL , containing 1 \times Taqman[®] Universal PCR Master Mix, No AmpErase[®] UNG, 1 \times Taqman Gene Expression Assay Mix (*RNase P*: P/N 431681 or *RAI1*: P/N Hs02570777_s1) at a final concentration of 900 nM of each primer, 250 nM of the probe, and 50 ng genomic DNA. All reactions were performed in triplicate and re-

peated at least once. PCR thermocycling conditions consisted of an initial polymerase activation and DNA denaturation step of 60°C for 15 min, followed by 40 cycles of 15 s at 95°C and 1 min at 60°C .

Q-PCR data analysis

Real-time PCR is a highly sensitive and specific assay that utilizes emission from fluorescent dyes (e.g., SYBR Green I) or fluorogenic probes (e.g., TaqMan Probes) as a direct measure of target amplification during the PCR reaction. Accumulated PCR products are measured when there is a noticeable increase in fluorescence above a set threshold level. The cycle at which this occurs is the threshold cycle (C_t). For quantification of gene copy number by real-time PCR, the C_t values of both an unknown sample and a calibrator sample are measured, and this difference represents n -fold copies of the target gene in the unknown sample, relative to the calibrator sample (Livak and Schmittgen, 2001).

Quantifying relative gene copies requires that the amplification efficiency of both reference and target genes are comparable. If amplification efficiencies are approximately equal, it is possible to employ the comparative C_t method, $\Delta\Delta C_t$, for determining relative gene copy (ABI PRISM User Bulletin #2). Efficiencies for *RNase P* (reference gene) and *RAI1* (target gene) were determined by constructing a standard curve over a 5 log dilution series and comparing the slopes of the resultant curves.

Background baseline and threshold levels for the amplification plots of *RAI1* and *RNase P* were automatically determined by the SDS Software 1.3.1 (Applied Biosystems). The threshold was set at 10 standard deviations above the mean baseline fluorescence within the logarithmic curve of the amplification plot. Using the relative quantification study of this program, *RAI1* copy number of the unknown sample was determined relative to the known copy number of a normal calibrator sample, using the expression: $2^{-(\Delta\Delta C_t \pm s)}$, where $\Delta\Delta C_t = [C_t \text{ } RAI1 \text{ (unknown sample)} - C_t \text{ } RNase P \text{ (unknown sample)}] - [C_t \text{ } RAI1 \text{ (calibrator sample)} - C_t \text{ } RNase P \text{ (calibrator sample)}]$. The standard deviation, s , is the difference of the standard deviations of the C_t values of *RAI1* and *RNase P*. An *RAI1* copy number of 1 is expected for normal diploid samples, 0.5 for samples with an *RAI1* deletion (SMS), and 1.5 for samples that have a duplication of *RAI1* (dup17p11.2 syndrome).

Results

In this study, we designed a Q-PCR assay to determine copy number of the *RAI1* gene, which lies within the critical deletion and duplication region for SMS and dup17p11.2 syndrome, respectively. The Taqman Gene Expression Assay specific to *RAI1* was chosen such that the primers and probe lie within the exon 6 boundary of this gene. *RNase P* was chosen as a reference for gene dosage because it is a single-copy gene and would be present as two copies in all individuals regardless of SMS or dup17p11.2 syndrome status.

The PCR amplification efficiency for the target gene and the reference gene was determined by constructing a standard curve over 5 log dilutions. The amplification efficiency based upon the slopes of the standard curves was 100% for *RAI1* and 97% for *RNase P*. Since the amplification efficiencies for both genes were approximately equivalent, it was

possible to use the comparative C_t method ($\Delta\Delta C_t$) to determine the relative copy number of *RAI1*, as outlined in Materials and Methods.

Amplification plots for each triplicate showed near overlap, indicating that the assay was highly reproducible between replicates. However, in cases where laboratory error or issues with DNA quality led to insufficient amplification, samples were repeated. We noted that DNA samples that had been extracted by the phenol chloroform method had to be repeated more often than those extracted by commercial kits. Further, optimal amplification occurred using 40–80 ng DNA per reaction. Lower concentrations yielded unreliable amplification results.

We validated our *RAI1* Q-PCR assay using 17 SMS patients, 1 dup17p11.2 syndrome patient, and 4 normal individuals. FISH was used to confirm the diagnoses for these samples prior to use in Q-PCR. To prevent bias, we blinded the *RAI1* status of these samples. *RAI1* copy number of each sample was calculated by the $\Delta\Delta C_t$ ratio of $2^{-(\Delta\Delta C_t \pm s)}$. All samples were calibrated against a normal control, carrying two copies of *RAI1*. Once the study was complete, the samples were then decoded to allow for comparison of their expected genotype with the results obtained by Q-PCR. By Q-PCR, all 17 previously diagnosed SMS patients were deemed to carry a single copy of *RAI1*, the 4 normal individuals had two copies of *RAI1*, while the dup17p11.2 syndrome patient carried three copies of this gene (Fig. 1A).

The blinded samples were further subjected to MLPA to verify the results obtained by Q-PCR. Samples deleted for the *RAI1* gene exhibited half peak heights for all *RAI1* probes tested as compared to a normal control individual (Fig. 1C, bottom). Conversely, samples that carried a duplication of *RAI1* had peak heights that were 1.5 times that of a normal control individual for all *RAI1* probes (Fig. 1D, bottom). The *RAI1* copy number status of the samples tested by MLPA confirmed the results we obtained by our Q-PCR assay as well as those by FISH (Fig. 1C, D, top).

We have established diagnostic ranges for detecting deletions and duplications of *RAI1* by Q-PCR based upon the samples that we have screened (Fig. 1B and Table 2). The diagnostic range for a *RAI1* deletion was 0.40–0.54 with a mean $\Delta\Delta C_t$ ratio of 0.47 ± 0.03 . The $\Delta\Delta C_t$ ratio for a duplication of *RAI1* ranged between 1.53 and 1.78 with a mean of 1.66 ± 0.10 . Samples from unrelated healthy individuals who were not previously screened for a deletion or duplication of the *RAI1* gene were used in the Q-PCR assay to determine a normal range. All 42 individuals were diploid for *RAI1* with a $\Delta\Delta C_t$ ratio that ranged from 0.72 to 1.28 and a mean of 0.98 ± 0.06 .

Discussion

In recent years, Q-PCR has been employed to determine gene copy number for a variety of syndromes, including Charcot-Marie Tooth disease type 1A and hereditary neuropathy with liability to pressure palsy (Aarskog and Vedeler, 2000; Ruiz-Ponte *et al.*, 2000; Kim *et al.*, 2003; Thiel *et al.*, 2003), hereditary motor and sensory neuropathy I (Thiel *et al.*, 2003), Down syndrome (Hu *et al.*, 2004), Rubinstein-Taybi syndrome (Coupry *et al.*, 2004), and von Hippel Lindau syndrome (Hoebeek *et al.*, 2005). Q-PCR offers several advantages in diagnostics, including speed, sensitivity, repro-

ducibility, and low cost. It has the added advantage that there is no post-PCR manipulation, thereby reducing the possibility of introducing contamination.

In this study, we describe a Q-PCR assay that can be used to diagnose SMS and dup17p11.2 syndrome, based upon copy number variation of the *RAI1* gene. Since our Q-PCR assay is targeted specifically to this gene, it is especially useful in diagnosing atypical deletion cases in which SMS is suspected, but cytogenetic analysis was interpreted as normal and/or FISH did not include a probe specific to *RAI1* (Vlamos *et al.*, 2005). To evaluate our Q-PCR assay, a blinded study was designed using samples with normal, deleted, or duplicated copies of *RAI1* (Fig. 1A). The copy number status was accurately determined in 100% of the cases. Our Q-PCR findings were validated using both FISH and MLPA, illustrating the sensitivity and specificity of this assay.

Further, we established diagnostic ranges for each set of individuals who are normal, deleted, or duplicated for *RAI1*. The $\Delta\Delta C_t$ ratio for an *RAI1* deletion ranged from 0.40 to 0.54 with a mean of 0.47 ± 0.03 , the $\Delta\Delta C_t$ ratio ranged between 1.53 and 1.78 with a mean of 1.66 ± 0.10 for *RAI1* duplications, and for a normal *RAI1* gene copy number this ratio was between 0.72 and 1.28 with a mean of 0.98 ± 0.06 (Table 2). Interestingly, we found that the Q-PCR results for SMS224, $\Delta\Delta C_t$ ratio = 1.78, were greater than our duplication control that had a $\Delta\Delta C_t$ ratio = 1.53 (Fig. 1A, B). Metaphase FISH and MLPA results indicated that this patient was duplicated for the *RAI1* gene (Fig. 1D).

Upon further investigation of SMS224 in our lab, it was determined by interphase FISH that this patient indeed had a duplication of 17p11.2 but was also 25% mosaic for tetrasomy 17p11.2p12 (Girirajan *et al.*, 2007b). Retrospectively, the mosaic tetrasomy for this region can possibly account for why our Q-PCR results were always greater than the expected $\Delta\Delta C_t$ ratio of 1.5 for a duplication of *RAI1*. It is, however, difficult to ascertain the extent of the effect that mosaicism lends to Q-PCR since we do not have any other mosaic deletion or duplication cases to evaluate at this time. But because of the limited number of duplication samples that we had available for Q-PCR testing, we have included the result for SMS224 within our *RAI1* Q-PCR duplication range. We expect that this range will fall in line with that of our control ($\Delta\Delta C_t$ ratio = 1.53 ± 0.11) once more samples have been screened.

Accurate quantification by Q-PCR may be affected by a number of factors that warrant consideration. We carried out all reactions in a 96-well plate with a total reaction volume of 10 μ L, which is half of what is recommended by the manufacturer. This reduction in reaction volume allowed for a marked decrease in the cost of reagents but did not appear to compromise our results, as reproducibility between replicates was consistent.

We noted, however, that amplification was affected by DNA quality whereby DNA that had been extracted using commercially available kits gave the most reliable results. Further, saliva provided high-quality DNA with added advantages of being a lower cost and far less invasive procedure compared to blood-based DNA collection. In cases where amplification was not sufficient because of poor DNA quality, new DNA samples were obtained and retested, yielding reproducible replicates. High-quality DNA is a critical factor for consistent amplification as well as contrib-

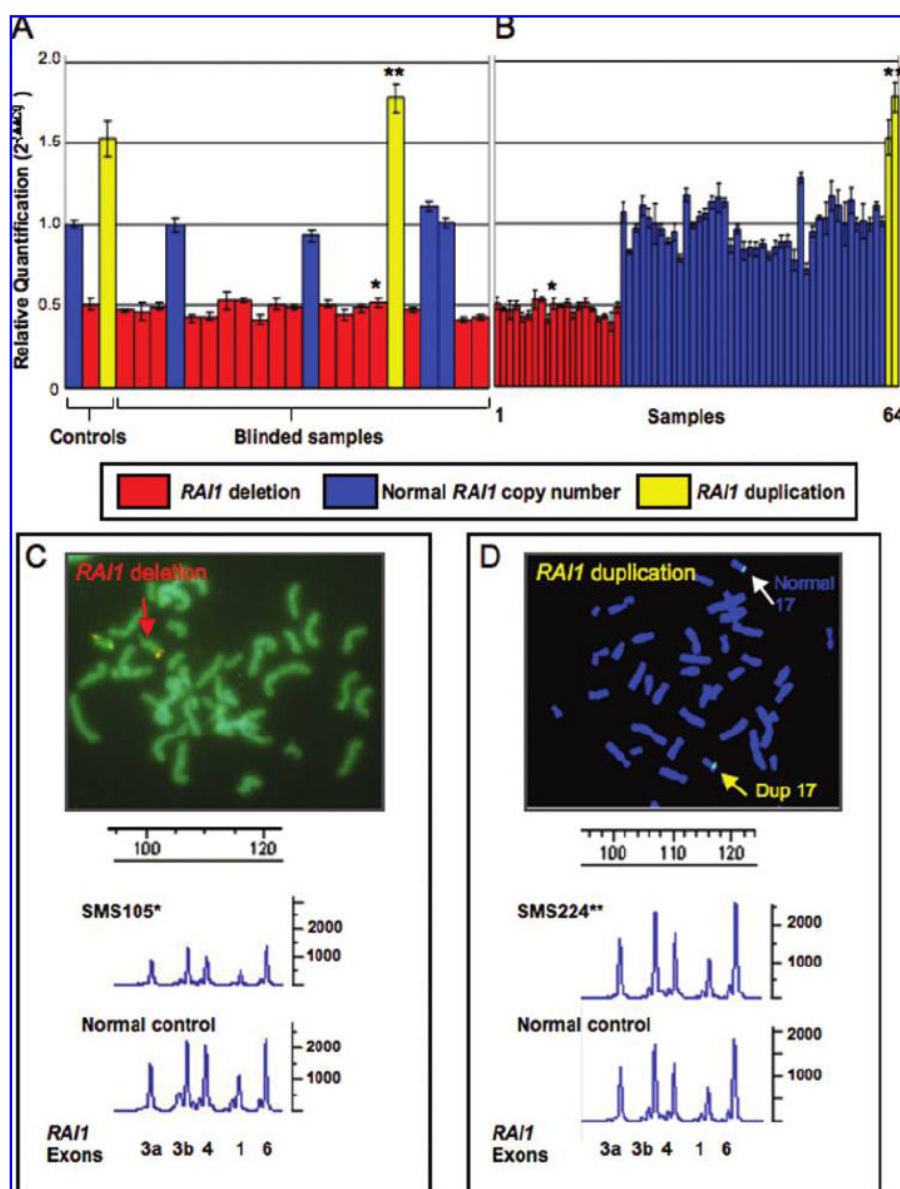


FIG. 1. Determining *RAI1* copy number variation by Q-PCR. (A) Mean results for the relative quantification, $2^{-\Delta\Delta C_t}$, and standard deviation of *RAI1* for 4 normal samples and 18 samples blinded to their previous diagnosis of either SMS or dup17p11.2 syndrome. Normal (blue), deletion (red), and duplication (yellow) controls were included in each run to ascertain the *RAI1* copy number status of the blinded sample. (B) All 64 samples assayed by Q-PCR provide nonoverlapping ranges for one (deletion), two (normal), or three (duplication) copies of *RAI1*. Q-PCR results were also validated by FISH and MLPA. Examples of FISH (top) and MLPA (bottom) results are shown for SMS (C) and dup17p11.2 syndrome (D). SMS105 is denoted with (*) and SMS224 with (**) in panels (A) and (B).

uting to a lower standard deviation between replicates (Thiel *et al.*, 2003).

Another important consideration when quantifying gene copy number is the use of an internal reference gene for normalization of sample-to-sample variation (Livak and Schmittgen, 2001). The choice of a suitable internal reference gene should be based upon whether the PCR amplification efficiencies of the target gene and the reference gene are similar. Amplification efficiencies closest to 100% ensure that accurate and reproducible results are obtained (ABI PRISM

User Bulletin #2). Our internal reference gene, *RNase P*, had an amplification efficiency of 97% making it almost equivalent to the 100% amplification efficiency of *RAI1*. Thus *RNase P* was a suitable internal reference gene for our *RAI1* Q-PCR assay.

With the results that we have obtained with our Q-PCR assay outlined here, we propose that *RAI1* Q-PCR is a reliable method for diagnosis of SMS and dup17p11.2. Q-PCR offers several advantages over traditional cytogenetic diagnostics such as FISH and more recent methods such as

TABLE 2. NORMAL, DELETED, AND DUPLICATED $\Delta\Delta C_T$ RATIOS DETECTED BY *RAI1* Q-PCR

Samples	Subjects ^a	Mean \pm SD ^b	Range
Normal	41	0.98 \pm 0.06	0.72–1.28
Deletion	21	0.47 \pm 0.03	0.40–0.54
Duplication	2	1.66 \pm 0.10	1.53–1.78

^aNumber of different individuals tested, including control samples.

^bMean copy number \pm standard deviation (SD).

MLPA. Of the three techniques used here, Q-PCR is the most cost effective and time conserving in terms of processing time and the acquisition of results, which are also important factors in patient diagnosis.

Based upon publicly available pricing from several diagnostic laboratories in the United States, we have found that the cost to the consumer ranges from US\$500–800 for Q-PCR, FISH, or MLPA for diagnosing SMS, dup17p11.2, or other microdeletion/microduplication syndromes. However, the estimated cost per sample, excluding labor and assuming that the laboratory has the infrastructure required to carry out each method, is approximately US\$150 for FISH, US\$20 for MLPA, and US\$9 for Q-PCR. It should be noted that this does not include the cost of including control samples or control probes that are required for relevant analyses in each of these methods, which would increase the costs stated here.

We estimate that the turnaround time, from the time that a sample is received until a diagnosis is rendered and a report generated, can be as little as 2 days for *RAI1* Q-PCR. The reaction set up and run time for Q-PCR can be completed in as little as 3 h. Comparatively, the turnaround time for FISH is approximately 7–10 days and for MLPA is 3–6 weeks. FISH is labor intensive and requires 30–35 h to complete. The turnaround time for FISH includes an additional time constraint of cell culturing for chromosome preparation that is unnecessary for Q-PCR or MLPA, as these two methods utilize genomic DNA. The long and variable turnaround time for MLPA is based on the fact that very few samples are sent for *RAI1* MLPA analysis; therefore, when samples are received they are placed in a batch system. Otherwise, MLPA for microdeletion/microduplication diagnosis can be performed within 24 h. Turnaround times for FISH and MLPA were based upon estimates given by national and international labs that currently perform these tests for SMS and dup17p11.2 syndrome.

In conclusion, we have developed a highly efficient, reliable, and cost-effective method of quantifying copy number aberrations of the *RAI1* gene. We have demonstrated that *RAI1* Q-PCR is capable of unequivocal diagnosis of SMS and dup17p11.2 syndrome and, further, offers several advantages over currently available techniques. We expect that as more diagnostic laboratories lean toward using methods that are economical but do not compromise on the accuracy of results, Q-PCR will be employed more routinely for screening gene copy number abnormalities.

Acknowledgments

The authors would like to acknowledge Sonia Benhamed (GeneDx, Gaithersburg, MD) for real-time PCR training. We would also like to thank Chris Miller (Applied Biosystems)

for his expertise during the initial setup of the *RAI1* Q-PCR assay. Our gratitude extends to all SMS patients and families that provided samples, without whom our research would not be possible. This work was funded by a grant from the U.S. National Institutes of Health (R01 HD38534) to S.H.E. and resources from Virginia Commonwealth University to S.H.E. This research was also supported, in part, by the Intramural Research Program of the National Human Genome Research Institute, National Institutes of Health. Financial support to H.T.T. was provided by Charles Sturt University through a CSU postgraduate scholarship.

References

- Aarskog NK, Vedeler CA (2000) Real-time quantitative polymerase chain reaction. A new method that detects both the peripheral myelin protein 22 duplication in Charcot-Marie-Tooth type 1A disease and the peripheral myelin protein 22 deletion in hereditary neuropathy with liability to pressure palsies. *Hum Genet* 107:494–498.
- ABI PRISM User Bulletin #2. ABI Prism 7700 Sequence Detection System, December 11, 1997 (updated 10/2001). <http://www.applied-biosystems.com>.
- Allanson JE, Greenberg F, Smith AC (1999) The face of Smith-Magenis syndrome: a subjective and objective study. *J Med Genet* 36:394–397.
- Bi W, Park SS, Shaw CJ, Withers MA, Patel PI, Lupski JR (2003) Reciprocal crossovers and a positional preference for strand exchange in recombination events resulting in deletion or duplication of chromosome 17p11.2. *Am J Hum Genet* 73:1302–1315.
- Bi W, Saifi GM, Shaw CJ, Walz K, Fonseca P, Wilson M, Potocki L, Lupski JR (2004) Mutations of *RAI1*, a PHD-containing protein, in nondeletion patients with Smith-Magenis syndrome. *Hum Genet* 115:515–524.
- Bunyan DJ, Eccles DM, Sillibourne J, Wilkins E, Thomas NS, Shea-Simonds J, Duncan PJ, Curtis CE, Robinson DO, Harvey JF, Cross NC (2004) Dosage analysis of cancer predisposition genes by multiplex ligation-dependent probe amplification. *Br J Cancer* 91:1155–1159.
- Chen KS, Manian P, Koeuth T, Potocki L, Zhao Q, Chinault AC, Lee CC, Lupski JR (1997) Homologous recombination of a flanking repeat gene cluster is a mechanism for a common contiguous gene deletion syndrome. *Nat Genet* 17:154–163.
- Coupry I, Monnet L, Attia AA, Taine L, Lacombe D, Arveiler B (2004) Analysis of CBP (CREBBP) gene deletions in Rubinstein-Taybi syndrome patients using real-time quantitative PCR. *Hum Mutat* 23:278–284.
- Girirajan S, Elsas LJ 2nd, Devriendt K, Elsea SH (2005) *RAI1* variations in Smith-Magenis syndrome patients without 17p11.2 deletions. *J Med Genet* 42:820–828.
- Girirajan S, Mendoza-Londono R, Vlangos CN, Dupuis L, Nowak NJ, Bunyan DJ, Hatchwell E, Elsea SH (2007a) Smith-Magenis syndrome and moyamoya disease in a patient with del(17)(p11.2p13.1). *Am J Med Genet A* 143A:999–1008.
- Girirajan S, Williams SR, Garben JY, Nowak NJ, Hatchwell E, Elsea S (2007b) 17p11.2p12 triplication and del(17)(q11.2q12) in a severely affected child with dup(17)(p11.2p12) syndrome. *Clin Genet* 72:47–58.
- Greenberg F, Guzzetta V, Montes de Oca-Luna R, Magenis RE, Smith AC, Richter SF, Kondo I, Dobyns WB, Patel PI, Lupski JR (1991) Molecular analysis of the Smith-Magenis syndrome: a possible contiguous-gene syndrome associated with del(17)(p11.2). *Am J Hum Genet* 49:1207–1218.

- Greenberg F, Lewis RA, Potocki L, Glaze D, Parke J, Killian J, Murphy MA, Williamson D, Brown F, Dutton R, McCluggage C, Friedman E, Sulek M, Lupski JR (1996) Multi-disciplinary clinical study of Smith-Magenis syndrome (deletion 17p11.2). *Am J Med Genet* 62:247–254.
- Gropman AL, Duncan WC, Smith AC (2006) Neurologic and developmental features of the Smith-Magenis syndrome (del 17p11.2). *Pediatr Neurol* 34:337–350.
- Hoebeek J, van der Lijdt R, Poppe B, de Smet E, Yigit N, Claes K, Zewald R, de Jong GJ, de Paepe A, Speleman F, Vandesompele J (2005) Rapid detection of VHL exon deletions using real-time quantitative PCR. *Lab Invest* 85:24–33.
- Hu Y, Zheng M, Xu Z, Wang X, Cui H (2004) Quantitative real-time PCR technique for rapid prenatal diagnosis of Down syndrome. *Prenat Diagn* 24:704–707.
- Kim SW, Lee KS, Jin HS, Lee TM, Koo SK, Lee YJ, Jung SC (2003) Rapid detection of duplication/deletion of the PMP22 gene in patients with Charcot-Marie-Tooth disease Type 1A and hereditary neuropathy with liability to pressure palsy by real-time quantitative PCR using SYBR Green I dye. *J Korean Med Sci* 18:727–732.
- Livak KJ, Schmittgen TD (2001) Analysis of relative gene expression data using real-time quantitative PCR and the 2⁻(Delta Delta C(T)) Method. *Methods* 25:402–408.
- Magenis RE, Brown MG, Allen L, Reiss J (1986) *De novo* partial duplication of 17p [dup(17)(p12→p11.2)]: clinical report. *Am J Med Genet* 24:415–420.
- Potocki L, Bi W, Treadwell-Deering D, Carvalho CM, Eifert A, Friedman EM, Glaze D, Krull K, Lee JA, Lewis RA, Mendoza-Londono R, Robbins-Furman P, Shaw C, Shi X, Weissenberger G, Withers M, Yatsenko SA, Zackai EH, Stankiewicz P, Lupski JR (2007) Characterization of Potocki-Lupski syndrome (dup(17)(p11.2p11.2)) and delineation of a dosage-sensitive critical interval that can convey an autism phenotype. *Am J Hum Genet* 80:633–649.
- Potocki L, Chen KS, Park SS, Osterholm DE, Withers MA, Kimonis V, Summers AM, Meschino WS, Anyane-Yeboah K, Kashork CD, Shaffer LG, Lupski JR (2000) Molecular mechanism for duplication 17p11.2—the homologous recombination reciprocal of the Smith-Magenis microdeletion. *Nat Genet* 24:84–87.
- Ruiz-Ponte C, Loidi L, Vega A, Carracedo A, Barros F (2000) Rapid real-time fluorescent PCR gene dosage test for the diagnosis of DNA duplications and deletions. *Clin Chem* 46:1574–1582.
- Slager RE, Newton TL, Vlangos CN, Finucane B, Elsea SH (2003) Mutations in *RAI1* associated with Smith-Magenis syndrome. *Nat Genet* 33:466–468.
- Smith ACM, McGavran L, Robinson J, Waldstein G, Macfarlane J, Zonona J, Reiss J, Lahr M, Allen L, Magenis E (1986) Interstitial deletion of (17)(p11.2p11.2) in nine patients. *Am J Med Genet* 24:393–414.
- Struthers JL, Carson N, McGill M, Khalifa MM (2002) Molecular screening for Smith-Magenis syndrome among patients with mental retardation of unknown cause. *J Med Genet* 39:E59.
- Thiel CT, Kraus C, Rauch A, Ekici AB, Rautenstrauss B, Reis A (2003) A new quantitative PCR multiplex assay for rapid analysis of chromosome 17p11.2-12 duplications and deletions leading to HMSN/HNPP. *Eur J Hum Genet* 11:170–178.
- Vlangos CN, Wilson M, Blancato J, Smith AC, Elsea SH (2005) Diagnostic FISH probes for del(17)(p11.2p11.2) associated with Smith-Magenis syndrome should contain the *RAI1* gene. *Am J Med Genet A* 132:278–282.
- Vlangos CN, Yim DK, Elsea SH (2003) Refinement of the Smith-Magenis syndrome critical region to approximately 950kb and assessment of 17p11.2 deletions. Are all deletions created equally? *Mol Genet Metab* 79:134–141.

Address reprint requests to:
 Sarah H. Elsea, Ph.D., FACMG
 Department of Pediatrics and Human Genetics
 Virginia Commonwealth University
 1101 E. Marshall St., 12-018 Sanger Hall
 P.O. Box 980441
 Richmond, VA 23298
 E-mail: selsea@vcu.edu

Appendix D

***Tom1l2* hypomorphic mice exhibit increased incidence of infections and tumors and abnormal immunologic response**

Santhosh Girirajan · Paula M. Hauck · Stephen Williams · Christopher N. Vlangos · Barbara B. Szomju · Sara Solaymani-Kohal · Philip D. Mosier · Kimber L. White Jr. · Kathleen McCoy · Sarah H. Elsea

Received: 20 November 2007 / Accepted: 28 January 2008 / Published online: 15 March 2008
 © Springer Science+Business Media, LLC 2008

Abstract Studies have shown that the TOM1 family of proteins, including TOM1 and TOM1L1, are actively involved in endosomal trafficking and function in the immune response. However, much less is known about the function of TOM1L2. To understand the biological importance of TOM1L2 and the potential significance of its cellular role, we created and evaluated *Tom1l2* gene-trapped mice with reduced *Tom1l2* expression. Mice hypomorphic for *Tom1l2* exhibited numerous infections and tumors compared to wild-type littermates. Associated with this increased risk for infection and tumor formation,

apparently healthy *Tom1l2* hypomorphs also had splenomegaly, elevated B- and T-cell counts, and an impaired humoral response, although at a reduced penetrance. Furthermore, cellular localization studies showed that a Tom1l2-GFP fusion protein colocalizes with Golgi compartments, supporting the role of Tom1l2 in cellular trafficking, while molecular modeling and bioinformatic analysis of Tom1l2 illustrated a structural basis for a functional role in trafficking. These results indicate a role for *Tom1l2* in the immune response and possibly in tumor suppression.

S. Girirajan and P. M. Hauck contributed equally to this work.

Electronic supplementary material The online version of this article (doi:10.1007/s00335-008-9100-6) contains supplementary material, which is available to authorized users.

S. Girirajan · S. Williams · S. H. Elsea (✉)
 Department of Human Genetics, Medical College of Virginia Campus, Virginia Commonwealth University, Richmond, VA 23298, USA
 e-mail: selsea@vcu.edu

P. M. Hauck · C. N. Vlangos · B. B. Szomju · S. Solaymani-Kohal · S. H. Elsea
 Department of Pediatrics, Medical College of Virginia Campus, Virginia Commonwealth University, Richmond, VA 23298, USA

Present Address:
 P. M. Hauck
 Molecular Oncology, McGuire Research Institute, Richmond, VA 23249, USA

Present Address:
 C. N. Vlangos
 Department of Pediatrics, University of Michigan, Ann Arbor, MI 48109, USA

Abbreviations

Tom1l2 Target of Myb-1-like 2
 Tom1l1 Target of Myb-1-like 1
 Tom1 Target of Myb-1

P. D. Mosier
 Department of Medicinal Chemistry and Center for the Study of Biological Complexity, Medical College of Virginia Campus, Virginia Commonwealth University, Richmond, VA 23298, USA

K. L. White Jr.
 Department of Pharmacology and Toxicology, Medical College of Virginia Campus, Virginia Commonwealth University, Richmond, VA 23298, USA

K. McCoy
 Department of Microbiology and Immunology, Medical College of Virginia Campus, Virginia Commonwealth University, Richmond, VA 23298, USA

Tollip	Toll interacting protein
SMS	Smith-Magenis syndrome
VHS	Vps27p/Hrs/Stam
GAT	GGA and Tom
GGA	Golgi localizing, Gamma-adaptin ear homology domain, ADP-ribosylation factor-binding protein
ARF1	ADP-ribosylation factor 1
SFK	Src family of protein kinases
IL-1R1	Interleukin-1 receptor type 1
SHIRPA	SmithKline Beecham Pharmaceuticals, Harwell MRC Mouse Genome Centre and Mammalian Genetics Unit, Imperial College School of Medicine at St Mary's, Royal London Hospital, St Bartholomew's, and the Royal London School of Medicine, Phenotype, Assessment

Introduction

Characterization of genes is of pivotal importance in understanding the biological processes that allow cells to function properly. This study focuses on *Tom1l2* (Target of Myb-1-Like 2), a 53.1-kb gene composed of 15 exons, encoding a 507-amino-acid protein (~55.7 kDa). *Tom1l2* belongs to a family of proteins involved in vesicular trafficking and endocytosis (Lohi and Lehto 1998). It is a homolog of the *Tom1* gene which was first discovered in a genetic screen to identify *Myb*-regulated genes (Burk et al. 1997). *Tom1* is a target of the proto-oncogene *v-Myb* when chicken myelomonocytic cells are transformed with avian myeloblastosis virus or avian leukemia virus E26 (Burk et al. 1997). The *Tom1* family of proteins, including *Tom1*, *Tom1l1* (alias *Srcasm/Jerry*), and *Tom1l2*, has a VHS (Vps27p/Hrs/Stam) domain, a GAT (GGA and Tom) domain, and clathrin-binding motifs. The VHS domain is involved in vesicular trafficking and endocytosis (Lohi and Lehto 1998), while the GAT domain of GGAs (Golgi localizing, Gamma-adaptin ear homology domain, ADP-ribosylation factor-binding protein) stabilizes membrane-bound ARF1 (ADP-ribosylation factor 1) in the GTP state (Takatsu et al. 2001). GGAs are monomeric clathrin adaptors (with clathrin boxes) that regulate transport and have been implicated in endosomal trafficking (Bonifacino 2004; Katoh et al. 2006). Clathrin-coated vesicles deliver cargo proteins from the plasma membrane and trans-Golgi network to the endosomes/lysosomes (Kirchhausen 2000).

Studies show that *Tom1* overexpression suppresses activation of transcription factors, including nuclear factor (NF)- κ B and activator protein (AP-1), induced by either interleukin-1 β or tumor necrosis factor- α , and that the VHS domain of *Tom1* is indispensable for its suppressive

activity (Yamakami and Yokosawa 2004). *Tom1* is required for sorting of IL-1R1 (interleukin-1, receptor type 1) in late endosomes using Toll interacting protein (Tollip) as an endosomal adaptor, and *Tom1* knockdown results in accumulation of IL-1R1 in late endosomes (Brissoni et al. 2006). Several studies have shown that *Tom1* interacts with Tollip, ubiquitin, endofin, and clathrin (Akutsu et al. 2005; Katoh et al. 2004; Seet and Hong 2005; Seet et al. 2004; Shiba et al. 2004; Yamakami and Yokosawa 2004). Recently, human *TOM1* was implicated in both bipolar affective disorder (BPAD) and schizophrenia by a gene-based SNP haplotype mapping of a BPAD linkage region on chromosome 22q12.3 (Potash et al. 2008).

A partial functional redundancy appears to exist between members of the *Tom1* family in regulating SFK (Src family of protein kinases) mitogenic signaling induced by growth factors (Franco et al. 2006). *Tom1l1* and *Tom1l2* act as adaptors for inhibition of mitogenesis (via disruption of SFK receptor complex formation), which is reversed by Myc expression or by SFK coexpression (Franco et al. 2006). In HEK293 cells, all human *TOM1* members associated with SRC, with a stronger interaction for *TOM1L1* and *TOM1L2* (Franco et al. 2006). In addition to SFK, the tyrosine motifs at the C-terminal region of *TOM1L1* mediate interactions with other signaling proteins such as GRB2, FYN, and the regulatory subunit of phosphoinositide 3-kinase, p85, in a phosphorylation-dependent manner (Puertollano 2005). Katoh et al. (2004) have shown that the GAT domains of *TOM1* and *TOM1L1* interact with both ubiquitin and TOLLIP. The VHS domain of *TOM1* has been shown to interact with HRS (hepatocyte growth factor-regulated tyrosine kinase substrate), whereas a PTAP (Pro-Thr-Ala-Pro) motif, located between the VHS and GAT domain of *TOM1L1*, is responsible for binding to TSG101 (tumor susceptibility gene 101) (Puertollano 2005). Furthermore, *TOM1L1* interacts with members of the multivesicular body-sorting machinery and may participate in the sorting of ubiquitinated proteins (Puertollano 2005). *TOM1L1* and *TOM1L2* differ from *TOM1* in that they do not directly interact with endofin (Seet et al. 2004); however, like *TOM1*, they do interact with TOLLIP and clathrin (Katoh et al. 2006).

Human *TOM1L2* maps to chromosome 17p11.2, a region that is deleted in 90% of patients with Smith-Magenis syndrome (SMS) (Lucas et al. 2001). Murine *Tom1l2* lies in the syntenic region on chromosome 11. SMS is characterized by a constellation of approximately 30 clinical features, including mental retardation, sleep disturbance, speech and developmental delay, self-injurious and stereotypical behaviors, craniofacial and skeletal abnormalities, frequent infections, and hypotonia (Greenberg et al. 1991, 1996). The *RAI1* gene is responsible for most features of SMS (Slager et al. 2003; Smith et al.

1986), while other genes within the 17p11.2 deletion region contribute to the variable features and severity of the disorder (Girirajan et al. 2006), modifying the overall phenotype. The specific contribution of individual genes lying within the 17p11.2 deletion region to the SMS phenotype is not known.

The gene-trap approach has been a useful tool in generating mutant mouse (Gossler et al. 1989; Skarnes et al. 1995), *Drosophila* (Bellen et al. 1989; Bier et al. 1989), and zebrafish (Amsterdam et al. 1999; Talbot and Hopkins 2000) lines, allowing for functional studies to investigate the role of the trapped gene. To understand the functional consequences of *TOM1L2* deficiency and to decipher its potential contribution to the clinical features of SMS, a *Tom1l2* gene-trap mouse was created. Studies were performed to characterize the behavioral and immunologic phenotypes in the *Tom1l2* heterozygous and homozygous mice. *Tom1l2* cellular expression pattern, molecular modeling, and bioinformatic studies were also performed to obtain structural evidence for functional similarity between *Tom1l2* and other *Tom1* family members.

Materials and methods

Creation of *Tom1l2*-targeted mice

Publicly accessible databases from the BayGenomics consortium (<http://www.baygenomics.ucsf.edu>) were queried with *Tom1l2* EST sequence via BLAST analysis (Skarnes et al. 1992, 1995; Stanford et al. 2001; Stryke et al. 2003). BLAST results identified the XG909 embryonic stem (ES) cell line which has the gene-trapping vector (pGT11xf) inserted between exons 10 and 11 in the mouse *Tom1l2* gene. XG909 ES cells were obtained and sent to the Transgenic Animal Model Core at The University of Michigan for injection into C57Bl/6 blastocysts. Chimeric males were mated to C57Bl/6J females to produce heterozygous (*Tom1l2*+/-) mice. The exact location of the insertion was determined by sequence analysis of a PCR product amplified using a vector-specific primer (5' CGTAAGGAGAAAATACCGCATC 3') and a *Tom1l2*-specific primer (5' CAGAAAGCCACTGGGAAGAG 3'). Amplification of 50–100 ng of template DNA was performed using 1.25 U of *Taq* polymerase in a cocktail consisting of 0.4 μ M of each primer, 0.2 mM dNTPs, and 2 \times PCR buffer (10 \times buffer contains 100 mM Tris-HCl, pH 8.3, 15 mM MgCl₂, 500 mM KCl, 0.01% gelatin). The samples were then subjected to an initial denaturation step at 94°C for 3 min, followed by 35 cycles of 94°C for 1 min, 60°C for 1 min, and 72°C for 1.5 min, followed by a final extension of 72°C for 10 min.

Genotyping of *Tom1l2* mice

DNA extraction Mouse tail (1–3 cm) was digested with 0.6 mg/ml proteinase K in TNES buffer (50 mM Tris, pH 7.5, 400 mM NaCl, and 100 mM EDTA, pH 8). DNA was then isolated using a standard phenol/chloroform procedure. Alternatively, DNA was extracted using the QIAamp DNA Minikit (Qiagen, Valencia, CA) as described in the Qiagen manual (tissue section).

Southern analysis Southern analysis was conducted by digesting 5 μ g of DNA with 10 U/ μ g *Bgl*I (New England Biolabs, Beverly, MA) and 2.5 mM spermidine and the result was electrophoresed on 1% Tris-acetate (TAE; 0.04 M Tris-acetate, 1 mM EDTA) agarose gels. Gel preparation, DNA transfer to an Amersham Hybond-N+ nylon or Hybond XL membrane, crosslinking, probe-labeling and preassociation, prehybridization, hybridization, and washes were conducted as described previously (Lucas et al. 2001). The probe was created by PCR amplification of *Tom1l2* intron 10 sequence (5' primer: CCCAAATGTGTCCACAGTTCTA, 3' primer: GGGTGGGAATGCACGACTAAA) followed by gel excision and band purification using the QiaQuick gel extraction kit (Qiagen) according to the manufacturer's instructions.

PCR genotyping The *Tom1l2*-specific primers (5' primer: GGTGAAGCTAACAGCCATGGCC, 3' primer: CCAGACAACAAATGCAGGTT) and insert-specific primers (5' primer: GACGTCTCGTTGCTGCATAA, 3' primer: GACCTGACCATGCAGAGGAT) were combined in each reaction. Amplification of 50–100 ng of template DNA was performed using the same cocktail and parameters as described above.

Tom1l2 expression analysis

Total RNA was isolated from 100 mg of brain, liver, or spleen tissues dissected from wild-type and *Tom1l2* gene-trapped mice using TRIzol reagent per the manufacturer's instructions. RNA was quantified using spectrophotometry, and 5 μ g RNA was reverse transcribed by first-strand cDNA synthesis using SuperScript II RT (Invitrogen, Carlsbad, CA). Brain, liver, and spleen cDNAs from each mouse were PCR amplified using *Tom1l2* primers (5' primer: CTTGGGGACAGAGAGTGTCTAG, 3' primer: CACAGGCAAAGAGCGCATCGTC) and a standard curve was generated. An internal control PCR was performed with primers for the *Rail* gene (5' primer: TGTCAGAAGACCTCGTGTC, 3' primer: GGGAAACAGTCAAAAGCTGC), which is unaffected by the gene trap. Each PCR product (2 μ l) was then loaded onto a 2% agarose gel and densitometry was performed using AlphaEaseFC software (Alpha Innotech, San Leandro, CA). A mean density for each tissue was

calculated for *Tom1l2* relative to endogenous *Rai1*. Wild-type expression levels were then set to 1.0.

Animal husbandry

Mice were separated by sex and housed 2–4 per cage with access to a standard diet of Prolab[®] RMH 2000 chow (PMI Nutrition International, Inc., Brentwood, MO), and water *ad libitum*. The mouse-room was maintained on a 12-h/12-h light/dark cycle and all testing was done during the light phase. Ambient temperature (70°F) and humidity (40%) were maintained. Animals used in this study were cared for in accordance with the guidelines of the Institutional Animal Care and Use Committee of Virginia Commonwealth University and the *Guide for the Care and Use of Laboratory Animals* (National Research Council 1996). The mice were initially kept in wood chip bedding but were later switched to corn cob bedding. Both bedding materials were sterilized prior to use.

Phenotypic assessment of *Tom1l2* mice

Assessments were conducted for 46 *Tom1l2* heterozygotes, 27 *Tom1l2* homozygotes, and 34 wild-type littermates. Mice of all genotypes were evaluated at 5, 10, 20, and 30 weeks. All animal studies were approved by the VCU IACUC committee. Physical assessment included whisker appearance and response, skin or fur abnormalities, condition of genital/rectal areas, nails and teeth, cage movement, and body measurements. The mice were weighed and body measurements, including distance between the bony landmarks of the craniofacial region and the limbs, were taken. In a fume hood, about 300 μ l of isoflurane was used to anesthetize the mouse by inhalation. The following measurements (in mm) of the mouse were recorded: inner eye to inner eye, base of ear to base of ear, tip of nose to top of head, length of trunk from mandible, front limbs (toe to hip), and hind limbs (toe to thigh). The sizes of heterozygotes and homozygotes were compared to wild-type littermates.

General behavior assessments included wild running, freezing, sniffing, licking, rearing, defecation, urination, and movement around entire cage. *Gait* was assessed by footprint analysis (dipping each foot in ink and allowing the mouse to traverse across white paper under a tunnel). The average distance between adjacent paw prints and the average stride length were calculated for each mouse. In a *cage top-hang test*, the mouse was allowed to hold on to a cage-top which was then inverted onto the cage. The time (in sec) the mouse remained hanging was noted. Three trials were completed, and the mean was determined. All tests were modified from the behavioral battery described by Crawley and Paylor (1997).

Sensorimotor reflexes observed include *postural reflex* (ability to remain upright while the cage is shaking in all directions for 10 sec each), *righting reflex* (time to right itself after being turned onto its back), and the response to being picked up by the tail (the normal response is to raise the head, extend extremities and reach for the ground when lowered). *Whisker response* was measured by touching the whiskers of a freely moving mouse (normal mouse will stop moving its whiskers and will turn its head on the side of the whiskers that was touched). *Eye blink and ear twitch response* was elicited by touching the corner of the eye and the tip of the ear (pinna), respectively, with the tip of a cotton swab. *Sound orientation* (a brief sharp sound was made to the left and right sides of the mouse and response of the mouse, such as turning to the direction of the sound, flinching, startle response, or freezing, was noted) was analyzed as well. Mice were also assessed for pain sensitivity. In this assay, the mouse was placed on the hot plate set to 55°C. The time (in sec) for the mouse to jump, pick up a paw, paw lick, or paw shake is recorded (maximum duration is set at 30 sec). Hyperalgesia is indicated by an extreme sensitivity to the painful stimulus.

Statistical analyses

Statistical analyses were performed using GraphPad Prism version 4.02 for Windows (GraphPad Software, San Diego, CA). All data were analyzed using nonparametric unpaired *t* test and one-way (genotype) or two-way (genotype \times age interval) analysis of variance (ANOVA). *Post hoc* comparisons were made using Bonferroni's multiple-comparison tests. Proportions of features in the genotypes were compared using Fisher's exact test. The level of significance was set at $P < 0.05$.

Histologic analysis

Spleens were isolated from *Tom1l2* mice and fixed in 4% paraformaldehyde/phosphate-buffered saline. Hematoxylin and eosin staining was performed at Michigan State University, Department of Pathology, according to standard procedures.

Hematologic evaluation

Blood was collected from the submandibular vein of mice of each genotype following standard protocols. Approximately 50 μ l of blood were collected in a samplette micro whole-blood collector containing EDTA (Kendall Health Care, Mansfield, MA). The samples were kept at 4°C until analysis of hemoglobin, hematocrit, MCV (mean corpuscular volume), MCH (mean corpuscular hemoglobin), MCHC (mean corpuscular hemoglobin concentration), platelet, WBC

(white blood cells), neutrophil, lymphocyte, monocyte, eosinophil, and basophil levels by the Comparative Pathology Lab (Davis, CA).

Flow cytometry

Monoclonal antibodies Cell-free culture supernatants from the following monoclonal antibody-producing B-cell hybridomas (American Type Culture Collection, Manassas, VA) were used for immunofluorescence staining: RA3-3A1 (anti-B220), GK1.5 (anti-CD4), and 53-6.72 (anti-CD8). Purified monoclonal anti-Mac-1 (M1/70), anti-Thy1.1 (OX-7), and fluoresceinated monoclonal anti-rat kappa light chain (MARK) antibodies were purchased from BD Biosciences Pharmingen (San Diego, CA). Biotinylated monoclonal anti-CD4 (GK1.5) antibody was purchased from eBioscience (San Diego, CA).

Immunofluorescence staining and flow cytometric analysis Single-cell suspensions of spleens, lymph nodes, and thymi were prepared, and cells were stained as previously described (Hartmann and McCoy 2004; Lewis et al. 1996). For one-color analysis, cells were incubated with monoclonal anti-B220, anti-CD4, anti-CD8, anti-Mac-1, or irrelevant anti-Thy-1.1 antibodies, followed by fluoresceinated MARK antibody. For two-color analysis, thymocytes were incubated with anti-CD8 or irrelevant anti-Thy1.1 antibodies followed by fluoresceinated MARK, and then the cells were incubated with biotinylated anti-CD4 antibody followed by phycoerythrin-conjugated streptavidin (Invitrogen, Carlsbad, CA). The fluorescence intensity of cells was measured with logarithmic amplification using a Becton-Dickinson FACScan (San Diego, CA) and analyzed by a G4 Macintosh computer. Data on 5,000 or 10,000 cells were collected, and forward-angle and side-scatter gates were set to exclude cell clumps and dead cells. To compare parameter measurements among the groups, values were analyzed by one-way ANOVA with a Dunnett's post-test. Significance was designated as $P < 0.05$.

Spleen IgM antibody-forming cell (AFC) response to sheep red blood cells

Using a modified hemolytic plaque assay of Jeme and Nordin (1963), the primary IgM response to sheep RBC was measured. Mice were sensitized with 7.5×10^7 sheep RBC (Lampire, Pipersville, PA) intravenously 4 days prior to sacrifice. On the day of sacrifice, spleen cell suspensions were prepared as previously described (Guo et al. 2001) and resuspended in RPMI 1640 (GibcoBRL, Grand Island, NY) medium with 10% fetal bovine serum (Hyclone, Logan, UT). Cell count was determined using a ZBII Coulter counter in the presence of ZAP-OGLOBIN II lytic reagent (Coulter Corporation, Miami, FL). An aliquot of

cells was added to a test tube containing warm agar (46–48°C), guinea pig complement, and sheep RBC. The mixture was thoroughly mixed, plated in a petri dish, and covered with a microscope coverslip to incubate for 3 h at 37°C. Developed plaques were counted with a Bellico plaque viewer (Bellico Glass, Inc, Vineland, NJ). Experimental results are expressed as specific activity (AFC/10⁶ spleen cells) and total spleen activity (AFC/spleen $\times 10^3$).

Anti-CD3 antibody-mediated T-cell proliferation

Proliferation of splenocytes in the presence of anti-CD3 antibody was performed as described by Guo et al. (2001). Briefly, single-spleen cell suspensions were prepared as above and resuspended in RPMI medium supplemented with 10% fetal bovine serum, sodium bicarbonate, HEPES, L-glutamine, gentamicin, and 2-mercaptoethanol. Splenocytes at 2×10^5 /well were cultured in the microtiter wells coated with or without 1 µg/ml anti-CD3 antibody (PharMingen, San Jose, CA) at 37°C at 5% CO₂ and 95% humidity. Prior to harvest on day 3, cells were pulsed with ³H-thymidine for 18–24 h. Incorporation of ³H-thymidine into the proliferating cells was used as the endpoint of the assay, and the data were expressed as CPM/2 $\times 10^5$ cells.

Natural killer cell activity

Activity of natural killer cells was assayed using the natural killer-sensitive target, Na⁵¹CrO₄-labeled YAC-1 cells, as described by Guo et al. (2001). Briefly, the splenocytes at different dilutions were mixed with the target cells to obtain effector:target ratios of 200:1, 100:1, 50:1, 25:1, 12.5:1, and 6.25:1. Spontaneous release was determined by adding medium to replicate cultures containing the target cells. Maximum release was determined by adding 0.1% Triton X-100 to YAC-1 cells. Natural killer cell-specific lysis (%) of ⁵¹Cr-labeled YAC-1 cells was used as the endpoint of the assay. Activity was calculated by the formula: (experimental release minus spontaneous release) / (maximum release minus spontaneous release) $\times 100\%$.

Bioinformatic analysis

Pairwise protein sequence alignments of TOM112 (Q6ZVM7), Tom112 (Q5SRX1), Tom1 (O88746), and Tom111 (Q923U0) were performed using the BioEdit sequence alignment editor, version 5.0.9 (Hall 1999), utilizing the ClustalW multiple alignment accessory application and the “full multiple alignment” setting. Following alignment similarity and identity was calculated using the BLOSUM62 matrix. The protein sequences were obtained from the Expert Protein Alignment System

(ExPASy) proteomics server of the Swiss Institute of Bioinformatics (SIB).

Creation of *Tom1l2*-GFP expressing cells

Construct preparation *Tom1l2* was PCR amplified from mouse genomic DNA (5' primer: ATATAATTTGCGGCCG CCCCCTTACCATggaggtcctgctgggaat) (3' primer: ATAT AAGGCGCGCCACCCCTTcagggcaagagcgcatcgctc) and cloned into pBluescript. *Tom1l2* was directionally cloned into pENTR (Invitrogen, Carlsbad, CA) with *NorI* and *AscI* (New England Biolabs, Beverly, MA) sites. *pENTR-Tom1l2* was then combined with pcDNA-DEST47 for an in-frame fusion with GFP, and an LRclonase reaction was performed according to the Gateway system instructions (Invitrogen). Digestions, ligation, transformations, and verification of all clones were conducted via standard molecular biology techniques.

Transient transfection and cellular localization of *Tom1l2* COS-7 monkey kidney fibroblasts were transfected with pDEST47-*Tom1l2* or a construct expressing GFP alone by Lipofectamine 2000 (Invitrogen). One day before transfection, cells were seeded on glass coverslips in DMEM medium at 2×10^5 cells/well in 6-well plates. *Tom1l2*-GFP plasmid DNA was complexed in serum-free media with Lipofectamine. After 20 min the complexes were added to COS-7 cells and cultured for 48 h. Transfected cells were stained with BODIPY TR C₅-ceramide (Molecular Probes, Eugene, OR) for visualization of the Golgi complex. Coverslips were mounted onto slides using Vectashield with DAPI (Vector Laboratories, Burlingame, CA) and examined under a Zeiss fluorescence microscope.

Molecular modeling

Homology modeling of the VHS and GAT domains of the mouse *Tom1l2* protein was performed using the automodel feature of the MODELLER program (version 8.1) (Fiser and Sali 2003; Sali and Blundell 1993). An unambiguous primary protein sequence alignment of the VHS and GAT regions of *Tom1* and *Tom1l2* was achieved with ClustalX version 1.83 using the default parameter settings (Chenna et al. 2003). Three-dimensional coordinates for the homology models were based on the high-resolution X-ray crystal structures of the VHS (Misra et al. 2000) and GAT (Akutsu et al. 2005) domains of the human *TOM1* protein. Subsequent structure optimization involved energy minimization of the protein domains using the Tripos Force Field in the SYBYL v7.3 (Tripos, Inc., St. Louis, MO) molecular modeling package. In the energy-minimization procedure, Gasteiger-Hückel charges were calculated and a distance-dependent dielectric constant ($D = 4.0$; cut-off = 8.0 Å) was employed. The stereochemical integrity

of the modeled domains was assessed using the PROCHECK utility (Laskowski 1993) and the ProTable facility within SYBYL. Figures depicting the two domains were prepared using SYBYL. Figure 8A, C, and D were prepared using SYBYL. Figure 8B was prepared using SPOCK v1.0b170 (Christopher 1998). The molecular surface depicted in Fig. 8B was colored by electrostatic surface potential with saturating colors at 20 kT (blue) and -20 kT (red) and a salt concentration of 150 mM. The electrostatic charges used in the calculation of the electrostatic surface were also calculated using SPOCK.

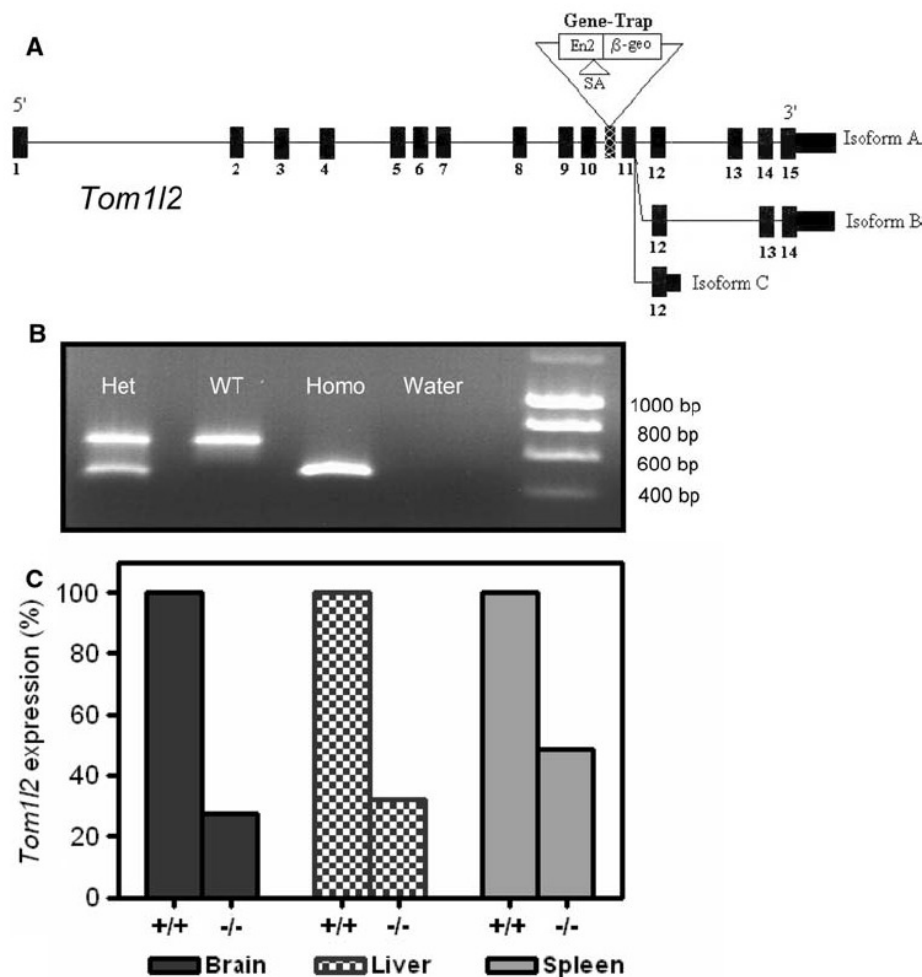
Results

Generation of *Tom1l2* gene-trapped mice

To assess the function of the *Tom1l2* gene, we created *Tom1l2*-deficient mice by gene-trapping (Gossler et al. 1989; Skames et al. 1995). The XG909 cell line (BayGenomics Consortium) (Stryke et al. 2003) carries a gene-trapping vector inserted between exons 10 and 11 of *Tom1l2*. The XG909 cell line was created from 129/OlaHsd embryonic stem cells, expanded, and injected into C57Bl/6J blastocysts for creation of chimeric mice. Chimeric XG909 males were mated with C57Bl/6J females to produce an F₁ line. *Tom1l2* heterozygote males and females from the F₁ generation (selected by coat color and verified by Southern analysis) were bred to obtain an F₂ generation. *Tom1l2* mouse breeding generated heterozygous, homozygous, and wild-type pups in expected Mendelian ratios. To identify the exact location of the vector insertion, a DNA fragment was PCR amplified from a homozygous mouse (see Methods) using a 5' primer specific to the gene-trapping vector and a 3' primer specific to the endogenous *Tom1l2* gene. Sequencing of this product localized the insert to intron 10, 1978 bases downstream from the end of exon 10 (Fig. 1A). Further genotyping was conducted by PCR, and wild-type, heterozygous, and homozygous mice were easily distinguished (Fig. 1B).

To determine whether these gene-trapped mice had reduced levels of *Tom1l2* expression, a semiquantitative RT-PCR was performed using primers designed to amplify a region downstream of the gene-trap insertion. Homozygous *Tom1l2* mouse brain revealed an approximately 80% reduction in *Tom1l2* expression compared with that of sibling wild-type littermates (Fig. 1C). Similarly, an ~70% and ~50% decrease in *Tom1l2* expression was observed in liver and spleen, respectively, of homozygous targeted animals as compared with wild-type mice (Fig. 1C). These results, similar to other those of published reports of gene-trapped mice (Stanford et al. 2001; Voss et al. 1998), indicate that the presence of the gene-trapping

Fig. 1 *Tom1l2* gene-trapped mice. (A) *Tom1l2* genomic structure and gene trap. All isoforms (a, b, and c) of *Tom1l2* are shown. The gene trap is located in intron 10, as shown. The vector splice acceptor site (SA) is indicated by the arrow. Note that insertion of the *En2* gene and β -geo interrupts all isoforms of *Tom1l2*. (B) *Tom1l2* PCR genotyping. The top band indicates the presence of the wild-type allele, while the appearance of the lower band indicates the presence of the gene-trapped allele. (C) RT-PCR of *Tom1l2* gene-trapped mice. Analysis of *Tom1l2* mRNA expression in brain, liver, and spleen of wild-type (+/+) and homozygous (-/-) *Tom1l2* gene-trapped mice indicates that the *Tom1l2*^{-/-} mice exhibit reduced expression as compared to wild-type



vector in the position described above was sufficient to reduce *Tom1l2* levels significantly, resulting in *Tom1l2* hypomorphic mice. The term hypomorph, for the purposes of this study, is used to signify that mice, homozygous for the insertion, produce reduced levels of *Tom1l2* mRNA. A true knockout would have no detectable levels of expression. Heterozygous mice have one wild-type copy of *Tom1l2* and one copy of the gene with the insertion and should not be considered hypomorphs.

Anxiety-related behaviors in *Tom1l2* hypomorphs

We evaluated craniofacial, skeletal, neurologic, and behavioral aspects of the *Tom1l2* mice. Phenotypic assessments were based on a comprehensive set of protocols adapted from the SHIRPA, the Irwin battery, and the test battery described by Crawley and Paylor (1997; Irwin 1968; Rogers et al. 1997). Preliminary assessments were performed to delineate abnormal characteristics, including health,

physical status, fecundity, and observable neurobehavioral features. Additional tests were employed to assess specific behavioral measures in all *Tom1l2* mice genotypes.

General behavioral evaluations showed significantly increased freezing response in the *Tom1l2* mice compared to wild-type mice (Fisher's exact test, $P < 0.05$; Table 1). Furthermore, a higher proportion of *Tom1l2* heterozygotes exhibited wild running (Table 1). To understand if the freezing behavior was related to fear or anxiety, open-field tests were performed. Heterozygous *Tom1l2* mice showed increased rearing in the open field compared with the wild-type animals, indicating fear- or anxiety-related behavior (Crawley and Paylor 1997). Physical assessments, including body weights, body lengths, and craniofacial measurements, were not significantly different among the genotypes (Supplementary Fig. 1 and data not shown). Other behavioral evaluations did not reveal any statistically significant effects due to reduced *Tom1l2* expression (Table 1).

Table 1 Phenotypic assessment of *Tom1l2* hypomorphic mice

	<i>Tom1l2</i> +/+	<i>Tom1l2</i> +/-	<i>Tom1l2</i> -/-
Number of mice evaluated	34	46	27
Physical assessment and simple reflexes (% abnormal)			
Whisker appearance	11.7	8.6	14.8
Bald patches (%)	8.8	17.4	22.2*
Condition of teeth ^a	3	2.1	7.4
Righting reflex	0	0	0
Sound orientation	0	0	0
Whisker response	0	0	0
Eye blink/ear twitch	0	0	0
Pupil constriction/dilation	0	0	0
General observational measurement (%)			
Wild running	8.6	17.6*	3.7
Freezing	2.1	17.6*	14.8*
Sniffing	100	100	100
Licking	100	100	100
Rearing			
5 weeks	8.8	17.3	11.1
10 weeks	5.8	15.2*	7.4
20 weeks	8.8	15.2*	7.4
30 weeks	8.8	13*	0
Defecation	100	100	100
Urination	100	100	100
Stereotypies	0	0	0
Sensorimotor reflexes and strength (% abnormal)			
Postural reflex	0	0	0
Cage-top hang test (latency in sec \pm SEM)			
Male (5 weeks)	42.8 \pm 4.9	47.3 \pm 3.5	42.4 \pm 5.2
Female (5 weeks)	52.1 \pm 3	56.4 \pm 1.3	55.4 \pm 3.8
Male (10 weeks)	26.7 \pm 4.3	32.3 \pm 5.1	34 \pm 6.1
Female (10 weeks)	51.63 \pm 4.8	48.9 \pm 4	52.1 \pm 2.9
Response to being picked up by tail	0	0	0
Hot-plate test (latency in sec \pm SEM)			
Male	4.3 \pm 0.03	3.7 \pm 0.73	3.8 \pm 0.36
Female	3.11 \pm 0.39	3.46 \pm 0.03	3.3 \pm 1

* Significantly different from the wild-type ($P < 0.05$)

^a Malocclusion of teeth

Tom1l2 gene-trapped mice exhibit increased incidence of infections and tumors

Physical assessments of *Tom1l2* homozygous, *Tom1l2* heterozygous, and wild-type littermates showed gross inflammatory lesions of the skin, including hair loss (bald patches), dermatitis, and skin ulcerations, in the *Tom1l2* mice compared with the wild-type mice (Tables 1 and 2). Homozygous mice showed more severe lesions than the heterozygotes, and wild-type mice rarely showed any abnormalities (Table 1). Initially, all mice were housed in woodchip bedding, which, with the benefit of retrospection, may have promoted the initiation and contributed to the severity of the infections observed. Eye manifestations

observed in *Tom1l2* mice included conjunctivitis, corneal ulcers, exophthalmos, and ocular asymmetry (Table 2). Later, the mice were transferred to cages with corncob bedding and the infections were not only less severe but were less frequent in the *Tom1l2* mice. Infections did not occur in wild-type animals from the same cage. Serologic investigations, including swab culture from sites of skin and eye infections, revealed the presence of *Staphylococcus aureus*, a common skin pathogen. Other infectious pathology included bronchopneumonia (2% incidence) and murine mycoplasmosis (1%). Overall, the incidence of skin/eye infections in *Tom1l2* mice was 15–20%. Although individual mice did not develop the entire array of observed health problems, *Tom1l2* mice at least 9 months

Table 2 Pathologies identified during gross organ and phenotypic assessment

<i>Tom1l2</i> +/-	<i>Tom1l2</i> -/-
Splenomegaly	Splenomegaly
Skin ulcers	Skin ulcers
Eye infections	Eye infections
Kyphosis	Malocclusion of teeth
Exophthalmos	Bladder hemorrhage
Ocular assymetry	Hemorrhagic mass near spleen
Corneal ulcer	Kyphosis
Excess fat in the abdomen	Hydrocephaly
Hydrocephaly	Pleural effusion
Emphysema of lung	Tumors
Tumors	Skin
Skin	Small, cystic kidneys
Soft tissue mass in vulva	Liver polyps
Lachrymal gland enlargement	Large ovarian mass
Lung tumor	Mammary gland tumor
Ovarian cyst	Kidney tumor
Dark mass on prostate	Bony tumor in the hind limb
Kidney tumors	Lung tumor

old manifested an array of complications typically resulting in euthanasia, including hemorrhagic bladder, hemorrhagic masses adjacent to spleen and ovary, and thoracic hemorrhage. Furthermore, a variety of tumors were observed in ~20% of *Tom1l2* mice. Tumors were not limited to any particular organ and developed within the lung, ovary, kidney, liver, prostate, abdomen, thorax, and skin (Table 2). The types of tumor ranged from primary and benign adenomas (pulmonary/brochoalveolar, renal) to noninvasive or invasive neoplasms (basal cell carcinoma of the skin, liver, and renal adenocarcinoma, lymphoid hyperplasia, and tumors of the mammary gland, ovaries, and prostate) and metastatic neoplasia (renal adenocarcinoma with secondaries in the liver and lymph nodes). In

addition, 3% of the *Tom1l2* mice developed excess fat deposition in the abdomen. None of these pathologies were observed in the wild-type littermates.

Splenomegaly in *Tom1l2* hypomorphs

Gross evaluation of spleens from homozygous mice older than 1 year revealed splenomegaly with weights from 1.5 to 2 times normal ($P < 0.01$). In one evaluation, four of six older *Tom1l2* mice had significantly larger, darker, abnormally shaped spleens. Homozygous mice showed an expanded splenic white pulp (Fig. 2A). Within the white pulp, both follicles (B-cell-enriched regions) and periarteriolar lymphoid sheath (T-cell-enriched regions) had increased cellularity. However, no germinal centers were present. There was no indication of erythropoiesis within the red pulp. Even apparently healthy homozygous mice from 12 to 16 weeks of age had significant splenomegaly (Fig. 2B). Body lengths and weights were assessed at 5, 10, 20 and 30 weeks of age and were not different among the genotypes (Supplementary Fig. 1). Therefore, differences in splenic weights are not due to differences in body size.

Because the white pulp is part of the immune system, we hypothesized that splenomegaly and the previously mentioned health issues were related. To further examine this possibility, a complete peripheral blood analysis was conducted on healthy mice of each genotype and sex (15-19 months old) (Fig. 3A). Although not statistically different, the total white blood cell (leukocyte) count in homozygous mice was decreased, with percentages of lymphocytes and neutrophils slightly lower than in wild-type mice, and the percentages of monocytes, eosinophils, and basophils were increased compared with those for wild-type mice (Fig. 3B). Homozygous mice had significantly lower platelet counts than wild-type mice (Fig. 3C), while the red blood cell (RBC) counts for all mice were normal (Fig. 3D). Other parameters concerning erythroid

Fig. 2 Enlarged spleens in *Tom1l2* mice. (A) Histologic tissue sections of spleen from a *Tom1l2* hypomorph (homozygous for the insertion), illustrating splenomegaly and enlarged white pulp (upper), and wild-type mouse (lower). Red (pink arrowheads) and white (white arrowheads) pulp are indicated. Scale bar = 1 mm. (B) Spleen weights for *Tom1l2*+/+ and *Tom1l2*-/- mice from 12 to 16 weeks of age. Mice from both sexes were evaluated

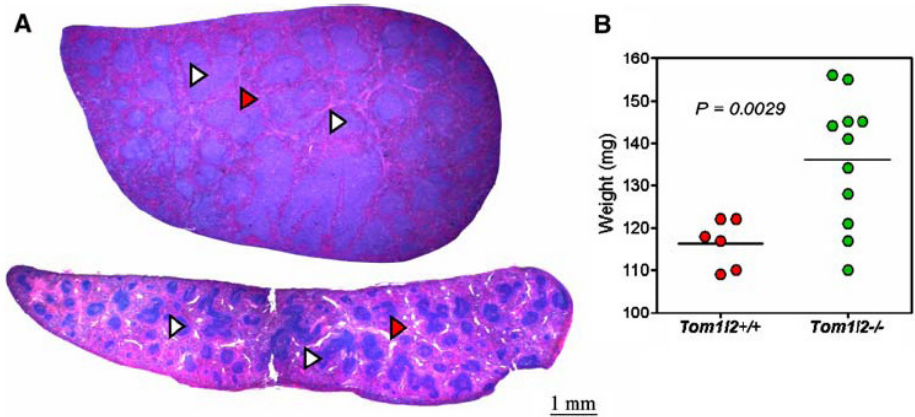
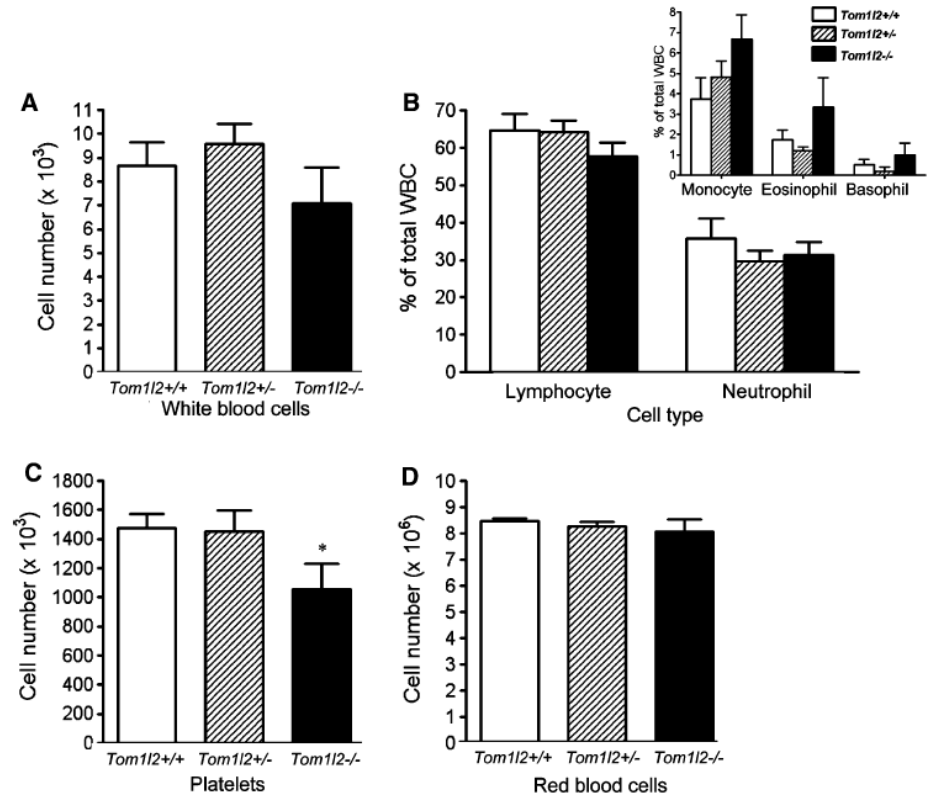


Fig. 3 Hematologic analyses of *Tom1l2* mice. (A) Total white blood cell count. (B) Percentages of lymphocytes and neutrophils. Inset: Percentages of monocytes, eosinophils, and basophils. (C) Platelet counts. Histogram represents *Tom1l2*^{+/+} (white bars), *Tom1l2*^{+/-} (hatched bars), and *Tom1l2*^{-/-} (black bars) mice



cells were also evaluated. Hemoglobin, hematocrit, mean corpuscular volume (MCV), mean corpuscular hemoglobin (MCH), and mean corpuscular hemoglobin concentration (MCHC) did not show any statistically significant differences among the genotypes (Supplementary Table 1). Thus, although homozygous mice had reduced platelet counts, they were not anemic. Overall, the decreased level of *Tom1l2* expression had no major effect on the erythroid system based on the examined parameters despite the darker color of the spleens in older mice.

Analyses of the cellular composition of major lymphoid organs, including spleen, lymph nodes, and thymus, were performed on mice that showed no signs of infection. For this purpose, young (7 weeks of age) and older (6 months of age) mice of each genotype were examined. A trend toward an increased number of nucleated cells (leukocytes) in the spleen was observed in homozygous mice for both age groups (Table 3). This increase in leukocytes likely explains the enlarged spleens in homozygous mice. By contrast, cellular counts for thymi for young mice were not different among the genotypes (Table 3). For evaluation of immune cell subpopulations, immunofluorescence staining and flow cytometric analysis were performed. Cells from the spleen, lymph nodes, and thymus were stained with monoclonal antibodies to detect CD4⁺ (helper T-cell marker), CD8⁺ (cytotoxic T marker), B220⁺ (B-cell marker),

Table 3 Number of nucleated cells ($\times 10^6$) in spleen and thymus in *Tom1l2* mice

Age and genotype	Nucleated cells ($\times 10^6$)	
	Spleen	Thymus
7 weeks		
<i>Tom1l2</i> ^{+/+}	91 \pm 55	126 \pm 50
<i>Tom1l2</i> ^{+/-}	80 \pm 36	130 \pm 82
<i>Tom1l2</i> ^{-/-}	114 \pm 76	107 \pm 60
6 months		
<i>Tom1l2</i> ^{+/+}	107 \pm 23	ND
<i>Tom1l2</i> ^{+/-}	123 \pm 54	ND
<i>Tom1l2</i> ^{-/-}	124 \pm 32	ND

and Mac-1⁺ (macrophage marker) molecules. The various thymocyte subpopulations, including CD4 single-positive, CD8 single-positive, CD4-CD8 double-positive, and CD4-CD8 double-negative cells, were virtually identical in all groups of young mice (data not shown), suggesting that thymic maturation was normal.

Spleens from 6-month-old hypomorphic mice showed a significant increase in the percentages of CD4⁺ helper T cells ($P = 0.05$) and CD8⁺ cytotoxic T cells ($P < 0.05$), while the percentage of macrophages was lower compared to the wild-type (Fig. 4B–D, Supplementary Table 2).

Although the difference was not statistically significant, B-cell levels tended to be elevated in spleens from both heterozygous and homozygous older mice (Fig. 4A, Supplementary Table 2). These results suggest that leukocyte subpopulations became skewed in older homozygous mice, while the relative proportion of the four cell types examined did not differ in the spleens of young mice (Supplementary Table 2). Lymph nodes of *Tom1l2* mice were not enlarged (data not shown) but had dramatically higher percentages of B cells and T cells in older mice and B cells in younger mice (Supplementary Table 2). The percentages of B cells, T cells, and macrophages in the lymph nodes from both young and old hypomorphic mice were highly variable compared to wild-type, which may suggest incomplete penetrance (Supplementary Table 2).

Reduced humoral immune response in *Tom1l2* hypomorphs

To assess immune competency of *Tom1l2* gene-trapped mice, we analyzed the ability of splenic cells to generate immune responses, which encompassed humoral

immunity, pan-T-cell response, and innate immunity. First, the IgM antibody-forming cell (AFC) response to T-dependent antigen sheep RBC was examined to evaluate humoral immunity (Jerne and Nordin 1963) (Fig. 5A). In homozygous mice, the specific activity (AFC/ 10^6 spleen cells) was decreased by $\sim 44\%$ ($P < 0.05$, $t = 2.4$; $df = 8$) and the total spleen activity (AFC/spleen) was decreased by $\sim 45\%$ ($P < 0.05$, $t = 2.39$; $df = 8$) compared with the controls (Fig. 5A, B). A reduction in the AFC response has been implicated in decreased host resistance to infectious agents in mice (Luster et al. 1988). However, the cells required for this humoral response were not decreased in *Tom1l2* homozygous mice. Generalized immune responsiveness of T cells was measured by cell proliferation induced with anti-CD3 antibody that crosslinks the T-cell receptor complex regardless of antigen specificity. The proliferative response of T cells was not statistically different between homozygous and wild-type mice (Fig. 5C). This result is surprising considering that the homozygous mice had 1.6-fold more T cells. Because a corresponding increase in the CD3 assay was not seen despite the higher levels of T cells in the homozygous mice, these data

Fig. 4 Altered splenocyte subpopulations in 6-month-old *Tom1l2* hypomorphs. (A) B220⁺ B cells. (B) CD4⁺ helper T cells. (C) CD8⁺ cytotoxic T cell. (D) Mac-1⁺ macrophages. * $P < 0.05$. + = In those samples that were fully penetrant, the differences observed were significant; $P < 0.05$.

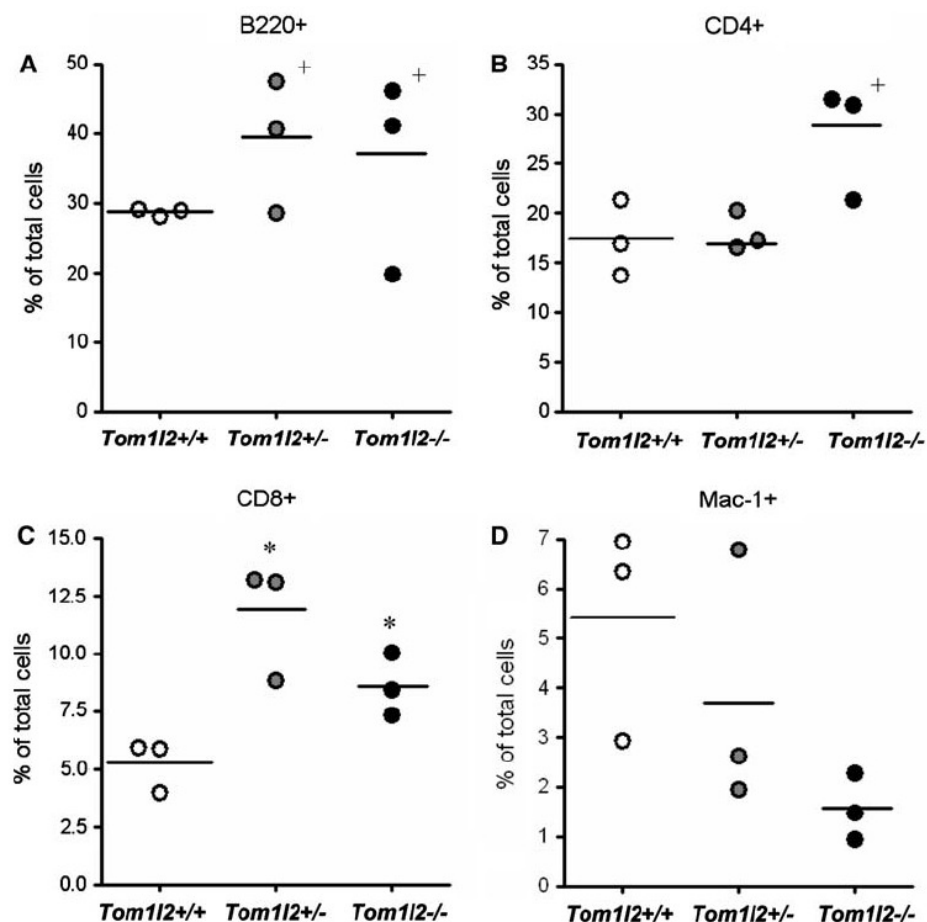
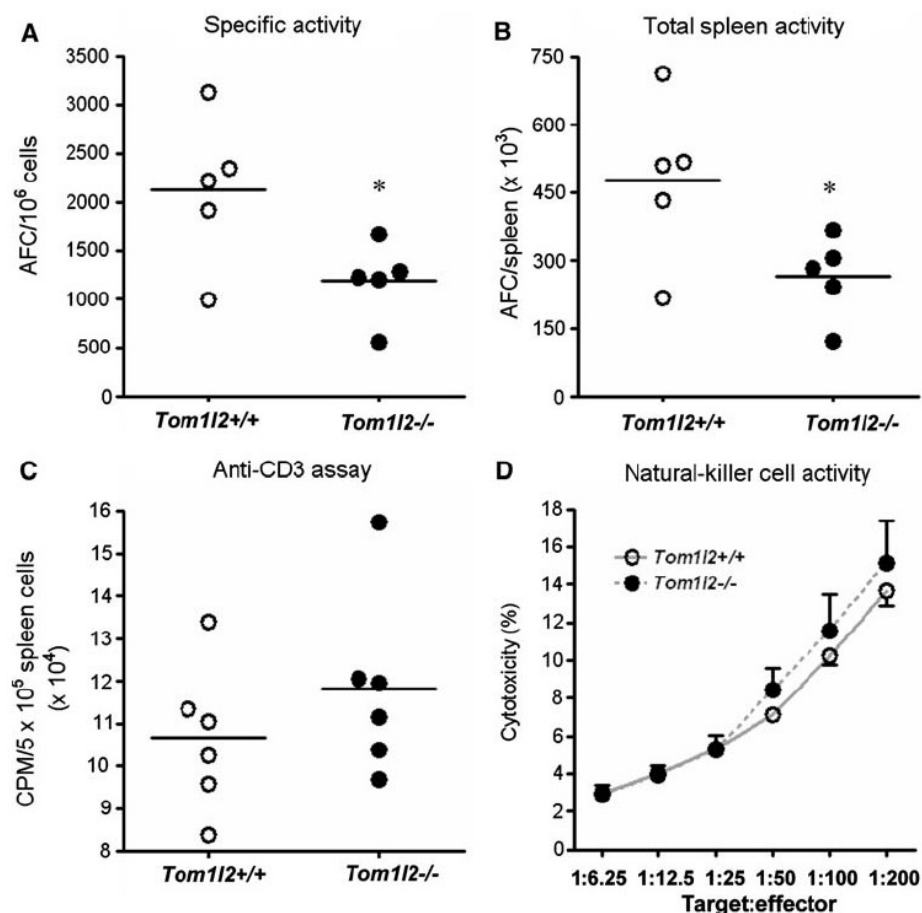


Fig. 5 Impaired adaptive immune responses by spleen cells from *Tom1l2* mice. IgM AFC response to the T-dependent sheep RBC antigen expressed as (A) specific splenic activity and (B) total splenic activity. (C) Pan-T-cell proliferative response to anti-CD3 antibody. (D) Natural killer cytotoxicity. * $P < 0.05$



confirm that there is a T-cell immune defect in the *Tom1l2* mice. Finally, innate immune responsiveness was evaluated by measuring natural killer cell cytotoxicity using ⁵¹Cr-labeled YAC-1 cells as the target at various target:effector ratios (Fig. 5D). Although increased cytotoxicity was observed at higher ratios with *Tom1l2*-deficient cells, no statistically significant difference was observed (Fig. 5D).

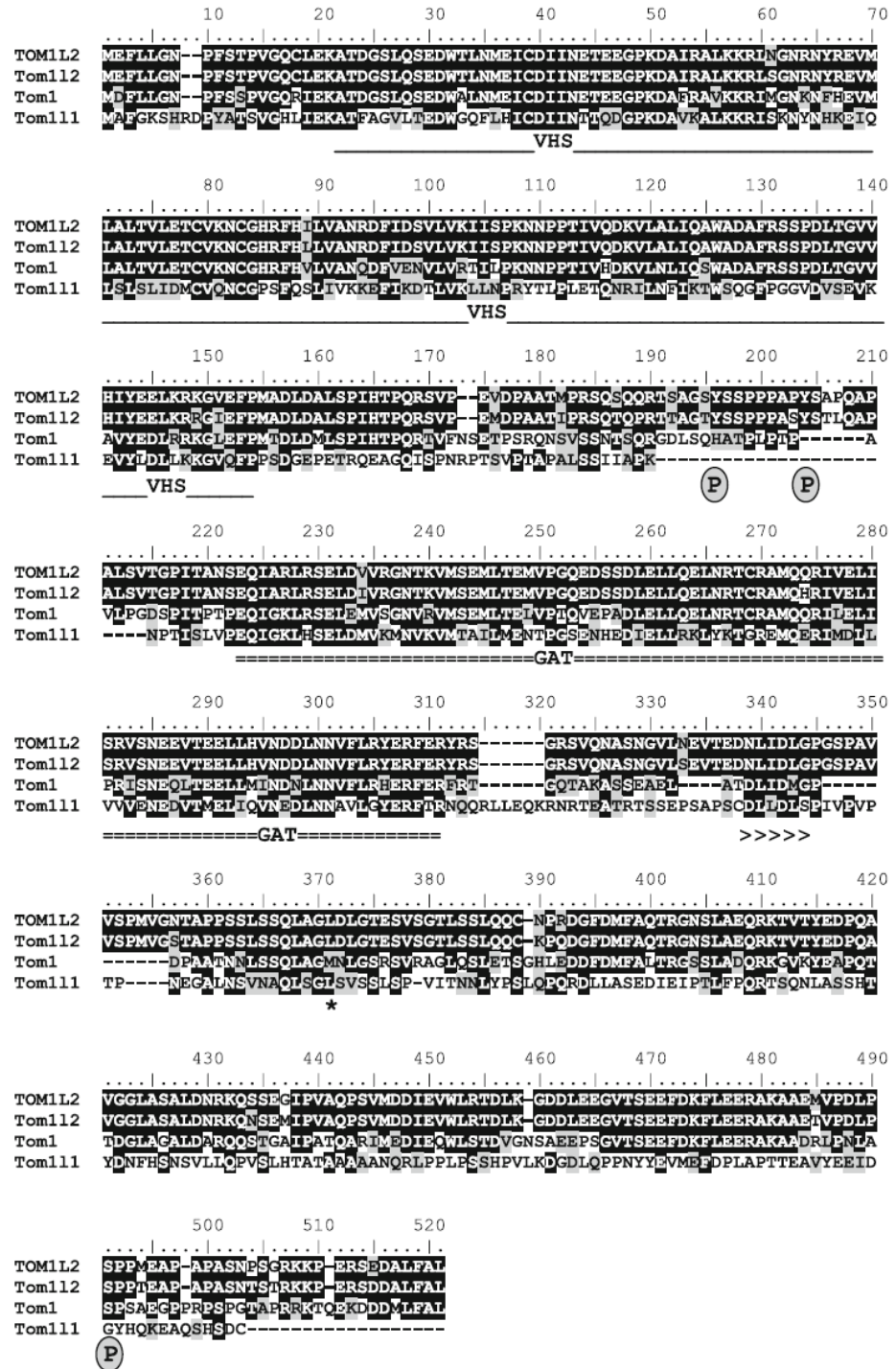
Tom1l2 belongs to Tom1 family of proteins and *Tom1l2* localizes to the trans-Golgi network

Bioinformatic studies were performed using the BioEdit pairwise sequence alignment editor. *Tom1l2* has 60.8% amino acid identity (74.2% similarity) to *Tom1* and 26.6% identity (47.3% similarity) to *Tom1l1* (Fig. 6, Supplementary Table 3). The mouse *Tom1l2* protein is 94.4% identical (97.8% similarity) to the human *TOMIL2*. Thus, a high level of similarity with conservation of functional domains exists among the *Tom1* family of proteins, indicating a common role in cellular biochemical processes.

A GFP-*Tom1l2* fusion construct (pDEST47-*Tom1l2*) was transfected into COS-7 monkey kidney fibroblasts. Forty-eight hours after transfection, the *Tom1l2*-GFP fusion protein colocalized with Bodipy TR Ceramide, which stains the Golgi apparatus (Fig. 7). Thus, the *Tom1l2*-GFP fusion protein colocalizes with Golgi compartments and vesicles, providing supporting evidence that *Tom1l2* is involved in trafficking and vesicular transport.

Molecular modeling was then performed based on protein homology using an unambiguous sequence alignment of the VHS and GAT domains of *Tom1* and *Tom1l2*. Three-dimensional coordinates based on known high-resolution X-ray structures of VHS and GAT domains (Akutsu et al. 2005; Misra et al. 2000) show structural similarity of these functional domains between *Tom1* and *Tom1l2* (Fig. 8). While the GAT domains of *TOM1* and *TOMIL1* interact with both ubiquitin and TOLLIP, interaction of ubiquitin with *TOMIL2* has not been shown (Katoh et al. 2004). Our molecular model suggests that *Tom1l2* likely provides cognate sites, similar to other members of *Tom1* family of proteins, for interactions with ubiquitin. Because a cellular trafficking role for *Tom1* is

Fig. 6 Tom112 belongs to the Tom1 family of proteins. Human TOM1L2 and murine Tom112, Tom1, and Tom111 are shown aligned in decreasing homology. The VHS (solid line) and GAT (dashed line) domains are indicated. The clathrin box (indicated by >>>>>) is also shown. Potential tyrosine and serine phosphorylation sites are indicated by P. The gene-trap vector (indicated by *) is inserted into *Tom112* intron 10, as shown, and affects all splice variants



already established (Lohi and Lehto 1998), our homology model of Tom112 provides structural evidence for a role in trafficking for Tom112 in the cell as well and provides supporting evidence for Tom112 interactions with ubiquitin.

Discussion

Tom112 gene-trapped mice were created to determine the biological significance of this protein. The vector insertion site, located in intron 10, affects all known splice variants

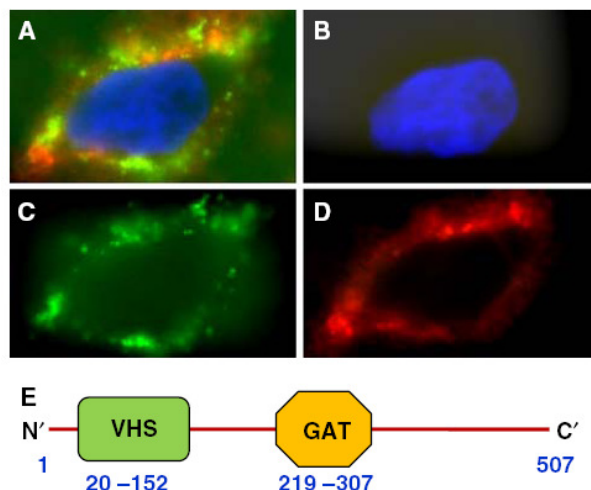


Fig. 7 Cellular localization of the Tom112 protein. Cells were imaged in live-cell format at 63 \times . (A) Tom112-GFP fusion protein expresses and localizes to Golgi compartment (yellow). (B) Nuclear staining (blue) with DAPI. (C) GFP (green) viewed under FITC filter. (D) Golgi apparatus stained with 2.5 μ M fluorescent ceramide (red) and viewed under Texas Red filter. (E) Schematic of the Tom112 protein with location of the VHS and GAT domains, with corresponding amino acid numbers (blue)

of Tom112 (isoforms a, b, and c). In concert with many other reported studies on gene-trapped mouse models (Serafini et al. 1996; Skarnes et al. 1992; Yeo et al. 1997), these *Tom112* mice are not total knockouts but instead are hypomorphs that show $\sim 30\%$ residual *Tom112* expression. A concern for any gene-trapping model is that the trapped gene may still function and have significant levels of normal protein being produced due to leakiness of the gene-trapped vector. This is the result of the cell transcription machinery effectively “skipping” or “reading over” the vector insert in the intron, thus allowing production of some normally functioning protein. Although a consistent difference between the genotypes was observed, extensive phenotypic variability in the hypomorphs was revealed in most of the immunologic studies. This variability could be due to the genetic background, modifier genes altering the phenotypic consequence, or incomplete penetrance of the immune system phenotype, perhaps requiring a “trigger” to induce the immunologic effects. The penetrance of individual phenotypes, including splenomegaly, skin and eye infections, and tumors, varied between 15% and 20% in *Tom112* mice; thus, overall penetrance for any aspect of the global immune phenotype is approximately 50–60%.

The most prominent phenotype of the *Tom112* hypomorphs was the high frequency of infections and tumors found in these mice. To further understand this phenotype, we performed gross organ dissections, histologic analysis, and immunologic studies. Gross organ observations showed

significant splenomegaly, further supported histologically by increased white pulp content. This was corroborated by an increase in CD4 $^{+}$ and CD8 $^{+}$ T cells and B cells in the spleen. While a corresponding increase in anti-CD3 proliferating T cells was expected in studies on humoral immune response, no significant difference was seen in the CD3 assay. The antibody-forming cell (AFC) assay is a sensitive indicator of the host’s ability to mount an antibody response to a specific antigen (Luster et al. 1988). When T-dependent antigen sRBC are employed as a trigger, the IgM antibody response requires a coordinated interaction of T cells, B cells, and antigen-presenting cells such as macrophages and/or dendritic cells (Luster et al. 1988; Yang et al. 2003). Any alteration in antigen processing or presentation, cytokine production and release by T cells, and proliferation and/or differentiation of T cells and B cells could affect the final immunologic response (Yang et al. 2003). A decrease in splenic IgM AFC response was observed for *Tom112* homozygous mice compared to wild-type littermates. Taken together, these results suggest that in spite of increased T-cell population in the spleens, leading to enlarged spleens, the number of functional T cells is low, indicating a defect in the T-cell immune response.

Functional genomic analysis suggests that *TOM112* is likely involved in trafficking, which is a critical and important part of normal cellular function. Trafficking has been shown to be important for a variety of developmental disorders, including Chediak-Higashi syndrome, an autosomal recessive disease characterized by variable degrees of oculocutaneous albinism, recurrent infections, and a mild bleeding tendency due to mutations in *CHS1* (*LYST*), a protein involved in the regulation of lysosomal trafficking (Zarzour et al. 2005). Our cellular localization studies showed that Tom112 is localized in the trans-Golgi-network and in cytoplasmic vesicles, consistent with the presence of a VHS domain in the N-terminus of TOM1L2/Tom112 (Lohi and Lehto 1998). Our homology-based molecular model not only confirms the structural similarity of VHS and GAT domains of Tom112 to other Tom1 family trafficking proteins, but it also supports a similar functional role for Tom112.

A review of the literature related to *TOLLIP*, *TOM1*, and *TOM1L1*, including *in vitro* and *in vivo* studies, shows that the phenotypic features in *Tom112* hypomorphs could be due to disruption of several interacting proteins and pathways. It is noteworthy that *TOLLIP*, which interacts with the GAT domain of TOM1L2 (Katoh et al. 2006), also interacts with the IL-1R (Katoh et al. 2004), a master regulator of inflammation and innate immunity. Furthermore, *TOM1*, which is functionally and structurally similar to TOM1L1 and TOM1L2, also interacts with IL-1R (Brissoni et al. 2006). Interestingly, Tom111 interacts with Fyn (Seykora et al. 2002), and mice with mutations in *Fyn*

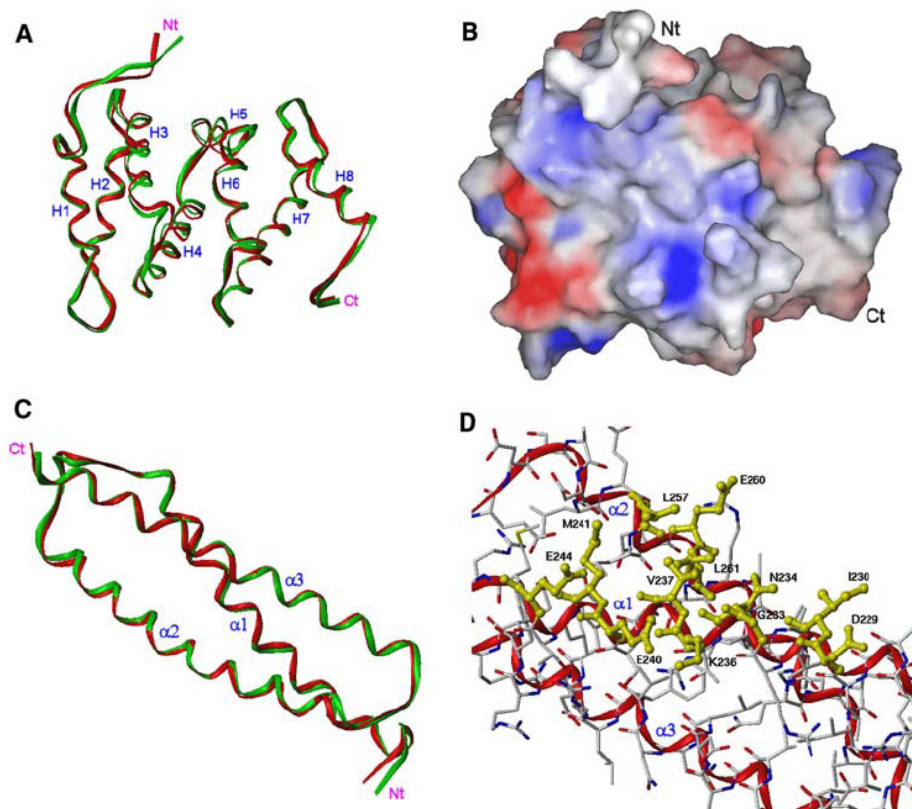


Fig. 8 Molecular modeling of Tom112 protein. (A) Ribbon diagrams depicting the secondary and tertiary structure of the VHS domains of TOM1 (green; residues Met1-Met153) crystal structure and Tom112 (red; residues Met1-Met153) homology model. Helix 1 through Helix 8 (H1-H8) and the N- and C-termini are labeled. The root-mean-square distance (RMSD) between the alpha carbon (C^α) atoms of TOM1 VHS and those in the corresponding Tom112 VHS model is 0.73 Å. (B) Molecular solvent-accessible surface of the Tom112 VHS domain. The surface is color-coded with respect to electrostatic surface potential, with acidic regions indicated in red and basic regions in blue. A pocket lined with basic residues can be seen, a

feature also found in the VHS domains of other proteins (Misra et al. 2000). (C) Ribbon diagrams depicting the higher-order structure of the GAT domains of TOM1 (green; residues Glu215-Gly307) crystal structure and Tom112 (red; residues Glu219-Gly311) homology model. Helices $\alpha 1$ ($\alpha 1$) through $\alpha 3$ ($\alpha 3$) and the N- and C-termini are labeled. The RMSD between the C^α atoms of TOM1 GAT and those in the corresponding Tom112 GAT model is 0.46 Å. (D) Residues on helices $\alpha 1$ and $\alpha 2$ in the Tom112 GAT domain are proposed to be the interaction site of ubiquitin based on cognate residues in the ubiquitin-TOM1 GAT domain crystal structure (Akutsu et al. 2005)

have immune defects, with abnormalities in lymphocyte development and impaired brain function (Grant et al. 1992; Stein et al. 1992). Given these data, it is reasonable to hypothesize that a decrease in *Tom112* expression would result in impaired immune responses.

Tom1 is also a direct target of both oncogenic forms of the *v-Myb* gene (Burk et al. 1997). *Myb* is involved in cell differentiation processes, including hematopoiesis (Burk and Klempnauer 1999; Oh and Reddy 1999), which is intriguing since *Tom112* hypomorphic mice have greater percentages of T cells in their spleens. In addition, *c-Kit* (Hogg et al. 1997) and *Bcl-2* (Frampton et al. 1996), well known for their prosurvival role in cancer, are upregulated by *v-Myb* along with *Tom1* (Burk et al. 1997). *Tom111* downregulation resulted in greater than twofold increase in mitogenic response induced by platelet-derived growth

factor (Franco et al. 2006), and TOM1L1 levels are decreased in cutaneous squamous cell carcinoma and associated precursor lesions (Li et al. 2005). Also, increased SFK activity is present in many human cancers and Tom111 acts as “rheostat” for activated SFKs that regulate cell proliferation (Aligayer et al. 2002; Biscardi et al. 2000; Park et al. 1993). Indeed, transgenic mice overexpressing a mutant *Tom111* exhibited a hyperproliferative skin phenotype (Li et al. 2007). Recently, expression profiling of osteosarcoma cell lines implicated *TOM1L2* as a candidate target gene for 17p amplicon-associated osteosarcomas (Atiye et al. 2005; van Dartel and Hulsebos 2004). These results are remarkable considering that *Tom112* hypomorphs have an increased incidence of tumors.

Understanding the role of *Tom112* in the immune response and its ultimate effect on immune function has

broad implications in the study of infectious disease, the immune response, and tumor development. If its deficiency results in increased incidence of malignancies, then understanding its function is paramount. Furthermore, evaluating this gene will help provide much needed data to direct any future development of pharmacotherapies related to this protein and its known pathways. The role of TOMIL2 in the Smith-Magenis syndrome, in which 90% of affected individuals are hemizygous for *TOMIL2*, may be pursued further as a cause for the immune abnormalities observed in these patients. By identifying the pathways in which TOMIL2 functions, we will be able to better understand and more effectively investigate the role of *TOMIL2* in immune deficiencies and human cancers.

Acknowledgments The authors thank Dr. Mario Dance from the VCU Department of Animal Resources for helping with collection of blood samples from mice. They acknowledge Valerie Vinoverski for assistance with GFP studies and Constance B. Hartmann for technical assistance with immunofluorescence staining and flow cytometry. They also thank the Transgenic Animal Model Core at the University of Michigan, the Histopathology Core at Michigan State University, and the Comparative Pathology Lab at UC Davis for mouse tissue and serum studies. This work was supported in part by NIH R01HD38534 (SHE), NIH P50DA05275 (KM), NIH R01ES07199 (KM), the Jeffress Foundation (SHE), the A. D. Williams Trust Fund (KM & SHE), and by resources from Michigan State University and Virginia Commonwealth University.

References

- Akutsu M, Kawasaki M, Katoh Y, Shiba T, Yamaguchi Y et al (2005) Structural basis for recognition of ubiquitinated cargo by Tom1-GAT domain. *FEBS Lett* 579:5385–5391
- Aligayer H, Boyd DD, Heiss MM, Abdalla EK, Curley SA et al (2002) Activation of Src kinase in primary colorectal carcinoma: an indicator of poor clinical prognosis. *Cancer* 94:344–351
- Amsterdam A, Burgess S, Golling G, Chen W, Sun Z et al (1999) A large-scale insertional mutagenesis screen in zebrafish. *Genes Dev* 13:2713–2724
- Atiye J, Wolf M, Kaur S, Monni O, Bohling T et al (2005) Gene amplifications in osteosarcoma-CGH microarray analysis. *Genes Chromosomes Cancer* 42:158–163
- Bellen HJ, O’Kane CJ, Wilson C, Grossniklaus U, Pearson RK et al (1989) P-element-mediated enhancer detection: a versatile method to study development in *Drosophila*. *Genes Dev* 3:1288–1300
- Bier E, Vaessin H, Shepherd S, Lee K, McCall K et al (1989) Searching for pattern and mutation in the *Drosophila* genome with a P-lacZ vector. *Genes Dev* 3:1273–1287
- Biscardi JS, Ishizawar RC, Silva CM, Parsons SJ (2000) Tyrosine kinase signalling in breast cancer: epidermal growth factor receptor and c-Src interactions in breast cancer. *Breast Cancer Res* 2:203–210
- Bonifacino JS (2004) The GGA proteins: adaptors on the move. *Nat Rev Mol Cell Biol* 5:23–32
- Brissoni B, Agostini L, Kropf M, Martinon F, Swoboda V et al (2006) Intracellular trafficking of interleukin-1 receptor I requires Tolip. *Curr Biol* 16:2265–2270
- Burk O, Klempnauer KH (1999) Myb and Ets transcription factors cooperate at the myb-inducible promoter of the tom-1 gene. *Biochim Biophys Acta* 1446:243–252
- Burk O, Worpenberg S, Haenig B, Klempnauer KH (1997) *tom-1*, a novel v-Myb target gene expressed in AMV- and E26-transformed myelomonocytic cells. *EMBO J* 16:1371–1380
- Chenna R, Sugawara H, Koike T, Lopez R, Gibson TJ et al (2003) Multiple sequence alignment with the clustal series of programs. *Nucleic Acids Res* 31:3497–3500
- Christopher JA (1998) SPOCK. Texas A&M University, College Station, TX
- Crawley JN, Paylor R (1997) A proposed test battery and constellations of specific behavioral paradigms to investigate the behavioral phenotypes of transgenic and knockout mice. *Horm Behav* 31:197–211
- Fiser A, Sali A (2003) Modeller: generation and refinement of homology-based protein structure models. *Methods Enzymol* 374:461–491
- Frampton J, Ramqvist T, Graf T (1996) v-Myb of E26 leukemia virus up-regulates bcl-2 and suppresses apoptosis in myeloid cells. *Genes Dev* 10:2720–2731
- Franco M, Furstoss O, Simon V, Benistant C, Hong WJ et al (2006) The adaptor protein Tom1L1 is a negative regulator of Src mitogenic signaling induced by growth factors. *Mol Cell Biol* 26:1932–1947
- Girirajan S, Vlangos CN, Szomju BB, Edelman E, Trevors CD et al (2006) Genotype-phenotype correlation in Smith-Magenis syndrome: evidence that multiple genes in 17p11.2 contribute to the clinical spectrum. *Genet Med* 8:417–427
- Gossler A, Joyner AL, Rossant J, Skarnes WC (1989) Mouse embryonic stem cells and reporter constructs to detect developmentally regulated genes. *Science* 244:463–465
- Grant SG, O’Dell TJ, Karl KA, Stein PL, Soriano P et al (1992) Impaired long-term potentiation, spatial learning, and hippocampal development in fyn mutant mice. *Science* 258:1903–1910
- Greenberg F, Guzzetta V, Montes de Oca-Luna R, Magenis RE, Smith AC et al (1991) Molecular analysis of the Smith-Magenis syndrome: a possible contiguous-gene syndrome associated with del(17)(p11.2). *Am J Hum Genet* 49:1207–1218
- Greenberg F, Lewis RA, Potocki L, Glaze D, Parke J et al (1996) Multi-disciplinary clinical study of Smith-Magenis syndrome (deletion 17p11.2). *Am J Med Genet* 62:247–254
- Guo TL, McCay JA, Karrow NA, Brown RD, Musgrove DL et al (2001) Immunotoxicity of sodium bromate in female B6C3F1 mice: a 28-day drinking water study. *Drug Chem Toxicol* 24:129–149
- Hall TA (1999) BioEdit: a user-friendly biological sequence alignment editor and analysis program for Windows 95/98/NT. *Nucleic Acids Symp Ser* 41:95–98
- Hartmann CB, McCoy KL (2004) Gallium arsenide exposure impairs processing of particulate antigen by macrophages: modification of the antigen reverses the functional defect. *Life Sci* 75:485–498
- Hogg A, Schirm S, Nakagoshi H, Bartley P, Ishii S et al (1997) Inactivation of a c-Myb/estrogen receptor fusion protein in transformed primary cells leads to granulocyte/macrophage differentiation and down regulation of c-kit but not c-myc or cdc2. *Oncogene* 15:2885–2898
- Irwin S (1968) Comprehensive observational assessment: Ia. A systematic, quantitative procedure for assessing the behavioral and physiologic state of the mouse. *Psychopharmacologia* 13:222–257
- Jerne NK, Nordin AA (1963) Plaque formation in agar by single antibody-producing cells. *Science* 140:405

- Katoh Y, Shiba Y, Mitsuhashi H, Yanagida Y, Takatsu H et al (2004) Tollip and Tom1 form a complex and recruit ubiquitin-conjugated proteins onto early endosomes. *J Biol Chem* 279:24435–24443
- Katoh Y, Imakagura H, Futatsumori M, Nakayama K (2006) Recruitment of clathrin onto endosomes by the Tom1-Tollip complex. *Biochem Biophys Res Commun* 341:143–149
- Kirchhausen T (2000) Clathrin. *Annu Rev Biochem* 69:699–727
- Laskowski RA, MacArthur MW, Moss DS, Thornton JM (1993) PROCHECK: a program to check the stereochemical quality of protein structures. *J Appl Crystallogr* 26:283–291
- Lewis TA, Munson AE, McCoy KL (1996) Gallium arsenide selectively suppresses antigen processing by splenic macrophages for CD4+ T cell activation. *J Pharmacol Exp Ther* 278:1244–1251
- Li W, Marshall C, Mei L, Dzubow L, Schmults C et al (2005) Srcasm modulates EGF and Src-kinase signaling in keratinocytes. *J Biol Chem* 280:6036–6046
- Li W, Marshall C, Mei L, Gelfand J, Seykora JT (2007) Srcasm corrects Fyn-induced epidermal hyperplasia by kinase down-regulation. *J Biol Chem* 282:1161–1169
- Lohi O, Lehto VP (1998) VHS domain marks a group of proteins involved in endocytosis and vesicular trafficking. *FEBS Lett* 440:255–257
- Lucas RE, Vlangos CN, Das P, Patel PI, Elsea SH (2001) Genomic organisation of the approximately 1.5 Mb Smith-Magenis syndrome critical interval: transcription map, genomic contig, and candidate gene analysis. *Eur J Hum Genet* 9:892–902
- Luster MI, Munson AE, Thomas PT, Holsapple MP, Fenters JD et al (1988) Development of a testing battery to assess chemical-induced immunotoxicity: National Toxicology Program's guidelines for immunotoxicity evaluation in mice. *Fundam Appl Toxicol* 10:2–19
- Misra S, Beach BM, Hurley JH (2000) Structure of the VHS domain of human *Tom1* (target of myb-1): insights into interactions with proteins and membranes. *Biochemistry* 39:11282–11290
- Oh IH, Reddy EP (1999) The myb gene family in cell growth, differentiation and apoptosis. *Oncogene* 18:3017–3033
- Park J, Meisler AI, Cartwright CA (1993) c-Yes tyrosine kinase activity in human colon carcinoma. *Oncogene* 8:2627–2635
- Potash JB, Buervenich S, Cox NJ, Zandi PP, Akula N et al (2008) Gene-based SNP mapping of a psychotic bipolar affective disorder linkage region on 22q12.3: Association with HMG2L1 and TOM1. *Am J Med Genet B Neuropsychiatr Genet* 147: 59–67
- Puertollano R (2005) Interactions of TOM1L1 with the multivesicular body sorting machinery. *J Biol Chem* 280:9258–9264
- Rogers DC, Fisher EM, Brown SD, Peters J, Hunter AJ et al (1997) Behavioral and functional analysis of mouse phenotype: SHIRPA, a proposed protocol for comprehensive phenotype assessment. *Mamm Genome* 8:711–713
- Sali A, Blundell TL (1993) Comparative protein modelling by satisfaction of spatial restraints. *J Mol Biol* 234:779–815
- Seet LF, Hong W (2005) Endofin recruits clathrin to early endosomes via TOM1. *J Cell Sci* 118:575–587
- Seet LF, Liu N, Hanson BJ, Hong W (2004) Endofin recruits TOM1 to endosomes. *J Biol Chem* 279:4670–4679
- Serafini T, Colamarino SA, Leonardo ED, Wang H, Beddington R et al (1996) Netrin-1 is required for commissural axon guidance in the developing vertebrate nervous system. *Cell* 87:1001–1014
- Seykora JT, Mei L, Dotto GP, Stein PL (2002) 'Srcasm: a novel Src activating and signaling molecule. *J Biol Chem* 277:2812–2822
- Shiba Y, Katoh Y, Shiba T, Yoshino K, Takatsu H et al (2004) GAT (GGA and Tom1) domain responsible for ubiquitin binding and ubiquitination. *J Biol Chem* 279:7105–7111
- Skarnes WC, Auerbach BA, Joyner AL (1992) A gene trap approach in mouse embryonic stem cells: the lacZ reported is activated by splicing, reflects endogenous gene expression, and is mutagenic in mice. *Genes Dev* 6:903–918
- Skarnes WC, Moss JE, Hurtley SM, Beddington RS (1995) Capturing genes encoding membrane and secreted proteins important for mouse development. *Proc Natl Acad Sci U S A* 92:6592–6596
- Slager RE, Newton TL, Vlangos CN, Finucane B, Elsea SH (2003) Mutations in RAI1 associated with Smith-Magenis syndrome. *Nat Genet* 33:466–468
- Smith AC, McGavran L, Robinson J, Waldstein G, Macfarlane J et al (1986) Interstitial deletion of (17)(p11.2p11.2) in nine patients. *Am J Med Genet* 24:393–414
- Stanford WL, Cohn JB, Cordes SP (2001) Gene-trap mutagenesis: past, present and beyond. *Nat Rev Genet* 2:756–768
- Stein PL, Lee HM, Rich S, Soriano P (1992) pp59fyn mutant mice display differential signaling in thymocytes and peripheral T cells. *Cell* 70:41–750
- Stryke D, Kawamoto M, Huang CC, Johns SJ, King LA et al (2003) BayGenomics: a resource of insertional mutations in mouse embryonic stem cells. *Nucleic Acids Res* 31:278–281
- Takatsu H, Katoh Y, Shiba Y, Nakayama K (2001) Golgi-localizing, gamma-adaptin ear homology domain, ADP-ribosylation factor-binding (GGA) proteins interact with acidic dileucine sequences within the cytoplasmic domains of sorting receptors through their Vps27p/Hrs/STAM (VHS) domains. *J Biol Chem* 276: 28541–28545
- Talbot WS, Hopkins N (2000) Zebrafish mutations and functional analysis of the vertebrate genome. *Genes Dev* 14:755–762
- van Dartel M, Hulsebos TJ (2004) Amplification and overexpression of genes in 17p11.2-p12 in osteosarcoma. *Cancer Genet Cytogenet* 153:77–80
- Voss AK, Thomas T, Gruss P (1998) Efficiency assessment of the gene trap approach. *Dev Dyn* 212:171–180
- Yamakami M, Yokosawa H (2004) Tom1 (target of Myb 1) is a novel negative regulator of interleukin-1- and tumor necrosis factor-induced signaling pathways. *Biol Pharm Bull* 27:564–566
- Yang HM, Butterworth L, Munson AE, Meade BJ (2003) Respiratory exposure to diesel exhaust particles decreases the spleen IgM response to a T cell-dependent antigen in female B6C3F1 mice. *Toxicol Sci* 71:207–216
- Yeo TT, Yang T, Massa SM, Zhang JS, Honkaniemi J et al (1997) Deficient LAR expression decreases basal forebrain cholinergic neuronal size and hippocampal cholinergic innervation. *J Neurosci Res* 47:348–360
- Zarzour W, Kleta R, Frangoul H, Suwannarat P, Jeong A et al (2005) Two novel CHS1 (LYST) mutations: clinical correlations in an infant with Chediak-Higashi syndrome. *Mol Genet Metab* 85:125–132

Copyright of *Mammalian Genome* is the property of Springer Science & Business Media B.V. and its content may not be copied or emailed to multiple sites or posted to a listserv without the copyright holder's express written permission. However, users may print, download, or email articles for individual use.

Appendix E

Overlapping genes identified in ChIP-Chip study (full names)

ATP-binding cassette, sub-family B (MDR/TAP), member 1;ABCB1
 ATP-binding cassette, sub-family B (MDR/TAP), member 1;ABCB1
 amylo-1, 6-glucosidase, 4-alpha-glucanotransferase (glycogen debranching enzyme, glycogen storage disease type III);AGL
 amylo-1, 6-glucosidase, 4-alpha-glucanotransferase (glycogen debranching enzyme, glycogen storage disease type III);AGL
 A kinase (PRKA) anchor protein 7;AKAP7
 A kinase (PRKA) anchor protein 7;AKAP7
 aldo-keto reductase family 1, member C1 (dihydrodiol dehydrogenase 1; 20-alpha (3-alpha)-hydroxysteroid dehydrogenase);AKR1C1
 aldo-keto reductase family 1, member C3 (3-alpha hydroxysteroid dehydrogenase, type II);AKR1C3
 aldo-keto reductase family 1, member C3 (3-alpha hydroxysteroid dehydrogenase, type II);AKR1C3
 amyotrophic lateral sclerosis 2 (juvenile) chromosome region, candidate 16;ALS2CR16
 amelogenin, Y-linked;AMELY
 amelogenin, Y-linked;AMELY
 amylase, alpha 2A; pancreatic;AMY2A
 amylase, alpha 2B (pancreatic);AMY2B
 annexin A1;ANXA1
 annexin A1;ANXA1
 APin protein;APIN
 adenine phosphoribosyltransferase;APRT
 adenine phosphoribosyltransferase;APRT
 Rho guanine nucleotide exchange factor (GEF) 7;ARHGEF7
 Rho guanine nucleotide exchange factor (GEF) 7;ARHGEF7
 N-acylsphingosine amidohydrolase (non-lysosomal ceramidase) 2;ASAH2
 N-acylsphingosine amidohydrolase (non-lysosomal ceramidase) 2;ASAH2
 ankyrin repeat and SOCS box-containing 4;ASB4
 activating transcription factor 6;ATF6
 activating transcription factor 6;ATF6
 ATP synthase, H⁺ transporting, mitochondrial F1 complex, epsilon subunit;ATP5E
 ATP synthase, H⁺ transporting, mitochondrial F1 complex, epsilon subunit;ATP5E
 5-azacytidine induced 2;AZI2
 5-azacytidine induced 2;AZI2
 bromodomain adjacent to zinc finger domain, 2B;BAZ2B
 bromodomain adjacent to zinc finger domain, 2B;BAZ2B
 butyrylcholinesterase;BCHE
 butyrylcholinesterase;BCHE
 bone morphogenetic protein 5;BMP5
 bone morphogenetic protein 5;BMP5

chromosome 10 open reading frame 61;C10orf61
 chromosome 10 open reading frame 61;C10orf61
 chromosome 10 open reading frame 68;C10orf68
 chromosome 10 open reading frame 68;C10orf68
 chromosome 14 open reading frame 10;C14orf10
 chromosome 14 open reading frame 10;C14orf10
 chromosome 14 open reading frame 150;C14orf150
 chromosome 16 open reading frame 73;C16orf73
 chromosome 18 open reading frame 9;C18orf9
 chromosome 20 open reading frame 103;C20orf103
 chromosome 20 open reading frame 103;C20orf103
 chromosome 21 open reading frame 34;C21orf34
 chromosome 21 open reading frame 34;C21orf34
 chromosome 3 open reading frame 58;C3orf58
 complement component 4 binding protein, beta;C4BPB
 complement component 4 binding protein, beta;C4BPB
 chromosome 4 open reading frame 22;C4orf22
 chromosome 4 open reading frame 7;C4orf7
 chromosome 4 open reading frame 7;C4orf7
 chromosome 5 open reading frame 36;C5orf36
 chromosome 9 open reading frame 102;C9orf102
 chromosome 9 open reading frame 150;C9orf150
 chromosome 9 open reading frame 150;C9orf150
 calcium binding protein 39-like;CAB39L
 calcium binding protein 39-like;CAB39L
 coiled-coil domain containing 46;CCDC46
 CD69 antigen (p60, early T-cell activation antigen);CD69
 CD69 molecule;CD69
 cadherin 12, type 2 (N-cadherin 2);CDH12
 cadherin 12, type 2 (N-cadherin 2);CDH12
 chromodomain protein, Y-linked, 2B;CDY2B
 centaurin, delta 1;CENTD1
 centaurin, delta 1;CENTD1
 centrosomal protein 76kDa;CEP76
 choline/ethanolamine phosphotransferase 1;CEPT1
 choline/ethanolamine phosphotransferase 1;CEPT1
 complement factor H;CFH
 cell adhesion molecule with homology to L1CAM (close homolog of L1);CHL1
 cell adhesion molecule with homology to L1CAM (close homolog of L1);CHL1
 chondrolectin;CHODL
 chondrolectin;CHODL
 cholinergic receptor, nicotinic, alpha 5;CHRNA5
 cholinergic receptor, nicotinic, alpha polypeptide 5;CHRNA5
 C-type lectin domain family 5, member A;CLEC5A
 C-type lectin domain family 5, member A;CLEC5A
 ciliary neurotrophic factor;CNTF

ciliary neurotrophic factor;CNTF
 component of oligomeric golgi complex 6;COG6
 component of oligomeric golgi complex 6;COG6
 COMM domain containing 3;COMMD3
 cereblon;CRBN
 cereblon;CRBN
 cAMP responsive element modulator;CREM
 cAMP responsive element modulator;CREM
 crystallin, gamma S;CRYGS
 crystallin, gamma S;CRYGS
 cylicin, basic protein of sperm head cytoskeleton 2;CYLC2
 cylicin, basic protein of sperm head cytoskeleton 2;CYLC2
 chromosome Y open reading frame 15A;CYorf15A
 chromosome Y open reading frame 15B;CYorf15B
 DEAD/H (Asp-Glu-Ala-Asp/His) box polypeptide 11 (CHL1-like helicase homolog, S. cerevisiae);DDX11
 defensin, beta 112;DEFB112
 defensin, beta 112;DEFB112
 diacylglycerol kinase, beta 90kDa;DGKB
 diacylglycerol kinase, beta 90kDa;DGKB
 diaphanous homolog 3 (Drosophila);DIAPH3
 diaphanous homolog 3 (Drosophila);DIAPH3
 DnaJ (Hsp40) homolog, subfamily C, member 5 beta;DNAJC5B
 DnaJ (Hsp40) homolog, subfamily C, member 5 beta;DNAJC5B
 dentin sialophosphoprotein;DSPP
 dentin sialophosphoprotein;DSPP
 dystrobrevin, alpha;DTNA
 dystrobrevin, alpha;DTNA
 elongation of very long chain fatty acids (FEN1/Elo2, SUR4/Elo3, yeast)-like 2;ELOVL2
 elongation of very long chain fatty acids (FEN1/Elo2, SUR4/Elo3, yeast)-like 2;ELOVL2
 eyes absent homolog 1 (Drosophila);EYA1
 eyes absent homolog 1 (Drosophila);EYA1
 family with sequence similarity 55, member D;FAM55D
 family with sequence similarity 55, member D;FAM55D
 F-box and leucine-rich repeat protein 7;FBXL7
 F-box and leucine-rich repeat protein 7;FBXL7
 F-box protein 4;FBXO4
 fibrinogen beta chain;FGB
 fibrinogen beta chain;FGB
 fibroblast growth factor 7 (keratinocyte growth factor);FGF7
 fibrinogen-like 2;FGL2
 fibrinogen-like 2;FGL2
 fumarate hydratase;FH
 fumarate hydratase;FH

hypothetical protein FLJ22662;FLJ22662
 hypothetical protein FLJ32745;FLJ32745
 FLJ44048 protein;FLJ44048
 forkhead box K2;FOXK2
 forkhead box K2;FOXK2
 forty-two-three domain containing 1;FYTTD1
 forty-two-three domain containing 1;FYTTD1
 gamma-aminobutyric acid (GABA) A receptor, gamma 1;GABRG1
 gamma-aminobutyric acid (GABA) A receptor, gamma 1;GABRG1
 UDP-N-acetyl-alpha-D-galactosamine:polypeptide N-acetylgalactosaminyltransferase 13
 (GalNAc-T13);GALNT13
 UDP-N-acetyl-alpha-D-galactosamine:polypeptide N-acetylgalactosaminyltransferase 13
 (GalNAc-T13);GALNT13
 UDP-N-acetyl-alpha-D-galactosamine:polypeptide N-acetylgalactosaminyltransferase-
 like 2;GALNTL2
 UDP-N-acetyl-alpha-D-galactosamine:polypeptide N-acetylgalactosaminyltransferase-
 like 2;GALNTL2
 GDNF family receptor alpha like;GFRAL
 glycine receptor, alpha 3;GLRA3
 glycine receptor, alpha 3;GLRA3
 G protein-coupled receptor 52;GPR52
 G protein-coupled receptor 52;GPR52
 HERV-H LTR-associating 2;HHLA2
 HERV-H LTR-associating 2;HHLA2
 histone 1, H2ac;HIST1H2AC
 histone cluster 1, H2ac;HIST1H2AC
 histone 1, H2bl;HIST1H2BL
 histone cluster 1, H2bl;HIST1H2BL
 histone 1, H2bm;HIST1H2BM
 histone cluster 1, H2bm;HIST1H2BM
 histone cluster 1, H3h;HIST1H3H
 histone 1, H4b;HIST1H4B
 histone cluster 1, H4b;HIST1H4B
 histone cluster 1, H4j;HIST1H4J
 major histocompatibility complex, class II, DP alpha 1;HLA-DPA1
 major histocompatibility complex, class II, DP alpha 1;HLA-DPA1
 major histocompatibility complex, class II, DP beta 1;HLA-DPB1
 major histocompatibility complex, class II, DP beta 1;HLA-DPB1
 hypothetical protein HS322B1A;HS322B1A
 heat shock transcription factor, Y-linked 1;HSFY1
 heat shock transcription factor, Y linked 2;HSFY2
 hereditary sensory neuropathy, type II;HSN2
 5-hydroxytryptamine (serotonin) receptor 2B;HTR2B
 5-hydroxytryptamine (serotonin) receptor 2B;HTR2B
 interferon, alpha 10;IFNA10
 interleukin 12 receptor, beta 2;IL12RB2

interleukin 12 receptor, beta 2;IL12RB2
 interleukin 15;IL15
 interleukin 15;IL15
 interleukin 17D;IL17D
 interleukin 17D;IL17D
 interphotoreceptor matrix proteoglycan 2;IMPG2
 interphotoreceptor matrix proteoglycan 2;IMPG2
 inversin;INVS
 inversin;INVS
 jumonji domain containing 1A;JMJD1A
 jumonji domain containing 1A;JMJD1A
 potassium channel, subfamily K, member 10;KCNK10
 potassium channel, subfamily K, member 10;KCNK10
 potassium large conductance calcium-activated channel, subfamily M, beta member 4;KCNMB4
 potassium large conductance calcium-activated channel, subfamily M, beta member 4;KCNMB4
 potassium channel tetramerisation domain containing 4;KCTD4
 potassium channel tetramerisation domain containing 4;KCTD4
 KIAA0391;KIAA0391
 KIAA0391;KIAA0391
 KIAA1712;KIAA1712
 KIAA1712;KIAA1712
 Kruppel-like factor 14;KLF14
 Kruppel-like factor 14;KLF14
 kelch-like 4 (Drosophila);KLHL4
 kelch-like 4 (Drosophila);KLHL4
 kelch-like 9 (Drosophila);KLHL9
 kelch-like 9 (Drosophila);KLHL9
 killer cell lectin-like receptor subfamily C, member 4;KLRC4
 killer cell lectin-like receptor subfamily K, member 1;KLRK1
 keratin 12 (Meesmann corneal dystrophy);KRT12
 keratin 12 (Meesmann corneal dystrophy);KRT12
 keratin 24;KRT24
 keratin 24;KRT24
 keratin associated protein 1-1;KRTAP1-1
 keratin associated protein 1-1;KRTAP1-1
 keratin associated protein 1-3;KRTAP1-3
 keratin associated protein 1-3;KRTAP1-3
 keratin associated protein 4-12;KRTAP4-12
 keratin associated protein 4-12;KRTAP4-12
 keratin associated protein 6-3;KRTAP6-3
 late cornified envelope 3B;LCE3B
 late cornified envelope 3B;LCE3B
 low density lipoprotein receptor (familial hypercholesterolemia);LDLR
 low density lipoprotein receptor (familial hypercholesterolemia);LDLR

lymphoid enhancer-binding factor 1;LEF1
 smooth muscle myosin heavy chain 11 isoform SM1-like;LOC129285
 C/EBP-induced protein;LOC81558
 latrophilin 2;LPHN2
 latrophilin 2;LPHN2
 leucine rich repeat neuronal 3;LRRN3
 leucine rich repeat neuronal 3;LRRN3
 leucine rich repeat transmembrane neuronal 4;LRRTM4
 leucine rich repeat transmembrane neuronal 4;LRRTM4
 liver-specific organic anion transporter 3;LST-3
 lumican;LUM
 lumican;LUM
 MAS1 oncogene-like;MAS1L
 MAS1 oncogene-like;MAS1L
 MADS box transcription enhancer factor 2, polypeptide A (myocyte enhancer factor 2A);MEF2A
 MADS box transcription enhancer factor 2, polypeptide A (myocyte enhancer factor 2A);MEF2A
 meprin A, alpha (PABA peptide hydrolase);MEP1A
 meprin A, alpha (PABA peptide hydrolase);MEP1A
 mannosyl (alpha-1,3-)-glycoprotein beta-1,4-N-acetylglucosaminyltransferase, isozyme C (putative);MGAT4C
 hypothetical protein MGC33530;MGC33530
 hypothetical protein MGC34713;MGC34713
 hypothetical protein MGC35043;MGC35043
 hypothetical protein MGC35212;MGC35212
 makorin, ring finger protein, 3;MKRN3
 makorin, ring finger protein, 3;MKRN3
 matrix metalloproteinase 13 (collagenase 3);MMP13
 matrix metalloproteinase 13 (collagenase 3);MMP13
 mitochondrial translational release factor 1-like;MTRF1L
 mitochondrial translational release factor 1-like;MTRF1L
 mucin 7, salivary;MUC7
 mucin 7, secreted;MUC7
 myosin, light chain 1, alkali; skeletal, fast;MYL1
 myosin, light polypeptide 1, alkali; skeletal, fast;MYL1
 nucleosome assembly protein 1-like 3;NAP1L3
 nucleosome assembly protein 1-like 3;NAP1L3
 odontogenic, ameloblast associated;ODAM
 osteoglycin (osteoinductive factor, mimecan);OGN
 osteoglycin (osteoinductive factor, mimecan);OGN
 osteomodulin;OMD
 osteomodulin;OMD
 olfactory receptor, family 10, subfamily T, member 2;OR10T2
 olfactory receptor, family 10, subfamily T, member 2;OR10T2
 olfactory receptor, family 11, subfamily H, member 4;OR11H4

olfactory receptor, family 11, subfamily H, member 4;OR11H4
 olfactory receptor, family 13, subfamily C, member 3;OR13C3
 olfactory receptor, family 13, subfamily C, member 3;OR13C3
 olfactory receptor, family 13, subfamily F, member 1;OR13F1
 olfactory receptor, family 13, subfamily F, member 1;OR13F1
 olfactory receptor, family 1, subfamily Q, member 1;OR1Q1
 olfactory receptor, family 1, subfamily Q, member 1;OR1Q1
 olfactory receptor, family 2, subfamily B, member 11;OR2B11
 olfactory receptor, family 2, subfamily J, member 3;OR2J3
 olfactory receptor, family 2, subfamily L, member 2;OR2L2
 olfactory receptor, family 2, subfamily L, member 2;OR2L2
 olfactory receptor, family 2, subfamily L, member 3;OR2L3
 olfactory receptor, family 2, subfamily M, member 5;OR2M5
 olfactory receptor, family 2, subfamily T, member 10;OR2T10
 olfactory receptor, family 2, subfamily T, member 4;OR2T4
 olfactory receptor, family 4, subfamily A, member 47;OR4A47
 olfactory receptor, family 4, subfamily C, member 16;OR4C16
 olfactory receptor, family 4, subfamily C, member 16;OR4C16
 olfactory receptor, family 51, subfamily A, member 7;OR51A7
 olfactory receptor, family 51, subfamily A, member 7;OR51A7
 olfactory receptor, family 52, subfamily A, member 1;OR52A1
 olfactory receptor, family 52, subfamily A, member 1;OR52A1
 olfactory receptor, family 52, subfamily N, member 5;OR52N5
 olfactory receptor, family 52, subfamily N, member 5;OR52N5
 olfactory receptor, family 56, subfamily B, member 1;OR56B1
 olfactory receptor, family 56, subfamily B, member 1;OR56B1
 olfactory receptor, family 5, subfamily B, member 2;OR5B2
 olfactory receptor, family 5, subfamily BU, member 1;OR5BU1
 olfactory receptor, family 5, subfamily H, member 14;OR5H14
 olfactory receptor, family 5, subfamily H, member 6;OR5H6
 olfactory receptor, family 5, subfamily H, member 6;OR5H6
 olfactory receptor, family 5, subfamily K, member 3;OR5K3
 olfactory receptor, family 5, subfamily K, member 4;OR5K4
 olfactory receptor, family 5, subfamily M, member 3;OR5M3
 olfactory receptor, family 5, subfamily M, member 3;OR5M3
 olfactory receptor, family 5, subfamily R, member 1;OR5R1
 olfactory receptor, family 5, subfamily T, member 2;OR5T2
 olfactory receptor, family 5, subfamily T, member 2;OR5T2
 olfactory receptor, family 5, subfamily V, member 1;OR5V1
 olfactory receptor, family 5, subfamily V, member 1;OR5V1
 olfactory receptor, family 5, subfamily W, member 2;OR5W2
 olfactory receptor, family 6, subfamily M, member 1;OR6M1
 olfactory receptor, family 6, subfamily M, member 1;OR6M1
 olfactory receptor, family 8, subfamily H, member 1;OR8H1
 olfactory receptor, family 8, subfamily H, member 2;OR8H2
 olfactory receptor, family 8, subfamily H, member 2;OR8H2

olfactory receptor, family 8, subfamily I, member 2;OR8I2
 olfactory receptor, family 8, subfamily I, member 2;OR8I2
 olfactory receptor, family 8, subfamily K, member 3;OR8K3
 olfactory receptor, family 8, subfamily K, member 3;OR8K3
 olfactory receptor, family 9, subfamily G, member 1;OR9G1
 olfactory receptor, family 9, subfamily G, member 1;OR9G1
 olfactory receptor, family 9, subfamily G, member 9;OR9G9
 OTU domain containing 6B;OTUD6B
 OTU domain containing 6B;OTUD6B
 palladin, cytoskeletal associated protein;PALLD
 protocadherin 11 X-linked;PCDH11X
 protocadherin 11 Y-linked;PCDH11Y
 protocadherin 15;PCDH15
 protocadherin 15;PCDH15
 protocadherin alpha 1;PCDHA1
 protocadherin alpha 11;PCDHA11
 protocadherin alpha 3;PCDHA3
 protocadherin beta 16;PCDHB16
 protocadherin beta 16;PCDHB16
 protocadherin beta 8;PCDHB8
 protocadherin beta 8;PCDHB8
 protocadherin gamma subfamily A, 12;PCDHGA12
 protocadherin gamma subfamily A, 9;PCDHGA9
 phosphodiesterase 1A, calmodulin-dependent;PDE1A
 phosphodiesterase 1A, calmodulin-dependent;PDE1A
 pleckstrin homology domain interacting protein;PHIP
 phytanoyl-CoA 2-hydroxylase interacting protein-like;PHYHIPL
 phytanoyl-CoA hydroxylase interacting protein-like;PHYHIPL
 phosphatidylinositol glycan anchor biosynthesis, class F;PIGF
 phosphatidylinositol glycan, class F;PIGF
 phospholipase C, beta 4;PLCB4
 phospholipase C, beta 4;PLCB4
 pleiotropic regulator 1 (PRL1 homolog, Arabidopsis);PLRG1
 pleiotropic regulator 1 (PRL1 homolog, Arabidopsis);PLRG1
 pro-melanin-concentrating hormone;PMCH
 pancreatic lipase;PNLIP
 pancreatic lipase;PNLIP
 POU domain, class 1, transcription factor 1 (Pit1, growth hormone factor 1);POU1F1
 POU domain, class 1, transcription factor 1 (Pit1, growth hormone factor 1);POU1F1
 protein kinase, cAMP-dependent, catalytic, beta;PRKACB
 protein kinase, cAMP-dependent, catalytic, beta;PRKACB
 RAP1B, member of RAS oncogene family;RAP1B
 RAP1B, member of RAS oncogene family;RAP1B
 regulator of G-protein signalling 21;RGS21
 ras homolog gene family, member B;RHOB
 ras homolog gene family, member B;RHOB

ring finger protein 17;RNF17
 ras responsive element binding protein 1;RREB1
 ras responsive element binding protein 1;RREB1
 arginine/serine-rich coiled-coil 1;RSRC1
 arginine/serine-rich coiled-coil 1;RSRC1
 serpin peptidase inhibitor, clade I (pancpin), member 2;SERPINI2
 serpin peptidase inhibitor, clade I (pancpin), member 2;SERPINI2
 sarcoglycan, gamma (35kDa dystrophin-associated glycoprotein);SGCG
 sarcoglycan, gamma (35kDa dystrophin-associated glycoprotein);SGCG
 sarcoglycan zeta;SGCZ
 sarcoglycan zeta;SGCZ
 short stature homeobox 2;SHOX2
 short stature homeobox 2;SHOX2
 sucrase-isomaltase (alpha-glucosidase);SI
 sucrase-isomaltase (alpha-glucosidase);SI
 silver homolog (mouse);SILV
 silver homolog (mouse);SILV
 solute carrier family 12 (sodium/potassium/chloride transporters), member 1;SLC12A1
 solute carrier family 12 (sodium/potassium/chloride transporters), member 1;SLC12A1
 solute carrier family 16 (monocarboxylic acid transporters), member 7;SLC16A7
 solute carrier family 16, member 7 (monocarboxylic acid transporter 2);SLC16A7
 solute carrier family 25, member 32;SLC25A32
 solute carrier family 25, member 32;SLC25A32
 solute carrier family 26, member 7;SLC26A7
 solute carrier family 26, member 7;SLC26A7
 solute carrier organic anion transporter family, member 1B3;SLCO1B3
 solute carrier organic anion transporter family, member 1B3;SLCO1B3
 SLIT and NTRK-like family, member 6;SLITRK6
 SLIT and NTRK-like family, member 6;SLITRK6
 structural maintenance of chromosomes 6;SMC6
 SMC6 structural maintenance of chromosomes 6-like 1 (yeast);SMC6L1
 syntaphilin;SNPH
 syntaphilin;SNPH
 small nuclear ribonucleoprotein polypeptide N;SNRPN
 Sp6 transcription factor;SP6
 Sp6 transcription factor;SP6
 sperm associated antigen 6;SPAG6
 sperm associated antigen 6;SPAG6
 sperm protein associated with the nucleus, X-linked, family member A1;SPANXA1
 SPANX family, member A2;SPANXA2
 SPANX family, member E;SPANXE
 spermatogenesis associated 18 homolog (rat);SPATA18
 spermatogenesis associated 18 homolog (rat);SPATA18
 TAF2 RNA polymerase II, TATA box binding protein (TBP)-associated factor,
 150kDa;TAF2
 TAF2 RNA polymerase II, TATA box binding protein (TBP)-associated factor,

150kDa;TAF2
 TGF-beta induced apoptosis protein 2;TAIP-2
 taste receptor, type 2, member 7;TAS2R7
 taste receptor, type 2, member 7;TAS2R7
 taste receptor, type 2, member 8;TAS2R8
 taste receptor, type 2, member 8;TAS2R8
 tudor domain containing 4;TDRD4
 testis expressed sequence 15;TEX15
 testis expressed sequence 15;TEX15
 transcription factor EC;TFEC
 transcription factor EC;TFEC
 transmembrane protein 77;TMEM77
 transmembrane protein 77;TMEM77
 transmembrane protease, serine 11B;TMPRSS11B
 transmembrane protease, serine 11B;TMPRSS11B
 tumor necrosis factor (ligand) superfamily, member 18;TNFSF18
 tumor necrosis factor (ligand) superfamily, member 18;TNFSF18
 tumor necrosis factor superfamily, member 5-induced protein 1;TNFSF5IP1
 tumor necrosis factor superfamily, member 5-induced protein 1;TNFSF5IP1
 transient receptor potential cation channel, subfamily C, member 3;TRPC3
 transient receptor potential cation channel, subfamily C, member 3;TRPC3
 transient receptor potential cation channel, subfamily M, member 8;TRPM8
 transient receptor potential cation channel, subfamily M, member 8;TRPM8
 tumor suppressor candidate 1;TUSC1
 tumor suppressor candidate 1;TUSC1
 thioredoxin domain containing 13;TXNDC13
 ubiquitin protein ligase E3A (human papilloma virus E6-associated protein, Angelman syndrome);UBE3A
 ubiquitin protein ligase E3A (human papilloma virus E6-associated protein, Angelman syndrome);UBE3A
 ubiquitin-fold modifier 1;UFM1
 ubiquitin-fold modifier 1;UFM1
 UDP glucuronosyltransferase 2 family, polypeptide A1;UGT2A1
 UDP glucuronosyltransferase 2 family, polypeptide A1;UGT2A1
 IVFI9356;UNQ9356
 urotensin 2 domain containing;UTS2D
 urotensin 2 domain containing;UTS2D
 ubiquitously transcribed tetratricopeptide repeat gene, Y-linked;UTY
 ubiquitously transcribed tetratricopeptide repeat gene, Y-linked;UTY
 V-set and transmembrane domain containing 2;VSTM2
 von Willebrand factor A domain containing 2;VWA2
 WD repeat domain 89;WDR89
 WD repeats and SOF1 domain containing;WDSOF1
 WD repeats and SOF1 domain containing;WDSOF1
 5'-3' exoribonuclease 1;XRN1
 5'-3' exoribonuclease 1;XRN1

Yip1 domain family, member 7;YIPF7

Yip1 domain family, member 7;YIPF7

zinc finger protein 306;ZNF306

zinc finger protein 306;ZNF306

zinc finger protein 614;ZNF614